October 2023

Distinct Nrf2 Signaling Thresholds Mediate Lung Tumor Initiation and Progression

Janine M. DeBlasi
University of South Florida

Distinct Nrf2 Signaling Thresholds Mediate Lung Tumor Initiation and Progression

by

Janine M. DeBlasi

A dissertation submitted in partial fulfillment
of the requirements for the degree of
Doctor of Philosophy
Department of Molecular Biosciences
College of Arts and Sciences
University of South Florida

Major Professor: Gina M. DeNicola, Ph.D.
Joseph L. Kissil, Ph.D.
Ana P. Gomes, Ph.D.
Elsa Flores, Ph.D.
Amer Beg, Ph.D.
Marcus Cooke, Ph.D.
Katerina Politi, Ph.D.

Date of Approval:
October 9, 2023

Keywords: Kelch-like ECH-associated protein 1 (KEAP1), Cancer, Genetically
engineered mouse model (GEMM)

Dedication

I would like to dedicate this dissertation to my stepsister Stacey and my grandmother Sadie. Stacey is a recurrent breast cancer survivor, and one of the strongest and liveliest individuals I know, along with being an incredible mother. She inspired me to pursue an education in cancer research, and I am forever grateful to call her my family. My grandmother, who we lost in February of 2022, is also a critical source of inspiration for me. She always believed in me and helped mold me into the happy and dedicated person I am today.

Acknowledgments

First, I would like to thank my mentor, Dr. Gina DeNicola. She has provided unwavering support, guidance, and taught me numerous invaluable things throughout my PhD experience. I will always be grateful for her extensive expertise, patience, and mentorship. I would also like to thank my committee members Dr. Ana Gomes, Dr. Joseph Kissil, Dr. Amer Beg, Dr. Elsa Flores, and Dr. Marcus Cooke for their feedback and support. Dr. Gomes and her lab also gave me helpful suggestions during our lab meetings that significantly contributed to my growth as a scientist. I would also like to thank Dr. Katerina Politi, for her willingness to serve as my external chair and share her insight in the field of lung cancer mouse modeling.

I also want to express my gratitude for the current and former members of the DeNicola Lab. Dr. Nathan Ward, who started mentoring me in the D'Agostino lab as a PhD student himself, and is now a PI of his own lab, has immensely contributed to my development in science. Dr. Laura Torrente, for being a wonderful, patient mentor and friend. Cheyenne Schneider, who has also been an amazing friend and lab mate. Dr. Chang Jiang, who has also been incredibly helpful, kind, and now has her own lab. Aimee Falzone, Samantha Caldwell, and Nicola Prieto, for their kindness and help with the mouse models used in my experiments. Dr. Yumi Kim, Dr. Paloma Gonzalez Sanchez, Andrea Mockabee Macias, and Amanda Sherwood, for their friendship and support in the lab. Dr. Yun Pyo Kang, for helping with the metabolomics in this study, and Sae Bom Lee, for both of their support and showing me kindness beginning when I

Table of Contents

List of Figures

List of Abbreviations

KEAP1	Kelch-like ECH associated protein 1
NRF2	Nuclear factor erythroid 2-related factor 2
NSCLC	non-small cell lung cancer
SCLC	small-cell lung cancer
LUAD	lung adenocarcinoma
SCC	squamous cell carcinoma
LCC	large cell carcinoma
KRAS	Kirsten rat sarcoma viral oncogene homolog
EGFR	epidermal growth factor receptor
ALK	anaplastic lymphoma kinase
STK11	serine threonine kinase 11
LKB1	liver kinase B1
GOF	gain-of-function
LOH	loss-of-heterozygosity
TP53	tumor protein p53
Cul3	Cullin 3
BTB	Broad complex, Tramtrack, and Bric-a-Brac
IVR	intervening region
bZIP	basic leucine zipper
CNC	cap 'n' collar
sMAF	small masculoaponeurotic fibrosarcoma
NQO1	NADPH dehydrogenase quinone 1
OGT	O-GlcNAc transferase
MGx	methylglyoxal
H_2O_2	hydrogen peroxide

NO	nitric oxide
SFN	sulforaphane
tBHQ	*tert*-butyl hydroquinone
FN3K	fructosamine-3-kinase
ARE	antioxidant response element
IHC	immunohistochemistry
G6P	glucose-6-phosphate
R5P	ribose-5-phosphate
PRPP	phosphoribosyl pyrophosphate
IMP	inosine monophosphate
F6P	fructose-6-phosphate
GA3P	glyceraldehyde-3-phosphate
3PG	3-phosphoglycerate
3-PHP	3-phosphohydroxypyruvate
3-PS	3-phosphoserine
10-Formyl-THF	10-formyl-tetrahydrofolate
DHFR	dihydrofolate reductase
CO	carbon monoxide
Asp	aspartate
Asn	asparagine
Glu	glutamate
Gly	glycine
ROS	reactive oxygen species
GSH	glutathione
GSSG	glutathione disulfide
TXN	thioredoxin
$NADP^+$	nicotinamide adenine dinucleotide phosphate, oxidized
NADPH	nicotinamide adenine dinucleotide phosphate, reduced
G6PD	glucose-6-phosphate dehydrogenase
PGD	phosphogluconate dehydrogenase
TALDO1	transaldolase 1

TKT	transketolase
PPAT	phosphoribosyl pyrophosphate amidotransferase
PPP	pentose phosphate pathway
MTHFD2	methylenetetrahydrofolate dehydrogenase 2
PHGDH	3-phosphoglycerate dehydrogenase
PSAT1	phosphoserine aminotransferase 1
SHMT1/2	serine hydroxymethyltransferase
ATF4	activating transcription factor 4
FECH	ferrochelatase
HMOX1	heme oxygenase 1
BLVRB1	biliverdin reductase B 1
FTH1	ferritin heavy chain
FTL	ferritin light chain
ME1	malic enzyme 1
IDH1	isocitrate dehydrogenase1
FAS	fatty acid synthase
GLS	glutaminase
ASNS	asparagine synthetase
TXNRD1	thioredoxin reductase 1
TXN	thioredoxin
SRXN1	sulfiredoxin
GSR	glutathione reductase
GCL	glutamate cysteine ligase
GCLC	glutamate-cysteine-ligase catalytic subunit
GCLM	glutamate-cysteine ligase modifier subunit
GPX4	glutathione peroxidase 4
PRDX	peroxiredoxin
SLC7A11/xCT	cystine glutamate antiporter
ASC	alanine-serine cysteine
CDO1	cysteine dioxygenase 1
NEAA	non-essential amino acid

HCC	hepatocellular carcinoma
ECM	extracellular matrix
FAO	fatty acid oxidation
GSK3β	glycogen synthase kinase-3 beta
β-TrCP	beta-transducin repeats-containing protein
ABC	ATP-binding cassette
GEMM	genetically engineered mouse model
CRISPR	clustered regularly interspaced short palindromic repeats
BACH1	BTB and CNC homology 1
TIGAR	TP53-induced glycolysis and apoptosis regulator
CA	conditionally active
LSL	lox-STOP-lox
WT	wild type
PA	poly A signal
MEF	mouse embryonic fibroblast
AAH	atypical adenomatous hyperplasia
BH	bronchiolar hyperplasia
ANOVA	analysis of variance
CC-3	cleaved capase-3
PGAM5	phosphoglycerate mutase 5
PALB2	partner and localizer of BRCA2
MCM3	mini-chromosome maintenance complex component 3
Ns	not significant
SPC	surfactant protein C
EV	empty vector
BSO	buthionine sulfoximine
AUC	area under the curve
ERK	extracellular signal-regulated kinase
4-HNE	4-hydroxynonenal
FFPE	formalin-fixed paraffin-embedded
NAC	N-Acetylcysteine

ALDH3A1   aldehyde dehydrogenase 3A1

DMSO   dimethyl sulfoxide

β-ME   beta-mercaptoethanol

GEO   gene expression omnibus

LC-HRMS   liquid chromatography - high resolution mass spectrometry

AMPK   AMP-activated protein kinase

Abstract

NRF2 is a redox-responsive transcription factor the directs the antioxidant

program and several critical metabolic processes. Mutations in NRF2 or its negative

regulator KEAP1 occur in up to one third of non-small cell lung cancers (NSCLCs) and

are often associated with resistance to therapy and poor outcomes. In the present

studies, murine alleles of the Keap1 and Nrf2 mutations found in human NSCLC were

developed and I comprehensively investigated their impact on tumor initiation and

progression. I observed that chronic Nrf2 stabilization by Keap1 loss-of-

function or Nrf2 activating mutation was not sufficient to cause lung tumor initiation,

even when p53 or Lkb1 were deleted. In the context of oncogenic $Kras^{G12D/+}$,

constitutive Nrf2 activation via Keap1/ Nrf2 mutation promoted lung tumor initiation and

early progression of hyperplasia to low-grade tumors.

When $Kras^{G12D/+}$ was combined with p53 deletion, I observed an

impairment in progression to advanced-grade tumors with $Keap1^{R554Q/R554Q}$ mutation,

which caused the most robust Nrf2 activation. I discovered that this progression block

was reversed by NRF2 deletion, indicating that the effects of Keap1 mutation in this

model were Nrf2-dependent. I also interrogated the effect of Nrf2 hyperactivation in

another mutational background, the $Kras^{G12D/+}$; $Lkb1^{fl/fl}$ model. Interestingly, $Nrf2^{D29H/+}$

mutation, which was the most activating towards Nrf2 in this model, blocked progression

to high-grade tumors, suggesting that excess levels of Nrf2 are detrimental to lung

tumor progression. Finally, I observed that NRF2 overexpression in KEAP1 mutant

human NSCLC cell lines impaired cell proliferation, viability, and anchorage-

independent colony formation. Collectively, these results establish the context-

dependence and activity threshold for NRF2 during the lung tumorigenic process.

Chapter One: Introduction[1]

Lung Cancer

Lung cancer continues to account for the highest number of cancer deaths among both men and women in the United States, with a 5-year survival rate of 21% for all stages (2). Lung cancer is divided into two main histological subtypes: small-cell lung cancer (SCLC) and non-small cell lung cancer (NSCLC), representing 15% and 85% of cases, respectively. NSCLC has a 5-year survival rate of ~16% and comprises adenocarcinomas (LUADs), squamous cell carcinomas (SCCs), and large cell carcinomas (LCCs), of which LUADs are the most common subtype and originate from distal airways (3, 4). SCLC, in contrast, arises from lung neuroendocrine stem cells and is considered the most aggressive histological subtype, with a 5-year survival rate of 7% (5). There are numerous treatment options available for LUAD patients including targeted therapy against Kirsten rat sarcoma viral oncogene homolog (KRAS), epidermal growth factor receptor (EGFR), and anaplastic lymphoma kinase (ALK), as well as platinum-based chemotherapy, and immunotherapy, depending on cancer stage (6). In contrast, there are limited options available for SCLC and SCC patients (7), actionable drivers found in LUAD, like EGFR and KRAS mutations, as well as ALK

---

[1] Note to reader: Portions of this chapter have been previously published in a review article in DeBlasi and DeNicola 2020, *Cancers (Basel)* (1). **J. M. DeBlasi** and **G. M. DeNicola:** Conceptualization, draft preparation, review and editing.

fusions, are rare in SCLC and SCC (4). Additional investigation is warranted into all clinical subtypes to improve clinical outcomes.

Genomic alterations in LUAD

Although there has been emerging progress in targeting driver oncogenes in lung LUADs, such as *KRAS* and *EGFR*, there are many tumors which lack actionable drivers. The most common gain-of-function (GOF) mutation in LUAD is *KRAS* which is altered in ~30% of cases (8). On the other hand, commonly mutated tumor suppressor genes in LUAD include tumor protein p53 (*TP53*), serine threonine kinase 11 (*STK11*), and Kelch-like ECH-associated protein 1 (*KEAP1*) (8); the biology of such genomic abnormalities and how they interact requires further investigation. The most frequently mutated tumor suppressor gene in all cancers, *TP53*, is regarded as the guardian of the genome, and can also regulate a vast number of metabolic processes, often conferring metabolic reprogramming when altered (9). *STK11* encodes for liver kinase B1 (LKB1) and is inactivated in ~20% of LUADs (10). LKB1 controls cell polarity, growth, motility, and metabolism, and when inactivated can cause metabolic deregulation and increased oxidative stress (11). KEAP1 negatively regulates nuclear factor-erythroid 2 p45-related factor 2 (NRF2, gene name: *NFE2L2*), which responds to oxidative stress within the cell and supports anabolic metabolism. Mutations in the KEAP1-NRF2 pathway occur in up to 30% of NSCLCs, promote constitutive accumulation of NRF2, and can confer resistance to therapy through detoxifying reactive oxygen species (ROS) (12).

KEAP1/ NRF2 Biology

KEAP1 is a member of the BTB-Kelch protein family and assembles with Cullin 3 (Cul3) and Rbx1 to comprise Cullin-RING ligases for proteasomal degradation of proteins like NRF2 (13). KEAP1 has three domains including the Broad complex, Tramtrack, and Bric-a-Brac (BTB) domain, which facilitates KEAP1 homodimerization and interaction with Cul3 (14), the intervening region (IVR) domain, which connects the BTB and Kelch domains and facilitates redox sensing, and the Kelch domain which mediates substrate binding and can bind to the low-affinity DLG or high-affinity ETGE motifs of NRF2 (15) **(Fig. 1.1)**. Throughout these domains, there are key cysteine residues that are modified upon electrophilic or oxidant exposure **(Fig. 1.2)** (15).

NRF2 is a cap "n" collar (CNC) family member of basic leucine zipper (bZIP) transcription factors that facilitates the antioxidant response. Once the key cysteine residues are modified, NRF2 can accumulate in the nucleus and promote expression of antioxidant enzymes and other metabolic pathways (15). NRF2 is comprised of several Neh domains (**Fig 1.1**). The Neh1 domain has the CNC bZIP region responsible for binding DNA and the small masculoaponeurotic fibrosarcoma (sMAF) proteins that dimerize with NRF2 (16). The Neh2 domain facilitates interaction with KEAP1 via its DLG and ETGE domains (17). The Neh3 domain is located at the C-terminus of NRF2 and is important for its transcriptional activity (18), in addition to the Neh4 and Neh5 domains, which comprise the transactivation domain and support transcription of NRF2 target genes (19). Finally, the Neh6 domain facilitates NRF2 negative regulation (independent of KEAP1) (20), and the Neh7 domain is involved in suppression of NRF2 transcription via the retinoid X receptor α (21).
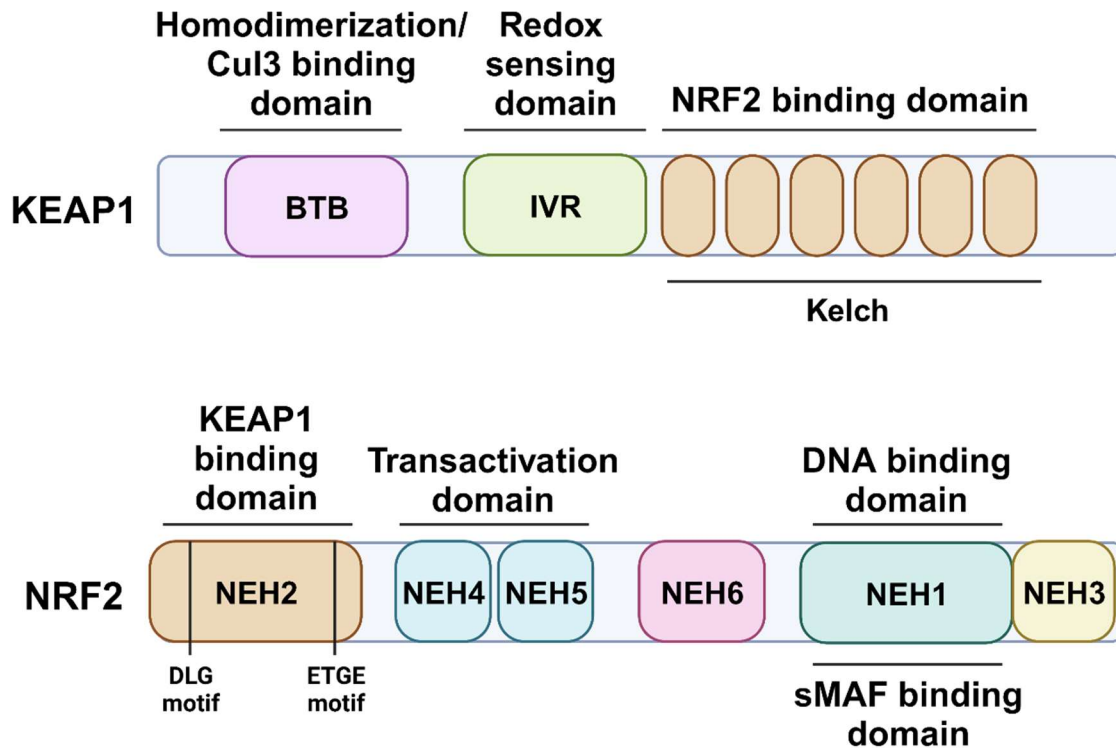
Figure 1.1. Domain structure of KEAP1 and NRF2 proteins. The KEAP1 protein contains the Bric-a-Brac (BTB), intervening region (IVR), and NRF2 binding domains. NRF2 is comprised of multiple Neh domains that play roles in NRF2-mediated transcriptional activation and regulation by KEAP1. Created with BioRender.com.

Transcriptional responses regulated by NRF2

The basic leucine zipper transcription factor NRF2 directs the transcription of both the antioxidant program and metabolic processes that support its function. NRF2 levels are controlled by its interaction with KEAP1, a substrate adaptor for a cullin 3 (CUL3)-based E3 ubiquitin ligase that targets NRF2 for ubiquitination and proteasomal degradation (22), as highlighted in **Figure 1.3**.
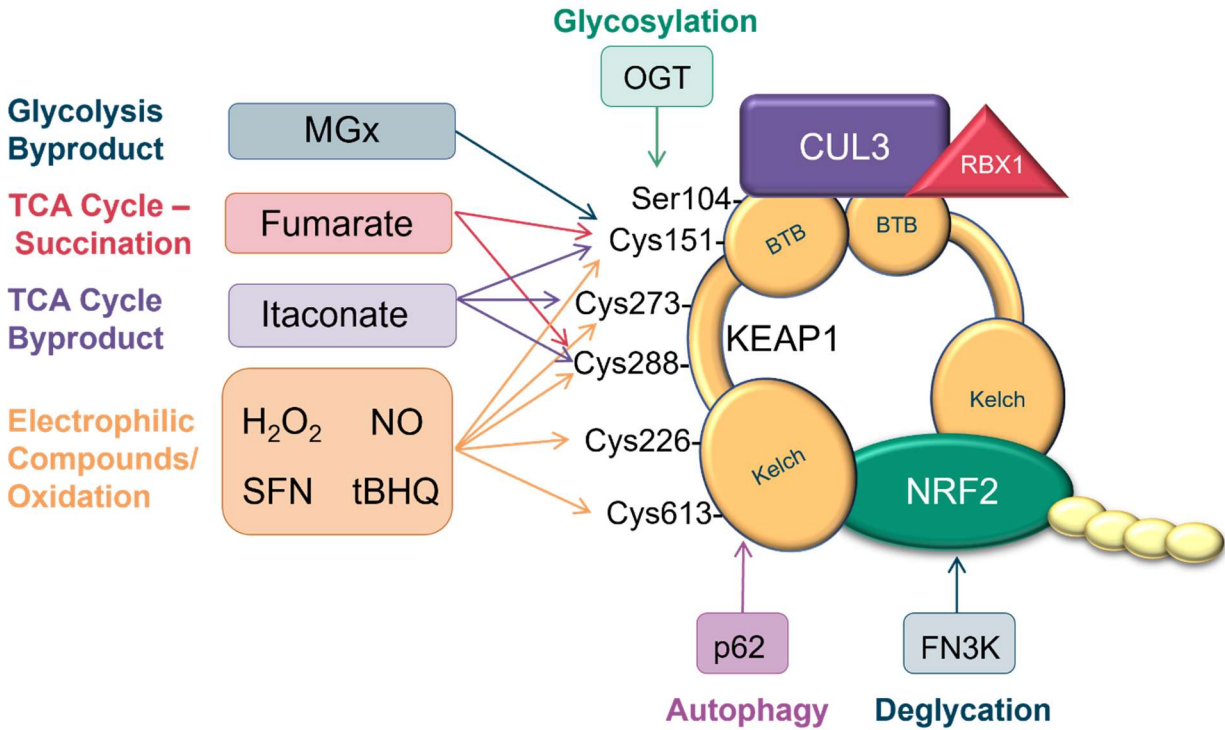
Figure 1.2. NRF2 is activated by oxidants, signaling molecules, and metabolites. KEAP1: KEAP1 is glycosylated by O-GlcNAc transferase (OGT) at serine 104. The glycolysis byproduct methylglyoxal (MGx) mediates a crosslink between cysteine 151 with arginine 135, activating the NRF2 transcriptional program. Further, NRF2 activation can result from fumarate-mediated succination of cysteines 151 and 288. The TCA cycle byproduct itaconate can also activate NRF2 by reacting with cysteines 151, 273, and 288. Hydrogen peroxide (H_2O_2), nitric oxide (NO), sulforaphane (SFN), and *tert*-butyl hydroquinone (tBHQ) can activate NRF2 by modifying cysteine residues 151, 273, 288, 226, and 613. The autophagy adaptor sequestome 1, p62, activates NRF2 by binding to the Kelch domain region of KEAP1. NRF2: NRF2 is destabilized by glycation, which is reversed by the enzyme Fructosamine-3-kinase (FN3K). This figure was previously published in *Cancers (Basel)*, DeBlasi and DeNicola 2020 (1).
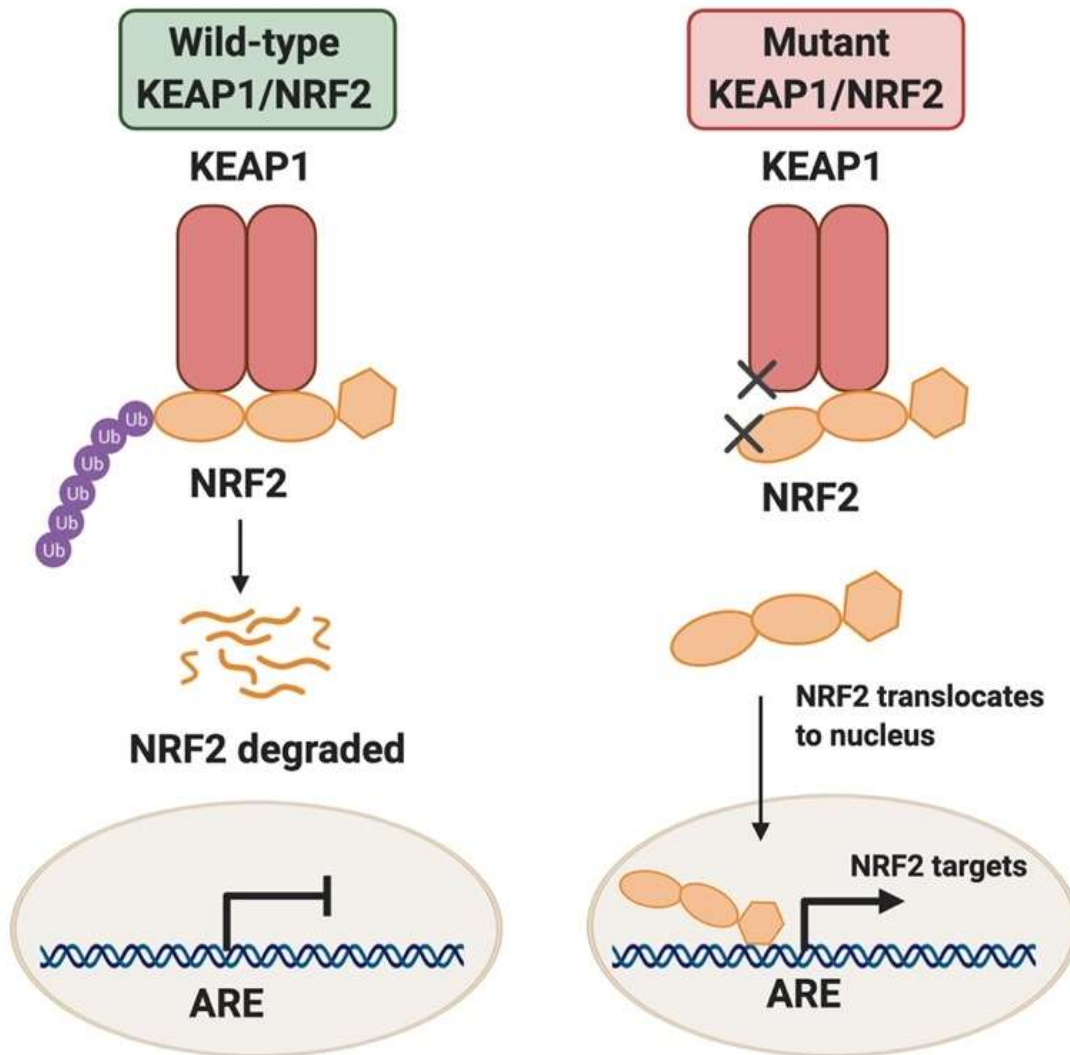
Figure 1.3. KEAP1/NRF2 regulation. Under non-stressed conditions KEAP1 directs ubiquitin-mediated degradation of NRF2, resulting in minimal transcription of NRF2 targets. Under oxidative or xenobiotic stress, or when the KEAP1/NRF2 pathway is mutated, NRF2 is stabilized and promotes transcription of antioxidant response element (ARE)-containing genes. Created with BioRender.com. This figure was previously published in *Cancers (Basel)*, DeBlasi and DeNicola 2020 (1).

NRF2 directs the antioxidant response

Oxidative stress refers to an imbalance in ROS production and elimination, and can cause damage to cells via oxidation (23). Xenobiotics can also cause oxidative stress and toxicity, warranting defense mechanisms via NRF2 (24). Following exposure to oxidative or xenobiotic stress, NRF2 binds to the antioxidant response element (ARE) of its target genes to promote transcription of phase II detoxifying enzymes (25). These enzymes play important roles in the antioxidant and stress responses, glutathione synthesis, and drug metabolism, among others, the description of which is expanded upon in the subsequent sections. Upregulation of these enzymes by NRF2 can be potentially exploited for chemoprevention by promoting carcinogen detoxification but can also cause resistance to chemotherapy, radiation, immunotherapy, and targeted therapies (26, 27, 28, 29, 30, 31, 32).

Over the past decade, advances in our understanding of the reprogramming of cellular metabolism in cancer cells have yielded insight into the complex biology of cancer. As this recently established cancer hallmark encompasses a plethora of pathways (33), there is still a lack of complete understanding into how metabolic pathways can be targeted in the treatment of cancer. NRF2 is emerging as a major regulator of cellular metabolism in both normal and cancer cells. In addition to orchestrating an antioxidant response to oxidative insults, there are emerging roles of NRF2 in promoting metabolic processes, including NADPH production (34, 35, 36, 37), and the metabolism of lipids (37, 38, 39, 40, 41), amino acids (cysteine (42, 43), glutamine(44, 45), serine/glycine (46, 47), asparagine (48)), nucleotides (35, 49), and iron/heme (37, 50, 51, 52, 53), as outlined in **Figures 1.3** and **1.4**. Although these

processes play an important role in supporting the antioxidant response in healthy cells, and may be exploitable for chemoprevention (30, 31, 32), they are hijacked by cancer cells to support proliferation and survival (54), warranting further investigation into the relationship between NRF2-regulated processes and tumorigenesis. Indeed, NRF2 regulates anabolic and catabolic metabolism, both of which can significantly impact tumorigenesis but are less well understood in the context of NRF2-driven cancer phenotypes.
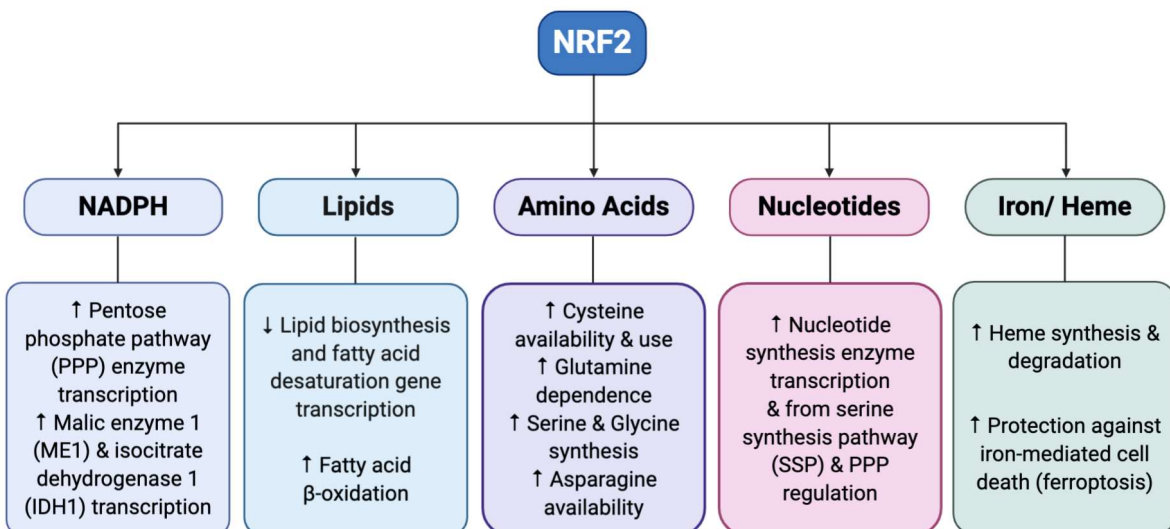
Figure 1.4. NRF2 directs numerous metabolic processes that impact cancer cell survival and proliferation. Several of these pathways include NADPH production and the metabolism of lipids, amino acids, nucleotides, and iron/heme. Created with BioRender.com. This figure was previously published in *Cancers (Basel)*, DeBlasi and DeNicola 2020 (1).
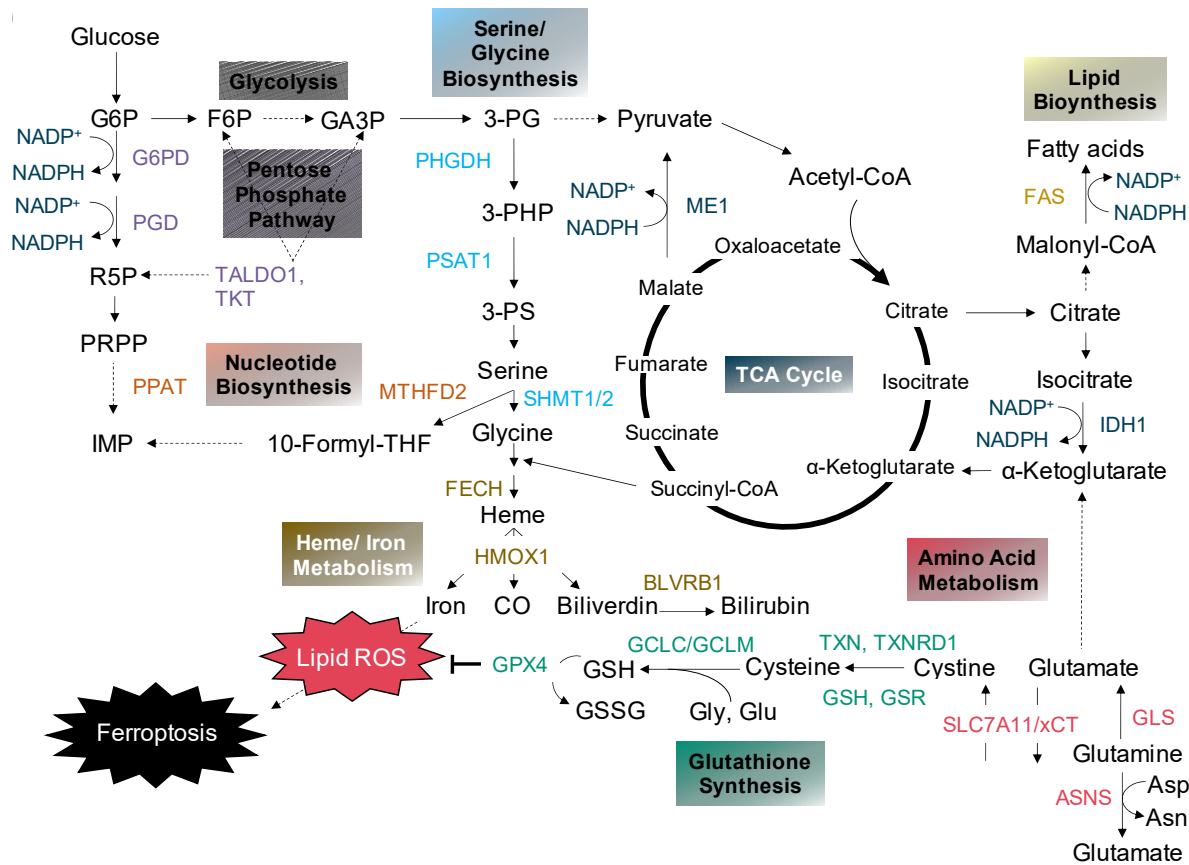
Figure 1.5. NRF2-regulated metabolic pathways. NRF2 directs the transcription of numerous genes that encode for metabolic enzymes and transporters, including those involved in the pentose phosphate pathway (G6PD, PGD, TALDO1, TKT), nucleotide biosynthesis (PPAT, MTHFD2), serine/ glycine biosynthesis (PHGDH, PSAT1, SHMT1/2), heme/iron metabolism (FECH, HMOX1, BLVRB1), glutathione synthesis and utilization (TXN, TXNRD1, GSH, GSR, GCLC, GCLM, GPX4), amino acid metabolism (GLS, ASNS, SLC7A11/xCT), NADPH production (ME1, IDH1), and lipid biosynthesis (FAS). This figure was previously published in *Cancers (Basel)*, DeBlasi and DeNicola 2020 (1).

NRF2's roles in detoxifying reactive oxygen species: cysteine, GSH, TXN

Cysteine is a semi-essential amino acid that can be taken up by cells in both its reduced (cysteine) and oxidized (cystine) forms. Cysteine transport is poorly characterized in both normal and tumor tissues and may involve the alanine-serine-cysteine (ASC), L-amino acid, and/or X_{AG} family of transporters (55, 56, 57). Alternatively, cysteine can be made by de novo synthesis through the reverse transulfuration pathway in some tissues (58). Further, cystine is transported via system x_c-, the cystine/glutamate antiporter (59). xCT, the protein encoded by SLC7A11, is a subunit of system x_c-, and is upregulated in many cancer types, including NSCLC, triple-negative breast cancer, and glioblastomas (60, 61, 62, 63, 64, 65). NRF2 increases intracellular cysteine availability through multiple mechanisms. NRF2 promotes the transcription of xCT to facilitate cystine entry into the cell (42).

One of the most critical aspects of NRF2-regulated processes is the antioxidant tripeptide glutathione (GSH), the most abundant antioxidant molecule in the cell (66). NRF2 promotes the use of cysteine for synthesizing GSH, which supports detoxification of oxidants and has been reported to support proliferation in both normal and cancer cells (67). GSH synthesis is regulated by availability of the amino acid cysteine and the enzyme glutamate cysteine ligase (GCL), which catalyzes the first step of GSH synthesis and is composed of the two subunits GCLC (catalytic) and GCLM (regulatory), both of which are NRF2 target genes (68, 69, 70, 71, 72). GCL facilitates the conjugation of cysteine and glutamate to produce γ-glutamylcysteine, a precursor for GSH (73). Although the regulation of cysteine metabolism by NRF2 robustly increases GSH levels following NRF2 activation, it is less clear whether NRF2-mediated cysteine accumulation promotes the

synthesis of other cysteine-derived metabolites. Beyond GCLC and GCLM, NRF2 also promotes expression of additional enzymes involved in GSH synthesis and utilization, including GSH reductase (GSR), GSH S-transferases and peroxidases (52). GSH peroxidase (GPX), along with peroxiredoxins (PRDXs) and catalase facilitate the conversion of H_2O_2 to water **(Fig. 1.6)**. Moreover, both GPXs and GSH S-transferases use GSH as a cofactor to detoxify ROS and lipid peroxides (74).

NRF2 also regulates expression of genes encoding proteins that reduce oxidized protein thiols, including thioredoxin (TXN) (75), thioredoxin reductase 1 (TXNRD1) (75), and sulfiredoxin (SRXN1) (76). These protein systems participate in the regeneration of PRDXs, which contribute to detoxification of H_2O_2 and peroxynitrite (77). Moreover, TXNRD1 and GSR function to regenerate oxidized TXN and GSH using NADPH for electron transfer (78, 79) **(Fig. 1.6)**. Both the GSH and TXN systems are critical in the antioxidant response and are complimentary, although further investigation is needed to understand their interplay. Collectively, these findings demonstrate the importance of NRF2 in protecting cells against oxidative stress.

Not all NRF2-regulated processes are favorable to cell proliferation

Our lab recently reported that cysteine accumulation mediated by NRF2 was a metabolic vulnerability in NSCLC cells as a consequence of stabilization of cysteine dioxygenase 1 (CDO1) and increased entry of cysteine into the taurine synthesis pathway (43). This led to wasteful and toxic product formation and depletion of NADPH as a consequence of excessive cystine reduction, which impaired NSCLC proliferation and antioxidant function. Notably, CDO1 is epigenetically silenced in NSCLC, particularly in

KEAP1 mutant adenocarcinomas. Consequently, not all NRF2-regulated processes are favorable.
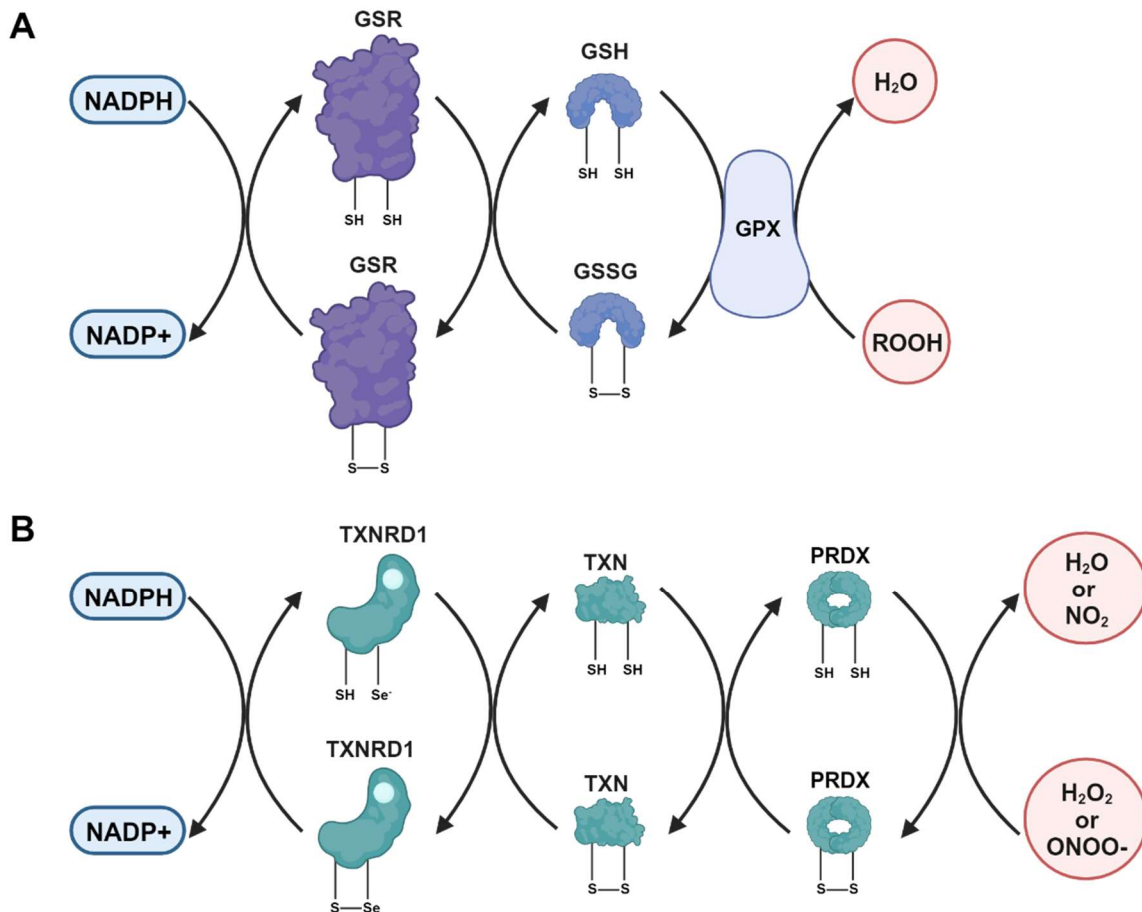
Figure 1.6. Overview of glutathione and thioredoxin systems. NADPH is used as an electron donor in the glutathione reductase (GSR) **(A)** and thioredoxin reductase (TXNRD1) **(B)** systems. Glutathione peroxidase (GPX) catalyzes the oxidation of glutathione (GSH) to glutathione disulfide (GSSG), as well as the conversion of H_2O_2 and lipid peroxides to water. Thioredoxin (TXN) contributes to regeneration of peroxiredoxins (PRDXs), which detoxify H_2O_2 and peroxynitrite. Created with BioRender.com.

Moreover, these consequences of NRF2 activation have also been linked to reductive stress, the accumulation of excessive reducing equivalents (80, 81, 82). In a mouse model of cardiomyopathy, Nrf2 activation was reported to promote reductive stress in association with increased GSH levels (80). Additionally, in human lung cancer cells, NRF2 activation caused reductive stress mediated by NADH, an important reduced nucleotide co-factor, resulting in decreased cell proliferation (82). These finds suggest that although NRF2 activation can protect cells from oxidative damage, there can still be detrimental effects from excess levels of NRF2.

Glutamine

NADPH is not the only cost of cystine import. Because xCT is a cystine-glutamate antiporter, cystine import must be matched by an equimolar amount of glutamate export. Accordingly, NRF2 active cells are in a glutamate-deficient state as a consequence of elevated xCT activity, which limits TCA cycle anaplerosis and increases reliance on glutamine catabolism to glutamate to support xCT flux (44, 45). In agreement with this metabolic vulnerability, KEAP1 mutant NSCLC cell lines, PDX models and Keap1-deficient mouse tumors demonstrate increased sensitivity to glutaminase inhibition with CB-389 (45, 61). Glutaminase inhibition has also been reported to prevent growth of recurrent breast tumor cells in a NRF2-dependent manner (49). In support of this NRF2-mediated dependence on glutamine, it has also been reported that cancer cells with high antioxidant capacity are dependent on non-essential amino acids (NEAAs) driven by xCT-mediated excretion of glutamate required for NEAA synthesis (83). This study also observed therapeutic efficacy in a Keap1 mutant mouse model treated with an inhibitor of glutaminase or asparaginase.

The connection between the KEAP1/NRF2 pathway and glutamine metabolism is not surprising, given that NRF2 upregulates glutaminase, which generates glutamate from glutamine (84). Recent work has also shown that KEAP1 mutant lung cancer cells are dependent on glutamine and the glutamine transporter ASCT2 (encoded by SLC1A5) (45). It has also been suggested that generation of TCA cycle intermediates by alternative pathways, such as IDH1 and ME1, may contribute to NRF2-mediated glutamine dependence (85). Furthermore, siRNA depletion of NRF2 in KEAP1 mutant NSCLC cells decreases incorporation of glutamate into GSH (35), suggesting that glutamate production from glutamine could support GSH synthesis. These studies highlight a metabolic vulnerability in NRF2-hyperactive cancer cells.

Serine/Glycine

Serine and glycine are NEAAs that contribute to diverse macromolecules within normal and cancer cells, including cysteine, sphingolipids, phospholipids, and nucleotides, among others (86, 87). Serine and glycine can be obtained from extracellular sources or synthesized de novo from glucose via the serine synthesis pathway (SSP). The SSP catalyzes the metabolism of the glycolytic intermediate 3-phosphoglycerate (3PG) by phosphoglycerate dehydrogenase (PHGDH) in the first and rate-limiting step. SSP-derived serine is subsequently metabolized to glycine in a reaction mediated by serine hydroxymethyl transferase (SHMT). NRF2 plays an important role in the regulation of SSP enzymes including PHGDH, phosphoserine aminotransferase 1 (PSAT1), and SHMT2 via the amino acid starvation-responsive activating transcription factor 4 (ATF4) (46). Suppression of serine synthesis in KEAP1 mutant NSCLC cell lines impaired the synthesis of GSH and nucleotides, and depleted cellular NADPH levels (46).

KRAS/KEAP1 mutant NSCLC cell lines were also found to depend on GLUT8 (SLC2A8) for serine biosynthesis, suggesting that serine synthesis addiction can also be targeted at the level of glucose availability (88). Beyond lung cancer, NRF2 SUMOylation in hepatocellular carcinoma (HCC) was shown to promote de novo serine synthesis via PHGDH upregulation, leading to serine accumulation and contributing to HCC maintenance (47). Finally, work has also linked serine availability and PHGDH to sphingolipid metabolism, with very low serine levels promoting toxic deoxysphingolipid synthesis (89, 90, 91). In alignment with these studies, earlier work demonstrates the importance of serine in supporting mitochondrial function through ceramide metabolism (92). Additional work is needed to determine whether sphingolipid metabolism is influenced by NRF2 activation in cancer.

Beyond NRF2 regulation, SSP activity is increased in diverse cancer types because of PHGDH amplification, overexpression, and posttranscriptional regulation (46, 93, 94, 95, 96, 97, 98, 99). To potentially exploit this, PHGDH inhibitors are being explored as treatments for cancer. PHGDH inhibition has demonstrated preclinical utility in xenograft models of colon cancer (91), as well as xenografts of breast cancer and renal cell carcinoma exhibiting brain metastases (100). The latter findings are also important for NSCLC patients, who can develop brain metastases (101, 102, 103), and thus may respond to PHGDH inhibition. Both PHGDH inhibitor treatment and whole-body Phgdh knockdown are non-toxic in mice, which suggests that PHGDH inhibitors may be safe for patients if adequate serine and glycine are present in the diet (89). In summary, these studies demonstrate inhibition of the SSP as a potential therapeutic modality in cancer.

Asparagine

Asparagine is another NEAA that can be obtained from extracellular sources or synthesized de novo. Asparagine synthetase (ASNS) catalyzes the transamidation of aspartate and glutamine to produce asparagine (104). ASNS, which like SSP enzymes is regulated by ATF4, plays an important role in maintaining asparagine levels under nutrient limiting conditions (105). Further, asparagine has been reported to protect against cell death from glutamine depletion, implicating its role as a metabolite used by cells to coordinate response to metabolic stress (106). NRF2 plays an important role in controlling asparagine availability through the regulation of ASNS. NRF2 regulated the binding of ATF4 to the ASNS promoter in KEAP1 mutant cells (46). Furthermore, NRF2 was essential for KRAS-mediated regulation of ATF4 under nutrient stress. In addition, deletion of KEAP1 enhanced the induction of ATF4 and ASNS following glutamine deprivation (48). Because asparagine depletion by L-asparaginase is a potential therapeutic strategy for the treatment of tumors, these studies suggest that the regulation of ASNS by NRF2 to increase asparagine availability may influence tumor response to L-asparaginase.

NADPH Production

The pentose phosphate pathway (PPP) is a major contributor to the cellular NADPH pool (107). NADPH is critical for the synthesis of fatty acids, cholesterol, mevalonate pathway products (108), nucleotides, folate (107, 109), and proline (54), all of which can support tumorigenesis. NADPH is also important for survival during ROS-mediated stress as a result of extracellular matrix (ECM) detachment (110). Further, the PPP is often altered in cancers to support cell survival and proliferation (111). The PPP

comprises both irreversible and reversible reactions that are divided into an oxidative branch and a non-oxidative branch. The irreversible oxidative branch uses glucose 6-phosphate (G6P) to produce ribose-5-phosphate (R5P) and NADPH, the latter of which is critical for redox homeostasis. The reversible non-oxidative branch, in contrast, supports the production of only R5P for nucleotide synthesis, and serves to link glycolysis and the PPP (112). The reversibility of this branch allows cells to synthesize R5P even when NADPH is high. NRF2 directly regulates the transcription of multiple PPP enzymes, including both oxidative PPP enzymes glucose-6-phosphate dehydrogenase (G6PD) and phosphogluconate dehydrogenase (PGD), and non-oxidative PPP enzymes transketolase (TKT) and transaldolase 1 (TALDO1) (35). Additionally, NRF2 has been observed to indirectly regulate this pathway through the attenuation of microRNAs miR-1 and miR-206, thereby enhancing PPP gene expression (36). Consequently, NRF2 can both directly and indirectly regulate the expression of PPP enzymes in both branches.

NRF2 also contributes to the NADPH pool via the transcriptional regulation of the NADPH-producing enzymes malic enzyme 1 (ME1) and isocitrate dehydrogenase 1 (IDH1) (35). Given this apparent redundancy in NADPH-generating pathways, one might think that targeting any one individually may not dramatically affect the NADPH pool. Indeed, Zhao et al. reported that despite increased NRF2-mediated transcription of genes involved in NADPH regeneration, the oxidative PPP contributed less to the NADPH pool, and consequently was less essential for the growth of KEAP1 mutant cells (113). Overall, these studies demonstrate the importance of KEAP1 mutational status when evaluating sensitivity to PPP inhibition in a therapeutic context. However, recent work suggests that the oxidative PPP plays a unique role in folate metabolism (107). Chen et al.

demonstrated that while the PPP, IDH1 and ME1 could all support cellular proliferation, only the PPP could maintain a normal NADPH/NADP+ ratio. Deletion of G6PD resulted in high NADP$^+$, leading to dihydrofolate reductase (DHFR) inhibition, and ultimately, impairment of folate-mediated biosynthesis in colon cancer cells, unveiling an important connection between NADPH and folate metabolism (107). Supportingly, Mitsuishi et al. found that silencing the PPP enzymes G6PD or TKT reduced tumor growth in a KEAP1 mutant NSCLC xenograft model in a similar manner to silencing NRF2 (35). Moreover, Best et al. observed that Keap1 mutant mouse lung tumors expressed high levels of Taldo1 and were more sensitive to inhibition of the PPP enzyme Pgd with 6-AN compared with their wild-type counterparts (34). Collectively, these studies highlight the regulation of the PPP by NRF2, which represents a critical metabolic vulnerability in vivo.

Lipid Metabolism

Lipid synthesis is a highly NADPH-consuming process that competes with cellular antioxidant systems for NADPH. NRF2 activation suppresses fatty acid synthesis and desaturation (37, 39) to increase NADPH for detoxification and anabolism in murine liver. While hepatocyte-specific deletion of Keap1 suppressed the expression of fatty acid synthesis and desaturation enzymes, deletion of Nrf2 increased their expression (37). A reduction in fatty acid synthesis enzymes and triglyceride accumulation was also observed in the livers from a Keap1 hypomorphic mouse model, which has elevated Nrf2 expression, fed a high-fat diet (39).

Although the ability of NRF2 to suppress lipogenesis has been established in liver, it is unclear whether this also occurs in tumor cells or how this would be compatible with the growth of a tumor with constitutive NRF2 stabilization. The co-occurrence of other

mutations in tumor suppressors and oncogenes, however, may alleviate this potential block. For example, in NSCLC, *KEAP1* mutant tumors tend to be highly enriched for alterations in serine/threonine kinase 11 (*STK11*), a gene that encodes for the liver kinase B1 (LKB1) (11). It has been suggested that *KEAP1* and *STK11* mutations may cooperate; Lkb1 deletion in MEFs causes increased glucose-dependent lipid biosynthesis and overall lipid content (114). This work suggests that LKB1-deficient tumor cells can divert NADPH into anabolic processes, potentially compensating for the lipid synthesis block conferred by NRF2. Indeed, Jeon and colleagues demonstrated that LKB1-deficient cancer cells increase NADPH consumption by fatty acid synthase (FAS) due to loss of AMPK-mediated regulation (115).

Furthermore, NRF2 has been recently reported to enhance mitochondrial fatty acid oxidation (FAO) (38). When Nrf2 is constitutively active as a result of Keap1 knockout, mitochondrial oxidation of both short-chain and long-chain fatty acids was increased; in contrast, Nfe2l2 knockout decreased their oxidation. It was also reported that expression of an activating Nfe2l2 mutant (Nrf2^{E79Q}) decreased adipogenesis in keratin 14 (KRT14)-positive mouse tissue (40). Further, RNA sequencing (RNAseq) profiling demonstrated that Nrf2^{E79Q} esophageal epithelial cells upregulated peroxisome proliferator activated receptor delta (PPARδ), which regulates FAO (40). More recently, Suzuki and colleagues showed the contribution of Nrf2 to weight gain in mice during space travel, where systemic Nfe2l2 knockout decreased FAO-related gene expression and white adipose tissue homeostasis, in agreement with previous studies demonstrating the importance of NRF2 in lipid metabolism (41). Overall, the role of NRF2-regulated fatty acid metabolism in

tumorigenesis requires further investigation, especially in the context of co-occurring mutations.

Nucleotide Synthesis

NRF2 supports nucleotide synthesis through both metabolic mechanisms and the transcriptional regulation of nucleotide synthesis enzymes. NRF2 regulates the activity of the PPP, which supports nucleotide metabolism by producing the R5P sugar backbone for nucleotide synthesis, and NADPH for the reduction of ribonucleotides to deoxyribonucleotides. Additionally, the SSP provides glycine for purine synthesis and one carbon units for the synthesis of both purines and pyrimidines. Furthermore, NRF2 directly regulates the expression of enzymes involved in de novo nucleotide synthesis. NRF2 knockdown decreases the mRNA expression of phosphoribosyl pyrophosphate amidotransferase (PPAT) and methylenetetrahydrofolate dehydrogenase 2 (MTHFD2) (35). PPAT adds an amine group from glutamine to phosphoribosyl pyrophosphate (PRPP) in the first step of purine synthesis, while MTHFD2 plays a critical role in the synthesis of the 10-Formyltetrahydrofolate molecules that are added to the purine ring in downstream steps. While nucleotide synthesis can support cancer cell proliferation, recent work has also shown that NRF2 signaling promotes transcriptional and metabolic reprogramming to support redox homeostasis and increase de novo nucleotide synthesis during breast tumor recurrence (49). Using in vivo CRISPR screening, Pgd of the oxidative PPP and Ppat were shown to be downstream NRF2 targets required for recurrent tumor growth. These studies highlight the importance of NRF2 in directing nucleotide metabolism for both tumor growth and recurrence.

Iron/Heme

Iron is essential for cellular metabolic processes, but labile, reactive iron can promote the formation of ROS, leading to cellular damage and death. To limit the detrimental effects of free iron, NRF2 regulates many genes involved in iron and heme metabolism, including heme oxygenase 1 (HMOX1) and the genes encoding the iron storage protein ferritin, ferritin heavy chain (FTH1) and ferritin light chain (FTL) (52). Importantly, many interactions between iron and oxygen occur via a porphyrin-bound form of iron, heme, which is in the center of several metabolic enzymes (116). NRF2 promotes the synthesis of heme through the regulation of ferrochelatase (FECH), and its transport via SLC48A1 (50). Surprisingly, NRF2 also promotes the degradation of heme through HMOX1 and biliverdin reductase B (BLVRB) (37, 51). HMOX1 encodes for a cytoprotective enzyme that catalyzes heme degradation, resulting in production of iron, biliverdin, and carbon monoxide (117). BLVRB1 subsequently reduces biliverdin to bilirubin, which is excreted. Many cellular processes rely on iron and heme, and the role of these enzymes in NRF2-mediated tumor initiation and progression is poorly understood.

In cancer, NRF2-mediated disruption of HMOX-1 and ferritin signaling can impact cancer cell proliferation, angiogenesis, metastasis, and response to therapy, which is usually influenced by the amount of ROS and iron present (118). HMOX-1 and NRF2 induction can protect against ferroptosis, an iron-mediated form of cell death. In HCC, Sun and colleagues reported that NRF2 protected HCC cells against ferroptosis via p62-mediated NRF2 stabilization. In this study, the anti-ferroptotic activity of NRF2 was dependent on NQO1, HMOX1, and FTH1 (119). NRF2 also transcriptionally regulates

glutathione peroxidase 4 (GPX4) (120), a key regulatory factor for ferroptosis that mitigates lipid peroxidation and consequent ferroptosis (121). Another key mediator of iron/heme metabolism is the transcription factor BACH1. Heme binds to BACH1, resulting in nuclear export and subsequent ubiquitin-mediated degradation, thereby limiting the amount of BACH1 available to bind DNA in complex with NRF2 (122); in contrast, when heme levels are low, BACH1 antagonizes the ability of NRF2 to activate HMOX1 to promote heme degradation (123). However, BACH1 plays important roles in cancer beyond its role in heme homeostasis. In a mouse model of lung adenocarcinoma, Keap1 deletion/Nrf2 activation promoted metastasis via Hmox1, which promoted the degradation of heme to induce the accumulation of Bach1, which regulated a battery of pro-metastatic genes (53). Collectively, these studies highlight the ways in which NRF2 can modulate iron/heme metabolism to impact tumor phenotypes.

While it has long been known that NRF2 is imperative to cellular homeostasis via its role in the antioxidant response, the regulation of metabolic pathways at the interface between antioxidant defense and cellular proliferation is an emerging and essential function of NRF2. The recent identification of the regulation of NRF2 by metabolic perturbations suggest that NRF2 plays a key role in metabolic homeostasis beyond supporting the antioxidant response. While some of these perturbations have been linked to cancer (e.g. fumarate hydratase mutations, p62 accumulation), further work is needed to determine whether others also play a causal role in tumorigenesis.

NRF2 is stabilized by KEAP1/NFE2L2 mutation

While NRF2 protein levels are highly inducible in normal cells in response to oxidative and xenobiotic stress or electrophile exposure, constitutive NRF2 expression is observed in several cancers (124, 125, 126, 127, 128, 129), including the squamous and adenocarcinoma subtypes of non-small cell lung cancer (NSCLC) (124), and squamous cancers of the esophagus, skin, larynx, and other tissues (127). NRF2 stabilization most commonly occurs via activating mutations and copy number amplifications of the *NFE2L2* gene or inactivating mutations or deletions in *KEAP1* or *CUL3*. Mutations in KEAP1 are usually missense loss-of-function mutations, and loss of heterozygosity (LOH) is often reported in patient tumors (124, 130, 131). NRF2 mutations, in contrast are primarily heterozygous and not associated with LOH (131). Mutations in KEAP1 can occur throughout the NRF2 binding domain, as well as the redox sensing domain **(Fig. 1.1)**. Mutations in NRF2 are in the DLG and ETGE motifs present in the domain that binds to KEAP1, and prevent degradation by KEAP1 **(Fig. 1.1)**

The context-dependence of NRF2 during different stages of tumorigenesis

The roles of NRF2 in tumorigenesis are context-dependent (34, 43, 45, 46, 53, 132, 133, 134, 135, 136, 137), and likely influenced by different aspects of metabolism. The role of ROS metabolism is better defined, however, and has been well-characterized during cancer initiation, progression, and metastasis (74). In healthy cells, activation of NRF2 promotes the transcription of anti-inflammatory and antioxidant genes that suppress the development of DNA damage and mutations that can initiate

tumor formation (138). In contrast, NRF2 supports the survival of transformed cells by protecting against oxidative damage to support their progression to more advanced-stage tumors. Consequently, NRF2 activation has been linked with resistance to both chemo- and radiotherapy (12, 138). NRF2 is known to regulate xenobiotic and drug efflux, including ATP binding cassette (ABC) transporters which relieve cellular stress but can confer resistance to chemotherapeutic agents (139, 140, 141).

Pro-tumorigenic effects of NRF2 activation in lung cancer in NSCLC

Mutations in the KEAP1/NRF2 pathway often confer poor outcomes in cancer patients (124, 125, 126, 127, 128, 129, 142, 143), and are associated with resistance to chemotherapy and radiation (12, 138). KEAP1/NRF2 mutations have also been reported to promote cancer cell survival (12), proliferation (137), metabolic reprogramming (35, 46, 61, 143), and metastasis (53). In human NSCLC cell lines, it was observed that shRNA-mediated NRF2 knockdown reduced cell survival in response to ionizing radiation, whereas Keap1-deficient mouse embryonic fibroblasts (MEFs) exhibited radio-resistance due to constitutive Nrf2 activation (12). Moreover, work from my supervisor showed that NRF2 activation is critical for the proliferation and tumorigenicity of human and mouse pancreatic cancer cells, as well as murine lung cancer cells *in vivo* (137).

In another study, NRF2 was reported to promote cancer cell proliferation by redirecting glucose and glutamine into anabolic metabolism and nucleotide synthesis via the PI3K-Akt pathway in both human and mouse cells (35). Work from my supervisor also showed that NRF2 supports nucleotide and glutathione synthesis by regulating expression of enzymes involved in serine and glycine biosynthesis in human NSCLC cells (46). Another study has also shown that NRF2 activation in both mouse and human

cancer cells causes an imbalance in central carbon metabolism via increasing dependence on glutamine as a result of limited glutamate availability (61).

There have also been several genetically engineered mouse models (GEMMs) utilized to further our understanding of the KEAP1/NRF2 pathway's role in lung cancer (34, 43, 45, 53, 132, 133, 134, 136, 137, 144, 145, 146). My supervisor's study showed that Nrf2 activation was critical for $Kras^{G12D}$ lung tumor initiation (137). Another study also reported that Nrf2 activation by Cre-mediated knockout of Keap1 resulted in a promotion of $Kras^{G12D}$-mediated lung tumorigenesis (34). Additionally, another group observed that Keap1 knockout promoted lung tumor initiation as measured by an increase in low grade tumors in the $Kras^{G12D}$ model of early lung adenocarcinoma (144).

In the aforementioned study, it was also observed that Nrf2 activation in the microenvironment impairs early progression of these Nrf2-active tumors (144), suggesting that the effects of Nrf2 are influenced by cell types in a tumor, including the microenvironment. Moreover, recent work has reported that CRISPR-mediated deletion of Keap1 increased lung tumor size and progression to grade 3 adenocarcinomas in the $Kras^{G12D}$; $p53^{fl/fl}$ model (45). This group also reported an increase in grade 3 tumor burden with Cre-mediated Keap1 knockout, although this was not reported as a proportion like their previous study (136), making it challenging to draw conclusions on the effects of Nrf2 activation on tumor progression. Additionally, grade 5 tumors were not reported in either of these studies, which usually occur in the $Kras^{G12D}$; $p53^{fl/fl}$ model. Moreover, another group also observed increased tumor size with CRISPR-mediated Keap1 deletion in the $Kras^{G12D}$ model. Interestingly, work from our lab has shown that $Keap1^{R554Q/R554Q}$-mediated Nrf2 activation significantly decreases lung tumor size in the

Kras$^{G12D/+}$; p53$^{fl/fl}$ model of lung adenocarcinoma (43). There have also been studies that did not observe changes in lung tumor initiation (147, 148) or size (134, 146, 148) with Nrf2 activation. Moreover, it's important to note that across these studies, there were varied phenotypes measured, experimental conditions, and time points.

Finally, Nrf2 has been reported to promote migration and invasion in the Kras^{G12D}; p53$^{fl/fl}$ lung cancer model with CRISPR-mediated Keap1 deletion through the transcription factor BTB and CNC homology 1 (BACH1) in a heme metabolism-dependent manner (53). In pancreatic cancer, a study by my supervisor showed that NRF2 loss can promote metastasis in the Kras$^{G12D/+}$; p53$^{R270H/+}$ model of pancreatic ductal adenocarcinoma (PDAC) (149). This increase in PDAC metastasis was also observed with deletion of TP53-induced glycolysis and apoptosis regulator (TIGAR), which was associated with increase ROS (149). It is likely that NRF2's effects on metastasis are dependent on tissue type, context, and ROS levels. Additional work is needed to determine NRF2's role(s) during lung tumor initiation and progression.

NRF2 in healthy cells: activation for chemoprevention

Because NRF2 facilitates cytoprotection and protects against oxidative damage, it is also important to determine whether NRF2 activators are suitable for chemoprevention in humans (30, 31, 32). NRF2 was first shown to play a critical role in the antioxidant response as well as phase II detoxification, limiting the deleterious effects of carcinogens (25). Additionally, it has been shown that mice with Nrf2 knockout are more susceptible to carcinogen exposure (150, 151). Accordingly, NRF2 activators have been explored as a means of chemoprevention, including sulforaphane (152) and oltipraz (29). However, because of NRF2's reported pro-tumorigenic roles, it was

unclear whether chronic NRF2 activation could be unsafe in healthy individuals. Previous work in mouse models has also shown that Nrf2 activation via Keap1 loss is insufficient to cause lung tumorigenesis, even in the absence of tumor suppressor genes (34, 133). Alongside these studies with NRF2 activation, there are also several NRF2 inhibitors being explored for potential application in KEAP1/NRF2 mutant cancers (153).

It is important to understand the contexts in which NRF2 can support or prevent cancer phenotypes. Moreover, previous studies have modeled Nrf2 activation by either conditionally knocking out Keap1 (34, 132, 133, 136, 144, 145) or CRISPR-mediated deletion of Keap1 (45, 53, 134, 146), but have not actually modeled KEAP1 mutations that occur in patients. Accordingly, the goal of the experiments performed in this dissertation were to comprehensively interrogate the effects of Keap1 and Nrf2 mutation and lung tumor initiation and progression.

Chapter Two: Keap1/ Nrf2 mutation is not sufficient

to cause lung tumorigenesis *in vivo*[2]

Introduction

It remains unknown whether long-term NRF2 activation is a safe strategy for cancer prevention in humans. Because NRF2 plays important roles in cellular protection and redox homeodynamics, there has been interest in pharmacological NRF2 activation for chemoprevention (30, 31, 32). Additional work is needed to determine whether constitutive NRF2 activation can transform normal cells. Additionally, whole body Nrf2 activation in mice via Keap1 deletion results in postnatal lethality because of constitutive Nrf2 activation (155), raising concerns about the feasibility of this approach in humans. To test whether chronic Nrf2 activation in the lung is sufficient for tumor initiation, I used mouse models made in our lab harboring Keap1 or Nrf2 mutation targeted to the lung and aged them. I also investigated the effect of these mutations in Lkb1- or p53-deficient background and aged them to 500 days. My hypothesis was that these

---

[2] Note to reader: Portions of this chapter have been previously published in DeBlasi et al. 2023, *Cancer Research* (154). **J.M. DeBlasi:** Data curation, formal analysis, investigation, visualization, methodology, writing–original draft, writing–review and editing. **A. Falzone, S. Caldwell, N. Prieto Farigua:** Mouse colony management and collections - Data curation, investigation, methodology, writing–review and editing. **J.R. Prigge, E.E. Schmidt:** Nrf2 antibody for IHC - Resources, writing–review and editing. **I.I.C. Chio:** Nrf2 targeting vector antibody for IHC - Resources, writing–review and editing. **F.A. Karreth:** ES cell targeting - Resources, methodology, writing–review and editing. **G.M. DeNicola:** Mouse models, RNA-sequencing - Conceptualization, resources, data curation, formal analysis, supervision, funding acquisition, investigation, methodology, writing–original draft, project administration, writing–review and editing.

mutations would not be sufficient to cause lung tumor initiation, consistent with prior studies that had determined the effect of Keap1 deletion out to 12-15 months (34, 133).

Keap1^{R554Q} and *Nfe2l2^{D29H}* murine alleles activate Nrf2-mediated transcription and metabolism

To understand how NRF2 activation affects lung cancer, our lab developed murine alleles of either the Keap1^{R554Q} or the Nrf2^{D29H} mutation found in NSCLC patients **(Fig. 2.1A** and **B)**. These mutations prevent Keap1-mediated degradation of Nrf2, allowing for stable, constitutive expression of Nrf2 and transcription of Nrf2 target genes (156, 157). The Keap1^{R554Q} mutation occurs in Keap1's Kelch domain, preventing Keap1 binding to Nrf2's DLG or ETGE motifs to facilitate Nrf2 degradation (156). The Nrf2^{D29H} mutation occurs in Nrf2's DLG motif, blocking Keap1-mediated degradation of Nrf2 (127). To generate the conditionally active *(CA)-Keap1^{R554Q}* allele, a wild-type *Keap1* cDNA of exons 3-5 flanked by loxP sites was added upstream of the R554Q mutation in endogenous exon 4 of the *Keap1* gene **(Fig. 2.1A)** (43). For the Lox-STOP-Lox *(LSL)-Nfe2l2^{D29H}* allele, a loxP-flanked transcriptional and translational STOP (LSL) cassette was added upstream of the D29H mutation in exon 2 of the endogenous *Nfe2l2* gene **(Fig. 2.1B).**
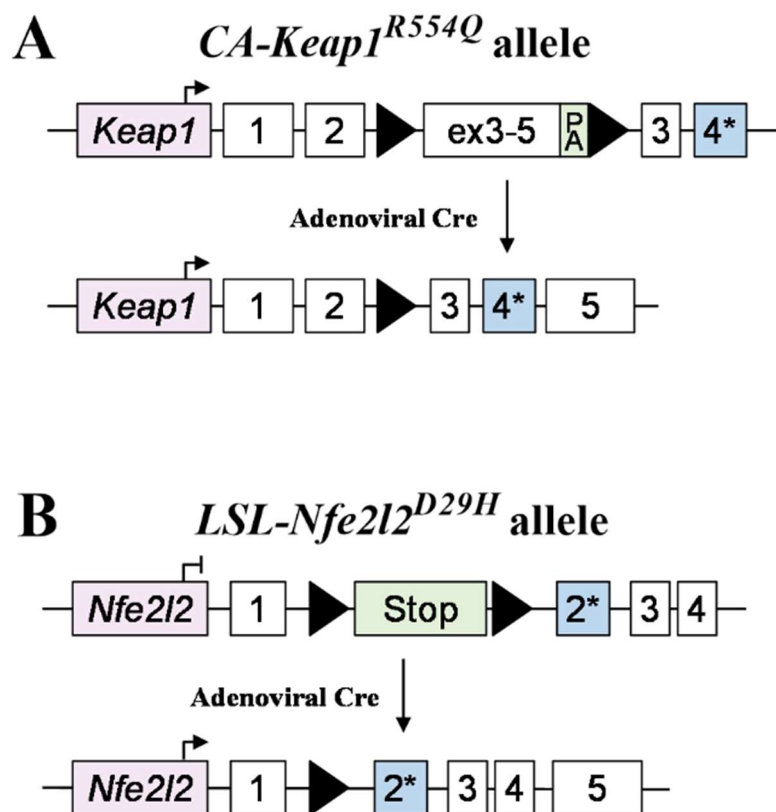
Figure 2.1. Development of mutant *Keap1* and *Nfe2l2* alleles found in human lung cancer. **(A)** The conditionally active (CA)-*Keap1R554Q* allele was generated by inserting a loxP-flanked, wild type (WT) *Keap1* cDNA containing exons 3-5 into intron 2 and introducing the R554Q mutation into endogenous exon 4 of the *Keap1* gene. Prior to intranasal installation of adenoviral-Cre recombinase Keap1 is wild type. Once the floxed cargo is excised, mutant Keap1R554Q is expressed. PA = poly A signal. **(B)** The Lox-STOP-Lox *(LSL)-Nfe2l2D29H* allele was created by inserting a STOP cassette flanked by loxP sites into intron 1 and introducing the D29H mutation in endogenous exon 2 of the *Nfe2l2* gene. Following Cre-mediated excision of the STOP cassette, mutant Nrf2D29H is expressed.

For both Keap1^{R554Q} and Nrf2^{D29H} alleles, Cre-mediated excision of the loxP-flanked cassettes allows for physiological expression of Keap1^{R554Q} or Nrf2^{D29H}, recapitulating NRF2 activation in human NSCLC. To validate the functionality of these alleles, an isogenic system using mouse embryonic fibroblasts (MEFs) was generated, which allowed the transition from a Nrf2-deficient state (Nrf2$^{LSL/LSL}$) to a Nrf2-stabilized state (Nrf2$^{D29H/D29H}$), or from a basal Nrf2 state (Keap1$^{+/+}$) to an activatedNrf2 state (Keap1$^{R554Q/R554Q}$). Using these MEFs, transcriptomic and metabolomic profiling was performed **(Fig. 2.2A-D)**. Transcriptomic profiling indicated that both Keap1$^{R554Q/R554Q}$ and Nrf2$^{D29H/D29H}$ MEFs demonstrated increased transcription of canonical Nrf2 target genes, including Nqo1, Srxn1, Txnrd1, and Gclc **(Fig. 2.2A** and **B)**. Non-targeted metabolomics revealed a robust increase in sulfur-containing metabolites, including glutathione, N-acetyl-L-cysteine, hypotaurine, and L-cystathionine in the Nrf2$^{D29H/D29H}$ MEFs, consistent with our lab's previous findings in Keap1$^{R554Q/R554Q}$ MEFs **(Fig. 2.2C and D)** (43).

It has also been previously reported that targeting the murine *Keap1* locus to generate a *Keap1^{flox}* allele resulted in the generation of a hypomorphic allele prior to Cre-mediated recombination, leading to whole body decreased Keap1 levels and increased Nrf2 transcriptional activity (158). To investigate whether our *CA-Keap1^{R554Q}* allele was hypomorphic, I first validated that MEFs with Keap1$^{+/+}$ or CA-Keap1$^{R554Q/R554Q}$ produced PCR products at the expected size **(Fig. 2.3A-C)**.
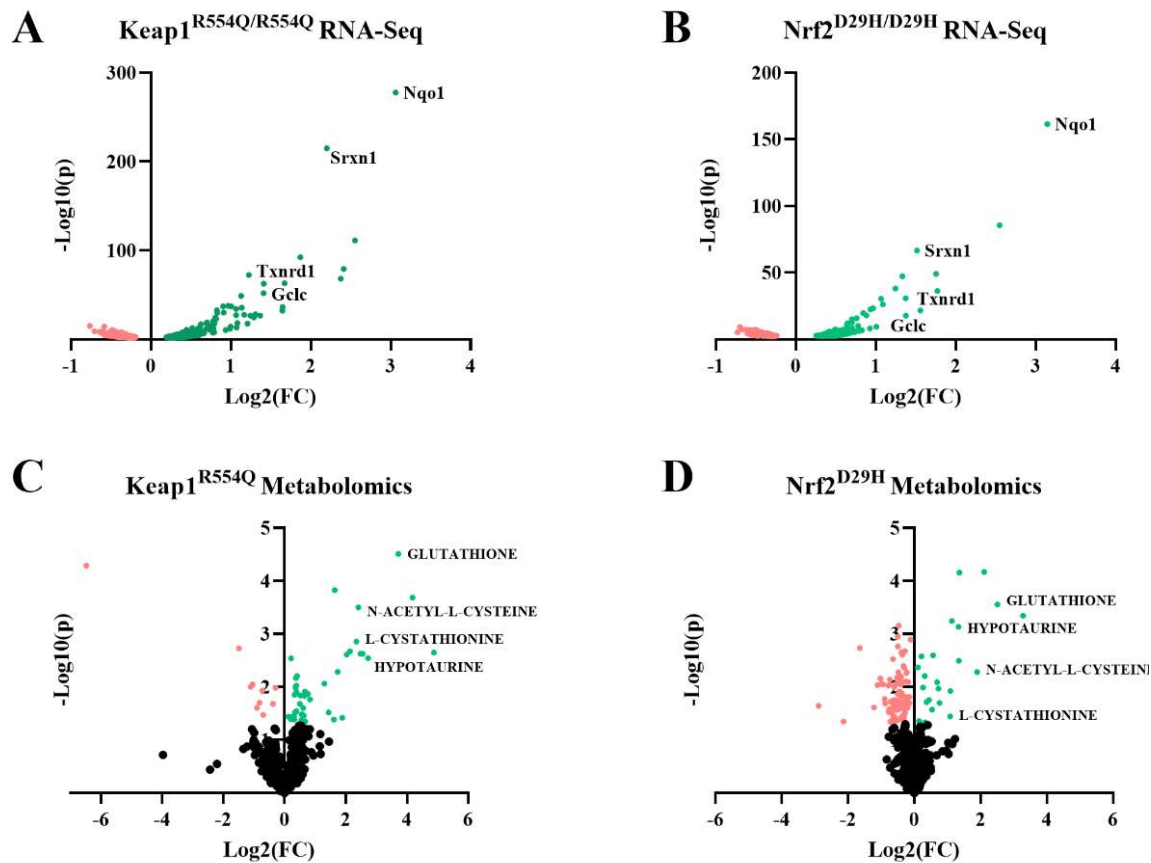
Figure 2.2. Mutant *Keap1* and *Nfe2l2* alleles activate Nrf2 transcriptional program and metabolism. **(A)** Volcano plot of RNA-sequencing data from murine embryonic fibroblasts (MEFs) expressing Keap1$^{R554Q/R554Q}$ compared to Keap1$^{+/+}$. N = 3 technical replicates, representative of two individual MEF lines. **(B)** Volcano plot of RNA-sequencing data from MEFs expressing Nrf2$^{D29H/D29H}$ compared to Nrf2$^{LSL/LSL}$, which lack Nrf2 expression. N = 3 technical replicates, representative of two individual MEF lines. **(C)** Volcano plot of LC-HRMS metabolomics profiling comparing Keap1$^{R554Q/R554Q}$ MEFs to Keap1$^{+/+}$ MEFs from our lab's previous study (43). N = 3 technical replicates, representative of two individual MEF lines. **(D)** LC-HRMS metabolomics profiling comparing Nrf2$^{D29H/D29H}$ MEFs to Nrf2$^{LSL/LSL}$ MEFs. N = 3 technical replicates, representative of two individual MEF lines.
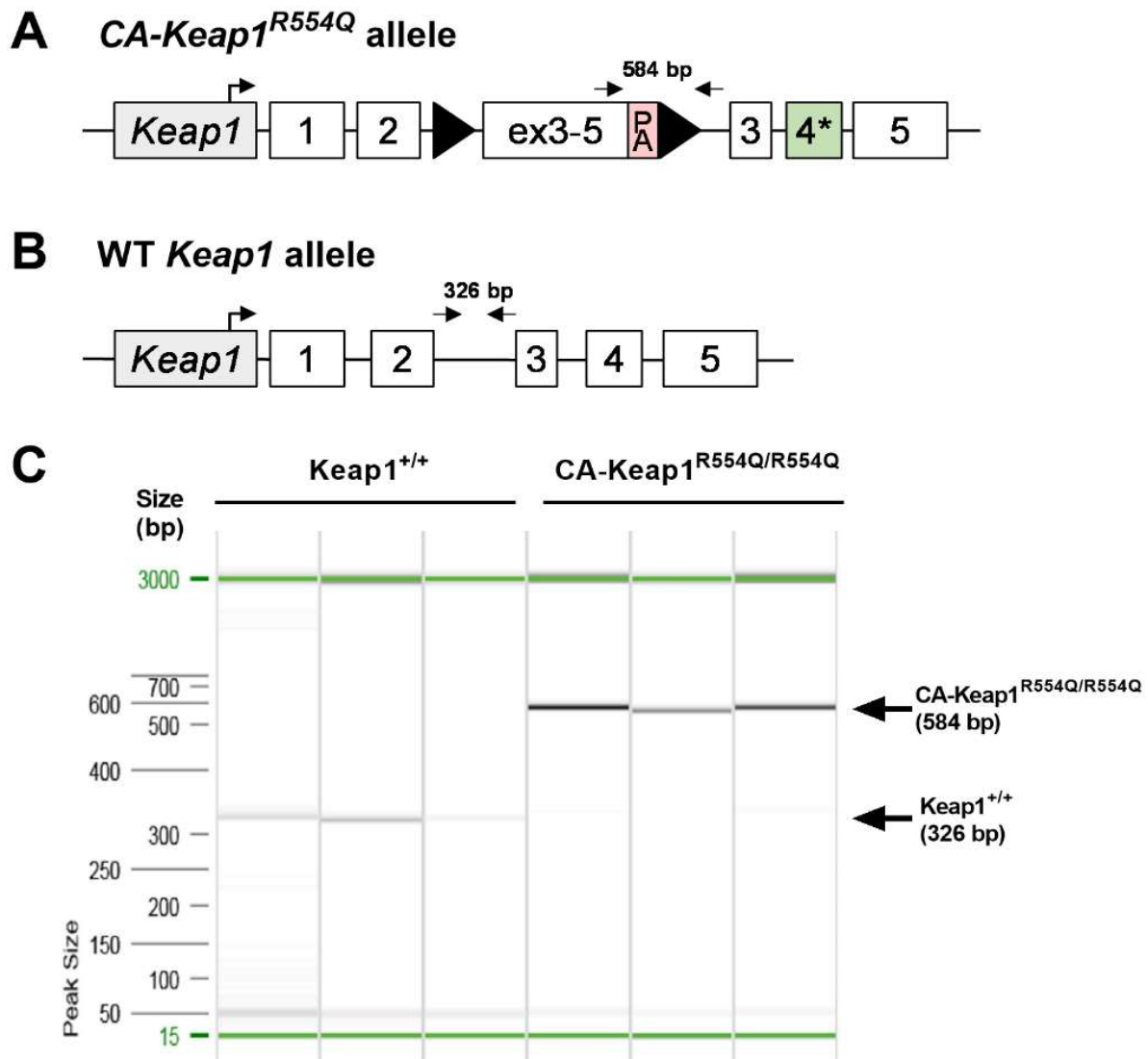
Figure 2.3. Validation of *CA-Keap1^{R554Q}* and WT *Keap1* alleles. Schematic of **(A)** *CA-Keap1^{R554Q}* and **(B)** WT *Keap1* alleles with genotyping primers. **(C)** Detection of *CA-Keap1^{R554Q}* and WT *Keap1* by QIAxcel electrophoresis. This figure was previously published in *Cancer Research*, DeBlasi et al. 2023 (154).

Next, I performed western blotting and did not find any differences in expression of Keap1, Nrf2, or Nrf2 target proteins Nqo1 and Gclc between CA-Keap1^{R554Q} and WT

Keap1 MEFs **(Fig. 2.4A).** My results indicate that the *CA-Keap1*[R554Q] allele is not hypomorphic. Overall, my data demonstrate that the mutant *Keap1*[R554Q] and *Nfe2l2*[D29H] alleles activate the Nrf2 transcriptional program and Nrf2-mediated metabolism.
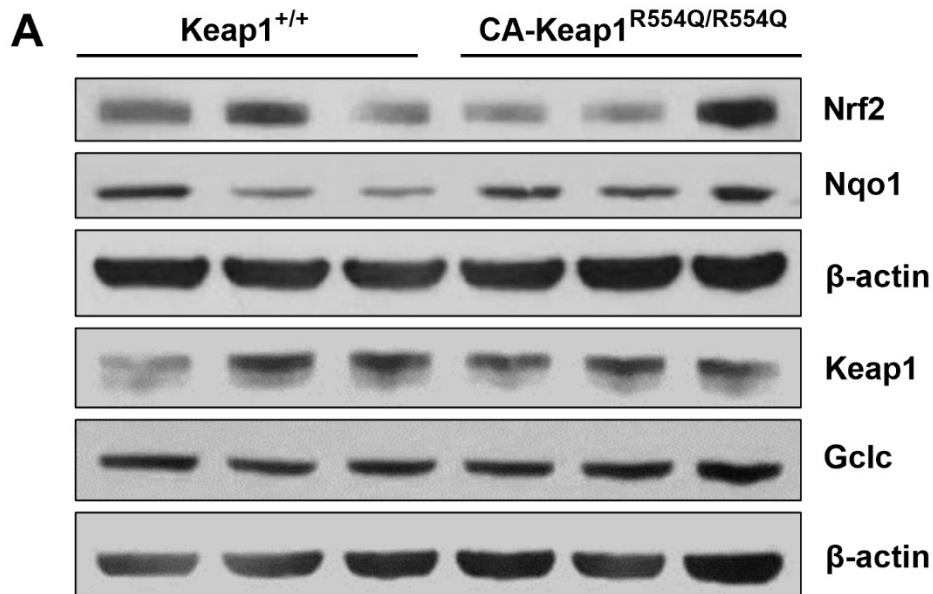
Figure 2.4. The *CA-Keap1*[R554Q] allele is not hypomorphic. **(A)** Western blot analysis of Nrf2, Nqo1, Keap1, Gclc, and β-actin expression in WT *Keap1* and *CA-Keap1*[R554Q/R554Q] MEFs (n=3 individual MEF lines from each genotype). This figure was previously published in *Cancer Research*, DeBlasi et al. 2023 (154).

Keap1 or Nrf2 mutation is not sufficient to initiate lung tumorigenesis

In human lung tumors, *KEAP1* inactivation is frequently biallelic(124), whereas *NFE2L2* mutations are frequently heterozygous (159). In order to test whether constitutive Nrf2 activation could initiate lung tumor formation, recombination of *Keap1* and *Nfe2l2* alleles was induced in the lungs of CA-Keap1[R554Q/+], CA-Keap1[R554Q/R554Q], or LSL-Nrf2[D29H/+] mice via intranasal installation of adenoviral-Cre. I observed no

significant differences in overall survival between wild-type and Keap1/Nrf2 mutant

groups, with the median overall survival ranging from approximately 650-750 days **(Fig.**

2.5A). Although I did observe tumors in some mice, these were age-associated tumors,

such as lymphoma. Furthermore, histological examination of the mouse lung to check

for the presence of lung tumors revealed that lung tumor-free survival was also not

different between the genotypes **(Fig. 2.5B)**.
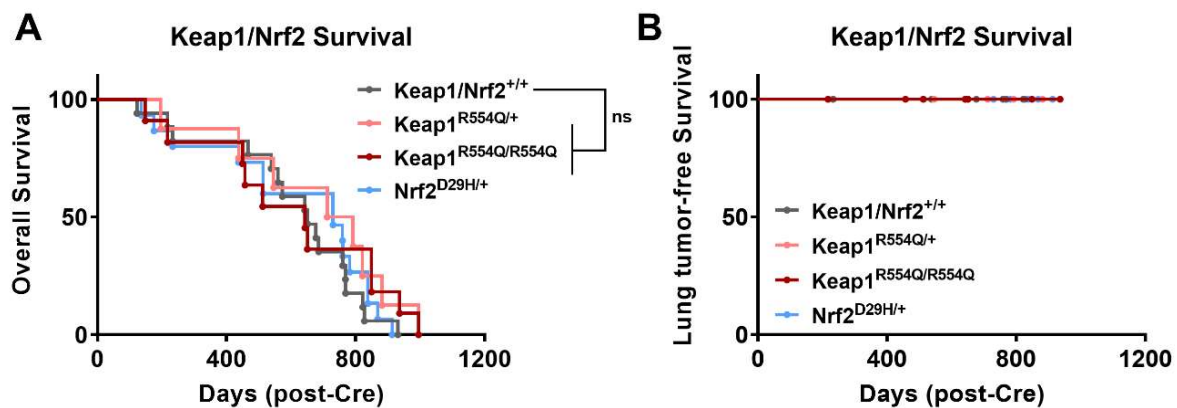
Figure 2.5. Mutation of Keap1 or Nrf2 does not impact overall or lung tumor-free
survival. **A,** Overall survival of Keap1/Nrf2 mutant mice. Keap1/Nrf2$^{+/+}$ (n=17),
Keap1$^{R554Q/+}$ (n=8); Keap1$^{R554Q/R554Q}$ (n=11); Nrf2$^{D29H/+}$ (n=15). Ns= not significant (Log-
rank (Mantel-Cox) test). **B,** Lung tumor-free survival of Keap1/Nrf2 mutant mice.
Keap1/Nrf2$^{+/+}$ (n=11), Keap1$^{R554Q/+}$ (n=4); Keap1$^{R554Q/R554Q}$ (n=8); Nrf2$^{D29H/+}$ (n=11). This
figure was previously published in *Cancer Research*, DeBlasi et al. 2023 (154).

My histological examination of lung tissues across genotypes revealed no

abnormal phenotypic changes in both alveolar and bronchiolar cells **(Fig. 2.6)**. These

results indicate that constitutive Nrf2 activation is not sufficient to induce lung tumor

formation.
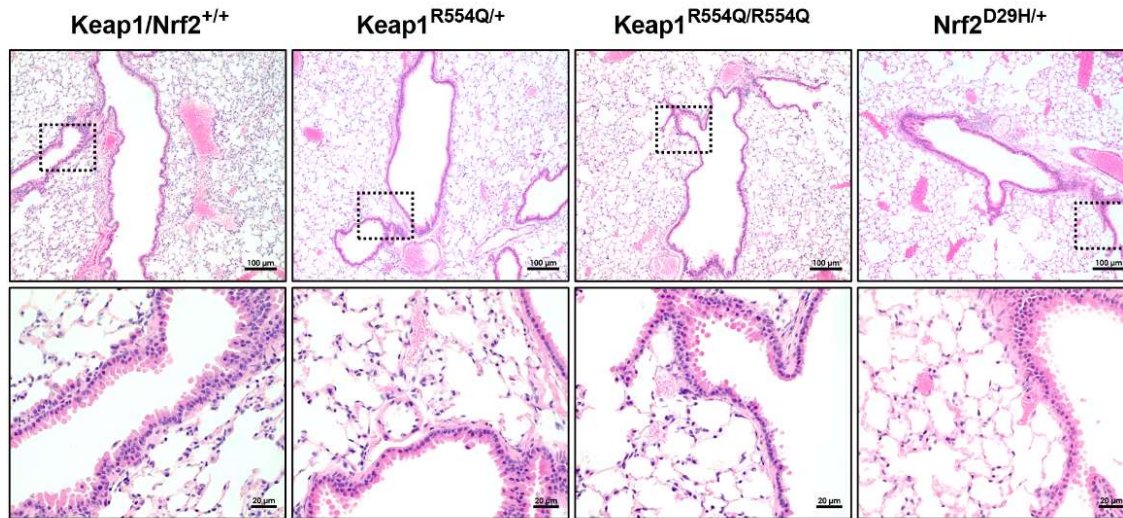
Figure 2.6. Mutation of Keap1 or Nrf2 is not sufficient to initiate lung tumorigenesis. Representative H&E of mouse lung depicting normal bronchiolar and alveolar cells [scale bars = 100 µm (top panel), 20 µm (bottom panel)]. This figure was previously published in *Cancer Research*, DeBlasi et al. 2023 (154).

Keap1 or Nrf2 mutation is not sufficient to initiate lung tumorigenesis in combination with tumor suppressor loss

In order to test whether tumor suppressor loss was required for constitutive Nrf2 activation to initiate lung tumorigenesis, mice harboring p53^{flox} or Lkb1^{flox} alleles were crossed with Keap1/Nrf2 mutant mice. Intranasal instillation of adenoviral Cre was used to concomitantly activate Nrf2 and delete these tumor suppressors in the lung **(Fig. 2.4)**. For these experiments, mice were aged to 500 days, at which timepoint all mice were euthanized and analyzed histologically for presence of lung tumors. First, I determined the effect of Nrf2$^{D29H/+}$, Keap1$^{R554Q/+}$, or Keap1$^{R554Q/R554Q}$ mutation in combination with p53 loss. Although there was a small number of these mice that succumbed to disease prior to 500 days, they developed age-associated tumors including lymphoma.

36

Importantly, I did not observe any differences in overall or lung tumor-free survival between groups **(Fig. 2.7A** and **B)**. When examining lung tissue histology, however, I observed dysplasia in the bronchioles of Keap1$^{R554Q/R554Q}$ mice with p53 deletion **(Fig. 2.7C)**. My observation is consistent with previous work reporting that tracheospheres derived from *Keap1$^{-/-}$;Trp53$^{-/-}$* cells had an aberrant morphology (132).
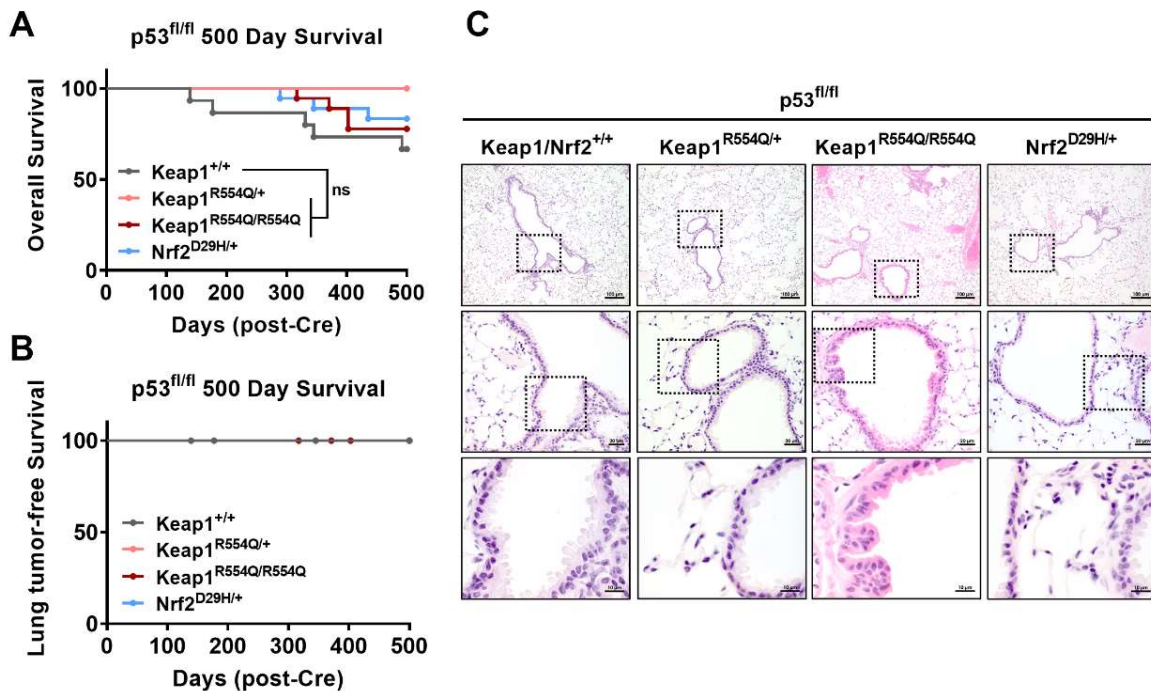
Figure 2.7. Mutation of Keap1 or Nrf2 is insufficient to initiate lung tumorigenesis with p53 loss. **A,** Overall survival of p53$^{fl/fl}$ mice expressing wild-type or mutant Keap1/Nrf2. Keap1/Nrf2$^{+/+}$ (n=15); Keap1$^{R554Q/+}$ (n=7); Keap1$^{R554Q/R554Q}$ (n=18); Nrf2$^{D29H/+}$ (n=18). Ns= not significant (Log-rank (Mantel-Cox) test). **B,** Lung tumor-free survival of p53$^{fl/fl}$ mice expressing wild-type or mutant Keap1/Nrf2. Keap1/Nrf2$^{+/+}$ (n=11); Keap1$^{R554Q/+}$ (n=6); Keap1$^{R554Q/R554Q}$ (n=16); Nrf2$^{D29H/+}$ (n=10). **C.** Representative H&E of mouse lung depicting bronchiolar and alveolar cells of the p53$^{fl/fl}$ models (scale bars = 100 μm (top panel), 20 μm (middle panel), 10 μm (bottom panel)). For **A** and **B**, mice were infected intranasally with adenoviral-Cre, followed by collection at 500 days to analyze lung tissue histology. This figure was previously published in *Cancer Research*, DeBlasi et al. 2023 (154).

Following my analyses in the p53$^{fl/fl}$ model, I investigated the effect of Nrf2$^{D29H/+}$, Keap1$^{R554Q/+}$ or Keap1$^{R554Q/R554Q}$ mutation in combination with Lkb1 deletion. Similar to what I observed with p53 deletion, I also did not find any differences in overall or lung tumor-free survival between groups **(Fig. 2.8A** and **B)**. Additionally, the bronchiolar and alveolar morphology was phenotypically normal across genotypes, in contrast to what was observed with p53 deletion **(Fig. 2.8C)**. My data indicate that Nrf2 activation is not sufficient to initiate lung tumorigenesis, even in the absence of tumor suppressor genes.
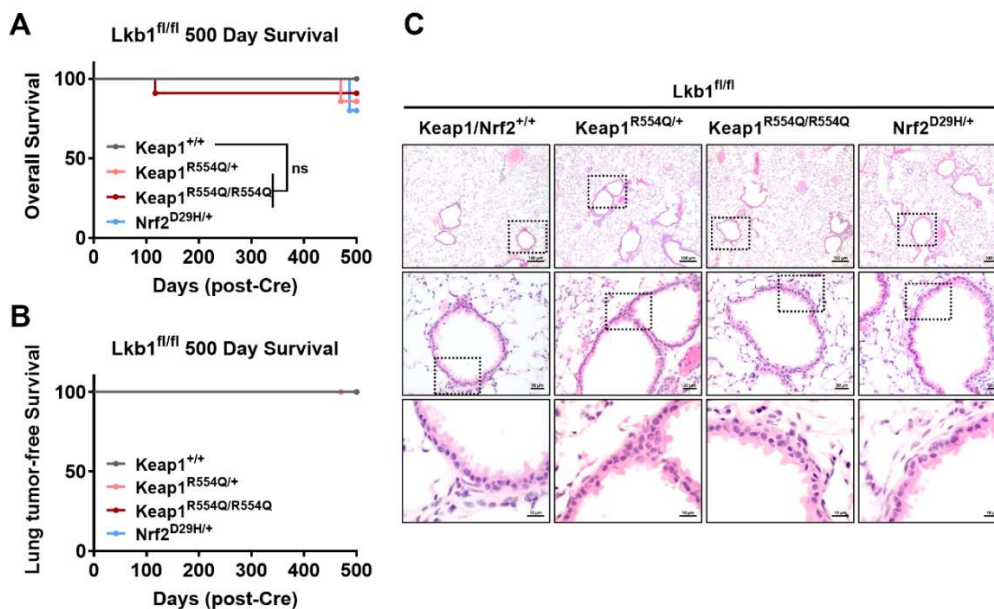
Figure 2.8. Mutation of Keap1 or Nrf2 is not sufficient to initiate lung tumorigenesis with Lkb1 loss. **A,** Overall survival of Lkb1$^{fl/fl}$ mice expressing wild-type or mutant Keap1/Nrf2. Keap1/Nrf2$^{+/+}$ (n=11); Keap1$^{R554Q/+}$ (n=7); Keap1$^{R554Q/R554Q}$ (n=11); Nrf2$^{D29H/+}$ (n=5). Ns= not significant (Log-rank (Mantel-Cox) test). **B,** Lung tumor-free survival of Lkb1$^{fl/fl}$ mice expressing wild-type or mutant Keap1/Nrf2. Keap1/Nrf2$^{+/+}$ (n=11); Keap1$^{R554Q/+}$ (n=6); Keap1$^{R554Q/R554Q}$ (n=9); Nrf2$^{D29H/+}$ (n=4). **C,** Representative H&E of mouse lung depicting bronchiolar and alveolar cells of the Lkb1$^{fl/fl}$ models (scale bars = 100 μm (top panel), 20 μm (middle panel), 10 μm (bottom panel)). For **A** and **B**, mice were infected intranasally with adenoviral-Cre, followed by collection at 500 days to analyze lung tissue histology. This figure was previously published in *Cancer Research*, DeBlasi et al. 2023 (154).

Discussion

I observed that our Keap1 and Nrf2 mutant alleles activated both Nrf2-mediated transcription and metabolism in MEFs, and that our Keap1^{R554Q} allele is not hypomorphic. My results also indicate that Nrf2 activation by Keap1 or Nrf2 mutation is not sufficient to cause lung tumor initiation, even with p53 or Lkb1 deletion. My results also corroborate studies that have determined the effect of Keap1 deletion out to 12-15 months (34, 133). I also observed bronchiolar dysplasia in mice with Keap1$^{R554Q/R554Q}$ mutation and p53 loss, reminiscent of a previous study in tracheospheres (132). Although there was dysplasia in this model, I did not observe this in wild type p53 cohorts. It is possible that bronchiolar cells are permissive for dysplasia because it's been reported that this cell type is sensitive to NRF2 hyperactivation in a Kras mutant, Keap1 deficient mouse model (34). This study also reported that bronchiolar cells are more enriched for Nrf2 target genes compared to alveolar cells (34), which could make them more sensitive to high Nrf2 levels. It's curious that I didn't observe this in the Lkb1$^{fl/fl}$ model, however, given that Lkb1 deletion has been reported to elevate Nrf2 activity in the context of Keap1 loss (160). Additionally, I did not analyze the allele recombination efficiency in our study. Although my IHC results in Chapters 3-4 demonstrate Nrf2 activation in the lung, I did not verify this in the wild-type Kras experiments; only genotyping was performed to verify that the alleles were present in the designated mouse cohorts. I could have performed PCR on the whole lung to assess recombination, but this may not have worked as only ~1% of cells are infected with this dose of virus. Additionally, although the mice were genotyped, we do not know the exact recombination efficiency, although my IHC results in Chapters 3-4 verify Nrf2

activation in tumor cells. Further investigation into how NRF2 activation affects different cell types in patients is warranted.

Moreover, it's important to consider that in this model, only a small percentage of cells in the lung were infected to activate NRF2. With pharmacological/ whole body NRF2 activation, all cells in the lung will be affected, unlike in this study. It's also unknown whether all the NRF2-activated cells in these models persist throughout the life of the mouse, or if some die off. To interrogate this, I could cross a reporter in with our Keap1/ Nrf2 alleles and track the cells over time *in vivo.* Another important consideration is the cell types affected by Nrf2 activation. In this study, Nrf2 was activated in primarily lung epithelial cells. In contrast, pharmacological NRF2 activators will affect all cells in the body, including stromal and immune cells. The recently developed NRF2 activator, omaveloxolone, was recently approved by the FDA for Friedreich's ataxia patients, suggesting that NRF2 activation can be safe in patients (161). Additional work and clinical study is needed to determine whether NRF2 activators are a safe strategy for chemoprevention.

Chapter Three: Nrf2 activation promotes lung tumor initiation and early progression in the Kras^{G12D} model[3]

Introduction

Among the multitude of available mouse models for the study these genomic alterations, all rely on Keap1 deletion via Cre-mediated excision of floxed alleles (34, 133) or CRISPR-Cas9 (45, 53, 134). While these models have proven useful and allowed for discoveries on the KEAP1/NRF2 pathway's role in lung tumorigenesis, they have limitations and may not fully recapitulate the effects of mutated Keap1, as mutation and deletion can have different effects. Furthermore, CRISPR-mediated deletion of KEAP1 in cells is variable (can be heterozygous or homozygous), and the Cas9 protein has been reported to exhibit immunogenicity by evoking the innate and adaptive immune responses (162). Some of these studies also report use of high viral titers than can strongly influence disease progression and have inflammatory effects (34, 133). To overcome these limitations and better understand the KEAP1-NRF2 axis, our lab has

---

[3] Note to reader: Portions of this chapter have been previously published in DeBlasi et al. 2023, *Cancer Research* (154). **J.M. DeBlasi:** Data curation, formal analysis, investigation, visualization, methodology, writing–original draft, writing–review and editing. **A. Falzone, S. Caldwell, N. Prieto Farigua:** Mouse colony management and collections - Data curation, investigation, methodology, writing–review and editing. **J.R. Prigge, E.E. Schmidt:** Nrf2 antibody for IHC - Resources, writing–review and editing. **I.I.C. Chio:** Nrf2 targeting vector antibody for IHC - Resources, writing–review and editing. **F.A. Karreth:** ES cell targeting - Resources, methodology, writing–review and editing. **G.M. DeNicola:** Mouse models, RNA-sequencing - Conceptualization, resources, data curation, formal analysis, supervision, funding acquisition, investigation, methodology, writing–original draft, project administration, writing–review and editing.

developed GEMMs expressing mutant Keap1 or Nrf2 via LOF or hyperactivation, respectively, both alterations present in human lung cancer. To thoroughly interrogate lung tumor initiation and early progression, I examined the effect of Keap1/ Nrf2 mutation in the Kras$^{G12D/+}$ model of early lung adenocarcinoma and measured lung tumor initiation and early progression. My hypothesis was that Nrf2 would promote lung tumor initiation and early progression, given that work from our lab and others has shown that Nrf2 is critical to Kras^{G12D}-mediated lung tumorigenesis in a GEMM (34, 137, 144).

Nrf2 activation cooperates with mutant Kras to promote lung tumor initiation and early progression

To determine how Keap1/Nrf2 mutation affect lung tumor initiation and early progression to low-grade adenocarcinoma, Keap1/Nrf2 mutant mice were crossed with the Kras$^{G12D/+}$ model of early lung adenocarcinoma and infected with intranasal adenoviral Cre to target all cell types in the lung. **(Fig. 3)** (163).
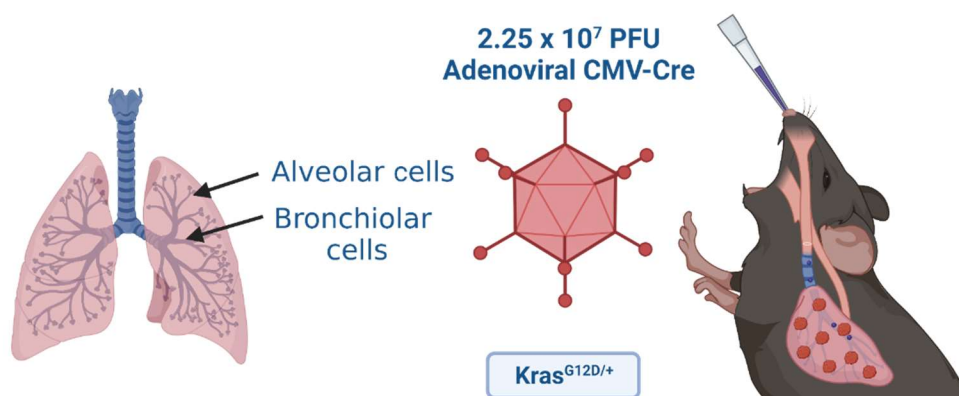
Figure 3. Using the Kras$^{G12D/+}$ mouse model to investigate lung tumor initiation. An overview of the amount of adenoviral-Cre used in the experiments for Chapter 3. Created with BioRender.com.

I observed no difference in survival between groups, with all mice succumbing to lung tumors with a median survival of approximately 200 days **(Fig. 3.1A** and **B)**.
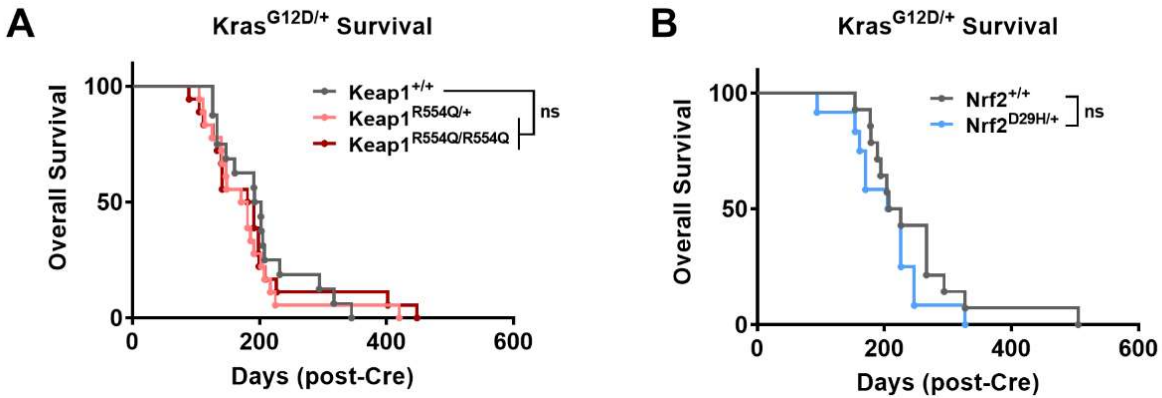
Figure 3.1. Keap1/Nrf2 mutation do not affect survival in the Kras$^{G12D/+}$ model. **A,** Overall survival of Keap1 mutant mice with Kras$^{G12D/+}$ mutation. Keap1$^{+/+}$ (n=16); Keap1$^{R554Q/+}$ (n=18); Keap1$^{R554Q/R554Q}$ (n=18). **B,** Overall survival of Nrf2 mutant mice with Kras$^{G12D/+}$ mutation. Nrf2$^{+/+}$ (n=14); Nrf2$^{D29H/+}$ (n=12). Ns = not significant (Log-rank (Mantel-Cox) test). This figure was previously published in *Cancer Research*, DeBlasi et al. 2023 (154).

I next verified that these mutations were activating toward Nrf2 in lung tumors by performing immunohistochemical (IHC) staining for Nrf2 and the canonical Nrf2 target Nqo1. I observed that Keap1$^{R554Q/R554Q}$ mutation resulted in the highest degree of Nrf2 activation, followed by Nrf2$^{D29H/+}$, and then Keap1$^{R554Q/+}$, compared to Keap1/Nrf2$^{+/+}$ expression **(Fig. 3.2A-D)**.
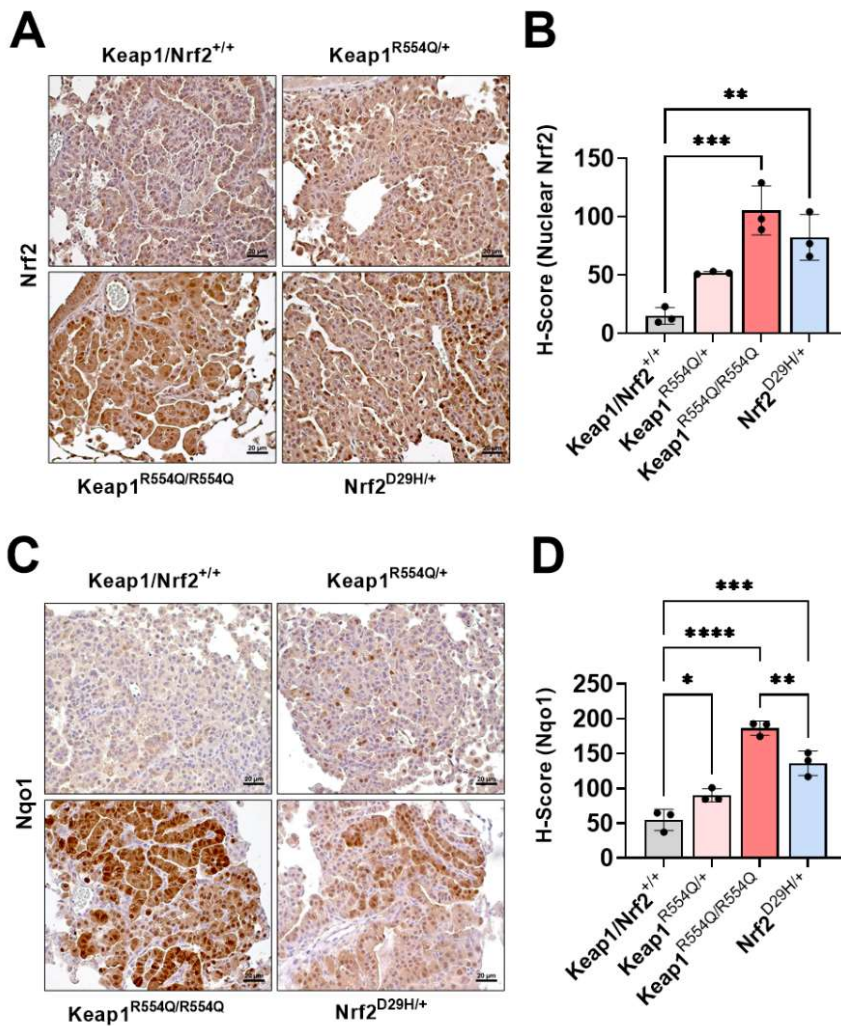
Figure 3.2. Homozygous Keap1 and heterozygous Nrf2 mutation result in Nrf2 activation in the Kras[G12D/+] model. **A,** Representative immunohistochemical (IHC) staining of Nrf2 in Keap1/Nrf2 mutant tumors with Kras[G12D/+] mutation (scale bars = 20 μm). **B,** H-scores for Nrf2 (nuclear) IHC staining. **C,** Representative immunohistochemical (IHC) staining of Nrf2 target Nqo1 (scale bars = 20 μm). **D,** H-scores for Nqo1 (whole cell) IHC staining. For **A-D**, N=3 mice per genotype and >20,000 tumor cells per mouse. *p<0.05, **p<0.01, ***p<0.001, ****p<0.0001 (one-way ANOVA). This figure was previously published in *Cancer Research*, DeBlasi et al. 2023 (154).

To determine whether Nrf2 activation affects lung tumor initiation, I quantified lung tumor number across the genotypes and observed that Keap1$^{R554Q/R554Q}$ and Nrf2$^{D29H/+}$ mutation significantly increased tumor number in the Kras$^{G12D/+}$ model **(Fig. 3.3A** and **B)**. This observation is consistent with previous studies using the Kras$^{G12D/+}$ model with Keap1 deletion (34, 144). Next, I tested whether Nrf2 affects early tumor progression by analyzing tumor grade. I quantified the distribution of atypical adenomatous and bronchiolar hyperplasia (AAH and BH, respectively) and tumors ranging from grades 1 (adenoma) to 5 (adenocarcinoma). I observed that Keap1$^{R554Q/R554Q}$ and Nrf2$^{D29H/+}$ mutation caused an increase in the proportion and number of grade 1 tumors compared to Keap1$^{R554Q/+}$ and Keap1/Nrf2$^{+/+}$ expression **(Figs. 3.3C, 3.4A)**. I also saw that grade 3 tumors were rare in this model across all genotypes, and an absence of grade 4 and grade 5 tumors **(Figs. 3.3C, 3.4A)** precluding the study of later tumor progression.

I also measured tumor size by grade and observed that the median tumor size did not differ between groups **(Fig. 3.4B)**. However, I did observe some modest differences in lesion size across the individual grades, including decreased AAH size in all Keap1/Nrf2 mutant models **(Fig. 3.4C).** Moreover, I observed that there was a decrease in grade 3 tumor burden across all Keap1/Nrf2 mutant models **(Fig. 3.3D)**, which resulted in decreased overall tumor burden **(Fig. 3.4D),** given that grade 3 tumors were much larger compared to other grades **(Fig. 3.4C)**. Grade 3 tumors were extremely rare in the Kras$^{G12D/+}$ model, however, limiting my ability to draw conclusions on the effect of Nrf2 activation on a small number of tumors. My results indicate that

constitutive Nrf2 activation cooperates with Kras$^{G12D/+}$ mutation to promote lung tumor initiation and early progression to low-grade tumors.
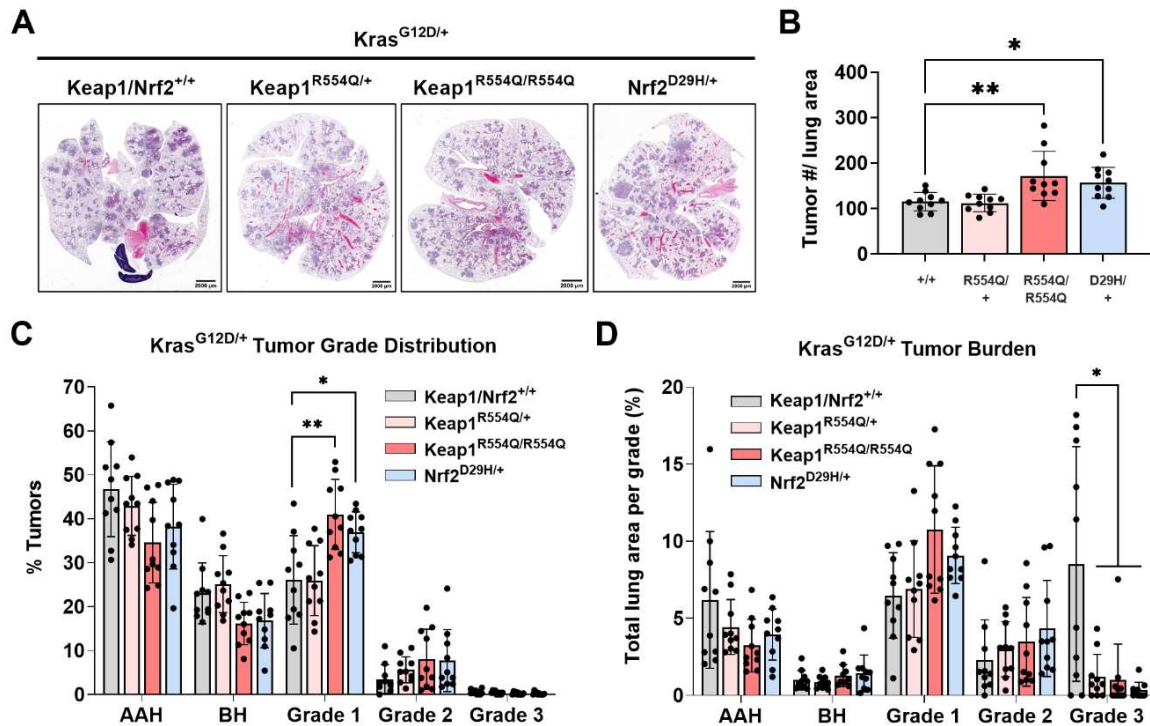
Figure 3.3. Keap1/Nrf2 mutation cooperates with Kras$^{G12D/+}$ to promote lung tumor initiation and early progression. **A,** Representative whole lung H&E-stained section (scale bars = 2000 μm). **B,** Tumor number per mouse in Keap1/Nrf2 mutant models normalized to lung area. *p<0.05, **p<0.01 (one-way ANOVA). **C,** Distribution of tumor grades across Keap1/Nrf2 mutant models. *p<0.05 (unpaired t test with Holm-Sidak's multiple comparisons test). AAH = atypical adenomatous hyperplasia. BH = bronchiolar hyperplasia. **D,** Fraction of lung tumor burden by grade (lung tumor area/ total lung area per grade). *p<0.05, **p<0.01 (unpaired t test with Holm-Sidak's multiple comparisons test). For both **C** and **D**, n=10 mice and ≥2,000 tumors per genotype. This figure was previously published in *Cancer Research*, DeBlasi et al. 2023 (154).
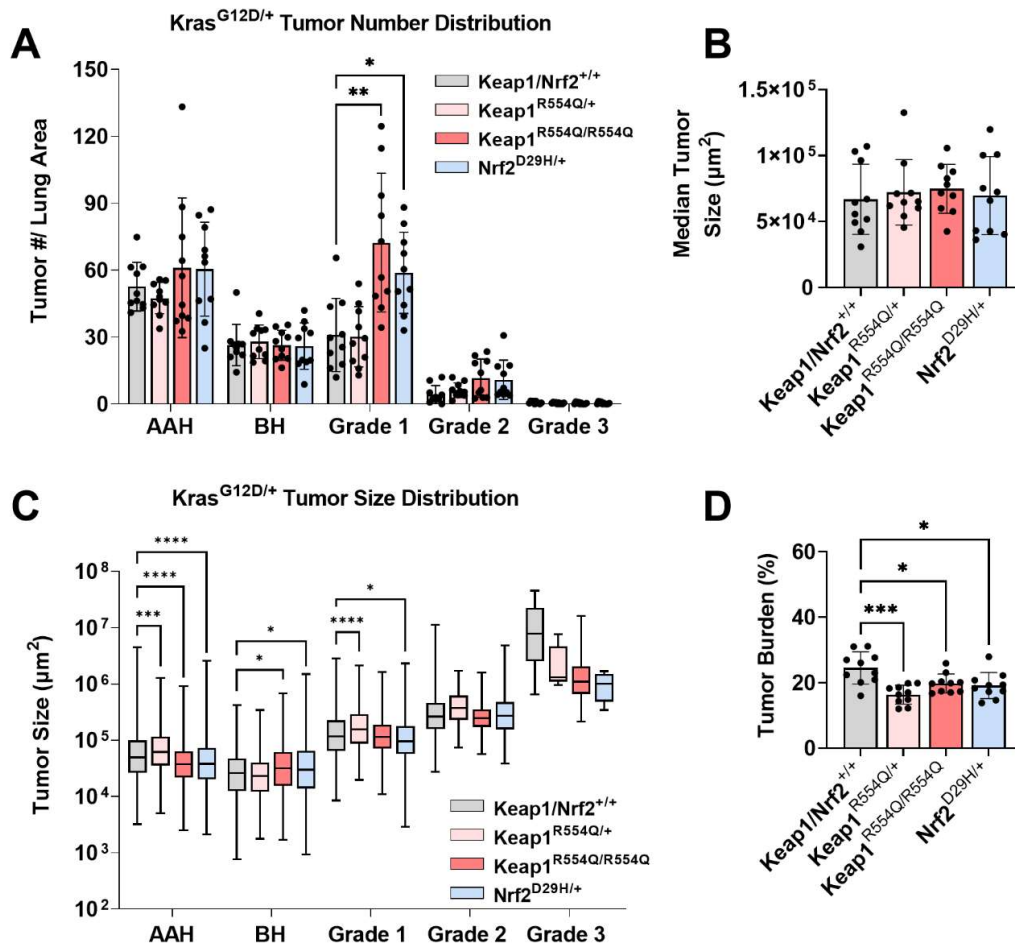
Figure 3.4. Lung tumor burden, size, and number quantification in the Kras[G12D/+] model with Keap1/Nrf2 mutation. **(A)** Distribution of tumor number by grade across Keap1/Nrf2 mutant models. N=10 mice per genotype, *p<0.05, **p<0.01 (unpaired t test with Holm-Sidak's multiple comparisons test). **(B)** Median tumor size per mouse for each genotype. *p<0.05 (one-way ANOVA). **(C)** Tumor size by grade across all mice per genotype. N=10 mice and ≥2,300 tumors per genotype, *p<0.05, ***p<0.001, ****p<0.0001 (Kruskal-Wallis test with Dunn's multiple comparisons test). **(D)** Overall tumor burden (%) calculated by dividing the total area of lung tumor by the total area of the lung. *p<0.05, ***p<0.001 (one-way ANOVA). This figure was previously published in *Cancer Research*, DeBlasi et al. 2023 (154).

Discussion

I observed that Nrf2 activation by Keap1$^{R554Q/R554Q}$ or Nrf2$^{D29H/+}$ mutation promoted lung tumor initiation and early progression to low-grade tumors in the Kras$^{G12D/+}$ model. My findings that Nrf2 activation promotes lung tumor initiation are consistent with previous studies (34, 137, 144), and support the critical role for NRF2 in the early stages of lung tumorigenesis. My supervisor's work showed that homozygous deletion of NRF2 reduced lung tumor number, burden, and AAH proliferation, and prolonged survival in the Kras^{G12D} model, highlighting the crucial role for Nrf2 in Kras^{G12D}-mediated lung tumor initiation (137). Another group showed that Nrf2 activation by Keap1 knockout in the Kras^{G12D} model promoted an increase in tumor number and proportion of low-grade tumors (adenomas), although this study used a higher titer of virus and conducted analysis 3 months post-Cre (34). An additional study in the Kras^{G12D} model observed also observed that Keap1 knockout increased tumor burden and the number of low-grade tumors at 9, 14, and 18 weeks post-Cre. Despite variable in methods between these studies, it seems consistent that Nrf2 activation supports Kras^{G12D} lung tumorigenesis.

Moreover, I observed that the Keap1$^{R554Q/R554Q}$ allele was the most activating towards Nrf2, followed by Nrf2$^{D29H/+}$, and then only modest activation in the Keap1$^{R554Q/+}$ model. I believe that this is because the KEAP1^{R554Q} mutation recapitulates a null allele with complete loss-of-function, as it does not bind NRF2 or suppress its transcription, allowing for high levels of NRF2 activation (156). Additionally, the NRF2^{D29H} mutation, which occurs in the low-affinity DLG motif (127), allows for escape of repression by KEAP1, although there is still one copy of WT NRF2 intact. Additionally, because this

mutation occurs in the DLG motif, there is still minimal binding with KEAP1, although degradation is impaired; this contrasts with mutations that occur in the ETGE motif, which usually do not have any KEAP1 binding (125). Interestingly, another group using a $Nrf2^{E79Q/+}$ mouse model of SCLC observed that aggressive SCLC tumors downregulate Nrf2 (164). I don't know how the degree of Nrf2 activation compares to the $Nrf2^{D29H}$ model, however; it may have slightly higher activity since KEAP1 binding would be completely impaired.

Since most KEAP1 mutant patient tumors undergo LOH/ have biallelic inactivation (124), it is likely that both copies need to be mutated in our mouse model to achieve sufficient Nrf2 activation. In contrast, most NRF2 mutations are heterozygous (165), as mutating one copy is sufficient to cause constitutive NRF2 activation. It is also likely that the amount of Keap1 and Nrf2 available varies with different mutations and can influence the degree of relative Nrf2 activity. It was also curious that all Keap1/ Nrf2 mutant models had decreased grade 3 tumor burden. Grade 3 tumors were very rare in this model, however, limiting my ability to compare tumor proportions of this grade, although the decreased burden suggests that Nrf2 may impair tumor progression. To ask this question, I next examined the effects of these mutations in the $Kras^{G12D/+}$; $p53^{fl/fl}$ model of lung adenocarcinoma, which develops high-grade tumors.

Chapter Four: Keap1 mutation impairs tumor progression

in the Kras^{G12D}; p53$^{fl/fl}$ model[4]

Introduction

Because I observed a decrease in grade 3 tumor burden in the Keap1/Nrf2 mutant models in my previous experiment **(Fig. 3.3D)**, this suggested that Nrf2 activation may impair progression to higher-grade tumors. To investigate this, I used the Kras$^{G12D/+}$; p53$^{fl/fl}$ model, which develops advanced-grade lung adenocarcinomas and can be used to study tumor progression **(Fig. 4)** (166). Additionally, in this Kras$^{G12D/+}$; p53$^{fl/fl}$ GEMM, our lab unexpectedly observed that Keap1$^{R554Q/R554Q}$ mutation significantly decreased tumor size (43). Although other groups have examined the effect of Keap1 deletion in the Kras$^{G12D/+}$; p53$^{fl/fl}$ model, phenotypes assayed varied, and they did not use Keap1 mutation (34, 53, 134, 146). Some authors reported that Keap1 deletion promoted adenocarcinoma progression (45, 136), while others observed no

---

[4] Note to reader: Portions of this chapter have been previously published in DeBlasi et al. 2023, *Cancer Research* (154). **J.M. DeBlasi:** Data curation, formal analysis, investigation, visualization, methodology, writing–original draft, writing–review and editing. **A. Falzone, S. Caldwell, N. Prieto Farigua:** Mouse colony management and collections - Data curation, investigation, methodology, writing–review and editing. **J.R. Prigge, E.E. Schmidt:** Nrf2 antibody for IHC - Resources, writing–review and editing. **I.I.C. Chio:** Nrf2 targeting vector antibody for IHC - Resources, writing–review and editing. **F.A. Karreth:** ES cell targeting - Resources, methodology, writing–review and editing. **G.M. DeNicola:** Mouse models, RNA-sequencing - Conceptualization, resources, data curation, formal analysis, supervision, funding acquisition, investigation, methodology, writing–original draft, project administration, writing–review and editing.

effect on tumor size (134, 146). Therefore, further investigation into Nrf2's effects on lung tumor initiation vs. progression was warranted.
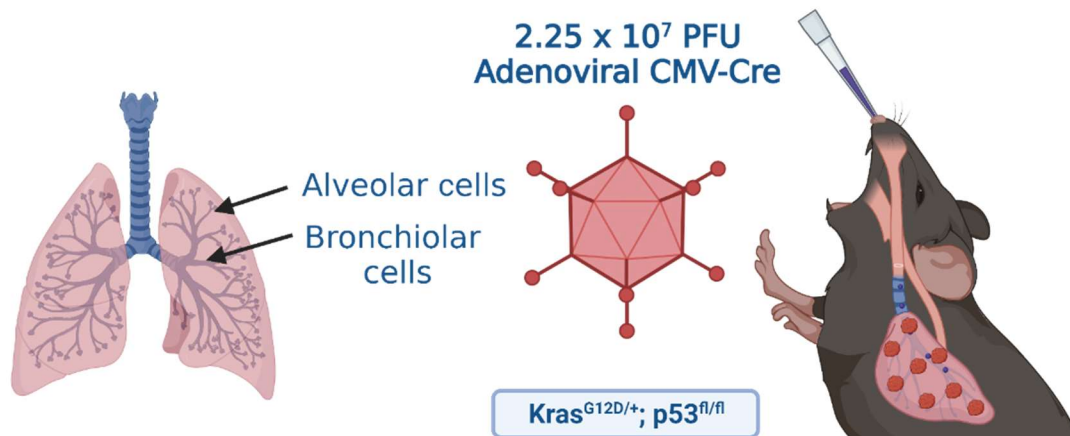
Figure 4. Using the Kras$^{G12D/+}$; p53$^{fl/fl}$ mouse model to investigate lung tumor progression. An overview of the amount of adenoviral-Cre used in the experiments for Chapters 4 and 5. Created with BioRender.com.

Nrf2 activation impairs lung adenocarcinoma progression

To determine how Keap1 and Nrf2 mutation affect tumor progression, I performed comprehensive phenotyping on KP tumors harboring Keap1 or Nrf2 mutation. Similar to my findings in the Kras$^{G12D/+}$ model **(Fig. 3.1)**, I observed no difference in overall survival of the KP model with Keap1 or Nrf2 mutation **(Fig. 4.1A and B)**.
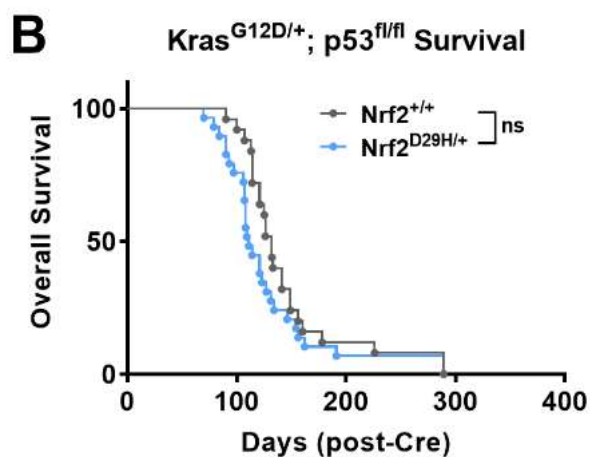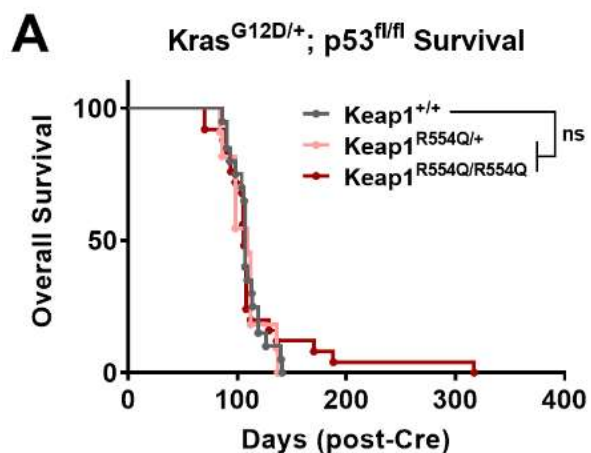
Figure 4.1. Keap1/ Nrf2 mutation do not affect survival in the Kras$^{G12D/+}$; p53$^{fl/fl}$ model. **A,** Overall survival of Kras$^{G12D/+}$; p53$^{fl/fl}$ mice with Keap1 mutation. Keap1$^{+/+}$ (n=20); Keap1$^{R554Q/+}$ (n=11); Keap1$^{R554Q/R554Q}$ (n=25). **B,** Overall survival of Kras$^{G12D/+}$; p53$^{fl/fl}$ mice with Nrf2 mutation. Nrf2$^{+/+}$ (n=25); Nrf2$^{D29H/+}$ (n=29). Ns = not significant (Log-rank (Mantel-Cox) test). This figure was previously published in *Cancer Research*, DeBlasi et al. 2023 (154).

Additionally, I observed that Keap1/Nrf2 mutation affected Nrf2 activation in a similar manner to the Kras$^{G12D/+}$ model, with Keap1$^{R554Q/R554Q}$ mutation being the most

activating, followed by Nrf2[D29H/+], and then Keap1[R554Q/+] compared to Keap1/Nrf2^{+/+} expression **(Fig. 4.2A-D)**.
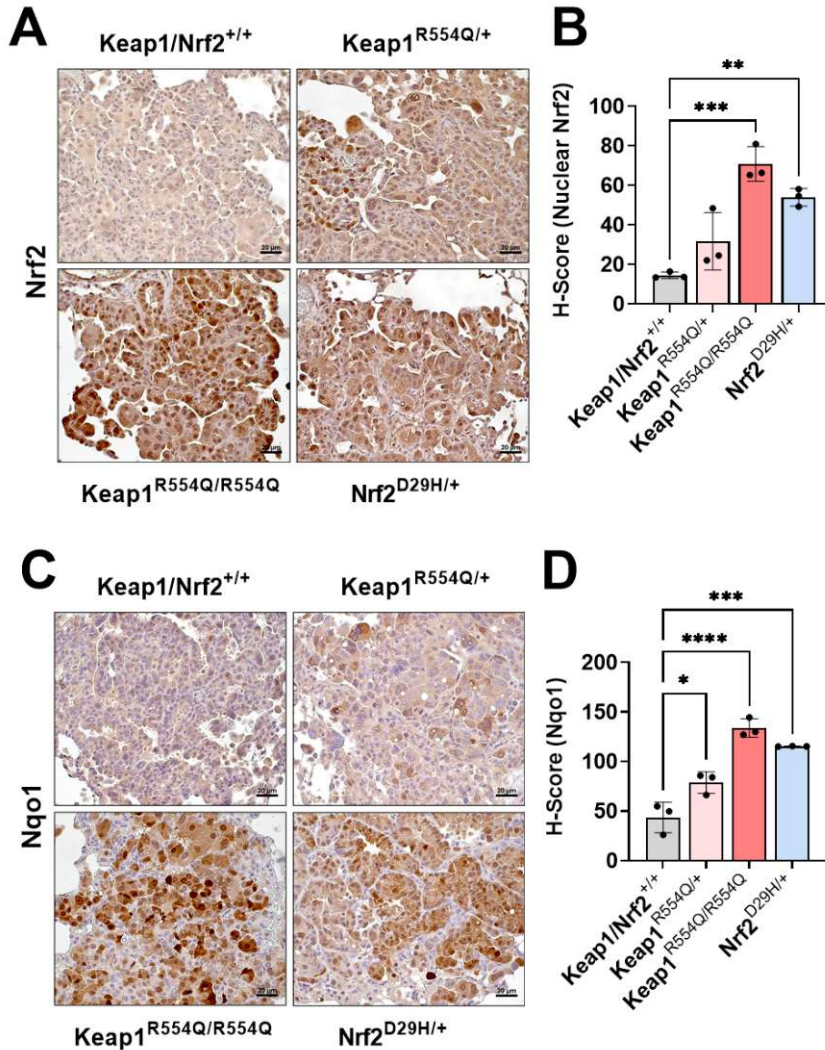
Figure 4.2. Keap1/ Nrf2 mutation constitutively activate Nrf2 in the Kras[G12D/+]; p53^{fl/fl} model. **A,** Representative immunohistochemical (IHC) staining of Nrf2 in Kras[G12D/+]; p53^{fl/fl} mice with Keap1/Nrf2 mutation (scale bars = 20 μm). **B,** H-scores for Nrf2 (nuclear) IHC staining. **C,** Representative immunohistochemical (IHC) staining of Nrf2 target Nqo1 (scale bars = 20 μm). **D,** H-scores for Nqo1 (whole cell) IHC staining. For **A-D**, N=3 mice per genotype and >20,000 tumor cells per mouse. *$p<0.05$, **$p<0.01$, ***$p<0.001$, ****$p<0.0001$ (one-way ANOVA). This figure was previously published in *Cancer Research*, DeBlasi et al. 2023 (154).

Upon histological examination, it was very apparent that Keap1$^{R554Q/R554Q}$ mice had decreased overall tumor burden **(Fig. 4.3A)**, which I verified upon quantitation **(Fig. 4.4A)**. Next, I examined tumor progression by tumor grading and observed a significant decrease in the proportion, number, and burden of grade 3 and 4 tumors in Keap1$^{R554Q/R554Q}$ mice **(Fig. 4.3B** and **C, Fig. 4.4B)**. I also observed a modest, non-significant decrease in the proportion, number, and burden of grade 3 and 4 tumors in Nrf2$^{D29H/+}$ mice **(Fig. 4.3B** and **C, 4.4B)**. Furthermore, I saw an increase in the proportion, number, and burden of grade 1 tumors in Keap1$^{R554Q/R554Q}$ mice, suggesting that there may be a threshold for Nrf2 to promote early progression to low-grade tumors, but impair late progression to advanced-grade tumors **(Fig. 4.3B** and **C, Fig. 4.4B)**. Accordingly, I hypothesized that there was likely a threshold effect for Nrf2 activation to allow vs. impair tumor progression. Although there were no differences in overall median tumor size between groups **(Fig. 4.4C)**, Keap1$^{R554Q/R554Q}$ AAH and grade 1 tumors were significantly smaller compared to their wild-type counterparts **(Fig. 4.4D)**.

Following my histological analyses, I examined whether tumors that progressed to the adenocarcinoma stage altered Nrf2 expression and/or activity to further interrogate my Nrf2 threshold hypothesis. To do this, I analyzed Nrf2 and Nqo1 expression across all tumor grades and hyperplasia (AAH, BH). My data revealed that Nrf2 and Nqo1 levels were highly elevated in grade 1 tumors of Keap1/Nrf2 mutant mice, with Nqo1 exhibiting increased nuclear localization in Keap1$^{R554Q/R554Q}$ tumors compared to Nrf2$^{D29H/+}$tumors **(Fig. 4.6A)**. As tumors progressed to higher grades, however, Nrf2 and Nqo1 levels were reduced in the Keap1/Nrf2 mutant models **(Fig. 4.6A-C)**. These data suggest that beyond a certain threshold, Nrf2 activation can impair

advanced-grade tumor progression, warranting selection for a more tolerable level of

Nrf2 expression and activity in higher-grade tumors.
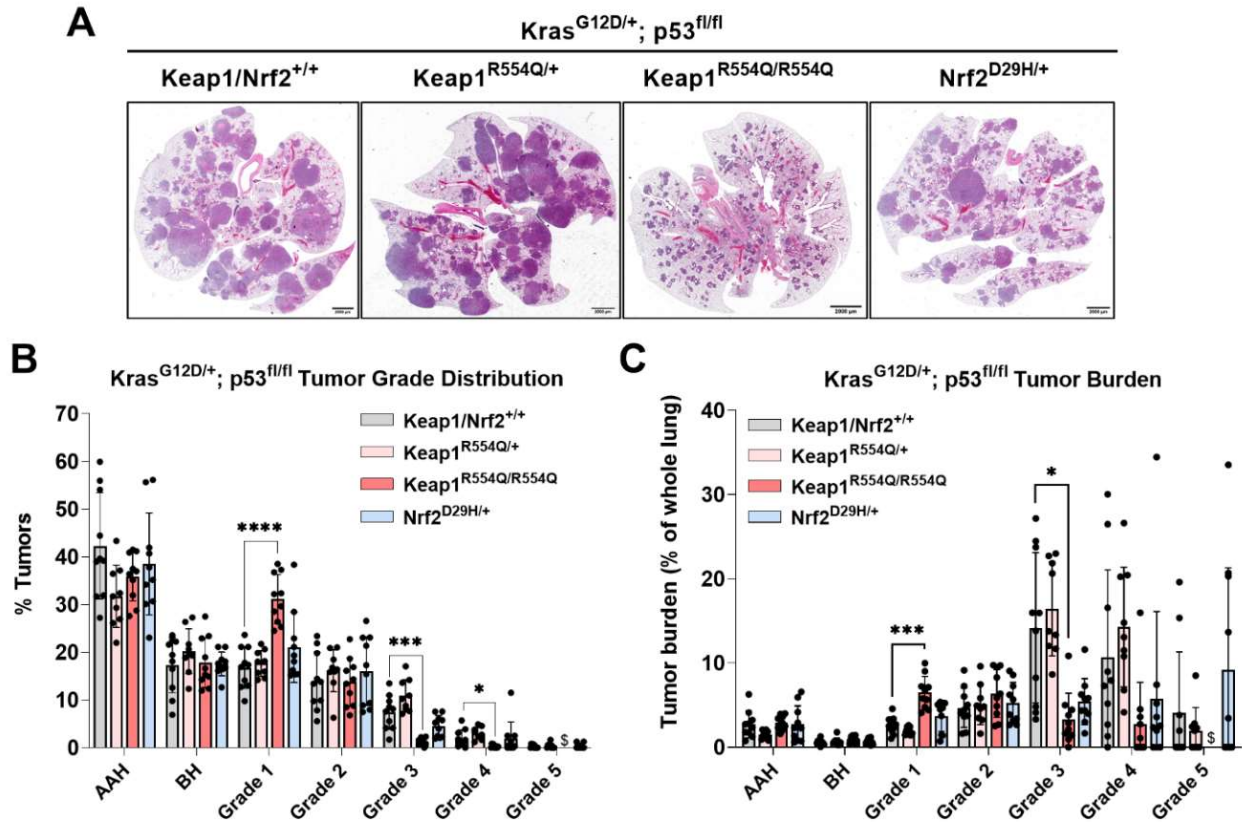
Figure 4.3. Homozygous Keap1[R554Q] impairs adenocarcinoma progression in the Kras[G12D/+]; p53^{fl/fl} model. **A,** Representative whole lung H&E-stained section (scale bars = 2000 μm). **B,** Distribution of tumor grades across Keap1/Nrf2 mutant models. *$p<0.05$ (unpaired t test with Holm-Sidak's multiple comparisons test). $ = fewer than three tumors detected across all mice. **C,** Fraction of lung tumor burden by grade (lung tumor area per grade/ total lung area). *$p<0.05$, ***$p<0.001$, ****$p<0.0001$ (unpaired t test with Holm-Sidak's multiple comparisons test). $ = fewer than three tumors detected across all mice. For both **B** and **C**, n≥9 mice and ≥1,900 tumors per genotype. Only one grade 5 tumor was found in the Keap1[R554Q/R554Q] cohort, and therefore was excluded from these analyses. This figure was previously published in *Cancer Research*, DeBlasi et al. 2023 (154).
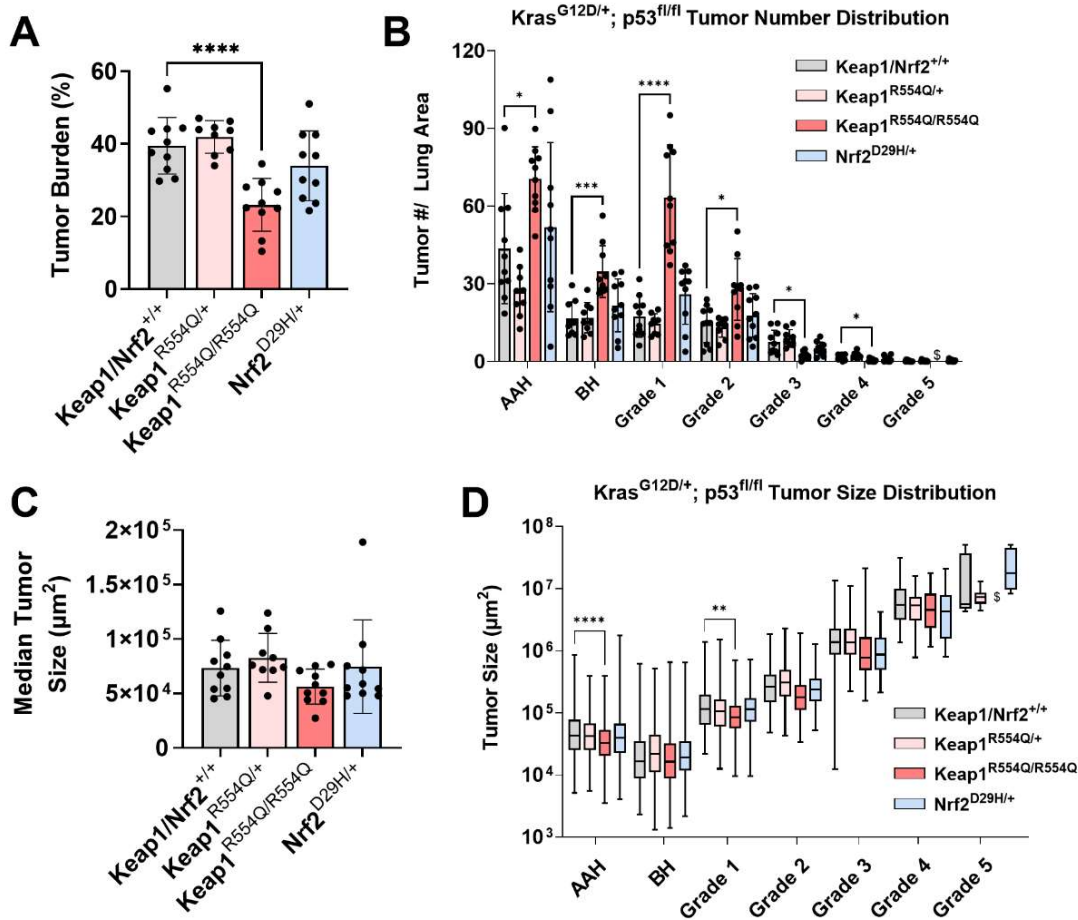
Figure 4.4. Lung tumor analysis in the Kras$^{G12D/+}$; p53$^{fl/fl}$ model with Keap1/Nrf2 mutation. **(A)** Overall tumor burden (%) calculated by dividing the total area of lung tumor by the total area of the lung. ****p<0.0001 (one-way ANOVA). **(B)** Distribution of tumor number by grade across Keap1/Nrf2 mutant models. N≥9 mice per genotype, *p<0.05, ***p<0.001, ****p<0.0001 (unpaired t test with Holm-Sidak's multiple comparisons test). $ = fewer than three tumors detected across all mice. **(C)** Median tumor size per mouse for each genotype (one-way ANOVA). **(D)** Tumor size by grade across all mice per genotype. N≥9 mice and ≥1,900 tumors per genotype. **p<0.01, ****p<0.0001 (Kruskal-Wallis test with Dunn's multiple comparisons test). $ = fewer than three tumors detected across all mice. For **(B)** and **(D)**, only one grade 5 tumor was found in the Keap1$^{R554Q/R554Q}$ cohort, and therefore was excluded from these analyses. This figure was previously published in *Cancer Research*, DeBlasi et al. 2023 (154).
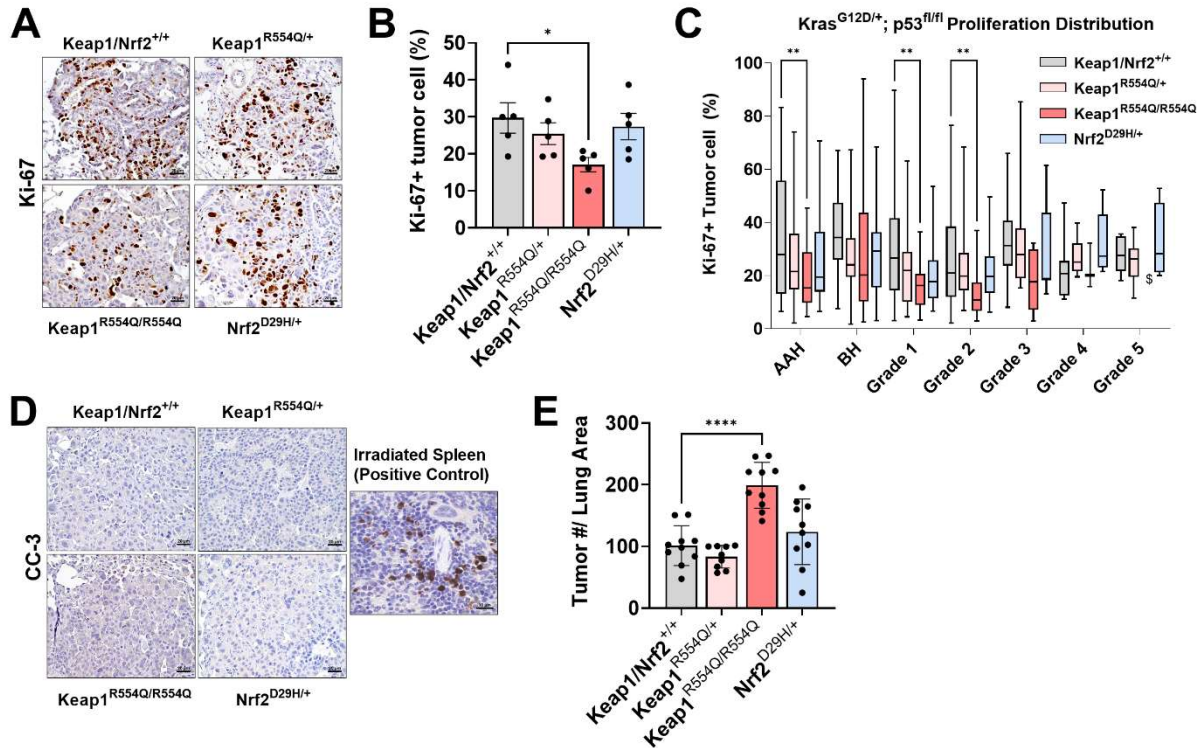
Figure 4.5. Lung tumor analysis and tumor cell proliferation/ death in the Kras[G12D/+]; p53^{fl/fl} model with Keap1/Nrf2 mutation. **(A)** Representative immunohistochemical (HC) staining of Ki-67 (scale bars = 20 μm). **(B)** Proportion of tumor cells positive for Ki-67 per mouse. *$p<0.05$ (one-way ANOVA). **(C)** Percentage of Ki-67 positive tumor cells in each tumor grade per genotype. N=5 mice per genotype, >20,000 tumor cells per mouse. **$p<0.01$ (unpaired t test with Holm-Sidak's multiple comparisons test). $ = fewer than three tumors detected across all mice. Only one grade 5 tumor was found in the Keap1[R554Q/R554Q] cohort, and therefore was excluded from these analyses. **(D)** Representative immunohistochemical (IHC) staining of cleaved caspase-3 (CC-3) (scale bars = 20 μm). N=5 mice per genotype. Positive control is BL6 mouse spleen 1 hour after irradiation with 7.5 Gy (scale bar = 10 μm). **(E)** Tumor number per mouse in Keap1/Nrf2 mutant models normalized to lung area. ****$p<0.0001$ (one-way ANOVA). This figure was previously published in *Cancer Research*, DeBlasi et al. 2023 (154).
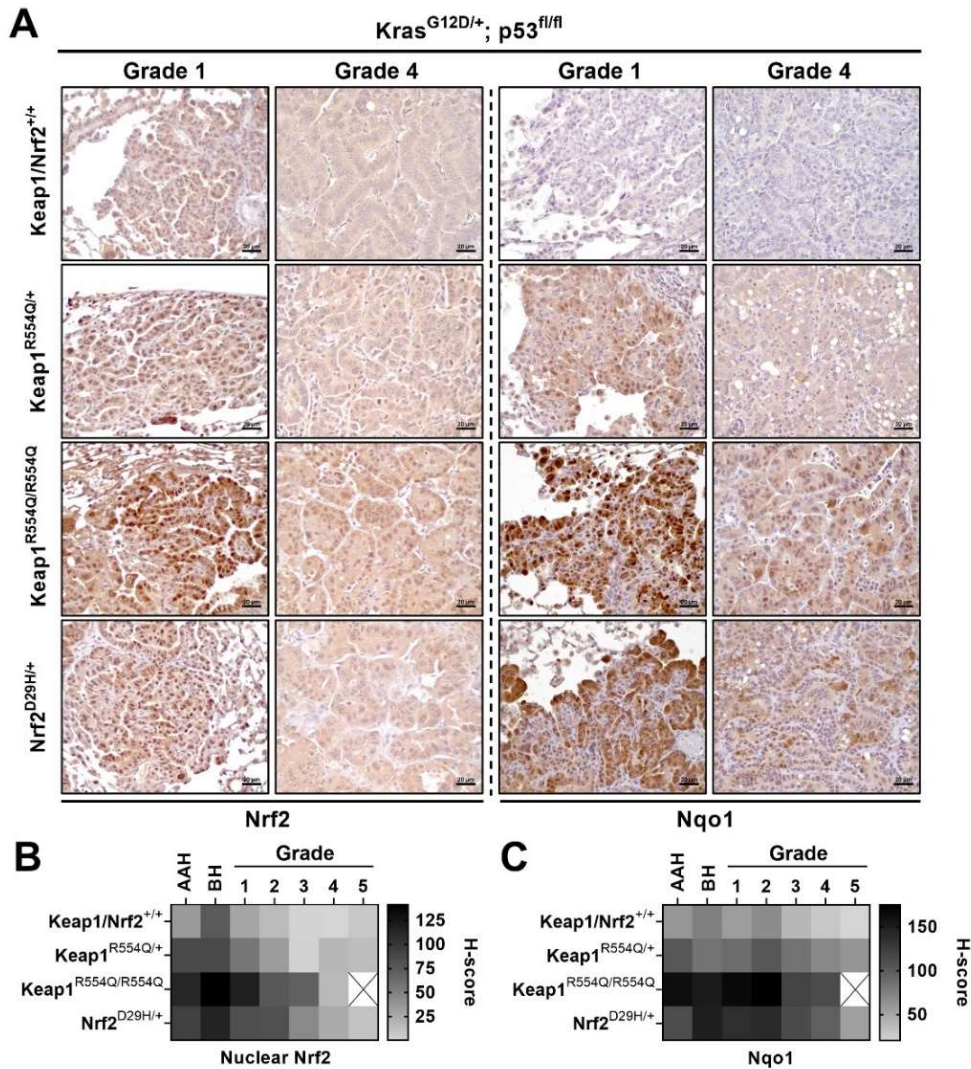
Figure 4.6. Nrf2 expression and activity is reduced in higher-grade tumors. **A,** Representative Nrf2 and Nqo1 IHC staining in grade 1 and 4 tumors from Kras[G12D/+]; p53^{fl/fl} mice with Keap1 or Nrf2 mutation (scale bars = 20 μm). **B, C** Heatmaps depicting the H-scores per grade from IHC staining for Nrf2 (nuclear) **(B)**, and the Nrf2 target Nqo1 (whole cell) **(C)**. N=3 mice per genotype, >20,000 tumor cells per mouse. Only one grade 5 tumor was found in the Keap1[R554Q/R554Q] cohort, and therefore was excluded from these analyses. This figure was previously published in *Cancer Research*, DeBlasi et al. 2023 (154).

Discussion

My results indicate the decreased tumor size with Keap1$^{R554Q/R554Q}$ mutation in the Kras$^{G12D/+}$; p53$^{fl/fl}$ model (43) was a result of blocked lung adenocarcinoma progression. It is curious that high levels of Nrf2 are favorable for promoting lung tumor initiation, but block progression. One potential reason for this could be that tumor cells need high levels of NRF2 to initiate and expand, but once tumors are established, high NRF2 is no longer needed. The models used in my experiments also don't recapitulate the stress experienced by patients in our models, such as tobacco smoke or air pollution, nor chemotherapy/ radiation, all of which could influence the level of NRF2 needed in tumors. In the presence of these factors, high levels of NRF2 may be beneficial to combat stress in the context of progression. I also observed that tumors across all genotypes downregulated Nrf2 expression and activity, indicating that high levels of Nrf2 may not be favorable for tumor progression. Although further investigation is needed to determine the mechanism of downregulation, possible methods could include methylation of the *Nfe2l2* promoter and/ or that other Nrf2 interacting proteins contributing to the decrease in Nrf2 levels, such as beta-transducin repeats-containing protein (β-TrCP)/ glycogen synthase kinase-3 beta (GSK3β), which can regulate Nrf2 stability (167).

It is also important to consider the potential reasons why high NRF2 activity could be detrimental to tumor cells. Possible mechanisms could include reductive stress and/ or a metabolic vulnerability. NRF2 hyperactivation is associated with reductive stress (80, 81), a state of excessive reducing equivalents, which can disrupt redox balance and be just as deleterious to tissue as oxidative stress, potentially impeding tumor

growth (168). It has been observed in human NSCLC cells that NRF2 can cause NADH-mediated reductive stress and subsequent impair proliferation (169). When considering if metabolic vulnerabilities can also contribute, work from our lab has shown that Nrf2 activation by Keap1$^{R554Q/R554Q}$ in the Kras$^{G12D/+}$; p53$^{fl/fl}$ model causes Cdo1 accumulation, which can lead to toxic metabolite formation, including cysteine sulfinic acid (CSA) and sulfite, and depletes NADPH (43). There have also been several studies showing that NRF2-active tumor cells (*in vitro* and *in vivo*) are dependent on glutaminolysis (45) and subsequently are sensitive to glutamate depletion mediated by the cystine-glutamate antiporter xCT (44, 61). Additional investigation is needed to determine if one or multiple mechanisms are contributing to the Nrf2-mediated progression defect in our mouse model and the proliferation/ viability impairment *in vitro*.

Moreover, the model with the highest degree of Nrf2 activation had the impairment in progression. It's likely that the levels of Nrf2 activation in the Nrf2$^{D29H/+}$ and Keap1$^{R554Q/+}$ models were tolerable for tumor progression. Although NRF2 activation/ KEAP1 inactivation have been reported to support tumorigenesis in many contexts, there are a few examples where KEAP1 inactivation has been detrimental to tumor progression and/ or normal tissue physiology. For example, Kras mutation and Keap1 deletion blocked pancreatic tumor progression and caused pancreatic atrophy (170). Postnatal lethality also occurs in a whole-body Keap1 deletion model in a Nrf2-dependent manner (155). There is also a possibility that p53 loss can influence Nrf2 activation, and subsequent effects on tumor progression. Importantly, p53 can suppress NRF2-dependent transcription of antioxidant response genes (171), suggesting that p53 loss may further enhance NRF2-mediated transcription in a model that already has high

NRF2 activity, leading to a block in tumor progression. Although this has been reported, I did not see notable differences in relative Nrf2 activity between the Kras$^{G12D/+}$ and Kras$^{G12D/+}$; p53$^{fl/fl}$ models. Therefore, it may be because the Kras$^{G12D/+}$; p53$^{fl/fl}$ model develops high-grade tumors and allows us to study tumor progression. Moreover, *KEAP1* and *TP53* mutations do not frequently co-occur in *KRAS* mutant lung adenocarcinoma (172), which could potentially explain tumor phenotypes in our mouse models with these mutations.

Chapter Five: Determining the role of Nrf2 in Keap1^{R554Q}-mediated tumor progression block[5]

Introduction

There are several studies that have shown that Keap1-deficient phenotypes are dependent on Nrf2. For example, in a study where Keap1 deletion impaired pancreatic tumor progression, this phenotype was reversed by both single-copy or homozygous deletion of Nrf2 (170), supporting a threshold effect for Nrf2. Additionally, in a model where systemic homozygous Keap1 deletion caused postnatal lethality, Nrf2 deletion rescued this phenotype (155). Studies like these high the dependence of Keap1-deficient phenotypes on Nrf2 activation, leading to my hypothesis that the block in progression in our model is Nrf2-dependent. Additionally, because I saw Nrf2 downregulation as tumors progress, I hypothesized that there is an activity threshold for Nrf2 in lung tumor progression. However, KEAP1 has additional substrates beyond NRF2 that have the potential to affect tumor progression, including phosphoglycerate

---

[5] Note to reader: Portions of this chapter have been previously published in DeBlasi et al. 2023, *Cancer Research* (154). **J.M. DeBlasi:** Data curation, formal analysis, investigation, visualization, methodology, writing–original draft, writing–review and editing. **A. Falzone, S. Caldwell, N. Prieto Farigua:** Mouse colony management and collections - Data curation, investigation, methodology, writing–review and editing. **J.R. Prigge, E.E. Schmidt:** Nrf2 antibody for IHC - Resources, writing–review and editing. **I.I.C. Chio:** Nrf2 targeting vector antibody for IHC - Resources, writing–review and editing. **F.A. Karreth:** ES cell targeting - Resources, methodology, writing–review and editing. **G.M. DeNicola:** Mouse models, RNA-sequencing - Conceptualization, resources, data curation, formal analysis, supervision, funding acquisition, investigation, methodology, writing–original draft, project administration, writing–review and editing.

mutase 5 (PGAM5) (173), partner and localizer of BRCA2 (PALB2) (174), mini-chromosome maintenance complex component 3 (MCM3) (175) and the BRCA2-interacting transcriptional repressor EMSY (176). These proteins play roles in DNA damage repair and mitochondrial homeostasis and may be disrupted upon Keap1 mutation. Therefore, I wanted to check whether the tumor progression block in our Keap1$^{R554Q/R554Q}$ model was dependent on Nrf2, and not other Keap1 substrates.

Single copy Nrf2 deletion rescues homozygous Keap1^{R554Q}-mediated tumor progression impairment

To test whether lowering Nrf2 levels could rescue the block in adenocarcinoma progression in the Keap1$^{R554Q/R554Q}$ model, a Nrf2^{flox} allele was crossed into the Kras$^{G12D/+}$; p53$^{fl/fl}$ and Kras$^{G12D/+}$; p53$^{fl/fl}$; Keap1$^{R554Q/R554Q}$ models. Because my supervisor's previous study revealed that complete Nrf2 deficiency impairs tumor initiation (137), I determined the effect of single copy Nrf2 deletion on tumor phenotypes. As in my previous experiment **(Figure 4.1A)**, I observed no difference in overall survival between cohorts with Keap1 mutation **(Fig. 5.1A)**. I also did not see differences in survival with heterozygous Nrf2 deletion. My supervisor's previous study did report an increase in median survival with Nrf2 deletion, although this was in the Kras$^{G12D/+}$ model with homozygous Nrf2 deletion (137). I also observed that Nrf2 deletion in the Keap1$^{R554Q/R554Q}$ model significantly reduced expression of Nrf2 and Nqo1 **(Fig. 5.1B-E, Fig. 5.2A and B)**.
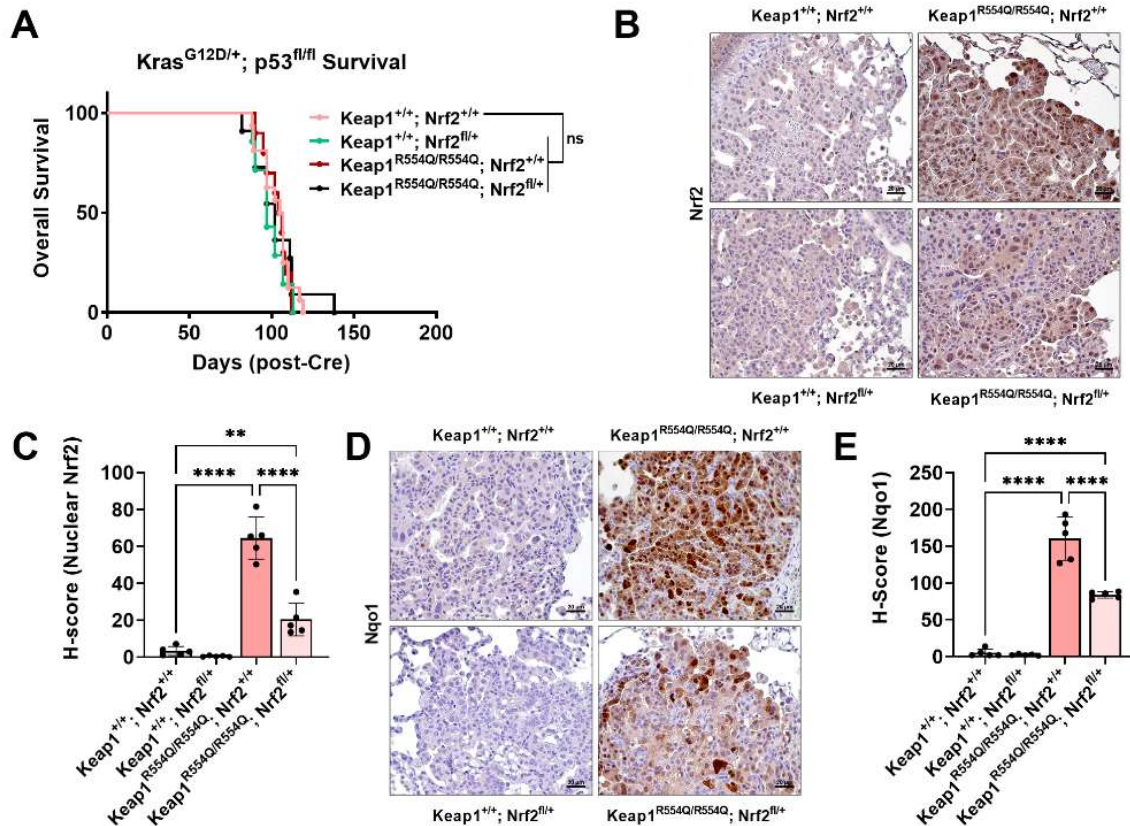
Figure 5.1. Single copy Nrf2 deletion decreases Nrf2 expression and activity in the Kras$^{G12D/+}$; p53$^{fl/fl}$ model with Keap1 mutation. **A,** Overall survival of Kras$^{G12D/+}$; p53$^{fl/fl}$ mice with Keap1 mutation and/ or single copy Nrf2 deletion. Keap1$^{+/+}$; Nrf2$^{+/+}$ (n=16), Keap1$^{+/+}$; Nrf2$^{fl/+}$ (n=7), Keap1$^{R554Q/R554Q}$; Nrf2$^{+/+}$ (n=10), Keap1$^{R554Q/R554Q}$; Nrf2$^{fl/+}$ (n=11). Ns = not significant (Log-rank (Mantel-Cox) test). **B,** Representative immunohistochemical (IHC) staining of Nrf2 in Kras$^{G12D/+}$; p53$^{fl/fl}$ mice with Keap1 mutation and/ or heterozygous Nrf2 deletion (scale bars = 20 μm). **C,** H-scores for Nrf2 (nuclear) IHC staining. **D,** Representative IHC staining of Nrf2 target Nqo1 (scale bars = 20 μm). **E,** H-scores for Nqo1 (whole-cell) IHC staining. For **B-E**, N=3 mice per genotype and >20,000 tumor cells per mouse. **p<0.01, ****p<0.0001 (one-way ANOVA). This figure was previously published in *Cancer Research*, DeBlasi et al. 2023 (154).

64

Moreover, as I previously observed, Nrf2 expression and activity was decreased in higher-grade tumors **(Fig. 5.2A and B).**
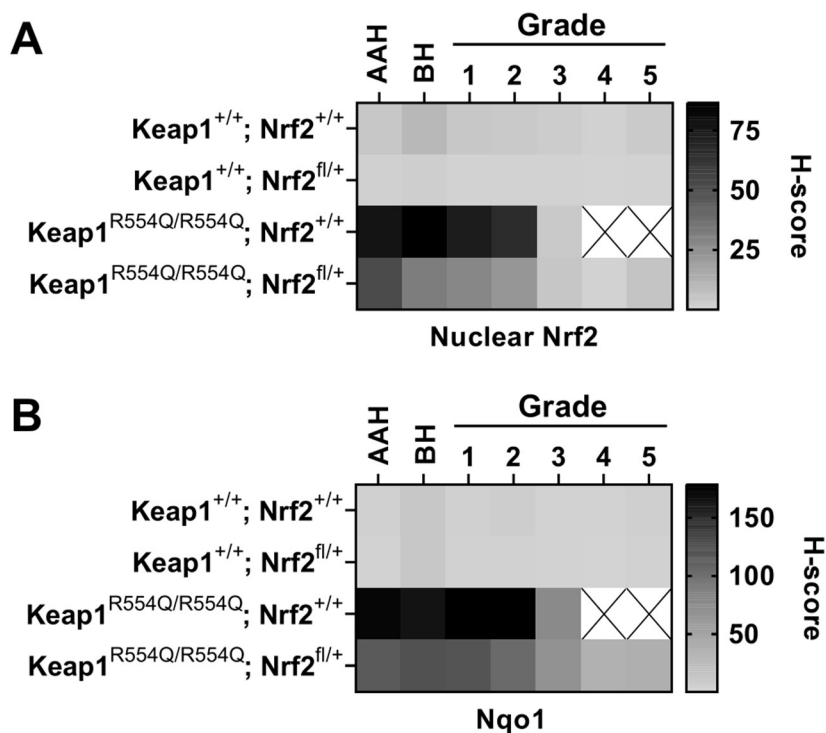
Figure 5.2. Immunohistochemical analysis of Nrf2 and Nqo1 across tumor grades in the Kras$^{G12D/+}$; p53$^{fl/fl}$ model with single copy Nrf2 deletion. **A** and **B,** Heatmaps depicting the H-scores per grade from IHC staining for Nrf2 (nuclear) **(A)** and the Nrf2 target Nqo1 (whole cell) **(B)**. N=3 mice per genotype, >20,000 tumor cells per mouse. Only one grade 4 and one grade 5 tumor were found in the Keap1$^{R554Q/R554Q}$; Nrf2$^{+/+}$ cohort, and therefore were excluded from these analyses. This figure was previously published in *Cancer Research*, DeBlasi et al. 2023 (154).

Upon histological examination of the lung tissue, I observed a striking difference in tumor burden, with single copy Nrf2 deletion having a minimal effect on the $Kras^{G12D/+}$; $p53^{fl/fl}$ model, while dramatically increasing burden in the $Kras^{G12D/+}$; $p53^{fl/fl}$; $Keap1^{R554Q/R554Q}$ model, which I confirmed by quantitation **(Fig. 5.3A, Fig. 5.4A)**. Tumor number and size were not significantly affected **(Fig. 5.4B and C-D)**. Upon tumor grading, I observed that $Keap1^{R554Q/R554Q}$ mutation blocked adenocarcinoma progression upon $Nrf2^{WT}$ expression **(Fig. 5.3B** and **C)**, in agreement with my previous experiment **(Fig. 4.3)**. Upon single copy Nrf2 deletion ($Nrf2^{flox/+}$), however, $Keap1^{R554Q/R554Q}$ mutation failed to impair lung tumor progression **(Fig. 5.3B** and **C)**. Additionally, the $Keap1^{R554Q/R554Q}$-mediated decrease in grade 3 tumor number and burden was rescued by single copy deletion of Nrf2 **(Fig. 5.3C, Fig. 5.4E)**. My data indicate that there is a threshold by which Nrf2 activation can promote or impair lung tumor initiation or progression.

Following my analyses in these models, I was also interested to see whether complete deletion of Nrf2 ($Nrf2^{fl/fl}$) would affect tumor initiation and progression, given the importance of Nrf2 in tumor initiation (34, 137, 144). Although I did not directly analyze these parameters, gross histological examination revealed that homozygous Nrf2 knockout did not negatively impact tumor number, burden or size **(Fig. 5.5A)**. Histological quantification is needed, however, to draw conclusions about tumor initiation and progression. Moreover, overall survival was not significantly affected with homozygous Nrf2 deletion **(Fig. 5.5 B).**
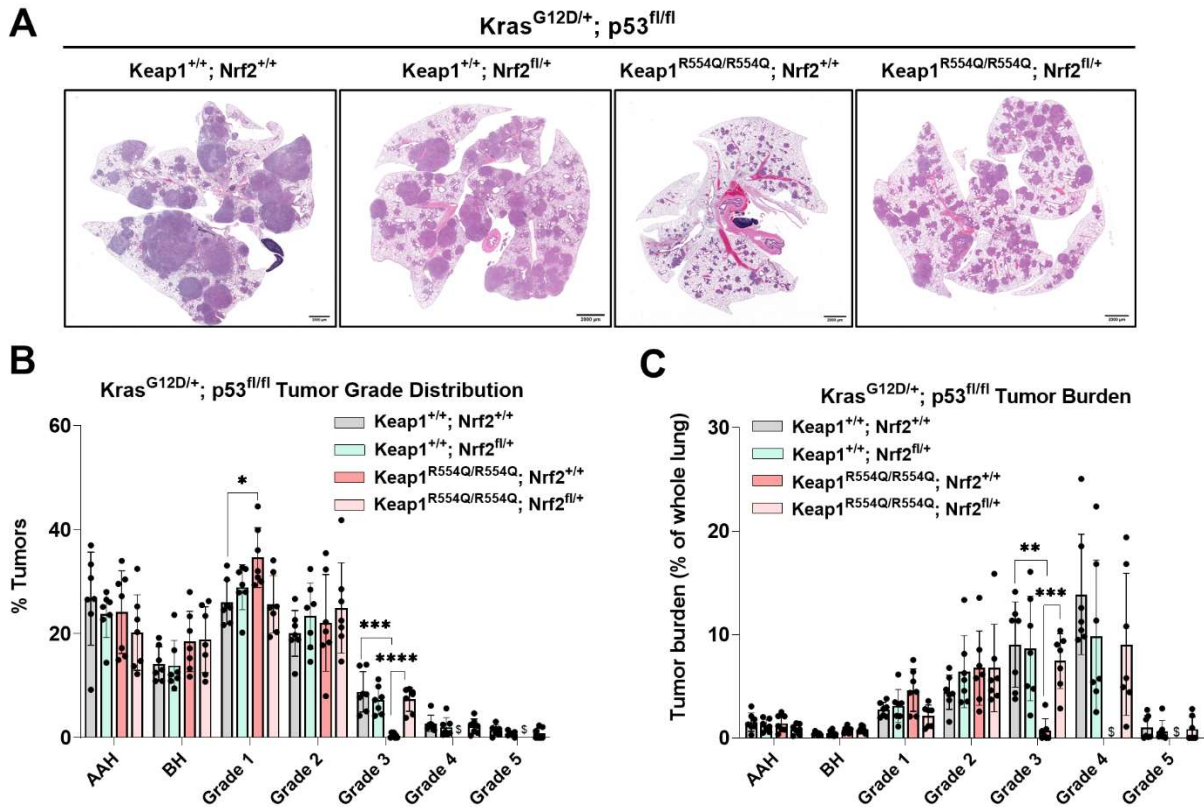
Figure 5.3. Single copy Nrf2 deletion rescues homozygous Keap1^{R554Q}-mediated adenocarcinoma progression impairment in the Kras$^{G12D/+}$; p53$^{fl/fl}$ model. **A,** Representative whole lung H&E-stained sections (scale bars = 2000 µm). **B,** Distribution of tumor grades across Keap1 mutant/ Nrf2-deleted models. *p<0.05, ***p<0.001, ****p<0.0001 (unpaired t test with Holm-Sidak's multiple comparisons test). $ = fewer than three tumors detected across all mice. **C,** Fraction of lung tumor burden by grade (lung tumor area per grade/ total lung area). **p<0.01, ***p<0.001 (unpaired t test with Holm-Sidak's multiple comparisons test). $ = fewer than 3 tumors detected across all mice. For both **G** and **H** n=7 mice and $\geq$1,000 tumors per genotype were analyzed. Only one grade 4 and one grade 5 tumor were found in the Keap1$^{R554Q/R554Q}$ cohort, and therefore were excluded from these analyses. This figure was previously published in *Cancer Research*, DeBlasi et al. 2023 (154).
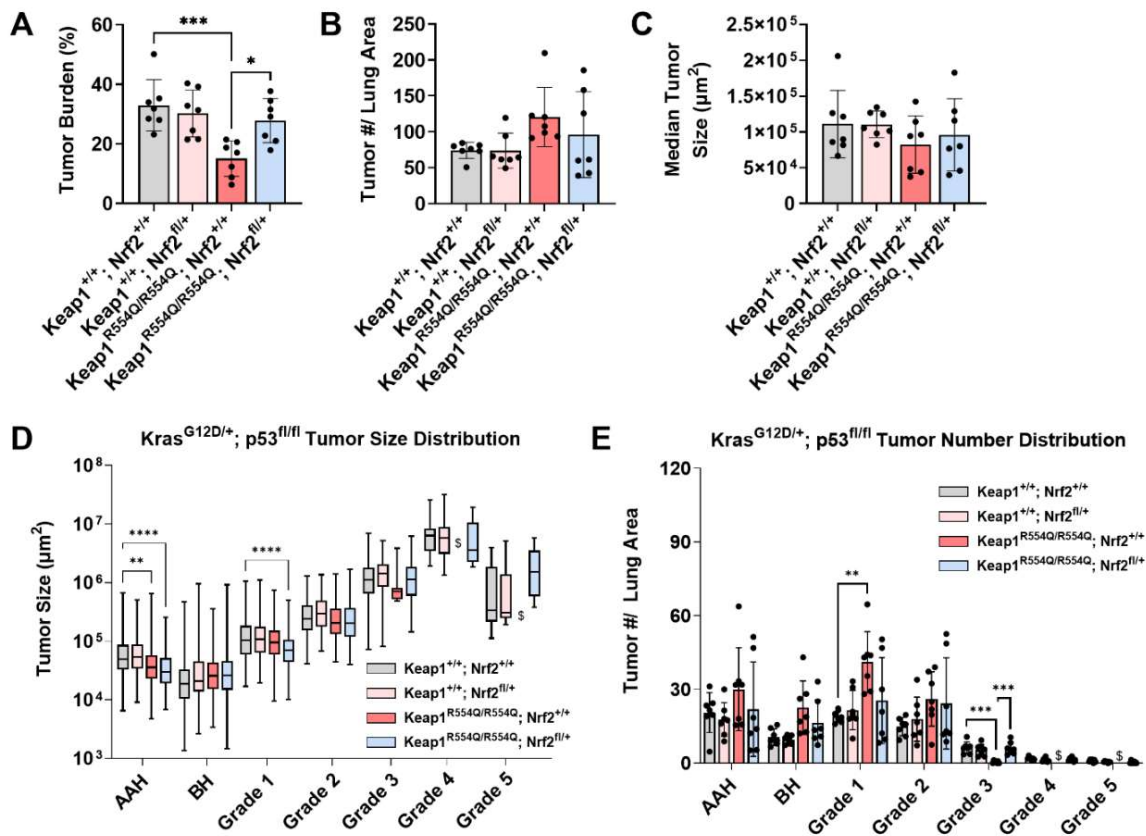
Figure 5.4. Lung tumor burden, size, and number quantification in the Kras$^{G12D/+}$; p53$^{fl/fl}$ model with single copy Nrf2 deletion. **A,** Overall tumor burden (%) calculated by dividing the total area of lung tumor by the total area of the lung. **B,** Tumor number per mouse normalized to lung area. **C,** Median tumor size per mouse for each genotype. For **A-C**, *p<0.05, ***p<0.001 (one-way ANOVA). **D,** Tumor size across all mice per genotype. N=7 mice and ≥1,000 tumors per genotype. **p<0.01, ****p<0.0001 (Kruskal-Wallis test with Dunn's multiple comparisons test). $ = fewer than three tumors detected across all mice. **E,** Distribution of tumor number by grade across Keap1/Nrf2 mutant models. N=7 mice per genotype, **p<0.01, ***p<0.001 (unpaired t test with Holm-Sidak's multiple comparisons test). $ = fewer than three tumors detected across all mice. For **D** and **E**, only one grade 4 and two grade 5 tumors were found in the Keap1$^{R554Q/R554Q}$; Nrf2$^{+/+}$ cohort, and therefore were excluded from these analyses. This figure was previously published in *Cancer Research*, DeBlasi et al. 2023 (154).
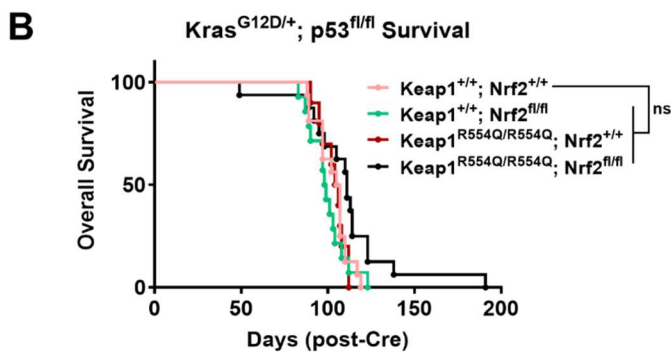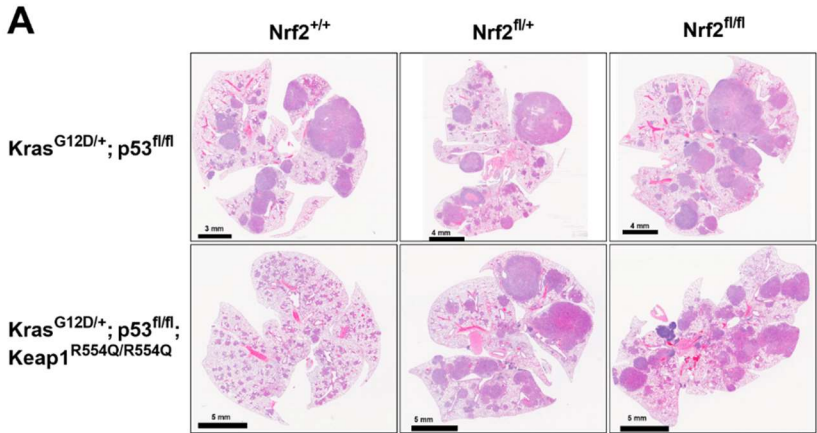
Figure 5.5. Homozygous Nrf2 deletion does not impact tumor burden, number, or size in Kras$^{G12D/+}$; p53$^{fl/fl}$ model but appears to increase tumor size/ burden in Kras$^{G12D/+}$; p53$^{fl/fl}$; Keap1$^{R554Q/R554Q}$ model. **A,** Representative whole lung H&E-stained section (scale bars = 4 or 5 mm). **B,** Overall survival of Kras$^{G12D/+}$; p53$^{fl/fl}$ mice with Keap1 mutation and/ or homozygous Nrf2 deletion. Keap1$^{+/+}$; Nrf2$^{+/+}$ (n=16), Keap1$^{+/+}$; Nrf2$^{fl/fl}$ (n=14), Keap1$^{R554Q/R554Q}$; Nrf2$^{+/+}$ (n=10), Keap1$^{R554Q/R554Q}$; Nrf2$^{fl/fl}$ (n=16). Ns = not significant (Log-rank (Mantel-Cox) test).

Discussion

I observed that the tumor progression block in the Keap1$^{R554Q/R554Q}$ model was dependent on Nrf2, given that single copy Nrf2 deletion rescued this phenotype. I observed that single copy deletion lowered Nrf2 to a more tolerable level, as indicated by IHC staining for Nrf2 and Nrf2 target Nqo1. Moreover, consistent with my previous

experiments, I saw that tumors downregulated Nrf2 expression and activity as they progressed. Interestingly, upon gross histological examination, I also saw that homozygous Nrf2 deletion did not affect tumor burden, number, or size. Although formal analysis is warranted, this examination suggests that concomitant Kras mutation and p53 loss may mitigate the necessity for Nrf2 activation during tumorigenesis and progression. Additionally, I don't know whether complete Nrf2 deletion was achieved in all tumors, nor the quantification of tumor number or grade. Another group using the Nrf2^{flox} allele reported that Nrf2 deletion in the bone marrow did not affect tumor burden in the Kras$^{G12D/+}$ lung cancer model with Nrf2 activated in tumor cells (144). They did, however, see that Nrf2 activation in immune cells prolonged survival of Nrf2-activated tumor-bearing mice, and rescued a Nrf2-activated tumor burden increase, suggesting that Nrf2 activation is important in the tumor microenvironment. Moreover, work from my supervisor also showed that whole body Nrf2 deletion in the Kras$^{G12D/+}$ model reduced lung tumor burden and prolonged survival (137). In this case, Nrf2 was deleted in both tumor and immune cells; it is likely that Nrf2 is critical for tumorigenesis in not only lung tumor cells, but also the tumor microenvironment.

It will be important to understand exactly how Nrf2 is downregulated during progression, and how Nrf2 activation/ inhibition affects different tumor grades to see whether this threshold is applicable to patient tumors. It should also be noted that Nrf2 is activated only in cancer cells in these experiments, and not in the microenvironment, which is an important consideration for the application of pharmacological Nrf2 activators, given that Nrf2 activation in the microenvironment can affect tumor growth (144, 177, 178).

Chapter Six: Keap1 and Nrf2 mutation have

differential effects in the Kras$^{G12D/+}$; Lkb1$^{fl/fl}$ model

Introduction

Although my results indicate that the tumor progression block in the

Keap1$^{R554Q/R554Q}$ model was dependent on Nrf2, I wanted to see if this was influenced

by mutational background. In *KRAS* mutant lung adenocarcinoma patients, *KEAP1* and

TP53 mutations co-occur in less than 25% of cases, whereas *KEAP1* and *STK11*

mutations co-occur in ~70% of cases (172, 179, 180). It has been suggested that

KEAP1 and *STK11* mutations may cooperate because NRF2 can increase availability of

NADPH for ROS detoxification (38), which may allow LKB1-deficient tumors to combat

oxidative stress and use NADPH for anabolic processes. Accordingly, I hypothesized

that mutational background may dictate how Nrf2 influences lung tumor progression.

Keap1/ Nrf2 mutation have differential effects in the Kras$^{G12D/+}$; Lkb1$^{fl/fl}$ model

To further investigate the effects of Nrf2 activation on tumor progression, our

Keap1/Nrf2 mutant models were crossed with the Kras$^{G12D/+}$; Lkb1$^{fl/fl}$ model **(Fig. 6)**.
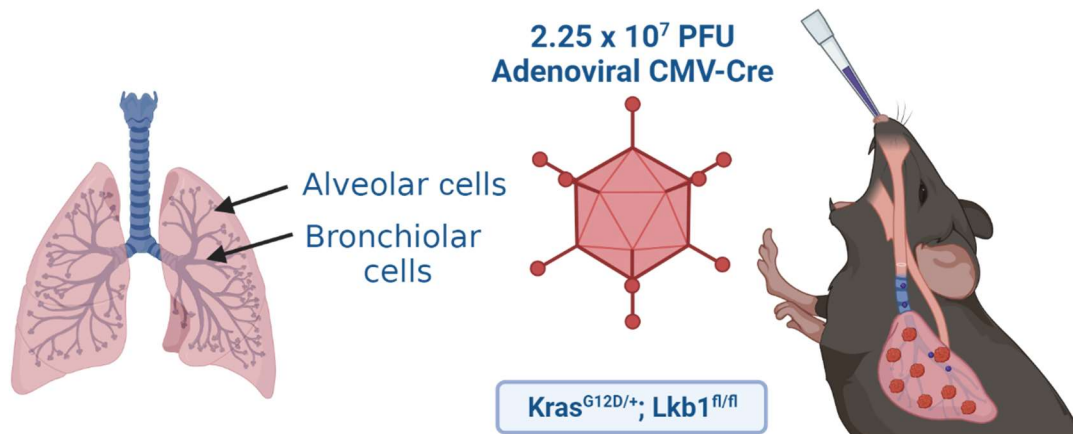
Figure 6. Using the Kras$^{G12D/+}$; Lkb1$^{fl/fl}$ mouse model to investigate how Keap1/ Nrf2 mutation affect tumor progression in a different mutational background. An overview of the amount of adenoviral-Cre used in the experiments for Figures 6.1 and 6.2. Created with BioRender.com.

Because *STK11* is frequently co-mutated with *KEAP1* in *KRAS* mutant lung adenocarcinoma patients, I hypothesized that this model may more closely recapitulate patient tumors compared to our KP experiments. I did not find any differences in overall survival with Keap1 mutation **(Fig. 6.1A)**. However, I observed a significant decrease in overall survival with the Nrf2$^{D29H/+}$ mutation **(Fig. 6.1B)**.
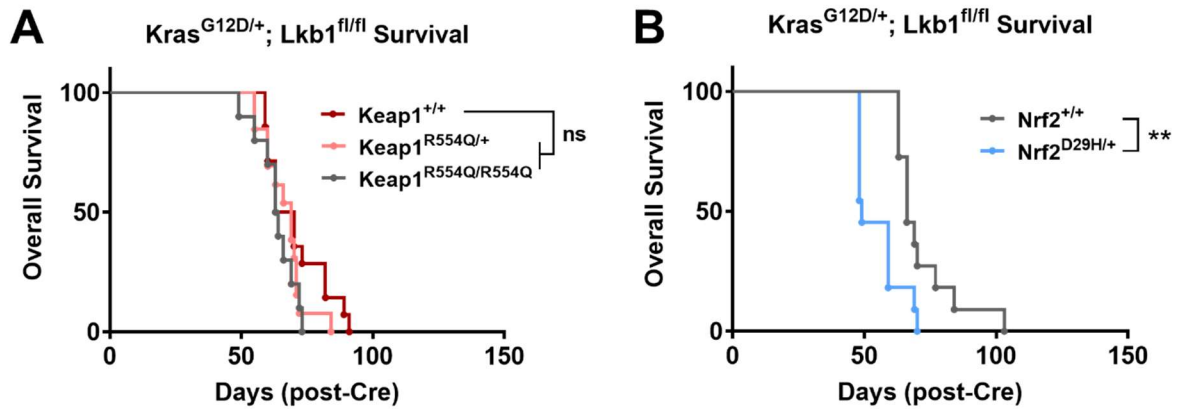
Figure 6.1. Nrf2 mutation decreases survival in the Kras$^{G12D/+}$; Lkb1$^{fl/fl}$ model. **A,** Overall survival of Keap1 mutant mice in Kras$^{G12D/+}$; Lkb1$^{fl/fl}$ model. Keap1$^{+/+}$ (n=14); Keap1$^{R554Q/+}$ (n=13); Keap1$^{R554Q/R554Q}$ (n=10). **B,** Overall survival of Nrf2 mutant mice in Kras$^{G12D/+}$; Lkb11$^{fl/fl}$ model. Nrf2$^{+/+}$ (n=11); Nrf2$^{D29H/+}$ (n=11). Ns, not significant; **, P<0.01 (Log-rank (Mantel-Cox) test).

I also examined Nrf2 activation in this model by performing IHC staining for the Nrf2 target Nqo1. Interestingly, I saw both Keap1$^{R554Q/R554Q}$ and Nrf2$^{D29H/+}$ mutations were similar activating, with the Nrf2$^{D29H/+}$ mutant trending slightly higher **(Fig. 6.2 A** and **B)**. Moreover, I saw only modest, non-significant activation with Keap1$^{R554Q/+}$, suggesting that Lkb1 deletion may influence the degree of Nrf2 activity. Moreover, because these mice died too rapidly, histological examination revealed an absence of high-grade tumors across all cohorts. Our data in the Kras$^{G12D/+}$; p53$^{fl/fl}$ model suggests that more stark differences in Nrf2 expression and activity are observed in adenocarcinomas, which could explain why Keap1$^{R554Q/R554Q}$ and Nrf2$^{D29H/+}$ were similarly activating.
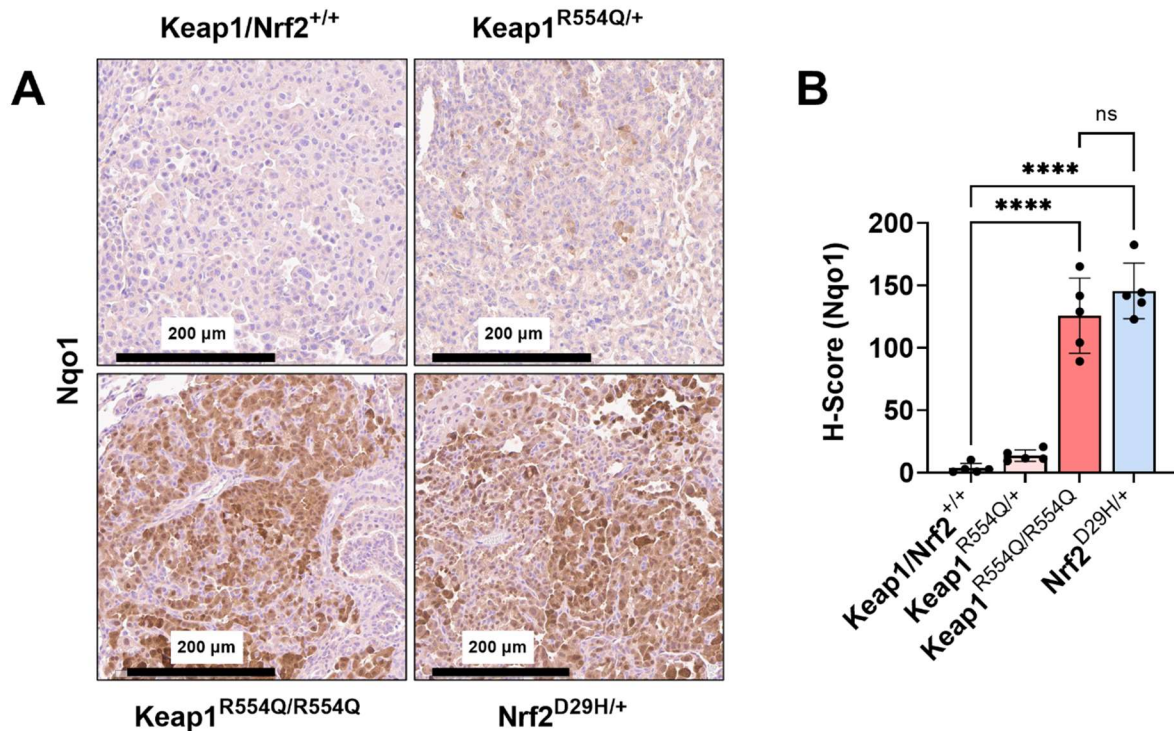
Figure 6.2. Keap1/ Nrf2 mutation significantly increase relative Nrf2 activity in the Kras$^{G12D/+}$; Lkb1$^{fl/fl}$ model. **A,** Representative immunohistochemical (IHC) staining of Nqo1 in Kras$^{G12D/+}$; Lkb1$^{fl/fl}$ mice with Keap1/Nrf2 mutation (scale bars = 200 μm). **B,** H-scores for Nqo1 IHC staining. N=5 mice per genotype and >20,000 tumor cells per mouse. ****$p<0.0001$ (one-way ANOVA).

Because the Nrf2$^{D29H/+}$ mice died sooner before their WT counterparts, I was unable to compare tumor burden and progression with these models. In order to fairly compare cohorts, and lower tumor multiplicity, I performed an additional experiment using a lower titer of adenovirus (10% of original dose) **(Fig. 6.3)**.
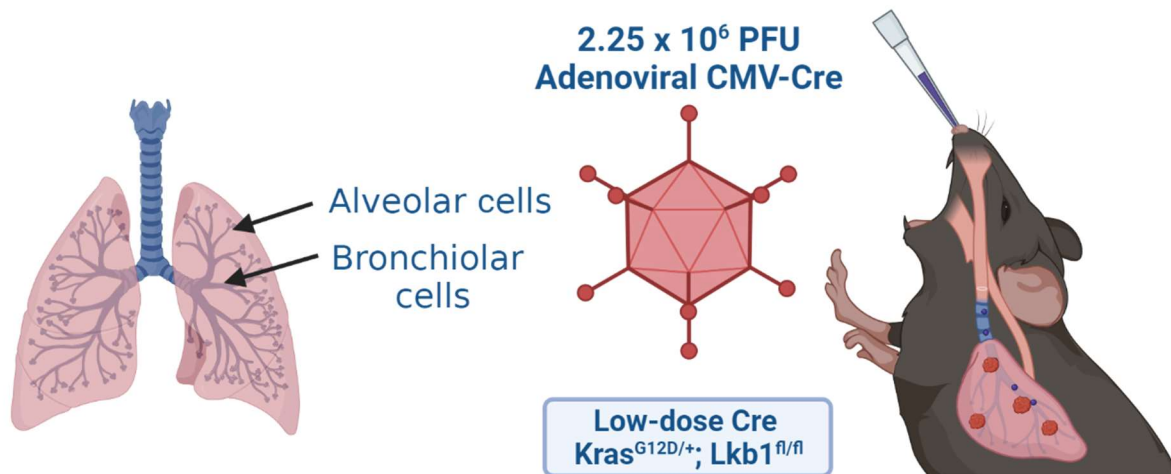
Figure 6.3. Using a lower dose of adenoviral-Cre in the Kras$^{G12D/+}$; Lkb1$^{fl/fl}$ mouse model to decrease tumor multiplicity of induction. An overview of the amount of adenoviral-Cre used in the experiments for Figures 6.4-6.7. Created with BioRender.com.

In this experiment, with a lower dose of adenoviral-Cre, I observed that neither Keap1 nor Nrf2 mutation affected overall survival **(Fig. 6.4 A** and **B).**
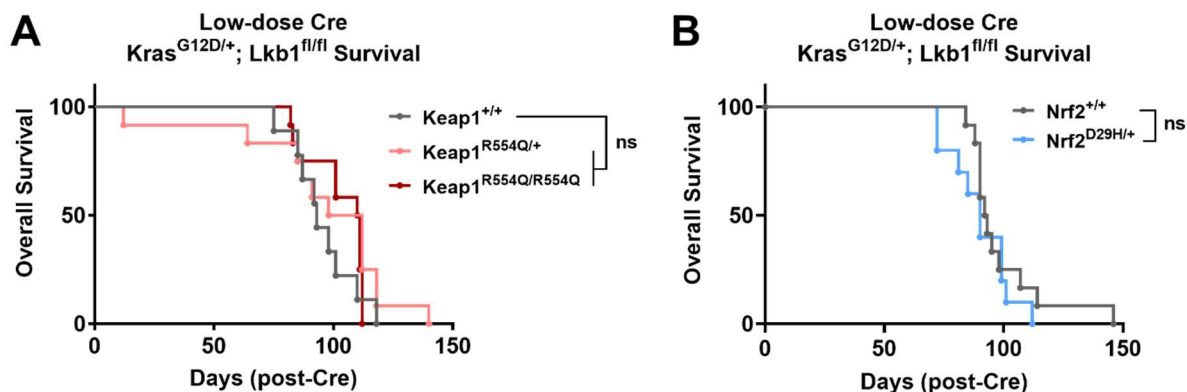
Figure 6.4. Keap1/ Nrf2 mutation do not affect survival in the low-dose Cre Kras$^{G12D/+}$; Lkb1$^{fl/fl}$ model. **A,** Overall survival of Keap1 mutant mice in Kras$^{G12D/+}$; Lkb11$^{fl/fl}$ model. Keap1$^{+/+}$ (n=9); Keap1$^{R554Q/+}$ (n=12); Keap1$^{R554Q/R554Q}$ (n=12). **B,** Overall survival of Nrf2 mutant mice with Kras$^{G12D/+}$; Lkb1$^{fl/fl}$ mutation. Nrf2$^{+/+}$ (n=12); Nrf2$^{D29H/+}$ (n=10). Ns, not significant (Log-rank (Mantel-Cox) test.

I next analyzed tumor progression via tumor grading. Histological examination revealed that Nrf2$^{D29H/+}$ mice had decreased tumor burden **(Fig. 6.5A)**, which I later validated with quantification **(Fig. 6.6E).** Upon tumor grading, I observed that Nrf2 mutant mice had increased early progression to low grade 2 tumors and a block in progression to advanced grade adenocarcinomas **(Fig. 6.5B** and **C).** I also saw a decrease in the proportion and burden of adenomatous, atypical hyperplasia (AAH), which is likely a result of those cells eventually progressing to low grade 2 tumors. Moreover, I observed that Keap1$^{R554Q/R554Q}$ mice had increased bronchiolar hyperplasia (BH) burden **(Fig. 6.5C)**, supporting the previously established role of Keap1 in bronchiolar cells (34).

I also examined additional parameters of my lung tumor analysis data. Consistent with my grading proportion results **(Fig. 6.5B)**, I saw that there was a lower number of AAH, grade 3 and grade 5 tumors in the Nrf2$^{D29H/+}$ cohort, as well as an increase in grade 2 tumors **(Fig. 6.6A)**. Interestingly, AAH and grade 1 lesions were also smaller with this genotype **(Fig. 6.6B)**. Moreover, although Keap1$^{R554Q/R554Q}$ did not affect progression in this model, this cohort had smaller AAH, grade 1, and grade 2 lesions **(Fig. 6.6B)**, suggesting that Keap1 mutation may also impair tumor cell proliferation in this model, as I had seen in the Kras$^{G12D/+}$; p53$^{fl/fl}$ model **(Figs. 4.4D, 4.5A** and **B)**. I saw a non-significant trend increase in tumor number in the Keap1$^{R554Q/R554Q}$ and Nrf2$^{D29H/+}$ cohorts **(Fig. 6.6C)**, supportive of a pro-initiation role for Nrf2 activation in our models. I also observed a decrease in overall tumor size in the Keap1$^{R554Q/R554Q}$ cohort **(Fig. 6.6D)**. Although I did not measure tumor cell proliferation

76

in this model, this data suggests that there was likely a lower proliferative index in this model, at least in AAH and grade 1/2 tumors. Finally, I saw a significant decrease in lung tumor burden in the Nrf2$^{D29H/+}$ cohort **(Fig. 6.6E)**, consistent with the progression block and decreased size of AAH and grade 1 tumors.
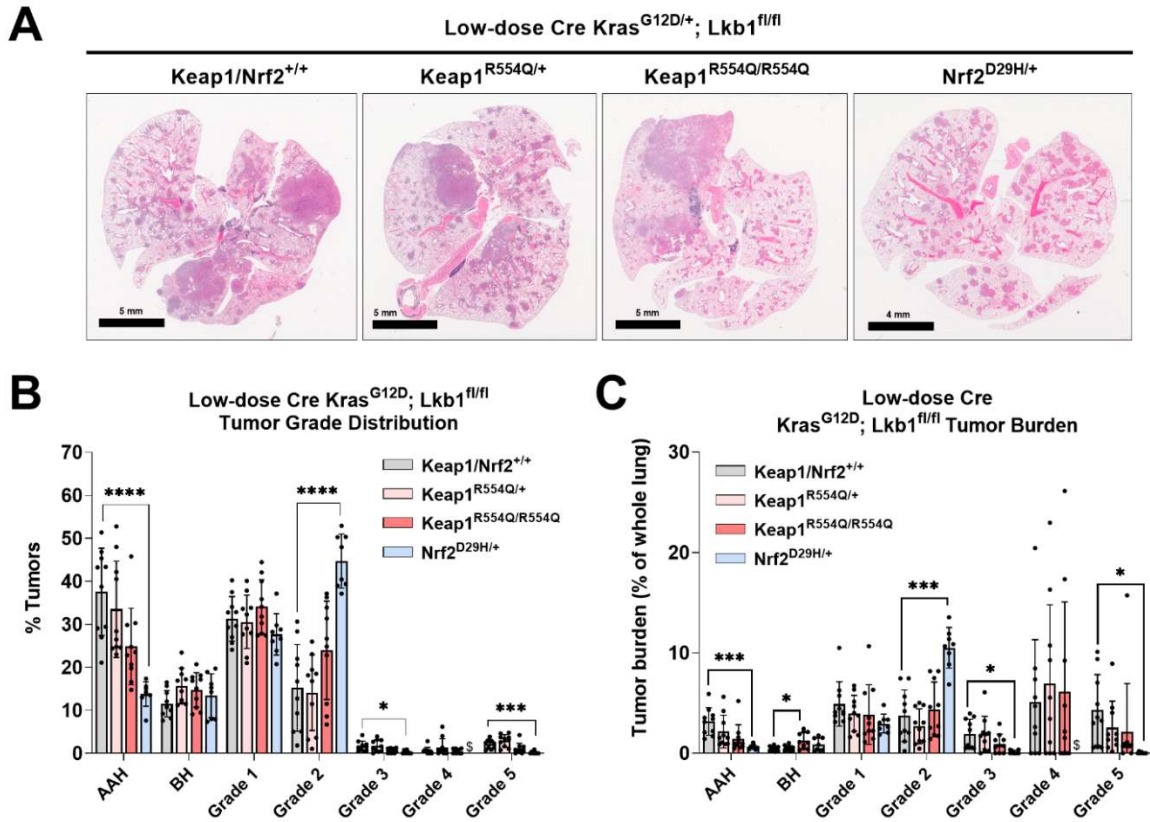
Figure 6.5. Nrf2^{D29H} promotes early progression but blocks adenocarcinoma progression in the Kras$^{G12D/+}$; Lkb1$^{fl/fl}$ model. **A,** Representative whole lung H&E-stained section (scale bars = 4 or 5 mm). **B,** Distribution of tumor grades across Keap1/Nrf2 mutant models. *p<0.05, ***p<0.001, ****p<0.0001 (unpaired t test with Holm-Sidak's multiple comparisons test). AAH = atypical adenomatous hyperplasia. BH = bronchiolar hyperplasia. **C,** Fraction of lung tumor burden by grade (lung tumor area/ total lung area per grade). *p<0.05, ***p<0.001 (unpaired t test with Holm-Sidak's multiple comparisons test). For both **B** and **C**, n$\geq$8 mice and $\geq$1,500 tumors per genotype. $ = fewer than three tumors detected across all mice.
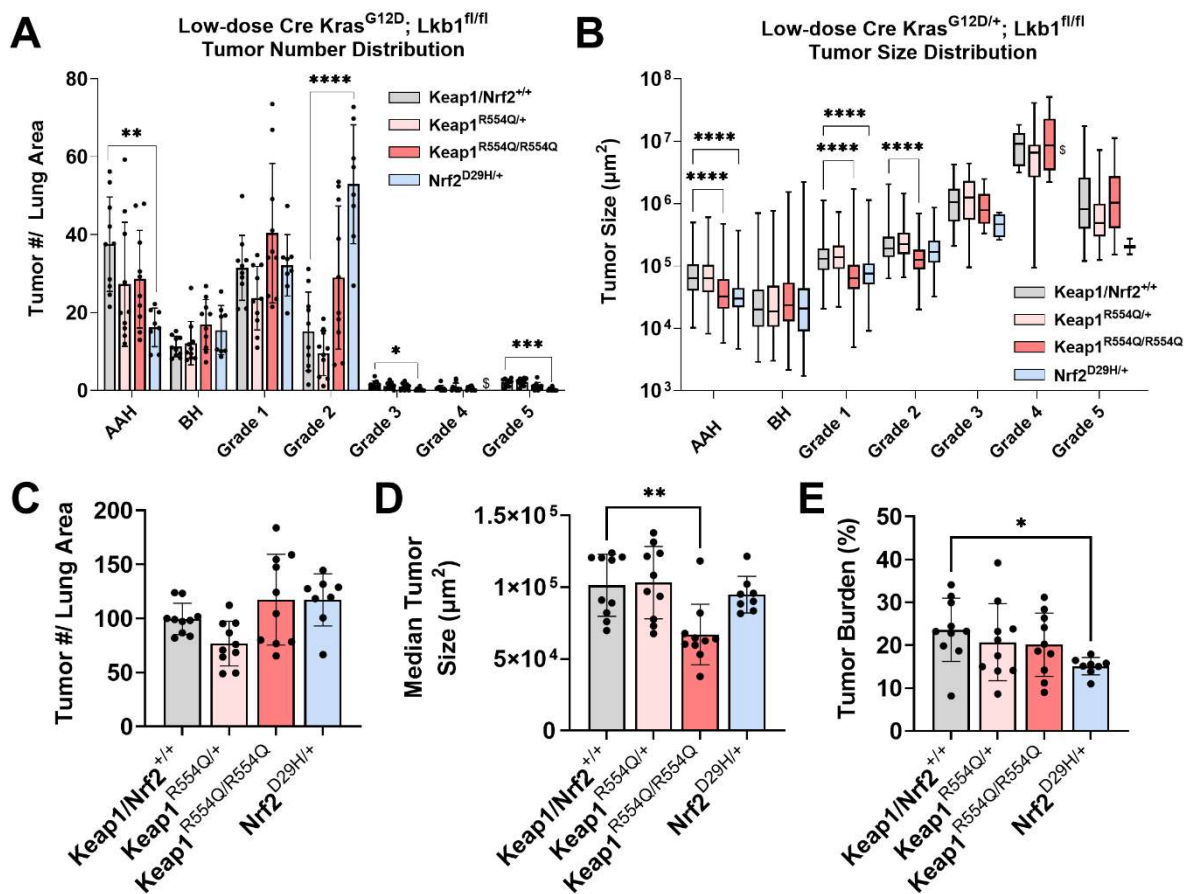
Figure 6.6. Lung tumor number, size, and burden in the Kras$^{G12D/+}$; Lkb1$^{fl/fl}$ model. **A,** Distribution of tumor number by grade across Keap1/Nrf2 mutant models. N≥8 mice per genotype, *p<0.05, **p<0.01, ***p<0.001, ****p<0.0001 (unpaired t test with Holm-Sidak's multiple comparisons test). $ = fewer than three tumors detected across all mice. **B,** Tumor size across all mice per genotype. N≥8 mice and ≥1,500 tumors per genotype. ****p<0.0001 (Kruskal-Wallis test with Dunn's multiple comparisons test). $ = fewer than three tumors detected across all mice. **C,** Tumor number per mouse normalized to lung area. **D,** Median tumor size per mouse for each genotype. **E,** Overall tumor burden (%) calculated by dividing the total area of lung tumor by the total area of the lung. For **C-E**, N≥8 mice per genotype. *p<0.05, **p<0.01 (one-way ANOVA).

Next, I analyzed Nrf2 expression and activity in our cohorts. I observed that Keap1$^{R554Q/+}$ was only modestly activating (non-significant) **(Fig. 6.7A** and **B)**. Interestingly, the Nrf2$^{D29H/+}$ mutation was the most activating towards Nrf2, followed by Keap1$^{R554Q/R554Q}$ **(Fig. 6.7A** and **B)**, indicating that these mutations can differentially affect Nrf2 activation in the context of Lkb1 vs. p53 deletion. Moreover, this supports my hypothesis for a threshold effect of Nrf2, where the cohort with the highest degree of Nrf2 activation (Nrf2$^{D29H/+}$) resulted in a tumor progression block. Although the Keap1$^{R554Q/R554Q}$ mutation did not cause a progression block in this model, it was associated with a reduction in size of some of the lesions, suggesting an anti-proliferative effect. Finally, I observed that Nrf2 expression and activity was downregulated with increasing tumor grade **(Fig. 6.7C** and **D)**.

Keap1 mutation does not block progression in the Kras$^{G12D/+}$; Lkb1$^{fl/fl}$ SPC Cre model

Although my findings in the Kras$^{G12D/+}$; Lkb1$^{fl/fl}$ model were consistent with a Nrf2 threshold effect, my results were partially confounded by the presence of large squamous tumors in this model. The Kras$^{G12D/+}$; Lkb1$^{fl/fl}$ model is well-studied; however, the mice form squamous tumors (181, 182), which are rarely observed in patients with *KRAS* and *STK11* mutations. In this model, I observed squamous and adenosquamous tumors in not only the Keap1/Nrf2$^{+/+}$ cohort, but also the Keap1$^{R554Q/+}$ and Keap1$^{R554Q/R554Q}$ cohorts. Interestingly, I did not observe any squamous tumors in the Nrf2$^{D29H/+}$ cohort, suggesting that Keap1 vs. Nrf2 mutation can affect different cell types. It's also possible that Nrf2$^{D29H/+}$ mutation did not support survival/ proliferation of cells

that give rise to squamous tumors. To address the caveat of squamous tumors, I also performed these experiments with a form of adenoviral-Cre specific to lung alveolar cells: surfactant protein C (SPC) Cre **(Fig. 6.8)** (183). Use of this Cre promotes adenocarcinoma formation, as alveolar type II cells are considered the primary cell-of-origin for lung adenocarcinoma (184, 185). In my SPC Cre experiments, I observed that neither Keap1 or Nrf2 mutation affected overall survival **(Fig. 6.9A** and **B)**.

Next, I measured tumor progression by performing tumor grading. Similar to the low-dose Cre experiment, I observed that Nrf2$^{D29H/+}$ mutation blocked progression to advanced grade 4 and 5 adenocarcinomas **(Fig. 6.10A-C)**. I did not see any changes in grade 3 tumors across the models, although these tumors were quite rare compared to the Kras$^{G12D/+}$; p53$^{fl/fl}$ model. As in my previous experiment **(Fig. 6.5B)**, I also saw a decrease in the proportion of AAH and an increase in early progression grade 2 tumors with Nrf2$^{D29H/+}$ mutation. Interestingly, I saw that Keap1$^{R554Q/+}$ significantly increased the proportion and burden of grade 5 adenocarcinomas **(Fig. 6.10B** and **C).** These findings suggest that excess high levels block tumor progression, whereas modest Nrf2 activation can accelerate progression in the context of Lkb1 deletion.
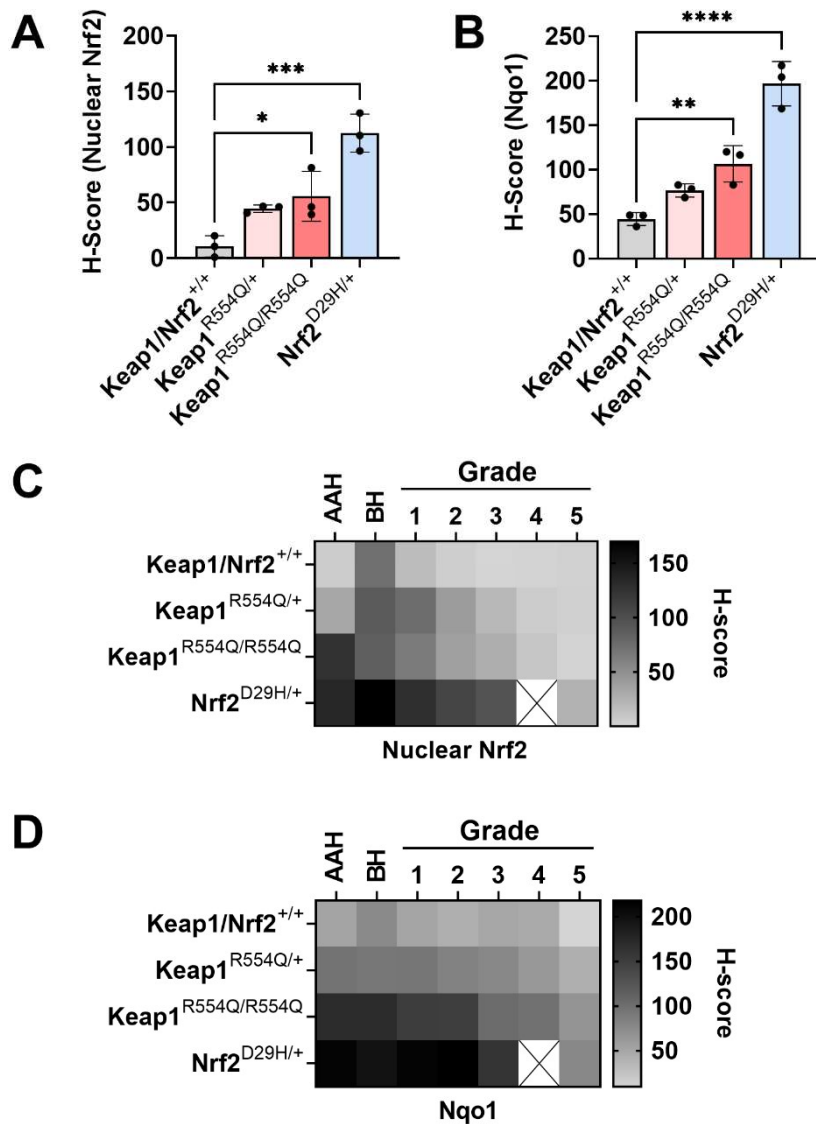
Figure 6.7. Keap1/ Nrf2 mutation constitutively activate Nrf2 in the low-dose Cre Kras$^{G12D/+}$; Lkb1$^{fl/fl}$ model. **A** and **B,** H-scores for Nrf2 (nuclear) **(A)** and Nqo1 (whole-cell) **(B)** immunohistochemical (IHC) staining. N=3 mice per genotype and >20,000 tumor cells per mouse. *p<0.05, **p<0.01, ***p<0.001, ****p<0.0001 (one-way ANOVA). **C** and **D,** Heatmaps depicting the H-scores per grade from IHC staining for Nrf2 (nuclear) **(C)** and the Nrf2 target Nqo1 (whole cell) **(D)**. N=3 mice per genotype, >20,000 tumor cells per mouse. Note that no grade 4 tumors were observed in the Nrf2$^{D29H/+}$ cohort.
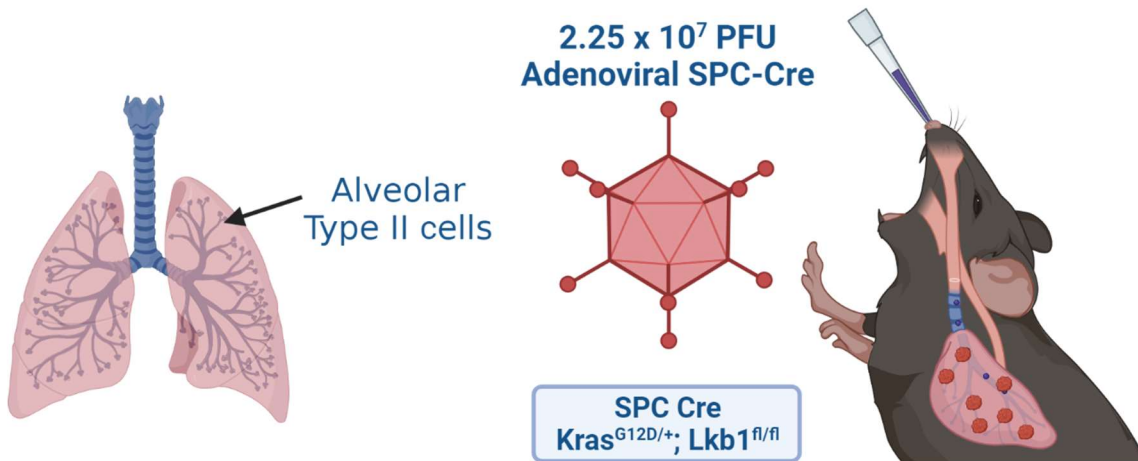
Figure 6.8. Using SPC Cre in the Kras$^{G12D/+}$; Lkb1$^{fl/fl}$ mouse model to target alveolar type II cells in the lung. An overview of the amount of adenoviral-Cre and cells targeted in the experiments for Figures 6.9-6.12. Created with BioRender.com.
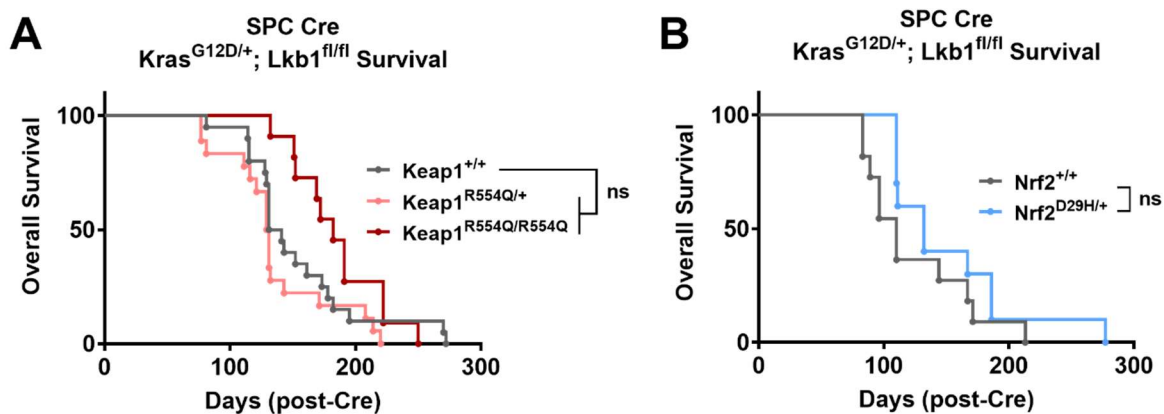
Figure 6.9. Keap1/ Nrf2 mutation do not affect survival in the SPC Cre Kras$^{G12D/+}$; Lkb1$^{fl/fl}$ model. **A,** Overall survival of Keap1 mutant mice in the Kras$^{G12D/+}$; Stk11$^{fl/fl}$ model. Keap1$^{+/+}$ (n=20); Keap1$^{R554Q/+}$ (n=18); Keap1$^{R554Q/R554Q}$ (n=11). **B,** Overall survival of Nrf2 mutant mice with Kras$^{G12D/+}$; Lkb1$^{fl/fl}$ mutation. Nrf2$^{+/+}$ (n=11); Nrf2$^{D29H/+}$ (n=10). Ns, not significant (Log-rank (Mantel-Cox) test).
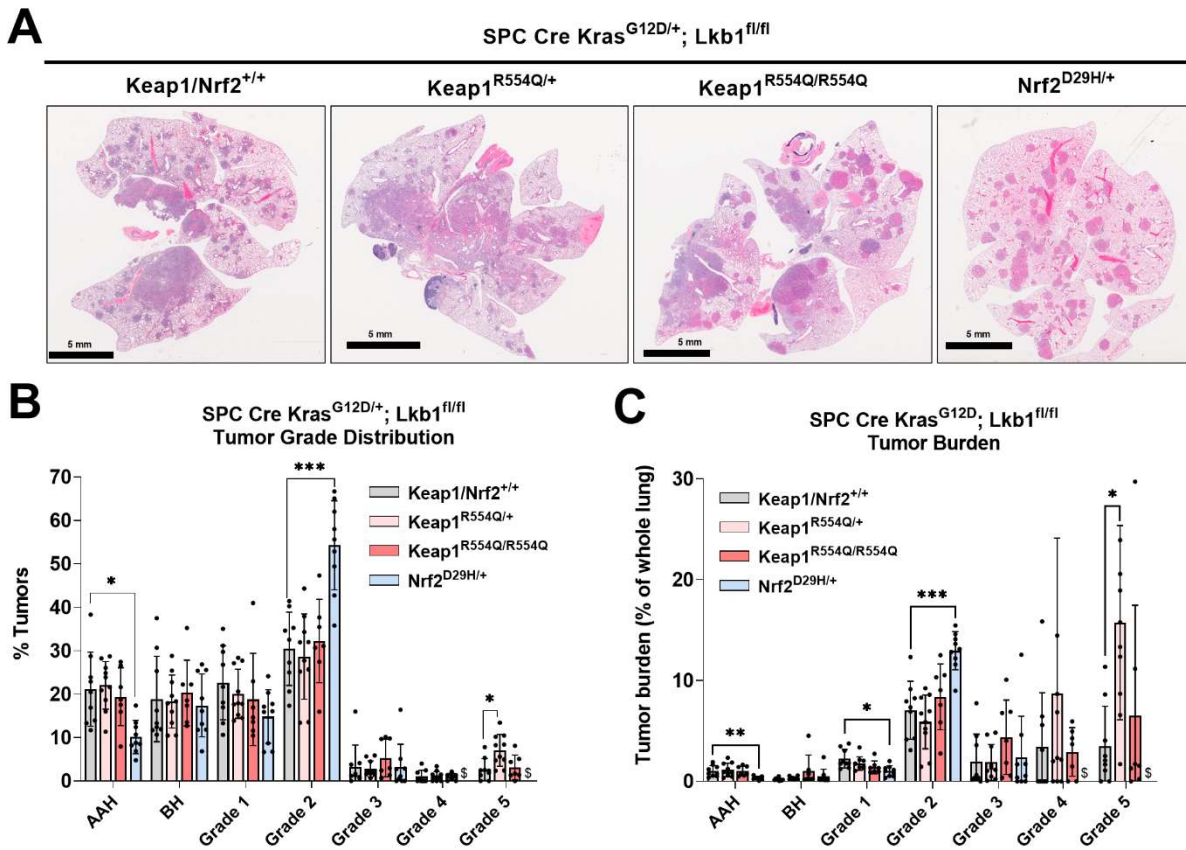
Figure 6.10. Keap1[R554Q/R554Q] mutation does not block adenocarcinoma progression in the SPC Cre Kras[G12D/+]; Lkb1^{fl/fl} model. **A,** Representative whole lung H&E-stained section (scale bars = 5000 μm). **B,** Distribution of tumor grades across Keap1/Nrf2 mutant models. *p<0.05, ***p<0.001 (unpaired t test with Holm-Sidak's multiple comparisons test). AAH = atypical adenomatous hyperplasia. BH = bronchiolar hyperplasia. **C,** Fraction of lung tumor burden by grade (lung tumor area/ total lung area per grade). *p<0.05, **p<0.01, ***p<0.001 (unpaired t test with Holm-Sidak's multiple comparisons test). For both **B** and **C**, n≥7 mice and ≥1,000 tumors per genotype. $ = fewer than three tumors detected across all mice. Only one grade 5 and two grade 4 tumors were detected in the Nrf2[D29H/+] cohort, and therefore were excluded from the analyses.

In accordance with these findings, I also observed that $Nrf2^{D29H/+}$ increased the number of grade 2 tumors, while $Keap1^{R554Q/+}$ increased the number of grade 5 tumors **(Fig. 6.11A)**. As with my low-dose Cre experiment, I observed smaller AAH and grade 1 with $Nrf2^{D29H/+}$ mutation, and smaller grade 1 tumors with $Keap1^{R554Q/R554Q}$ mutation **(Fig. 6.11B)**. Finally, although I didn't see any changes in overall tumor number or tumor size **(Fig. 6.11C** and **D)**, I did see increased tumor burden with $Keap1^{R554Q/+}$ mutation **(Fig. 6.11E)**, which is likely accounted for by the increase in grade 5 tumor burden I observed **(Fig. 6.10C).**

I next measured Nrf2 activation in this model by performing IHC staining for Nrf2 and Nqo1. Interestingly, I saw that Nrf2 was similarly expressed across all models with Keap1/ Nrf2 mutation **(Fig. 6.12A)**. I did, however, see differences in relative Nrf2 activity, where the $Nrf2^{D29H/+}$ cohort had the most intense Nqo1 staining, followed by $Keap1^{R554Q/R554Q}$, and a non-significant trend increase in the $Keap1^{R554Q/+}$ genotype **(Fig. 6.12B)**. In this model, my data suggest that the level of Nrf2 activity (rather than total levels) may be more important for progression of tumors originating from alveolar type II cells. Additionally, as in my previous experiments, I saw that all tumors downregulated Nrf2 expression and activity as they progressed **(6.12C** and **D)**, consistent with selection of a more optimal level of Nrf2 activation for tumor progression.
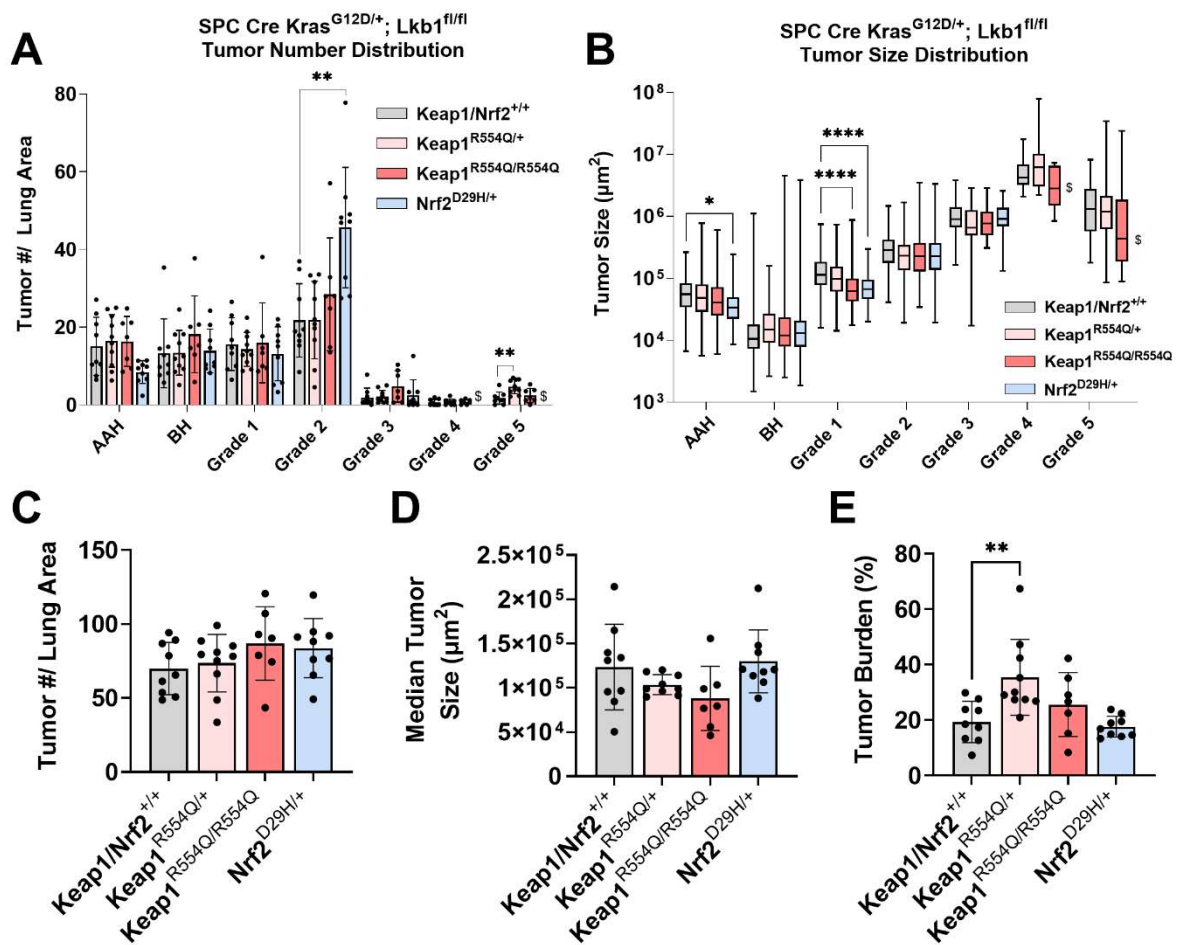
Figure 6.11. Lung tumor number, size, and burden in the SPC Cre Kras$^{G12D/+}$; Lkb1$^{fl/fl}$ model. **A,** Distribution of tumor number by grade across Keap1/Nrf2 mutant models. N$\geq$8 mice per genotype, *p<0.05, **p<0.01, ***p<0.001, ****p<0.0001 (unpaired t test with Holm-Sidak's multiple comparisons test). $ = fewer than three tumors detected across all mice. **B,** Tumor size across all mice per genotype. N$\geq$8 mice and $\geq$1,500 tumors per genotype. ****p<0.0001 (Kruskal-Wallis test with Dunn's multiple comparisons test). $ = fewer than three tumors detected across all mice. **C,** Tumor number per mouse normalized to lung area. **D,** Median tumor size per mouse for each genotype. **E,** Overall tumor burden (%) calculated by dividing the total area of lung tumor by the total area of the lung. For **C-E**, N$\geq$8 mice per genotype. *p<0.05, **p<0.01 (one-way ANOVA).

Figure 6.12. Keap1/ Nrf2 mutation activate Nrf2 in the SPC Cre Kras$^{G12D/+}$; Lkb1$^{fl/fl}$ model. **A** and **B,** H-scores for Nrf2 (nuclear) **(A)** and Nqo1 (whole-cell) **(B)** immunohistochemical (IHC) staining. N=3* mice per genotype and >20,000 tumor cells per mouse. *Note that there are only 2 mice in the Keap1/Nrf2$^{+/+}$ cohort. *p<0.05, **p<0.01, ***p<0.001, ****p<0.0001 (one-way ANOVA). **C** and **D,** Heatmaps depicting the H-scores per grade from IHC staining for Nrf2 (nuclear) **(C)** and the Nrf2 target Nqo1 (whole cell) **(D)**. N=3* mice per genotype, >20,000 tumor cells per mouse. *Note that there are only 2 mice in the Keap1/Nrf2$^{+/+}$ cohort. Only one grade 5 and two grade 4 tumors were detected in the Nrf2$^{D29H/+}$ cohort, and therefore were excluded from the analyses.

Next, I performed IHC staining for Nrf2 and Nqo1 across all of our models to be able to compare how Nrf2 activation was impacted. The models with the highest level of Nrf2 and Nqo1 expression were the ones that had a promotion of early tumor progression to low-grade tumors, namely Keap1$^{R554Q/R554Q}$ and Nrf2$^{D29H/+}$ in the Kras$^{G12D/+}$ cohort, Keap1$^{R554Q/R554Q}$ in the Kras$^{G12D/+}$; p53$^{fl/fl}$ cohort, and Nrf2$^{D29H/+}$ in both Kras$^{G12D/+}$; Lkb1$^{fl/fl}$ cohorts **(Fig. 6.13A** and **B)**. These models, except Kras$^{G12D/+}$, were also associated with a block in tumor progression, suggesting that excessively high levels of Nrf2 activation can promote early tumor progression, but impair progression to high-grade tumors.

Finally, I wanted to test the effect of Keap1/Nrf2 mutation on expression of another Nrf2 target gene, Taldo1. I performed IHC staining for Taldo1 and observed levels of relative Nrf2 activity comparable to my findings with Nqo1 **(Fig. 6.14)**. I saw that Keap1$^{R554Q/R554Q}$ was the most activating in the Kras$^{G12D/+}$ and Kras$^{G12D/+}$; p53$^{fl/fl}$ models, while Nrf2$^{D29H/+}$ was the most activating in both Kras$^{G12D/+}$; Lkb1$^{fl/fl}$ models. I also observed that tumors downregulated Taldo1 expression as they progressed.
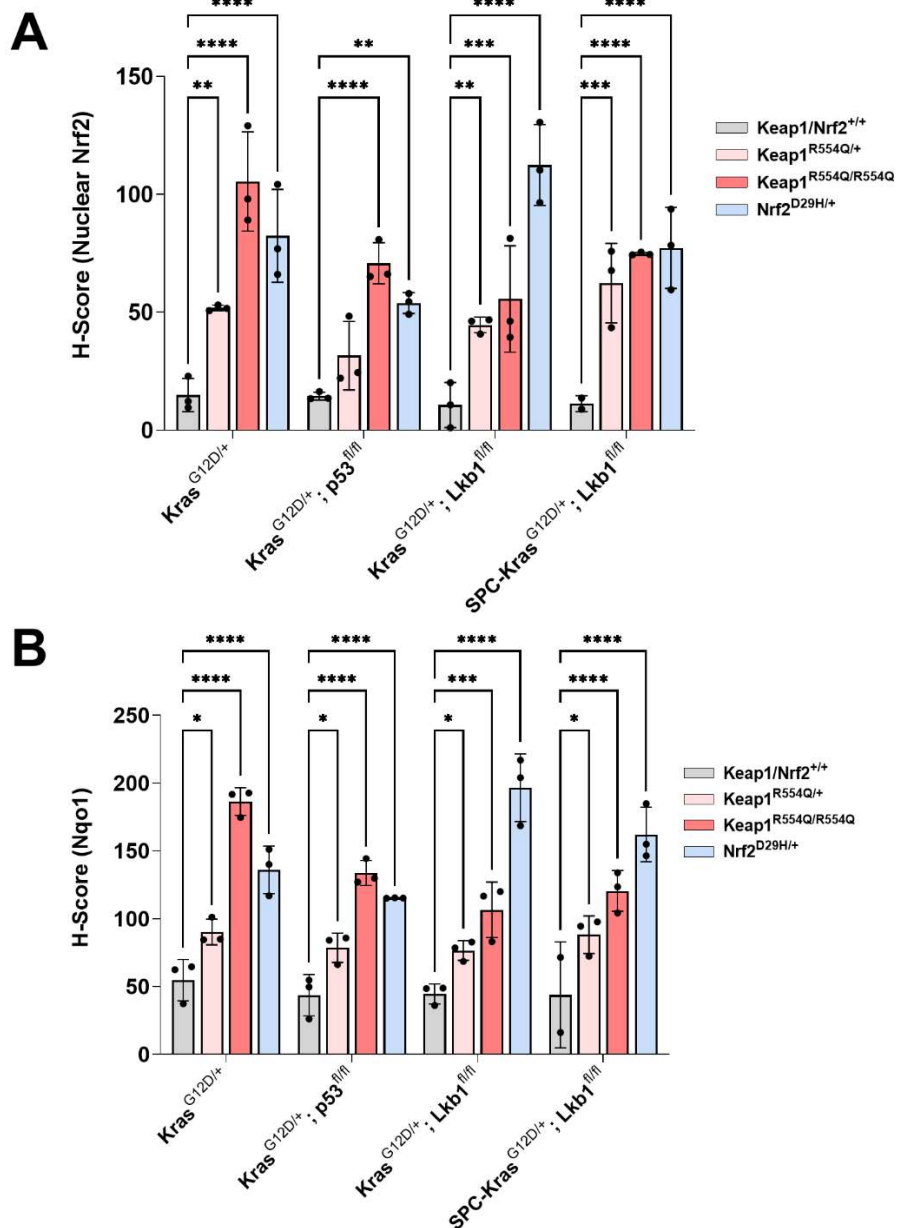
Figure 6.13. Nrf2 activation across all models with Keap1/ Nrf2 mutation. **A** and **B,** H-scores for nuclear Nrf2 **(A)** and whole-cell Nqo1 **(B)** immunohistochemical staining across the Kras$^{G12D/+}$, Kras$^{G12D/+}$; p53$^{fl/fl}$, low-dose Cre Kras$^{G12D/+}$; Lkb1$^{fl/fl}$, and SPC Cre Kras$^{G12D/+}$; Lkb1$^{fl/fl}$ models. N=3* mice per genotype, >20,000 tumor cells per mouse. *Note that there are only 2 mice in the SPC-Kras$^{G12D/+}$; Lkb1$^{fl/fl}$ Keap1/Nrf2$^{+/+}$ cohort. *p<0.05, ***p<0.001, ****p<0.0001 (two-way ANOVA with Dunnett's multiple comparisons test).
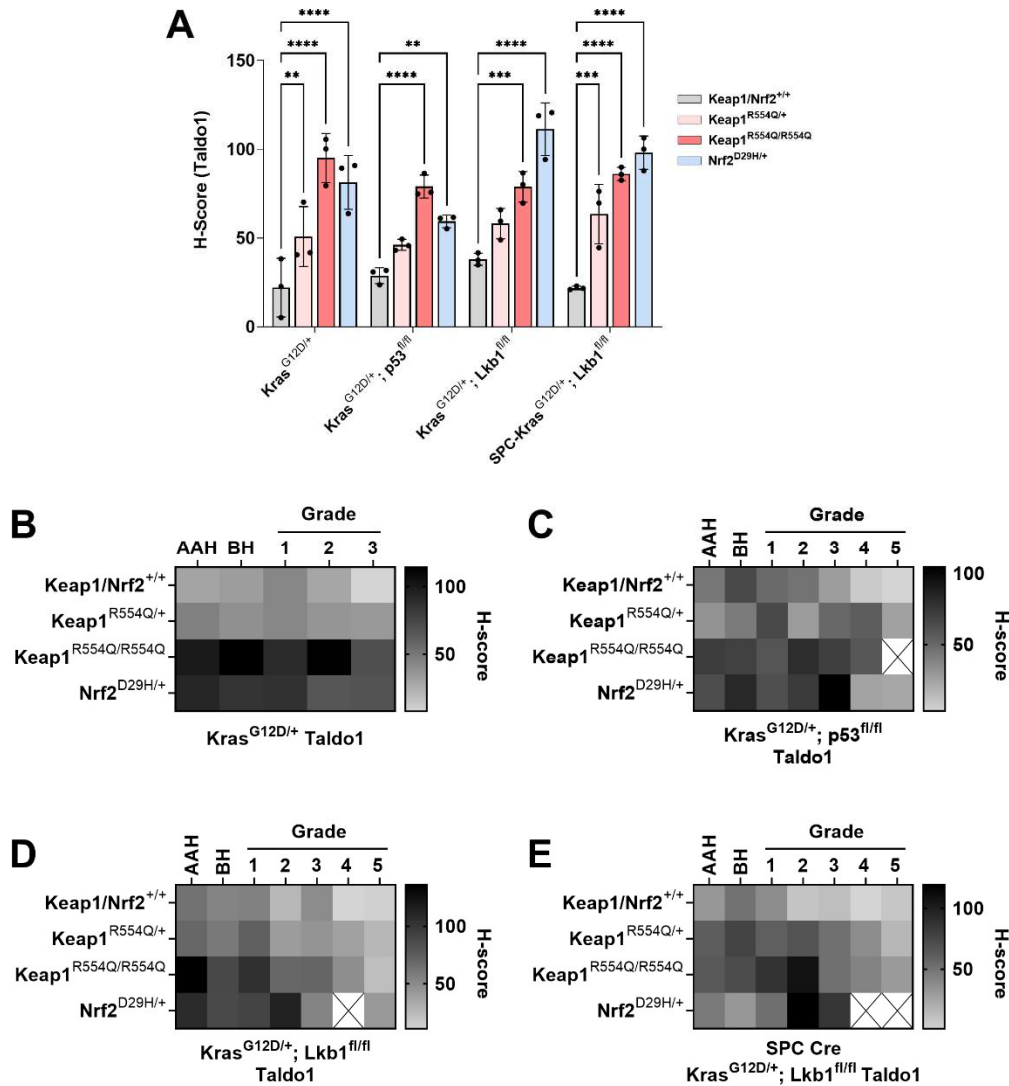
Figure 6.14. Keap1/ Nrf2 mutation increase expression of Nrf2 target gene Taldo1. **A,** H-scores for whole-cell Taldo1 across the Kras[G12D/+], Kras[G12D/+]; p53^{fl/fl}, low-dose Cre Kras[G12D/+]; Lkb1^{fl/fl}, and SPC Cre Kras[G12D/+]; Lkb1^{fl/fl} models. **p<0.01, ***p<0.001, ****p<0.0001 (two-way ANOVA with Dunnett's multiple comparisons test). **B-E,** Heatmaps depicting the H-scores per grade from IHC staining for Taldo1. For **A-E,** N=3 mice per genotype, >20,000 tumor cells per mouse. Note that no grade 4 tumors were found in the Kras[G12D/+]; Lkb1^{fl/fl}; Nrf2[D29H/+] cohort. Only one grade 5 tumor was found in the Kras[G12D/+]; p53^{fl/fl}; Keap1[R554Q/R554Q] cohort, one grade 5 and two grade 4 tumors in the SPC Kras[G12D/+]; Lkb1^{fl/fl}; Nrf2[D29H/+] cohort, and therefore were excluded from the analyses.

Discussion

I discovered that the Nrf2$^{D29H/+}$ mutation was the most activating in the Kras$^{G12D/+}$; Lkb1$^{fl/fl}$ model, in contrast to what I had observed in the Kras$^{G12D/+}$; and Kras$^{G12D/+}$; p53$^{fl/fl}$ models, where Keap1$^{R554Q/R554Q}$ was the most activating towards Nrf2. Further investigation is warranted to determine why these mutations differentially effect Nrf2 activation in different mutational backgrounds. It has also previously been reported that NRF2 activity is increased with co-mutation *of STK11/KEAP1* compared to *KEAP1* mutation alone (160), which may partially explain the differences I see between the models. To interrogate this, I could check what is bound to Nrf2 in both backgrounds and determine whether this affects activity. For example, β-TrCP can bind to the Neh6 domain of NRF2, causing NRF2 ubiquitination (20). AMP-activated protein kinase (AMPK), which is activated by LKB1, can disrupt this binding through GSK3β, which could affect NRF2 activation (186). I also would need to determine the relative expression of both Keap1 and Nrf2 between the models.

I also observed that the most activating mutant, Nrf2$^{D29H/+}$, promoted early progression and blocked advanced-grade adenocarcinoma progression, reminiscent of what I had observed with Keap1$^{R554Q/R554Q}$ in the Kras$^{G12D/+}$; p53$^{fl/fl}$ model. These results support a threshold effect for Nrf2 during lung tumor initiation and progression. It is also interesting that Nrf2$^{D29H/+}$ decreased overall survival in our first experiment, but not when the adenovirus dose was lowered or SPC Cre was used. In our initial experiment, the mice died as a result of hyperplasia, rather than advanced tumors, as I saw that Nrf2$^{D29H/+}$ mice had extensive tumor burden characterized by numerous small tumors.

This finding fits with my previous experiment showing that Nrf2 activation promotes lung tumor initiation and low-grade tumor progression **(Figure 3.3)**.

It seemed that the SPC Cre model is most representative of the human condition, as this Cre was specific to the hypothesized cell-of-origin for lung adenocarcinoma, alveolar type II cells. Moreover, squamous cell carcinoma patients rarely have mutations in *STK11* or *KRAS*. My experiments with CMV Cre in this model were confounded by the presence of squamous tumors, although I did not observe any in the Nrf2$^{D29H/+}$ cohort. It was also curious that Keap1$^{R554Q/+}$ promoted progression to grade 5 tumors in the SPC Cre model, which may be supportive of an optimal Nrf2 level needed to cooperate with Lkb1 deletion. Moreover, in lung cancer patient tumors with a KEAP1 mutation, loss-of-heterozygosity is often observed, indicating that tumors usually start with only one copy mutated. This could be partially why the Keap1$^{R554Q/+}$ promoted tumor progression in this Lkb1-deficient model. Overall, my data supports a threshold effect for Nrf2 in lung tumor initiation and progression, given that the models with the highest degree of Nrf2 activation promote early progression but block adenocarcinoma progression.

Chapter Seven: Understanding the mechanisms by which NRF2 hyperactivation can impair tumor cell proliferation and progression[6]

Introduction

Because my data suggested evidence for a Nrf2 threshold *in vivo*, I wanted to see if I could further interrogate this using an *in vitro* system. One hypothesis for why excess Nrf2 activation could be detrimental to tumor progression was the potential for reductive stress, an accumulation of excess reducing equivalents that has been linked to NRF2 activation (80, 81) and can have detrimental effects on cell proliferation. To interrogate this mechanism, I overexpressed NRF2 in a panel of Keap1 mutant NSCLC cell lines and evaluated their phenotype. I also performed experiments to determine whether the effects of NRF2 are based on its target genes. Finally, I used IHC to interrogate potential mechanisms related to the tumor progression block.

---

[6] Note to reader: Portions of this chapter have been previously published in DeBlasi et al. 2023, *Cancer Research* (154). **J.M. DeBlasi:** Data curation, formal analysis, investigation, visualization, methodology, writing–original draft, writing–review and editing. **A. Falzone, S. Caldwell, N. Prieto Farigua:** Mouse colony management and collections - Data curation, investigation, methodology, writing–review and editing. **J.R. Prigge, E.E. Schmidt:** Nrf2 antibody for IHC - Resources, writing–review and editing. **I.I.C. Chio:** Nrf2 targeting vector antibody for IHC - Resources, writing–review and editing. **F.A. Karreth:** ES cell targeting - Resources, methodology, writing–review and editing. **G.M. DeNicola:** Mouse models, RNA-sequencing - Conceptualization, resources, data curation, formal analysis, supervision, funding acquisition, investigation, methodology, writing–original draft, project administration, writing–review and editing.

KEAP1 mutations are associated with NRF2 dependence in NSCLC

Previous work has reported that KEAP1 mutant lung cancer cells are "NRF2-addicted" meaning that they depend on NRF2 for their proliferation (187). To support this, analysis of DepMap data (188) indicated that NSCLC cell lines with high NRF2 activity (46), which were enriched for KEAP1 mutations, demonstrated dependence on NRF2 **(Fig. 7.1A)**.
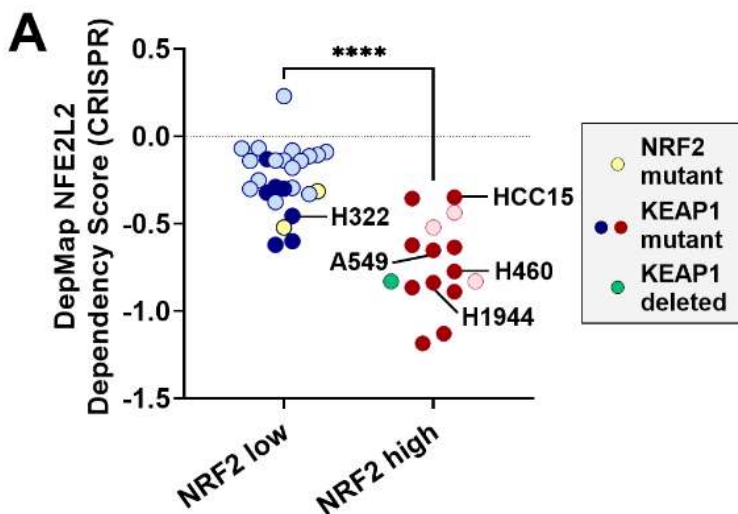
Figure 7.1. NSCLC cells with high NRF2 activity exhibit NRF2 dependence. **A,** Dependency scores obtained from DepMap(188) and represented as *NFEL2* 22Q2 Public+Score, Chronos for NSCLC cell lines previously determined to have high or low NRF2 activity(46). NRF2 mutant line symbols are represented by yellow, KEAP1 mutant lines by dark red or dark blue, and KEAP1 deleted lines by green. ***p<0.0001 (unpaired t-test). This figure was previously published in *Cancer Research*, DeBlasi et al. 2023 (154).

NRF2 overexpression impairs NSCLC cell proliferation, viability, and anchorage-independent colony formation

To directly interrogate my hypothesis that excess NRF2 activation above a specific threshold is detrimental to lung tumor cell proliferation, I used lentiviral transduction to overexpress wild-type NRF2 in five KEAP1 mutant lung cancer cell lines (H1944, H322, A549, HCC15, H460). I verified overexpression of NRF2 via western blot analysis of NRF2 and targets GCLC, xCT, and GSR **(Fig. 7.2A)**. I observed increased expression of NRF2 in all cell lines and increased expression of NRF2 targets upon lentiviral transduction, indicating that NRF2 binding sites were not saturated by the level of NRF2 in these cells **(Fig. 7.2A)**. I then examined the effect of NRF2 overexpression on cell proliferation and viability over the course of four days using live cell imaging **(Fig. 7.2B-F)**. Similar to what I observed in the $Kras^{G12D/+}$; $p53^{fl/fl}$ model upon $Keap1^{R554Q/R554Q}$ mutation, I observed that NRF2 overexpression decreased cell proliferation in all cell lines **(Fig. 7.2E)**. Additionally, I saw that NRF2 overexpression increased cell death in 4 out of 5 cell lines **(Fig. 7.2F)**.
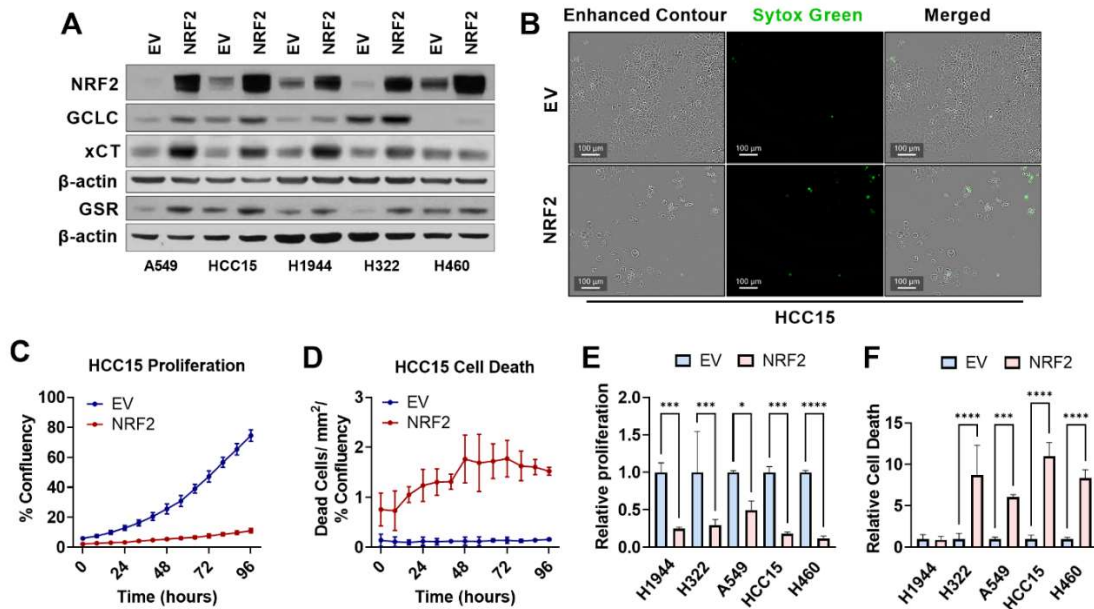
Figure 7.2. NRF2 overexpression impairs lung cancer cell proliferation and viability. **A,** Western blot analysis of NRF2, β-actin, and NRF2 target GCLC, xCT, and GSR expression in *KEAP1* mutant lung cancer cell lines transduced with pLX317-empty vector (EV) or pLX317-NRF2 (NRF2). **B,** Representative images of HCC15 cells transduced with EV or NRF2 demonstrating cell confluency (enhanced contour) and cell death (Sytox Green) (scale bars = 100 μm). **C, D,** Analysis of EV and NRF2 HCC15 cell proliferation and death over 96 hours. Proliferation is represented as % confluency at each time point, and cell death as the number of Sytox Green positive cells per area normalized to % confluency. N=3 technical replicates per cell line, and two independent experiments. **E, F,** Area under the curve (AUC) analysis of cell proliferation **(E)** and Sytox Green-positive cell death **(F)** in KEAP1 mutant lung cancer cells lines +/- NRF2, normalized to empty vector control. *p<0.05, ***p<0.001, ****p<0.0001 (one-way ANOVA). For **B-F** NSCLC cells were seeded in triplicate in 96-well plates at a density of 2,500 cells/ well. This figure was previously published in *Cancer Research*, DeBlasi et al. 2023 (154).

I also observed impaired anchorage-independent colony formation in soft agar in all cell lines **(Fig. 7.2H** and **I)**. These results suggest that there is an optimal threshold of NRF2 expression and activity permissive for lung cancer cells *in vitro*, and that excessive NRF2 activation can impair lung cancer phenotypes.
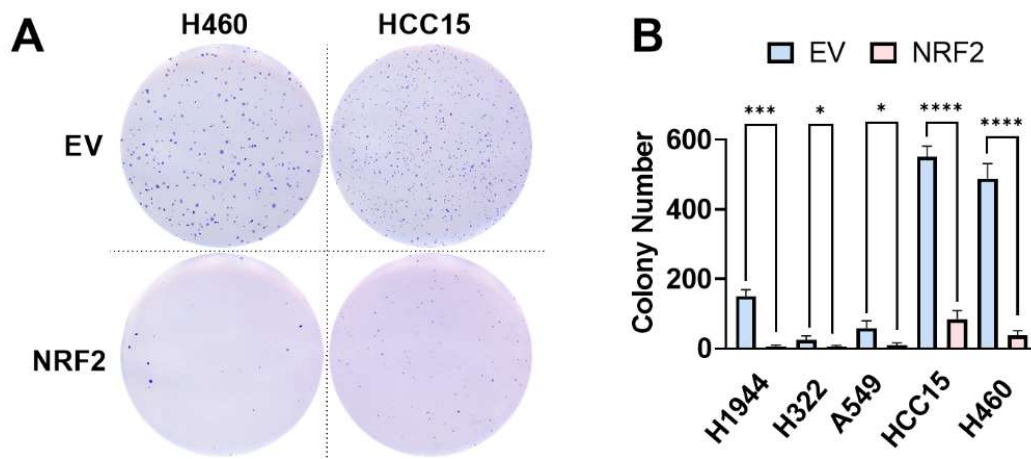
Figure 7.3. NRF2 overexpression impairs anchorage-independent soft agar colony formation. **A,** Representative images of H460 and HCC15 soft agar colony formation +/- NRF2. **B,** Quantification of soft agar colony number of *KEAP1* mutant lung cancer cell lines. *p<0.05 (one-way ANOVA). N=3 technical replicates per cell line, two independent experiments. For **A** and **B,** 5,000 cells per well were seeded in 6-well plates in triplicate. This figure was previously published in *Cancer Research*, DeBlasi et al. 2023 (154).

Investigating how excess Nrf2 activation can impair tumor cell proliferation

I next wanted to interrogate the mechanism(s) by which high levels of Nrf2 could impair tumor cell proliferation and tumor progression. First, I determined whether the effects of NRF2 were dependent on its target genes. In order to this, Cheyenne Schneider in our lab created a transcriptionally inactive version of NRF2 lacking the transactivation domain (ΔNEH4/5), where NRF2 could still bind DNA, but there would be no transcription of its target genes, as previously described by another group (19). I overexpressed empty vector (EV) control, wild-type (WT) NRF2, and ΔNEH4/5 NRF2 in a panel of Keap1 mutant NSCLC cell lines. I observed comparable expression of NRF2 with WT and ΔNEH4/5 overexpression (**Fig. 7.4. A).** Moreover, while I saw induction of NRF2 target genes GSR and HMOX1 with WT NRF2 overexpression in most of the cell lines, I did not see this induction in the ΔNEH4/5 mutant, indicating a lack of NRF2 transcriptional activity. Additionally, I saw that unlike WT NRF2, ΔNEH4/5 NRF2 did not impair NSCLC cell proliferation or viability **(Fig. 7.4 B** and **C),** indicating that NRF2's antiproliferative effects are dependent on its transcriptional activity.
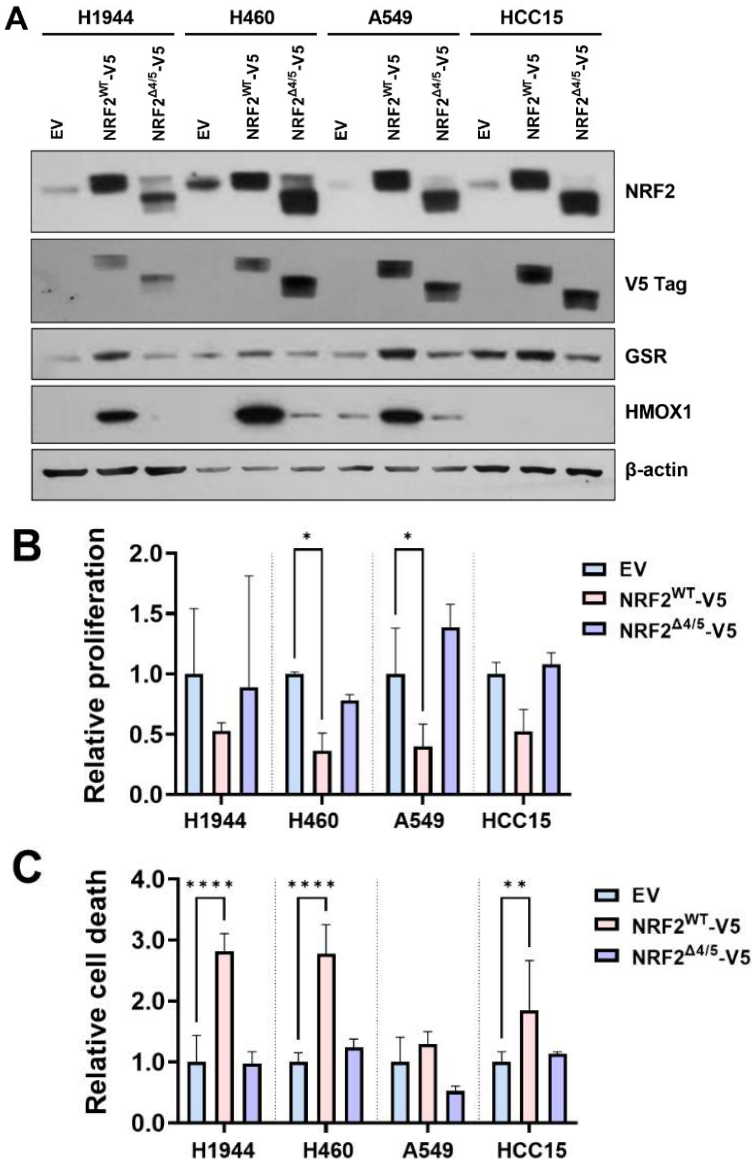
Figure 7.4. Transcriptionally inactive NRF2 does not impair tumor cell proliferation or viability. **A,** Western blot analysis of NRF2, V5 tag, β-actin, and NRF2 targets GSR and HMOX1 expression in *KEAP1* mutant lung cancer cell lines transduced with PLX317-empty vector (EV), PLX317-NRF2^WT-V5, or PLX317-NRF2^Δ4/5-V5. **B, C,** Area under the curve (AUC) analysis of cell proliferation **(B)** and Sytox Green-positive cell death **(B)** in KEAP1 mutant lung cancer cells lines, normalized to empty vector control. Proliferation is represented as % confluency at each time point, and cell death as the number of Sytox Green positive cells per area normalized to % confluency. N=3 technical replicates per cell line. *p<0.05, **p<0.01, ****p<0.0001 (one-way ANOVA). For **B-C**, NSCLC cells were seeded in triplicate in 96-well plates at a density of 2,500 cells/ well.

Next, because my results suggests that Nrf2's effects are transcriptional, I

performed experiments to test whether reductive stress was contributing to the NRF2-

mediated proliferation and viability defect. NRF2-mediated transcriptional regulation of

the GSH and TXN systems could promote excess reducing equivalents, as previously

observed in a mouse model of cardiomyopathy (80). NRF2 has also been recently

reported to promote reductive stress via NADH in NSCLC cell lines (82). To test the

hypothesis that excess reducing equivalents are responsible for NRF2's effects *in vitro*,

I treated H460 and HCC15 cells with buthionine sulfoximine (BSO) to block gamma-

glutamylcysteine synthetase and subsequent GSH synthesis, auranofin to inhibit

TXNRD1, or erastin to inhibit xCT/ impair cysteine metabolism/ GSH synthesis. I used

concentrations of these drugs previously validated by our lab (89, 189) and performed

the treatment upon selection for NRF2 overexpression or empty vector control

expression. I observed that none of these drugs rescued the proliferation or viability

defect caused by NRF2 overexpression **(Fig. 7.5)**.
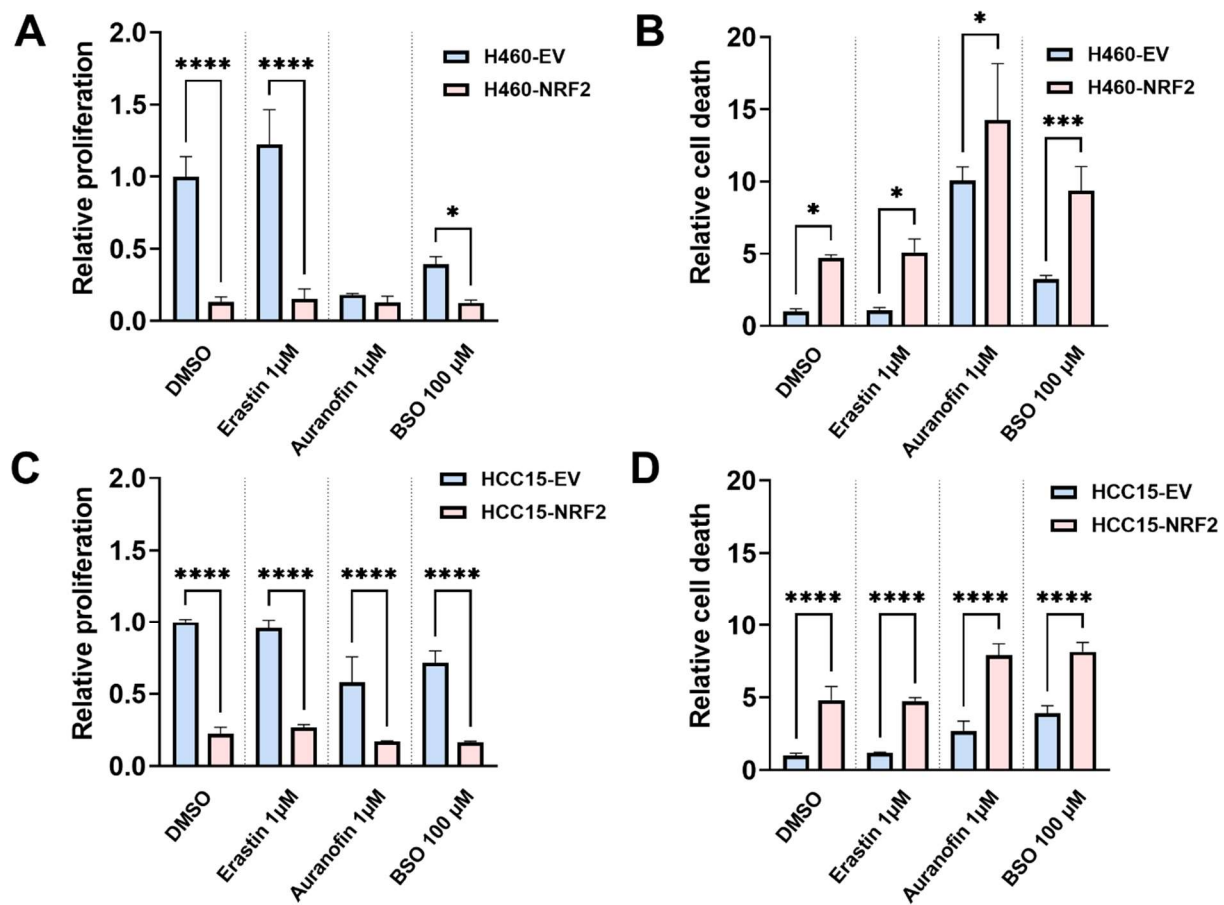
Figure 7.5. Blocking cysteine metabolism or inducing ROS does not rescue NRF2-mediated proliferation or viability defect in H460 or HCC15 cells. **A-D**, Area under the curve (AUC) analysis of cell proliferation **(A, C)** and Sytox Green-positive cell death **(B, D)** in H460 and HCC15 cells +/- NRF2, normalized to empty vector control treated with DMSO. *$p < 0.05$, ***$p < 0.001$, ****$p < 0.0001$ (one-way ANOVA). Cells were seeded in triplicate in 96-well plate at a density of 2,500 cells/ well.

In another attempt to see if GSH was mediating NRF2's toxicity, I also examined

the effects of CRISPR-mediated deletion of GSR. I used GSR knockout A549 cell

generated by Chang Jiang in our lab and performed overexpression of NRF2 to see if

this could protect against NRF2's effects. I did not observe any rescue effect **(Fig. 7.6)**,

suggesting that glutathione may not be responsible for NRF2's detrimental effects *in*

vitro.
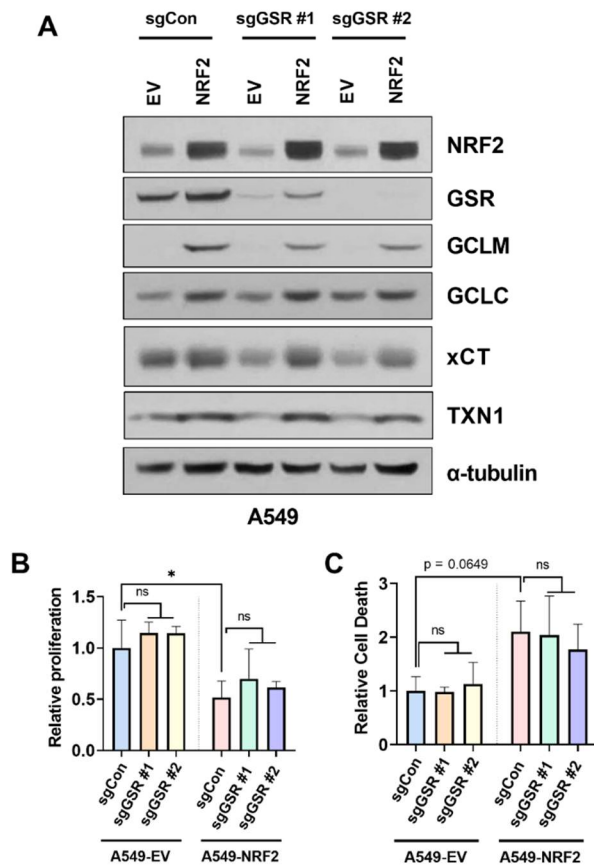
Figure 7.6. GSR deletion does not rescue NRF2-mediated proliferation defect in A549
cells. **A,** Western blot analysis of NRF2, α-tubulin, NRF2 targets GSR, GCLM, GCLC,
xCT, TXN1 expression in A549 cells transduced with pLX317-empty vector (EV) or
pLX317-NRF2 (NRF2). **B, C,** Area under the curve (AUC) analysis of cell proliferation
(B) and Sytox Green-positive cell death **(C)** in A549 cells +/- NRF2, normalized to empty
vector control with sgControl (sgCon). *$p < 0.05$, ns=non-significant (one-way ANOVA).
Cells were seeded in triplicate in 96-well plate at a density of 2,500 cells/ well.

Understanding how excess Nrf2 activation can impair tumor progression

Alongside my *in vitro* experiments, I also wanted to investigate potential mechanism(s) for the progression block in our mouse models. My supervisor previously observed in a pancreatic cancer mouse model that Nrf2 deletion promoted metastasis to the lung, and that this was associated with increased extracellular signal-regulated kinase (ERK) activity (149). I hypothesized that excess Nrf2 activation in our model may be decreasing ERK activity, suppressing invasiveness and progression. To test this, I performed IHC staining for phospho-ERK in Keap1/ Nrf2$^{+/+}$ and. I did not observe any meaningful changes in staining across cohorts, possibly indicating either a technical/ lack of specificity issue, or no actual changes in this pathway in our model **(Fig. 7.7A and B)**. A previous study showed that phospho-ERK staining was increased in adenocarcinomas compared to adenomas in the Kras$^{G12D/+}$; p53$^{fl/fl}$ model (190), which I did not observe. This study measured phospho-ERK staining in 7- and 10-week-old tumors, however, whereas I measured at end-of-life (~14-17 weeks), so it is also possible that tumors do not need to upregulate phospho-ERK at this later time point.
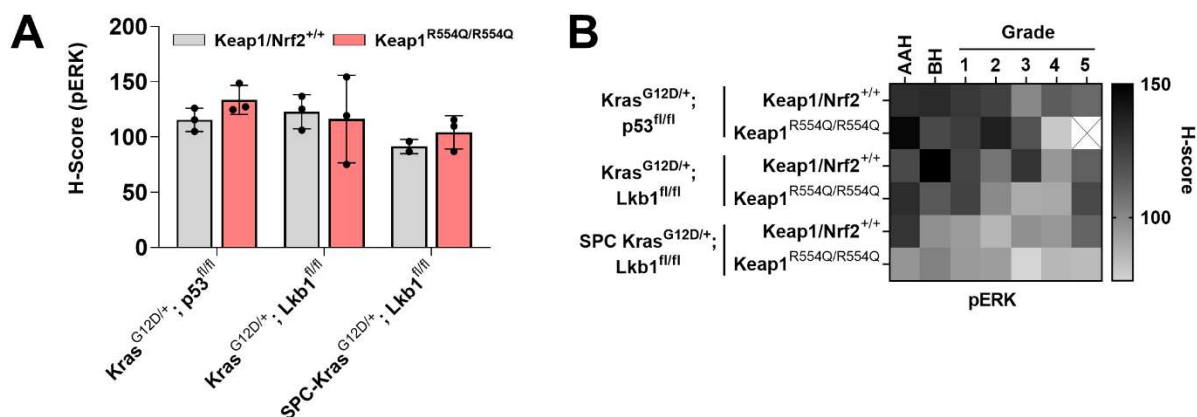
Figure 7.7. Nrf2 activation does not affect phospho-ERK levels in Keap1[R554Q/R554Q] mutant models. **A,** H-scores for phospho-ERK (pERK) IHC staining across mouse models with or without homozygous Keap1 mutation. Two-way ANOVA with Dunnett's multiple comparisons test. **B,** Heatmaps depicting the H-scores per grade from IHC staining for pERK staining. N=3* mice per genotype, >20,000 tumor cells per mouse. *Note that there are only 2 mice in the SPC-Kras[G12D/+]; Lkb1^{fl/fl} Keap1/Nrf2^{+/+} cohort. Only one grade 5 tumor was found in the Keap1[R554Q/R554Q] cohort, and therefore was excluded from these analyses.

Next, to test my hypothesis that redox status is altered in Keap1/ Nrf2 mutant tumors I performed IHC staining for 4-HNE, a by-product and marker of lipid peroxidation. I did not see any significant changes in staining, except for an increase in lipid peroxidation in the Kras[G12D/+]; Lkb1^{fl/fl}; Nrf2[D29H/+] model **(Fig. 7.8A-E)**. This may be an artifact though, given that NRF2 is important for mitigating lipid peroxidation (191), and suggests that 4-HNE may not be a good indicator of NRF2 activation/ overall oxidation status in these models. Moreover, although 4-HNE can induce oxidative stress, at low concentrations it has been reported that 4-HNE can be cytoprotective through NRF2-mediated TXNRD1 activation (192). This crosstalk may influence the IHC results, and there is also a possibility for lack of antibody specificity in this experiment since I did not use a positive control.
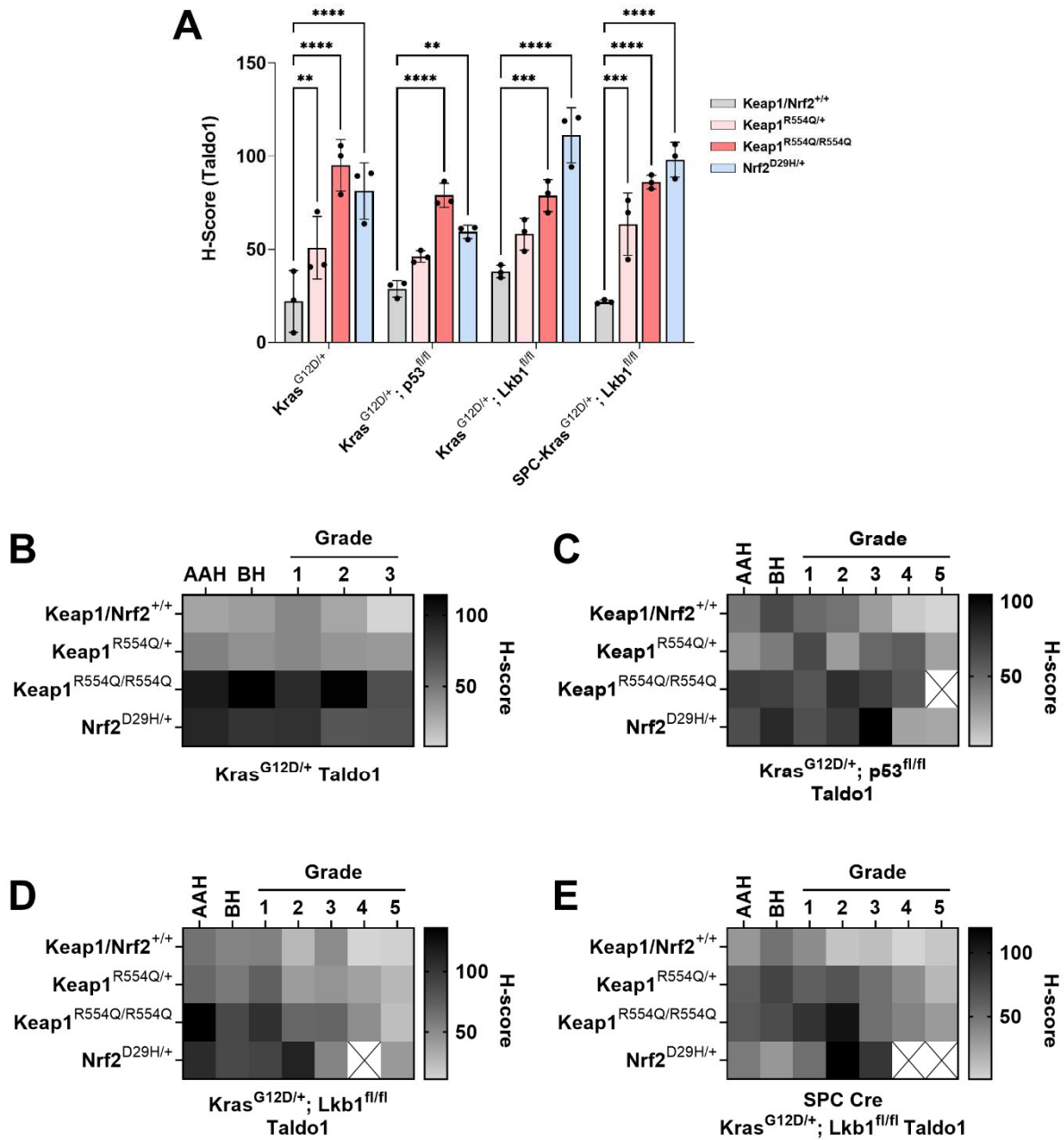
Figure 7.8. Keap1/ Nrf2 mutation differentially affect lipid peroxidation across Kras$^{G12D/+}$ mouse models. **A,** H-scores for 4-HNE IHC staining across Keap1/ Nrf2 mutant mouse models. *p<0.05 (two-way ANOVA with Dunnett's multiple comparisons test). **B-E,** Heatmaps depicting the H-scores per grade from IHC staining for 4-HNE. For **A-E**, n=3 mice per genotype, >20,000 tumor cells per mouse.

Discussion

I observed that wild type NRF2 overexpression impairs NSCLC cell lines proliferation, viability, and anchorage-independent colony formation. I also observed that these effects were dependent on NRF2 target genes, as overexpression of a transcriptionally inactive version of NRF2 did not impair cancer phenotypes. Although I did not see any rescue effects with my drug treatment or sgGSR experiments, it is possible that the timing of drug treatment was too late (i.e., I could have pre-treated with these drugs prior to selection), and/or that GSH, TXN, nor xCT are contributing to NRF2's detrimental effects. Looking at redox status could be informative as to whether reductive stress is a possible mechanism. I also did not test NADH-mediated reductive stress, which was reported by another group using a pharmacological NRF2 activator *in vitro* (82). In addition to measuring the NADH/NAD+ ratio in cell lines with NRF2 overexpression, I could also treat cells with the NAD+ precursor α-ketobutyrate to promote NADH recycling.

Moreover, I did not observe any changes *in vivo* with pERK or 4-HNE staining, which could potentially be due to lack of antibody specificity. Regarding pERK, it has been previously observed that pERK expression is low in low-grade adenomas, but high in adenocarcinomas in the $Kras^{G12D/+}$; $p53^{fl/fl}$ model (190). It is also possible that lipid peroxidation may not change even if there are changes in NADPH/ NADP+, NADH/ NAD+, or GSH/GSSG ratios, warranting the need for a direct measure of protein redox states in the mouse models and cell lines with NRF2 overexpression. A technical limitation faced with this approach, however, was that the tumors in the $Kras^{G12D/+}$; $p53^{fl/fl}$; $Keap1^{R554Q/R554Q}$ model were too small to cut out and freeze. I only had formalin-

fixed paraffin-embedded (FFPE) tissue, therefore limiting my ability to conduct assays where frozen tissue is needed.

Additional work is needed to determine the mechanism(s) by which NRF2 impairs cell proliferation and viability, as well as tumor progression. Additional experiments could also include treating Kras$^{G12D/+}$; p53$^{fl/fl}$; Keap1$^{R554Q/R554Q}$ mice with BSO to block glutathione synthesis or auranofin to inhibit thioredoxin reductase and see if this rescues the progression block, and/ or treating Kras$^{G12D/+}$; p53$^{fl/fl}$ mice with N-Acetylcysteine (NAC) to see if this phenocopies the effects of Nrf2 activation via the accumulation of reducing equivalents. Ongoing work in our lab will also determine whether knockout of major cytosolic reductases, glutathione reductase (GSR), or thioredoxin reductase 1 (TXNRD1) rescues the Keap1$^{R554Q/R554Q}$-mediated progression block.

Chapter Eight: Implications and Future Directions[7]

My data indicate that constitutive Nrf2 activation is not sufficient to initiate lung tumorigenesis, even in the context of of tumor suppressor deletion (p53 or Lkb1 up to 500 days). These findings correspond with previous work demonstrating that Keap1 loss is insufficient to cause lung tumor formation, alone (133), and also in the context of p53 or Lkb1 deletion up to ~350-450 days (34). Additionally, this work is important when considering NRF2 activation as a potential modality for chemoprevention. Beyond NRF2 activators that have been explored for this purpose (29, 152), omaveloxolone, a newly developed NRF2 activator, has been FDA-approved in patients with Friedreich's ataxia, and is safe with minimal toxicity (161). It would be interesting to see how the $Kras^{G12D/+}$; $p53^{fl/fl}$ and $Kras^{G12D/+}$; $Lkb1^{fl/fl}$ models respond to pharmacological Nrf2 activation, given that we've only tested the effects of Nrf2 activation prior to lung tumor initiation. Moreover, this treatment would activate Nrf2 in the microenvironment, unlike our mouse models. Since a previous study showed that Nrf2 activation in immune cells impairs early progression of Nrf2-active tumors, it is possible that a pharmacological Nrf2 activator may have a similar effect *in vivo*. Moreover, it would be important to titrate the level of Nrf2 activation with the drug, as a certain threshold is likely needed to impair late tumor progression. A potential challenge could be if excess Nrf2 activation

---

[7] Note to reader: Portions of this chapter have been previously published in a review article in DeBlasi and DeNicola 2020, *Cancers (Basel)* (1). J. M. DeBlasi and G. M. DeNicola: Conceptualization, draft preparation, review and editing.

becomes detrimental to immune cells as well, although this has not been previously reported. I also discovered that Nrf2 activation promotes lung tumor initiation in the Kras$^{G12D/+}$ model of early lung adenocarcinoma. These findings corroborate previous studies showing that Keap1 deletion promotes initiation in the Kras$^{G12D/+}$ model (34, 144). My results also unexpectedly revealed that excess Nrf2 activation can impair tumor progression in both the Kras$^{G12D/+}$; p53$^{fl/fl}$ and Kras$^{G12D/+}$; Lkb1$^{fl/fl}$ models in a dosage-dependent manner. These findings are summarized in **Figure 8**.
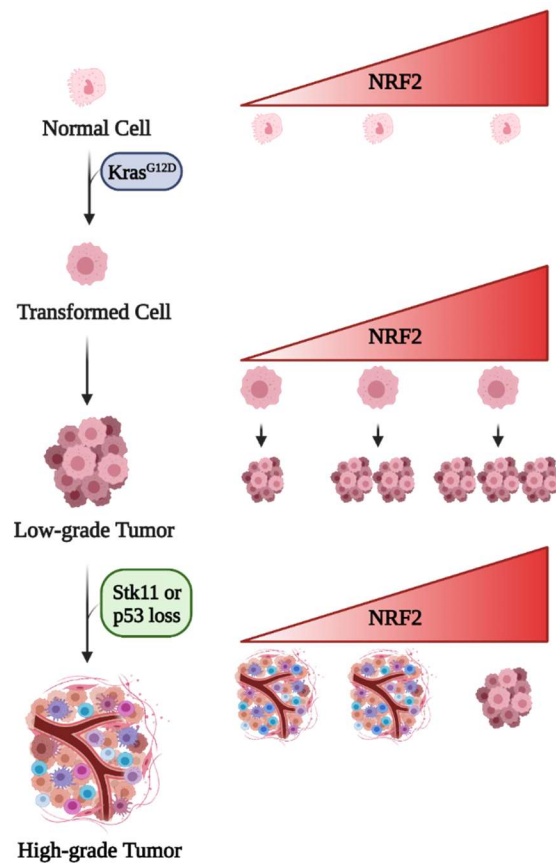
Figure 8. Working model of Nrf2 threshold in lung tumor initiation and progression. NRF2 exhibits context-dependent roles in lung tumorigenesis and progression. NRF2 activation is not sufficient to transform normal cells, even in the absence of tumor suppressor genes, but can promote Kras^{G12D} lung tumor initiation. At low levels, Nrf2 permits tumor progression; however, at high levels, Nrf2 blocks progression to advanced-grade tumors. Created with BioRender.com

Previous work from our lab reveal that the Keap1$^{R554Q/R554Q}$ mutation caused smaller tumors in the Kras$^{G12D/+}$; p53$^{fl/fl}$ model (43), which my analyses revealed is a result of impaired tumor progression caused by high Nrf2 activity. This observation of blocked tumor progression with Nrf2 activation has not reported by other groups studying Nrf2 in lung cancer mouse models. Some studies observed the Keap1 deletion promotes adenocarcinoma progression (45, 136), whereas others did not analyze tumor grade (34, 134, 146). The studies that reported increased progression with Keap1 inactivation used either a floxed allele (136) or CRISPR-mediated deletion (45). It's possible that complete Keap1 deletion was not achieved in all lung tumor cells, thus resulting in more modest Nrf2 activation compared to our Keap1/ Nrf2 mutant models. CRISPR-mediated deletion in cells is also variable (can be heterozygous or homozygous), and the Cas9 protein has been reported to cause immunogenicity (162), which can influence disease progression. Additionally, there are distinct biological differences between deletion vs. mutation of Keap1. These studies also did not observe any grade 5 tumors in the Kras$^{G12D/+}$; p53$^{fl/fl}$ model (45, 136), unlike studies by us and others (154, 166, 193), and they did not analyze hyperplasia. Moreover, they did not check whether Nrf2 levels were downregulated in higher-grade tumors.

It is curious that Keap1$^{R554Q/R554Q}$ blocked progression in the Kras$^{G12D/+}$; p53$^{fl/fl}$ model, whereas Nrf2$^{D29H/+}$ blocked progression in the Kras$^{G12D/+}$; Lkb1$^{fl/fl}$ model. Further investigation is warranted to determine why Keap1 mutation is more activating in the context of p53 loss, whereas Nrf2 mutation is more activating with Lkb1 deletion. Previous work has shown that Keap1 mutation and Lkb1 deletion cooperate to enhance Nrf2 activity (compared to Keap1 mutation alone) (160), but it is still unclear if this

applies to the mouse models in my experiments, and why Keap1 vs. Nrf2 mutation elicit different effects in different mutational backgrounds. There could be influences from the tumor microenvironment, and/ or the relative expression of Keap1/ Nrf2 in these models. Moreover, in the mouse genome, *Keap1* and *Stk11* are located on different chromosomes, whereas in humans, *KEAP1* and *STK11* are both on chromosome 19 (160). Therefore, it is likely a combination of external factors that dictate how these mutations influence tumor phenotypes and relative Nrf2 activity. Furthermore, Nrf2's threshold-dependent effects are comparable to what has been previously reported for oncogenes Myc and Ras, where low levels support transformation and cell proliferation, but excess levels can cause senescence or cell death (194, 195).

An important consideration for this work was whether the block in progression in the Keap1$^{R554Q/R554Q}$ model was dependent on Nrf2. Beyond NRF2, KEAP1 has additional substrates that play roles in mitochondrial homeostasis and DNA. damage repair, including PGAM5 (173), PALB2 (174), MCM3 (175) and EMSY (176). It is plausible that dysregulation of these proteins could impair tumor progression. Although this possibility cannot be entirely excluded, my data suggests that Nrf2 hyperactivation plays a direct role in the Keap1^{R554Q}-mediated tumor progression block, given that Nrf2 deletion rescues this phenotype. This is also supported by the finding that high levels of Nrf2 via Nrf2$^{D29H/+}$ in the Kras$^{G12D/+}$; Lkb1$^{fl/fl}$ model also block progression, and that overexpression of NRF2 in human lung cancer cell lines impairs their proliferation, viability, and anchorage-independent growth. Moreover, I observed that lung tumors downregulate Nrf2 expression and activity during tumor progression, suggesting that high levels of Nrf2 are not favorable for progression.

In corroboration with these results, it has been reported that a Keap1-binding defective Nrf2^{E79Q} mouse model of small-cell lung cancer (SCLC) with p53/ p16 inactivation (164) exhibited downregulation of Nrf2 in aggressive SCLC tumors, although the mechanism of how tumors downregulate Nrf2 is yet to be elucidated. It is also still unclear how exactly Nrf2 can prevent tumor progression. Potential metabolic vulnerabilities linked to NRF2 activation that could explain this include CDO1-mediated toxic metabolite formation/ NADPH depletion (43), xCT-mediated glutamate depletion (44, 45, 61), and reductive stress via aldehyde dehydrogenase 3A1 (ALDH3A1) (169). Additional work is needed to determine if these metabolic liabilities or other mechanisms regulate NRF2-mediated progression and proliferation defects.

It is challenging to determine in which contexts NRF2 activation is advantageous, given that KEAP1 and NRF2 mutations are common in NSCLC patients and associated with poor prognosis. In patient data, it's been observed that KEAP1 mutations are an initiating driver along with KRAS and TP53 mutations in lung adenocarcinoma (196), which agrees with my finding that Nrf2 activation promotes lung tumor initiation, and suggests that additional mutations may be required to overcome a NRF2-mediated progression block.

Although my results did not indicate that NRF2 activation conferred poor outcomes in our mouse models, it's important to acknowledge that our models do not capture all the features of patient tumors. For example, the mice did not develop metastases with sufficient frequency, preventing examination of the effect of Nrf2 activation on metastasis as previously reported (53). Additionally, mice are not exposed to tobacco smoke and other environmental carcinogens where NRF2 activation may

promote survival (26, 27, 28, 29). I have also not tested the response of these models to chemotherapy, targeted therapy, immunotherapy, or radiation, of which resistance to is commonly reported in patients with *KEAP1/ NRF2* mutation. KEAP1 inactivation or NRF2 hyperactivation causes accumulation of NRF2, leading to increased expression of antioxidant enzymes and drug efflux pumps (197), which can contribute to therapeutic resistance. Moreover, this resistance is usually observed in advanced tumors, where high levels of NRF2 activation are likely beneficial for tumors to evade therapy, unlike in our mouse models where there's an absence of stress/ therapy.

Further investigation is needed to verify whether these approaches can be translated clinically. First, it needs to be understood how exactly NRF2 is downregulated during tumor progression, and how pharmacological NRF2 activation/ inhibition affects different tumor grades in our mouse models. These experiments will be important to clarify the NRF2 threshold, and how pharmacological activation of NRF2 compares to *KEAP1/NRF2* mutation. Additionally, our mouse models only activate NRF2 in tumor cells, whereas pharmacological NRF2 activation will affect NRF2 levels in the microenvironment, which can also affect tumor growth (144, 177, 178). It would also be of value to look at NRF2 expression in patient tumors and see if this is affected by the degree of differentiation. Based on my findings in our mouse models, I would except more advanced/ poor differentiated patient tumors to have less NRF2 expression compared to less advanced tumors. Collectively, this work will further elucidate the contexts in which NRF2 can support and impair lung tumor initiation and progression, respectively. These findings highlight the diverse roles that NRF2 plays during different stages of tumorigenesis in various contexts, and the distinct roles for ROS metabolism

and metabolic regulation. Additional experiments are warranted to understand how

NRF2 regulates redox status and tumor progression in our mouse models.

Chapter 9: Materials and Methods

Mice

Mice were housed and bred in accordance with the ethical regulations and approval of the IACUC (protocols #: IS00003893R and IS00007922R). Generation of the Keap1 targeting vector was previously described (43). Briefly, the *CA-Keap1^R554Q* allele (Keap1^tm1Gmdn^, MGI: 7327097) was made by inserting a wild-type *Keap1* cDNA containing exons 3-5 flanked by loxP sites upstream of the R554Q mutation in exon 4 of the *Keap1* gene. *Keap1* was targeted in C10 murine ES cells and cells were selected with blasticidin. To make the *LSL-Nfe2l2^D29H^* allele (Nfe2l2^tm1Gmdn^, MGI: 7327101), a STOP cassette flanked by loxP sites was inserted into intron 1 and codon 29 in endogenous exon 2 was mutated from an aspartic acid to a histidine. The endogenous *Nfe2l2* locus was targeted in C10 murine ES cells and puromycin was used to select positive cells. For both alleles, positive clones were screened by copy number real-time PCR and injected into blastocysts. Genotyping primers were as follows: for the *Keap1*^R554Q^ allele: Mutant forward: 5'-ATGGCCACACTTTTCTGGAC-3'; wild-type (WT) forward: 5'-GGGGGTAGAGGGAGGAGAAT-3'; Common reverse: 5'-GCCACCCTATTCACAGACCA-3'. The WT PCR product was 326 bp and the mutant PCR product 584 bp. For the *Nfe2l2*^D29H^ allele: WT forward: 5'-GAGGCAGGTAGTTCTCTGAGTTTG-3'; Common reverse: 5'-GCAAATGCACTGAGACACTCAT-3'; Mutant forward: 5'-

CTAGCCACCATGGCTTGAGT-3'. The WT PCR product was 189 bp and the mutant PCR product 282 bp. All mice were maintained on a mixed C57BL/6 genetic background. In addition to Keap1^{R554Q} and Nrf2^{D29H} mice, p53^{flox} (RRID:IMSR_JAX:008462); Stk11^{flox} (RRID:IMSR_JAX:014143); Nrf2^{flox} (RRID:IMSR_JAX:025433); and LSL-Kras$^{G12D/+}$ (RRID:IMSR_JAX:008179) mice were used. For mouse lung tumor experiments, intranasal installation of 2.25×10^7 PFU adenoviral-Cre or SPC Cre (University of Iowa) was used to induce lung tumors as previously described (163). For low-dose adenoviral-Cre experiments in the Kras$^{G12D/+}$; Stk11$^{fl/fl}$ model, 2.25×10^6 PFU was used to induce lung tumors. Adenoviral infections were performed under isofluorane anesthesia.

Murine embryonic fibroblast generation and culture

MEFs were isolated from E13.5-14.5-day old embryos and maintained in pyruvate-free DMEM (Corning) containing 10% FBS, 100 units/mL penicillin and 100 µg/mL streptomycin (Gibco) in a humidified incubator with 5% CO_2 and 95% air at 37 °C. MEFs were used within four passages and infected with control empty adenovirus or adenoviral-Cre (University of Iowa) at an approximate multiplicity of infection of 500.

RNA-sequencing preparation and analysis

Samples were prepared using the RNeasy plus mini kit (Qiagen, 74134). RNA quality was checked with the QIAxcel RNA QC kit (Qiagen, 929104). Additional RNA QC, sequencing, mapping to the mouse genome, and analysis were performed by Novogene. Differentially expressed genes (DESeq2) with $p < 0.05$ were included in the volcano plot.

LC-HRMS conditions for MEF non-targeted metabolomics

Sample preparation and conditions were previously described (43). Briefly, cells were extracted in 80% methanol and analyzed by liquid chromatography-high resolutions mass spectrometry (LC-HRMS) using a Vanquish UPLC systems coupled to a Q Exactive HF mass spectrometer. A Luna 3 μm HILIC 200 Å, LC Column 100 × 2 mm (Phenomenex, Torrance, CA, Part N: 00D-4449-B0) was used for chromatographic separation. Both positive and negative mode were used for the MS1 scan. Data analysis was done using El Maven v0.3.1 (198). The identification of metabolites was based on comparison of retention time and m/z value of sample peaks with an internal library (MSMLS Library, Sigma Aldrich).

Immunohistochemistry (IHC)

Mouse lung tissue was fixed with 10% formalin overnight, transferred to 70% ethanol and paraffin embedded to be sectioned. Unstained tissue sections were de-paraffinized in xylene followed by rehydration in a graded alcohol series. Antigen retrieval was performed by boiling in 10 mM citrate buffer (pH 6). Antibodies used for IHC include affinity-purified NRF2 (1:150 or 1:300) (199), NQO1 (Sigma Aldrich, RRID:AB_1079501, 1:500, 0.4 μg/ mL), Ki-67 (Cell Signaling Technology, RRID:AB_2620142, 1:200, 1.35 μg/ mL), Cleaved Caspase-3 (Cell Signaling Technology, RRID:AB_2070042, 1:1000, 0.04 μg/ mL), phospho-ERK (Cell Signaling Technology, RRID:AB_331772, 1:400, 0.13 μg/ mL), Taldo1 (Sigma-Aldrich, RRID:AB_10675127, 1:1000, 0.1 μg/ mL). Following overnight incubation at 4 °C in primary antibody, the ImmPRESS HRP goat anti-rabbit kit (Vector Laboratories,

RRID:AB_2631198) was used as directed by manufacturer's instructions. DAB peroxidase (HRP) substrate (Vector Laboratories, SK-4105) was used to develop immunohistochemical staining, followed by counterstaining with hematoxylin (Vector Laboratories, H-3404). Slides were scanned with the Aperio imager at 20x and the H-score of at least five representative regions/ mouse was analyzed with QuPath software(200). Representative images were captured using the Axio Lab.A1 microscope at 40x (Carl Zeiss Microimaging Inc.).

Tumor grading analysis and histology

Lung tumor grading was performed manually as previously described (166). Tumor grading distribution percentages were calculated by dividing the number of tumors in a specific grade by the total number of tumors per mouse. Tumor burden by grade was calculated by dividing the area of the lung covered by a specific tumor grade by the total lung area.

NSCLC cell lines and culture

Human lung cancer cell lines used include H1944 (RRID:CVCL_1508), H322 (RRID:CVCL_1556), A549 (RRID:CVCL_0023), HCC15 (RRID:CVCL_2057), and H460 (RRID:CVCL_0459) and were previously described (46). All cell lines were acquired from an authentic source (Hamon Cancer Center Collection). Cells were cultured in RPMI 1640 (Gibco) containing 5% FBS without antibiotics in a humidified incubator with 5% CO_2 and 95% air at 37 °C. Cells were confirmed to be free of mycoplasma with the MycoAlert kit (Lonza) immediately upon receipt and aliquots were frozen. Cell lines were tested monthly for mycoplasma and used within 10-20 passages.

Lentivirus generation and infection of NSCLC cells

Lentiviruses were made by transfecting Lenti-X 293T cells (Takara 632180) overnight with polyethylenimine (PEI), lentiviral plasmid (pLX317-NRF2^{WT}(130)), pLX317-NRF2^{WT}-V5, pLX317-NRF2$^{\Delta 4/5}$-V5, or the control pLX317 empty vector(43)), and packaging plasmids pCMV-dR8.2 dvpr (RRID:Addgene_8455) and pCMV-VSV-G (RRID:Addgene_8454) in DMEM containing 10% FBS. Expression of the V5 tag and deletion of NEH4/5 domains were performed via site-directed mutagenesis performed by Cheyenne Schneider (New England BioLabs E0554). To generate NRF2-overexpressing cells, NSCLC cells were transduced for 24 h with lentiviruses in medium containing polybrene (8 µg/mL). After transduction, infected cells were selected with 0.5 µg/mL (H1944, H322, H460) or 1 µg/mL (A549, HCC15) puromycin for 72 h. Immediately following selection, cells were seeded in respective puromycin concentrations for the indicated assays. For sgGSR experiments, A549 sgCon and sgGSR cells were generated by Chang Jiang as previously described (201). First, lentiviral transduction was used to stably express *Streptococcus pyogenes* Cas9 in A549 cells, followed by selection with 4 µg/mL blastocidin. Following this, A549s were transduced with guide RNAs against GSR (sgGSR) or non-targeting (sgCon) and selected with 1 µg/mL puromycin. Following validation of GSR knockout, lentiviral NRF2 overexpression was performed as described above in cells stably expressing guide RNAs.

Cell proliferation and cell death assays

NSCLC cells were monitored with the CELLCYTE X[TM] live cell imaging instrument (Cytena) over the course of 96 hours. Prior to imaging, SYTOX Green nucleic acid stain (Thermo Fisher Scientific, S7020) was added to medium at a final concentration of 20 nM. Images were acquired from each well at 8-hour intervals and analyzed using CellCyte Studio (CELLINK). Cell confluency was represented as the % of the image covered by cells. The number of dead cells was normalized to cell confluency [number of Sytox Green positive cells/ mm^2/ cell confluency]. The area under the curve (AUC) values were calculated by summing the proliferation or normalized dead cell number at each time point. For drug treatments, cells were treated upon replacing the medium with selection antibiotic following transduction. Auranofin (#A6733) was obtained from Sigma Aldrich. L-Buthionine-(S,R)-Sulfoximine (BSO) (#14484) and erastin (#17754) were obtained from Cayman Chemical. All drugs were dissolved in DMSO (#N182) from VWR Scientific Inc. As a control, DMSO was used at a final concentration of 0.2%.

Western blotting

Cells were lysed in ice-cold RIPA buffer with protease inhibitors (Fisher Scientific, PIA32955) followed by sonication in a water bath sonicator (Diagenode). Protein was quantified using the DC protein assay (Bio-Rad). Lysates were prepared with 6X SDS sample buffer containing 12% (v/v) β-ME (VWR) and separated on Bolt[TM] or NuPAGE 4-12% Bis-Tris gels (Invitrogen). SDS-PAGE separation was followed by transfer to 0.45 μm nitrocellulose membranes (GE Healthcare). The membranes were blocked in

5% non-fat milk in Tris-buffered saline with 0.1% Tween 20 (TBST). For immunoblotting, the following antibodies diluted in 5% milk in TBST were used: KEAP1 (Millipore Sigma, RRID:AB_2921362, 1:2000, 0.5 µg/ mL), NRF2 (Cell Signaling Technologies, D1Z9C, RRID:AB_2715528, 1:1000, 1.11 µg/ mL), NQO1 (Sigma Aldrich, RRID:AB_1079501, 1:1000, 0.2 µg/ mL), GCLC (Sana Cruz Biotechnology, H-5, RRID:AB_2736837, 1:1000, 0.2 µg/ mL), xCT (abcam, RRID:AB_778944, 1:1000, 1 µg/ mL), GSR (Santa Cruz Biotechnology, RRID:AB_2295121, 1:1000, 0.2 µg/ mL), β-actin (Invitrogen AM4302, RRID:AB_2536382, 1:100,000, Lot #2666237). V5 tag (Cell Signaling Technologies, D3H8Q, RRID:AB_2687461, 1:1000, 0.192 µg/ mL), HMOX1 (Enzo, RRID:AB_10617276, 1:1000, 1 µg/ mL), TXN1 (Cell Signaling Technologies, C63C6, RRID:AB_2272594, 1:1000, Lot #3), GCLM (GeneTex, RRID: AB_10730087, 1:1000, 0.33 µg/ mL). HRP secondary antibodies used include goat anti-rabbit IgG (Jackson ImmunoResearch Labs, RRID: AB_2313567, 1:10,000, 0.08 µg/ mL), goat anti-mouse IgG (Jackson ImmunoResearch Labs, RRID:AB_10015289, 1:10,000, 0.24 µg/ mL), and goat anti-rat IgG (Jackson ImmunoResearch Labs, RRID:AB_2338128, 1:10,000, 0.24 µg/ mL). Membranes were developed with Clarity ECL substrate (Bio-Rad) or a luminol-based homemade ECL substrate.

Soft agar colony formation assays

6-well plates were coated with a 0.8% agar prepared in RPMI. NSCLC cells were then seeded in 0.4% agar in RPMI. After the cell/ agar mixture solidified, RPMI medium containing 10% FBS, Pen/Strep and puromycin was added to each well and replenished every few days. Colonies were allowed to form for 10–16 days, and wells were stained

with 0.01% crystal violet in a 4% paraformaldehyde in PBS solution. Plates were scanned on a flatbed scanner and ImageJ was used to quantify colonies.

DepMap Analysis

NFE2L2 dependency scores were downloaded from the DepMap database v. 22Q2 (188). Values were plotted from CRISPR (DepMap 22Q2 Public+Score, Chronos) for non-small cell lung cancer cell lines that my supervisor previously evaluated for high or low NRF2 activity (46).

Quantification and statistical analysis

Graphpad Prism9 software was used for statistical analyses and P values < 0.05 were considered significant, with symbols as follows: *p<0.05, **p<0.01, ***p<0.001, ****p<0.0001. All data is represented as mean +/- standard deviation unless otherwise stated. For all experiments, similar variances between groups were observed.

Data Availability

The gene expression data generated in this thesis are publicly available in Gene Expression Omnibus (GEO) at GSE212942. The data for the NFE2L2 dependency scores analyzed in this study were obtained from the DepMap database v. 22Q2 at https://depmap.org/portal/download/all/.

References

1. DeBlasi JM, DeNicola GM. Dissecting the Crosstalk between NRF2 Signaling and Metabolic Processes in Cancer. Cancers (Basel). 2020;12(10).

2. Siegel RL, Miller KD, Fuchs HE, Jemal A. Cancer statistics, 2022. CA: A Cancer Journal for Clinicians. 2022;72(1):7-33.

3. Inamura K. Lung cancer: understanding its molecular pathology and the 2015 wHO classification. Frontiers in Oncology. 2017.

4. Testa U, Castelli G, Pelosi E. Lung Cancers: Molecular Characterization, Clonal Heterogeneity and Evolution, and Cancer Stem Cells. Cancers (Basel). 2018;10(8).

5. Liang J, Guan X, Bao G, Yao Y, Zhong X. Molecular subtyping of small cell lung cancer. Semin Cancer Biol. 2022;86(Pt 2):450-62.

6. Veluswamy R, Mack PC, Houldsworth J, Elkhouly E, Hirsch FR. KRAS G12C-Mutant Non-Small Cell Lung Cancer: Biology, Developmental Therapeutics, and Molecular Testing. J Mol Diagn. 2021;23(5):507-20.

7. Ferone G, Lee MC, Sage J, Berns A. Cells of origin of lung cancers: lessons from mouse studies. Genes Dev. 2020;34(15-16):1017-32.

8. Collisson EA, Campbell JD, Brooks AN, et al. Comprehensive molecular profiling of lung adenocarcinoma: The cancer genome atlas research network. Nature. 2014.

9. Lacroix M, Riscal R, Arena G, Linares LK, Le Cam L. Metabolic functions of the tumor suppressor p53: Implications in normal physiology, metabolic disorders, and cancer. 2020.

10. Sanchez-Cespedes MP, Esteller M, Nomoto S, Trink B, Engles JM, Westra WH, Herman JG, Sidransky D. Inactivation of LKB1 / STK11 Is a Common Event in Adenocarcinomas of the Lung Inactivation of LKB1 / STK11 Is a Common Event in Adenocarcinomas of the Lung 1. Cancer Research. 2002;62:3659-62.

11. Lizcano JM, Göransson O, Toth R, Deak M, Morrice NA, Boudeau J, Hawley SA, Udd L, Mäkelä TP, Hardie DG, Alessi DR. LKB1 is a master kinase that activates 13 kinases of the AMPK subfamily, including MARK/PAR-1. The EMBO Journal. 2004;23(4):833-43.

12. Singh A, Bodas M, Wakabayashi N, Bunz F, Biswal S. Gain of Nrf2 function in non-small-cell lung cancer cells confers radioresistance. Antioxidants and Redox Signaling. 2010.

13. Canning P, Sorrell FJ, Bullock AN. Structural basis of Keap1 interactions with Nrf2. Free Radic Biol Med. 2015;88(Pt B):101-7.

14. Cleasby A, Yon J, Day PJ, Richardson C, Tickle IJ, Williams PA, Callahan JF, Carr R, Concha N, Kerns JK, Qi H, Sweitzer T, Ward P, Davies TG. Structure of the BTB domain of Keap1 and its interaction with the triterpenoid antagonist CDDO. PLoS One. 2014;9(6):e98896.

15. Crisman E, Duarte P, Dauden E, Cuadrado A, Rodríguez-Franco MI, López MG, León R. KEAP1-NRF2 protein-protein interaction inhibitors: Design, pharmacological properties and therapeutic potential. Med Res Rev. 2023;43(1):237-87.

16. Motohashi H, Katsuoka F, Engel JD, Yamamoto M. Small Maf proteins serve as transcriptional cofactors for keratinocyte differentiation in the Keap1–Nrf2 regulatory pathway. Proceedings of the National Academy of Sciences. 2004;101(17):6379-84.

17. Itoh K, Wakabayashi N, Katoh Y, Ishii T, Igarashi K, Engel JD, Yamamoto M. Keap1 represses nuclear activation of antioxidant responsive elements by Nrf2 through binding to the amino-terminal Neh2 domain. Genes Dev. 1999;13(1):76-86.

18. Nioi P, Nguyen T, Sherratt PJ, Pickett CB. The carboxy-terminal Neh3 domain of Nrf2 is required for transcriptional activation. Mol Cell Biol. 2005;25(24):10895-906.

19. Katoh Y, Itoh K, Yoshida E, Miyagishi M, Fukamizu A, Yamamoto M. Two domains of Nrf2 cooperatively bind CBP, a CREB binding protein, and synergistically activate transcription. Genes to Cells. 2001;6(10):857-68.

20. Chowdhry S, Zhang Y, McMahon M, Sutherland C, Cuadrado A, Hayes JD. Nrf2 is controlled by two distinct β-TrCP recognition motifs in its Neh6 domain, one of which can be modulated by GSK-3 activity. Oncogene. 2013;32(32):3765-81.

21. Wang H, Liu K, Geng M, Gao P, Wu X, Hai Y, Li Y, Li Y, Luo L, Hayes JD. RXRα inhibits the NRF2-ARE signaling pathway through a direct interaction with the Neh7 domain of NRF2. Cancer research. 2013;73(10):3097-108.

22. Dayalan Naidu S, Dinkova-Kostova AT. KEAP1, a cysteine-based sensor and a drug target for the prevention and treatment of chronic disease. Open Biol. 2020;10(6):200105-.

23. Lushchak VI, Storey KB. Oxidative stress concept updated: Definitions, classifications, and regulatory pathways implicated. Excli j. 2021;20:956-67.

24. Shen G, Kong AN. Nrf2 plays an important role in coordinated regulation of Phase II drug metabolism enzymes and Phase III drug transporters. Biopharm Drug Dispos. 2009;30(7):345-55.

25. Itoh K, Chiba T, Takahashi S, Ishii T, Igarashi K, Katoh Y, Oyake T, Hayashi N, Satoh K, Hatayama I, Yamamoto M, Nabeshima Y. An Nrf2/small Maf heterodimer mediates the induction of phase II detoxifying enzyme genes through antioxidant response elements. Biochem Biophys Res Commun. 1997;236(2):313-22.

26. Ramos-Gomez M, Dolan PM, Itoh K, Yamamoto M, Kensler TW. Interactive effects of nrf2 genotype and oltipraz on benzo[a]pyrene–DNA adducts and tumor yield in mice. Carcinogenesis. 2003;24(3):461-7.

27. Ramos-Gomez M, Kwak M-K, Dolan PM, Itoh K, Yamamoto M, Talalay P, Kensler TW. Sensitivity to carcinogenesis is increased and chemoprotective efficacy of enzyme inducers is lost in <i>nrf2</i> transcription factor-deficient mice. Proceedings of the National Academy of Sciences. 2001;98(6):3410-5.

28. Aoki Y, Sato H, Nishimura N, Takahashi S, Itoh K, Yamamoto M. Accelerated DNA adduct formation in the lung of the Nrf2 knockout mouse exposed to diesel exhaust. Toxicol Appl Pharmacol. 2001;173(3):154-60.

29. Iida K, Itoh K, Kumagai Y, Oyasu R, Hattori K, Kawai K, Shimazui T, Akaza H, Yamamoto M. Nrf2 Is Essential for the Chemopreventive Efficacy of Oltipraz against Urinary Bladder Carcinogenesis. Cancer Research. 2004;64(18):6424-31.

30. Kensler TW, Wakabayashi N. Nrf2: friend or foe for chemoprevention? Carcinogenesis. 2010;31(1):90-9.

31. Schmidlin CJ, Shakya A, Dodson M, Chapman E, Zhang DD. The intricacies of NRF2 regulation in cancer. Semin Cancer Biol. 2021;76:110-9.

32. Telkoparan-Akillilar P, Suzen S, Saso L. Pharmacological Applications of Nrf2 Inhibitors as Potential Antineoplastic Drugs. Int J Mol Sci. 2019;20(8).

33. Hanahan D, Weinberg RA. Hallmarks of Cancer: The Next Generation. Cell. 2011;144(5):646-74.

34. Best SA, Ding S, Kersbergen A, Dong X, Song JY, Xie Y, Reljic B, Li K, Vince JE, Rathi V, Wright GM, Ritchie ME, Sutherland KD. Distinct initiating events underpin the immune and metabolic heterogeneity of KRAS-mutant lung adenocarcinoma. Nature Communications. 2019;10(1):1-14.

35. Mitsuishi Y, Taguchi K, Kawatani Y, Shibata T, Nukiwa T, Aburatani H, Yamamoto M, Motohashi H. Nrf2 redirects glucose and glutamine into anabolic pathways in metabolic reprogramming. Cancer Cell. 2012;22(1):66-79.

36. Singh A, Happel C, Manna SK, Acquaah-Mensah G, Carrerero J, Kumar S, Nasipuri P, Krausz KW, Wakabayashi N, Dewi R, Boros LG, Gonzalez FJ, Gabrielson E, Wong KK, Girnun G, Biswal S. Transcription factor NRF2 regulates miR-1 and miR-206 to drive tumorigenesis. J Clin Invest. 2013;123(7):2921-34.

37. Wu KC, Cui JY, Klaassen CD. Beneficial role of Nrf2 in regulating NADPH generation and consumption. Toxicol Sci. 2011;123(2):590-600.

38. Ludtmann MHR, Angelova PR, Zhang Y, Abramov AY, Dinkova-Kostova AT. Nrf2 affects the efficiency of mitochondrial fatty acid oxidation. Biochemical Journal. 2014.

39. Slocum SL, Skoko JJ, Wakabayashi N, Aja S, Yamamoto M, Kensler TW, Chartoumpekis DV. Keap1/Nrf2 pathway activation leads to a repressed hepatic gluconeogenic and lipogenic program in mice on a high-fat diet. Arch Biochem Biophys. 2016;591:57-65.

40. Bowman BM, Montgomery SA, Schrank TP, Simon JM, Ptacek TS, Tamir TY, Muvlaney KM, Weir SJ, Nguyen TT, Murphy RM, Makowski L, Hayes DN, Chen XL, Randell SH, Weissman BE, Major MB. A conditional mouse expressing an activating mutation in NRF2 displays hyperplasia of the upper gastrointestinal tract and decreased white adipose tissue. J Pathol. 2020.

41. Suzuki T, Uruno A, Yumoto A, Taguchi K, Suzuki M, Harada N, Ryoke R, Naganuma E, Osanai N, Goto A, Suda H, Browne R, Otsuki A, Katsuoka F, Zorzi M, Yamazaki T, Saigusa D, Koshiba S, Nakamura T, Fukumoto S, Ikehata H, Nishikawa K, Suzuki N, Hirano I, Shimizu R, Oishi T, Motohashi H, Tsubouchi H, Okada R, Kudo T, Shimomura M, Kensler TW, Mizuno H, Shirakawa M, Takahashi S, Shiba D, Yamamoto M. Nrf2 contributes to the weight gain of mice during space travel. Commun Biol. 2020;3(1):496.

42. Sasaki H, Sato H, Kuriyama-Matsumura K, Sato K, Maebara K, Wang H, Tamba M, Itoh K, Yamamoto M, Bannai S. Electrophile response element-mediated induction of the cystine/glutamate exchange transporter gene expression. Journal of Biological Chemistry. 2002;277(47):44765-71.

43. Kang YP, Torrente L, Falzone A, Elkins CM, Liu M, Asara JM, Dibble CC, Denicola GM. Cysteine dioxygenase 1 is a metabolic liability for non-small cell lung cancer. eLife. 2019.

44. Muir A, Danai LV, Gui DY, Waingarten CY, Lewis CA, Vander Heiden MG. Environmental cystine drives glutamine anaplerosis and sensitizes cancer cells to glutaminase inhibition. Elife. 2017;6.

45. Romero R, Sayin VI, Davidson SM, Bauer MR, Singh SX, Leboeuf SE, Karakousi TR, Ellis DC, Bhutkar A, Sánchez-Rivera FJ, Subbaraj L, Martinez B, Bronson RT, Prigge JR, Schmidt EE, Thomas CJ, Goparaju C, Davies A, Dolgalev I, Heguy A, Allaj V, Poirier JT, Moreira AL, Rudin CM, Pass HI, Vander Heiden MG, Jacks T, Papagiannakopoulos T. Keap1 loss promotes Kras-driven lung cancer and results in dependence on glutaminolysis. Nature Medicine. 2017.

46. DeNicola GM, Chen PH, Mullarky E, Sudderth JA, Hu Z, Wu D, Tang H, Xie Y, Asara JM, Huffman KE, Wistuba II, Minna JD, DeBerardinis RJ, Cantley LC. NRF2 regulates serine biosynthesis in non-small cell lung cancer. Nature Genetics. 2015;47(12):1475-81.

47. Guo H, Xu J, Zheng Q, He J, Zhou W, Wang K, Huang X, Fan Q, Ma J, Cheng J, Mei W, Xing R, Cai R. NRF2 SUMOylation promotes de novo serine synthesis and maintains HCC tumorigenesis. Cancer Lett. 2019;466:39-48.

48. Gwinn DM, Lee AG, Briones-Martin-Del-Campo M, Conn CS, Simpson DR, Scott AI, Le A, Cowan TM, Ruggero D, Sweet-Cordero EA. Oncogenic KRAS Regulates Amino Acid Homeostasis and Asparagine Biosynthesis via ATF4 and Alters Sensitivity to L-Asparaginase. Cancer cell. 2018;33(1):91-107.e6.

49. Fox DB, Garcia NMG, McKinney BJ, Lupo R, Noteware LC, Newcomb R, Liu J, Locasale JW, Hirschey MD, Alvarez JV. NRF2 activation promotes the recurrence of dormant tumour cells through regulation of redox and nucleotide metabolism. Nat Metab. 2020;2(4):318-34.

50. Campbell MR, Karaca M, Adamski KN, Chorley BN, Wang X, Bell DA. Novel hematopoietic target genes in the NRF2-mediated transcriptional pathway. Oxid Med Cell Longev. 2013;2013:120305.

51. Hirotsu Y, Katsuoka F, Funayama R, Nagashima T, Nishida Y, Nakayama K, Engel JD, Yamamoto M. Nrf2-MafG heterodimers contribute globally to antioxidant and metabolic networks. Nucleic Acids Res. 2012;40(20):10228-39.

52. Kensler TW, Wakabayashi N, Biswal S. Cell survival responses to environmental stresses via the Keap1-Nrf2-ARE pathway. Annu Rev Pharmacol Toxicol. 2007;47:89-116.

53. Lignitto L, LeBoeuf SE, Homer H, Jiang S, Askenazi M, Karakousi TR, Pass HI, Bhutkar AJ, Tsirigos A, Ueberheide B, Sayin VI, Papagiannakopoulos T, Pagano M. Nrf2 Activation Promotes Lung Cancer Metastasis by Inhibiting the Degradation of Bach1. Cell. 2019;178(2):316-29.e18.

54. Ahn CS, Metallo CM. Mitochondria as biosynthetic factories for cancer proliferation. Cancer Metab. 2015;3(1):1.

55. Zerangue N, Kavanaugh MP. Interaction of L-cysteine with a human excitatory amino acid transporter. J Physiol. 1996;493 (Pt 2):419-23.

56. Knickelbein RG, Seres T, Lam G, Johnston RB, Jr., Warshaw JB. Characterization of multiple cysteine and cystine transporters in rat alveolar type II cells. Am J Physiol. 1997;273(6):L1147-55.

57. Chen Y, Swanson RA. The glutamate transporters EAAT2 and EAAT3 mediate cysteine uptake in cortical neuron cultures. J Neurochem. 2003;84(6):1332-9.

58. Combs JA, DeNicola GM. The Non-Essential Amino Acid Cysteine Becomes Essential for Tumor Proliferation and Survival. Cancers (Basel). 2019;11(5).

59. Lewerenz J, Hewett SJ, Huang Y, Lambros M, Gout PW, Kalivas PW, Massie A, Smolders I, Methner A, Pergande M, Smith SB, Ganapathy V, Maher P. The cystine/glutamate antiporter system x(c)(-) in health and disease: from molecular mechanisms to novel therapeutic opportunities. Antioxid Redox Signal. 2013;18(5):522-55.

60. Gu Y, Albuquerque CP, Braas D, Zhang W, Villa GR, Bi J, Ikegami S, Masui K, Gini B, Yang H, Gahman TC, Shiau AK, Cloughesy TF, Christofk HR, Zhou H, Guan KL, Mischel PS. mTORC2 Regulates Amino Acid Metabolism in Cancer by Phosphorylation of the Cystine-Glutamate Antiporter xCT. Mol Cell. 2017;67(1):128-38 e7.

61. Sayin VI, LeBoeuf SE, Singh SX, Davidson SM, Biancur D, Guzelhan BS, Alvarez SW, Wu WL, Karakousi TR, Zavitsanou AM, Ubriaco J, Muir A, Karagiannis D, Morris PJ, Thomas CJ, Possemato R, Vander Heiden MG, Papagiannakopoulos T. Activation of the NRF2 antioxidant program generates an imbalance in central carbon metabolism in cancer. Elife. 2017;6.

62. Lanzardo S, Conti L, Rooke R, Ruiu R, Accart N, Bolli E, Arigoni M, Macagno M, Barrera G, Pizzimenti S, Aurisicchio L, Calogero RA, Cavallo F. Immunotargeting of Antigen xCT Attenuates Stem-like Cell Behavior and Metastatic Progression in Breast Cancer. Cancer Res. 2016;76(1):62-72.

63. Briggs KJ, Koivunen P, Cao S, Backus KM, Olenchock BA, Patel H, Zhang Q, Signoretti S, Gerfen GJ, Richardson AL, Witkiewicz AK, Cravatt BF, Clardy J, Kaelin WG, Jr. Paracrine Induction of HIF by Glutamate in Breast Cancer: EglN1 Senses Cysteine. Cell. 2016;166(1):126-39.

64. Sleire L, Skeie BS, Netland IA, Forde HE, Dodoo E, Selheim F, Leiss L, Heggdal JI, Pedersen PH, Wang J, Enger PO. Drug repurposing: sulfasalazine sensitizes gliomas to gamma knife radiosurgery by blocking cystine uptake through system Xc-, leading to glutathione depletion. Oncogene. 2015;34(49):5951-9.

65. Polewski MD, Reveron-Thornton RF, Cherryholmes GA, Marinov GK, Cassady K, Aboody KS. Increased Expression of System xc- in Glioblastoma Confers an Altered Metabolic State and Temozolomide Resistance. Mol Cancer Res. 2016;14(12):1229-42.

66. Espinosa-Diez C, Miguel V, Mennerich D, Kietzmann T, Sánchez-Pérez P, Cadenas S, Lamas S. Antioxidant responses and cellular adjustments to oxidative stress. Redox Biol. 2015;6:183-97.

67. Traverso N, Ricciarelli R, Nitti M, Marengo B, Furfaro AL, Pronzato MA, Marinari UM, Domenicotti C. Role of Glutathione in Cancer Progression and Chemoresistance. Oxidative Medicine and Cellular Longevity. 2013;2013:972913.

68. Wild AC, Moinova HR, Mulcahy RT. Regulation of gamma-glutamylcysteine synthetase subunit gene expression by the transcription factor Nrf2. J Biol Chem. 1999;274(47):33627-36.

69. Moinova HR, Mulcahy RT. Up-regulation of the human gamma-glutamylcysteine synthetase regulatory subunit gene involves binding of Nrf-2 to an electrophile responsive element. Biochem Biophys Res Commun. 1999;261(3):661-8.

70. Solis WA, Dalton TP, Dieter MZ, Freshwater S, Harrer JM, He L, Shertzer HG, Nebert DW. Glutamate-cysteine ligase modifier subunit: mouse Gclm gene structure and regulation by agents that cause oxidative stress. Biochem Pharmacol. 2002;63(9):1739-54.

71. Bea F, Hudson FN, Chait A, Kavanagh TJ, Rosenfeld ME. Induction of glutathione synthesis in macrophages by oxidized low-density lipoproteins is mediated by consensus antioxidant response elements. Circ Res. 2003;92(4):386-93.

72. Sekhar KR, Crooks PA, Sonar VN, Friedman DB, Chan JY, Meredith MJ, Starnes JH, Kelton KR, Summar SR, Sasi S, Freeman ML. NADPH oxidase activity is essential for Keap1/Nrf2-mediated induction of GCLC in response to 2-indol-3-yl-methylenequinuclidin-3-ols. Cancer Res. 2003;63(17):5636-45.

73. Lu SC. Regulation of glutathione synthesis. Mol Aspects Med. 2009;30(1-2):42-59.

74. Harris IS, DeNicola GM. The Complex Interplay between Antioxidants and ROS in Cancer. Trends in Cell Biology. 2020:1-12.

75. Hawkes HJ, Karlenius TC, Tonissen KF. Regulation of the human thioredoxin gene promoter and its key substrates: a study of functional and putative regulatory elements. Biochim Biophys Acta. 2014;1840(1):303-14.

76. Abbas K, Breton J, Planson A-G, Bouton C, Bignon J, Seguin C, Riquier S, Toledano MB, Drapier J-C. Nitric oxide activates an Nrf2/sulfiredoxin antioxidant pathway in macrophages. Free Radical Biology and Medicine. 2011;51(1):107-14.

77. Trujillo M, Clippe A, Manta B, Ferrer-Sueta G, Smeets A, Declercq J-P, Knoops B, Radi R. Pre-steady state kinetic characterization of human peroxiredoxin 5: Taking advantage of Trp84 fluorescence increase upon oxidation. Archives of Biochemistry and Biophysics. 2007;467(1):95-106.

78. Arnér ESJ. Focus on mammalian thioredoxin reductases — Important selenoproteins with versatile functions. Biochimica et Biophysica Acta (BBA) - General Subjects. 2009;1790(6):495-526.

79. Lu SC. Glutathione synthesis. Biochim Biophys Acta. 2013;1830(5):3143-53.

80. Rajasekaran NS, Varadharaj S, Khanderao GD, Davidson CJ, Kannan S, Firpo MA, Zweier JL, Benjamin IJ. Sustained activation of nuclear erythroid 2-related factor 2/antioxidant response element signaling promotes reductive stress in the human mutant protein aggregation cardiomyopathy in mice. Antioxidants and Redox Signaling. 2011.

81. Dialynas G, Shrestha OK, Ponce JM, Zwerger M, Thiemann DA, Young GH, Moore SA, Yu L, Lammerding J, Wallrath LL. Myopathic Lamin Mutations Cause Reductive Stress and Activate the Nrf2/Keap-1 Pathway. PLoS Genetics. 2015.

82. Weiss-Sadan T, Ge M, de Groot A, Carlin A, Gohar M, Fischer H, Shi L, Wei T-Y, Adelmann CH, Vornbäumen T, Dürr BR, Takahashi M, Richter M, Zhang J, Yang T-Y, Vijay V, Hayashi M, Fischer DE, Hata AN, Papaginanakopoulos T, Mostoslavsky R, Bardeesy N, Bar-Peled L. NRF2 activation induces NADH-reductive stress providing a metabolic vulnerability in lung cancer. bioRxiv. 2022:2022.08.31.506025.

83. LeBoeuf SE, Wu WL, Karakousi TR, Karadal B, Jackson SR, Davidson SM, Wong KK, Koralov SB, Sayin VI, Papagiannakopoulos T. Activation of Oxidative Stress Response in Cancer Generates a Druggable Dependency on Exogenous Non-essential Amino Acids. Cell Metab. 2020;31(2):339-50.e4.

84. Agyeman AS, Chaerkady R, Shaw PG, Davidson NE, Visvanathan K, Pandey A, Kensler TW. Transcriptomic and proteomic profiling of KEAP1 disrupted and sulforaphane-treated human breast epithelial cells reveals common expression profiles. Breast Cancer Research and Treatment. 2012;132(1):175-87.

85. Hayes JD, Dinkova-Kostova AT. The Nrf2 regulatory network provides an interface between redox and intermediary metabolism. Trends Biochem Sci. 2014;39(4):199-218.

86. Locasale JW. Serine, glycine and one-carbon units: cancer metabolism in full circle. Nat Rev Cancer. 2013;13(8):572-83.

87. Li AM, Ye J. Reprogramming of serine, glycine and one-carbon metabolism in cancer. Biochim Biophys Acta Mol Basis Dis. 2020;1866(10):165841.

88. McMillan EA, Ryu MJ, Diep CH, Mendiratta S, Clemenceau JR, Vaden RM, Kim JH, Motoyaji T, Covington KR, Peyton M, Huffman K, Wu X, Girard L, Sung Y, Chen PH, Mallipeddi PL, Lee JY, Hanson J, Voruganti S, Yu Y, Park S, Sudderth J, DeSevo C, Muzny DM, Doddapaneni H, Gazdar A, Gibbs RA, Hwang TH, Heymach JV, Wistuba I, Coombes KR, Williams NS, Wheeler DA, MacMillan JB, Deberardinis RJ, Roth MG, Posner BA, Minna JD, Kim HS, White MA. Chemistry-First Approach for Nomination of Personalized Treatment in Lung Cancer. Cell. 2018;173(4):864-78 e29.

89. Kang YP, Falzone A, Liu M, Gonzalez-Sanchez P, Choi BH, Coloff JL, Saller JJ, Karreth FA, DeNicola GM. PHGDH supports liver ceramide synthesis and sustains lipid homeostasis. Cancer Metab. 2020;8:6.

90. Gantner ML, Eade K, Wallace M, Handzlik MK, Fallon R, Trombley J, Bonelli R, Giles S, Harkins-Perry S, Heeren TFC, Sauer L, Ideguchi Y, Baldini M, Scheppke L, Dorrell MI, Kitano M, Hart BJ, Cai C, Nagasaki T, Badur MG, Okada M, Woods SM, Egan C, Gillies M, Guymer R, Eichler F, Bahlo M, Fruttiger M, Allikmets R, Bernstein PS, Metallo CM, Friedlander M. Serine and Lipid Metabolism in Macular Disease and Peripheral Neuropathy. N Engl J Med. 2019;381(15):1422-33.

91. Muthusamy T, Cordes T, Handzlik MK, You L, Lim EW, Gengatharan J, Pinto AFM, Badur MG, Kolar MJ, Wallace M, Saghatelian A, Metallo CM. Serine restriction alters sphingolipid diversity to constrain tumour growth. Nature. 2020.

92. Gao X, Lee K, Reid MA, Sanderson SM, Qiu C, Li S, Liu J, Locasale JW. Serine Availability Influences Mitochondrial Dynamics and Function through Lipid Metabolism. Cell Rep. 2018;22(13):3507-20.

93. Possemato R, Marks KM, Shaul YD, Pacold ME, Kim D, Birsoy K, Sethumadhavan S, Woo HK, Jang HG, Jha AK, Chen WW, Barrett FG, Stransky N, Tsun ZY, Cowley GS, Barretina J, Kalaany NY, Hsu PP, Ottina K, Chan AM, Yuan B, Garraway LA, Root DE, Mino-Kenudson M, Brachtel EF, Driggers EM, Sabatini DM. Functional genomics reveal that the serine synthesis pathway is essential in breast cancer. Nature. 2011;476(7360):346-50.

94. Ding J, Li T, Wang X, Zhao E, Choi JH, Yang L, Zha Y, Dong Z, Huang S, Asara JM, Cui H, Ding HF. The histone H3 methyltransferase G9A epigenetically activates the serine-glycine synthesis pathway to sustain cancer cell survival and proliferation. Cell Metab. 2013;18(6):896-907.

95. Hitosugi T, Zhou L, Elf S, Fan J, Kang HB, Seo JH, Shan C, Dai Q, Zhang L, Xie J, Gu TL, Jin P, Alečković M, LeRoy G, Kang Y, Sudderth JA, DeBerardinis RJ, Luan CH, Chen GZ, Muller S, Shin DM, Owonikoko TK, Lonial S, Arellano ML, Khoury HJ, Khuri FR, Lee BH, Ye K, Boggon TJ, Kang S, He C, Chen J. Phosphoglycerate mutase 1 coordinates glycolysis and biosynthesis to promote tumor growth. Cancer Cell. 2012;22(5):585-600.

96. Locasale JW, Grassian AR, Melman T, Lyssiotis CA, Mattaini KR, Bass AJ, Heffron G, Metallo CM, Muranen T, Sharfi H, Sasaki AT, Anastasiou D, Mullarky E, Vokes NI, Sasaki M, Beroukhim R, Stephanopoulos G, Ligon AH, Meyerson M, Richardson AL, Chin L, Wagner G, Asara JM, Brugge JS, Cantley LC, Vander Heiden MG. Phosphoglycerate dehydrogenase diverts glycolytic flux and contributes to oncogenesis. Nat Genet. 2011;43(9):869-74.

97. Ma L, Tao Y, Duran A, Llado V, Galvez A, Barger JF, Castilla EA, Chen J, Yajima T, Porollo A, Medvedovic M, Brill LM, Plas DR, Riedl SJ, Leitges M, Diaz-Meco MT, Richardson AD, Moscat J. Control of nutrient stress-induced metabolic reprogramming by PKCζ in tumorigenesis. Cell. 2013;152(3):599-611.

98. Ou Y, Wang SJ, Jiang L, Zheng B, Gu W. p53 Protein-mediated regulation of phosphoglycerate dehydrogenase (PHGDH) is crucial for the apoptotic response upon serine starvation. J Biol Chem. 2015;290(1):457-66.

99. Tameire F, Verginadis, II, Leli NM, Polte C, Conn CS, Ojha R, Salas Salinas C, Chinga F, Monroy AM, Fu W, Wang P, Kossenkov A, Ye J, Amaravadi RK, Ignatova Z, Fuchs SY, Diehl JA, Ruggero D, Koumenis C. ATF4 couples MYC-dependent translational activity to bioenergetic demands during tumour progression. Nat Cell Biol. 2019;21(7):889-99.

100. Ngo B, Kim E, Osorio-Vasquez V, Doll S, Bustraan S, Liang RJ, Luengo A, Davidson SM, Ali A, Ferraro GB, Fischer GM, Eskandari R, Kang DS, Ni J, Plasger A, Rajasekhar VK, Kastenhuber ER, Bacha S, Sriram RK, Stein BD, Bakhoum SF, Snuderl M, Cotzia P, Healey JH, Mainolfi N, Suri V, Friedman A, Manfredi M, Sabatini DM, Jones DR, Yu M, Zhao JJ, Jain RK, Keshari KR, Davies MA, Heiden MGV, Hernando E, Mann M, Cantley LC, Pacold ME. Limited Environmental Serine and Glycine Confer Brain Metastasis Sensitivity to PHGDH Inhibition. Cancer Discov. 2020.

101. Shin DY, Na, II, Kim CH, Park S, Baek H, Yang SH. EGFR mutation and brain metastasis in pulmonary adenocarcinomas. J Thorac Oncol. 2014;9(2):195-9.

102. Hendriks LE, Smit EF, Vosse BA, Mellema WW, Heideman DA, Bootsma GP, Westenend M, Pitz C, de Vries GJ, Houben R, Grunberg K, Bendek M, Speel EJ, Dingemans AM. EGFR mutated non-small cell lung cancer patients: more prone to development of bone and brain metastases? Lung Cancer. 2014;84(1):86-91.

103. Tamura T, Kurishima K, Nakazawa K, Kagohashi K, Ishikawa H, Satoh H, Hizawa N. Specific organ metastases and survival in metastatic non-small-cell lung cancer. Mol Clin Oncol. 2015;3(1):217-21.

104. Balasubramanian MN, Butterworth EA, Kilberg MS. Asparagine synthetase: regulation by cell stress and involvement in tumor biology. Am J Physiol Endocrinol Metab. 2013;304(8):E789-99.

105. Ye J, Kumanova M, Hart LS, Sloane K, Zhang H, De Panis DN, Bobrovnikova-Marjon E, Diehl JA, Ron D, Koumenis C. The GCN2-ATF4 pathway is critical for tumour cell survival and proliferation in response to nutrient deprivation. EMBO J. 2010;29(12):2082-96.

106. Zhang J, Fan J, Venneti S, Cross JR, Takagi T, Bhinder B, Djaballah H, Kanai M, Cheng EH, Judkins AR, Pawel B, Baggs J, Cherry S, Rabinowitz JD, Thompson CB. Asparagine plays a critical role in regulating cellular adaptation to glutamine depletion. Mol Cell. 2014;56(2):205-18.

107. Chen L, Zhang Z, Hoshino A, Zheng HD, Morley M, Arany Z, Rabinowitz JD. NADPH production by the oxidative pentose-phosphate pathway supports folate metabolism. Nat Metab. 2019;1:404-15.

108. Mullen PJ, Yu R, Longo J, Archer MC, Penn LZ. The interplay between cell signalling and the mevalonate pathway in cancer. Nat Rev Cancer. 2016;16(11):718-31.

109. Fan J, Ye J, Kamphorst JJ, Shlomi T, Thompson CB, Rabinowitz JD. Quantitative flux analysis reveals folate-dependent NADPH production. Nature. 2014;510(7504):298-302.

110. Mason JA, Hagel KR, Hawk MA, Schafer ZT. Metabolism during ECM Detachment: Achilles Heel of Cancer Cells? Trends Cancer. 2017;3(7):475-81.

111. Jiang P, Du W, Wu M. Regulation of the pentose phosphate pathway in cancer. Protein Cell. 2014;5(8):592-602.

112. Patra KC, Hay N. The pentose phosphate pathway and cancer. Trends Biochem Sci. 2014;39(8):347-54.

113. Zhao D, Badur MG, Luebeck J, Magana JH, Birmingham A, Sasik R, Ahn CS, Ideker T, Metallo CM, Mali P. Combinatorial CRISPR-Cas9 Metabolic Screens Reveal Critical Redox Control Points Dependent on the KEAP1-NRF2 Regulatory Axis. Mol Cell. 2018;69(4):699-708 e7.

114. Faubert B, Vincent EE, Griss T, Samborska B, Izreig S, Svensson RU, Mamer OA, Avizonis D, Shackelford DB, Shaw RJ, Jones RG. Loss of the tumor suppressor LKB1 promotes metabolic reprogramming of cancer cells via HIF-1α. Proc Natl Acad Sci U S A. 2014.

115. Jeon SM, Chandel NS, Hay N. AMPK regulates NADPH homeostasis to promote tumour cell survival during energy stress. Nature. 2012.

116. Kerins MJ, Ooi A. The Roles of NRF2 in Modulating Cellular Iron Homeostasis. Antioxid Redox Signal. 2018;29(17):1756-73.

117. Loboda A, Damulewicz M, Pyza E, Jozkowicz A, Dulak J. Role of Nrf2/HO-1 system in development, oxidative stress response and diseases: an evolutionarily conserved mechanism. Cell Mol Life Sci. 2016;73(17):3221-47.

118. Chiang SK, Chen SE, Chang LC. A Dual Role of Heme Oxygenase-1 in Cancer Cells. Int J Mol Sci. 2018;20(1).

119. Sun X, Ou Z, Chen R, Niu X, Chen D, Kang R, Tang D. Activation of the p62-Keap1-NRF2 pathway protects against ferroptosis in hepatocellular carcinoma cells. Hepatology. 2016;63(1):173-84.

120. Salazar M, Rojo AI, Velasco D, de Sagarra RM, Cuadrado A. Glycogen synthase kinase-3beta inhibits the xenobiotic and antioxidant cell response by direct phosphorylation and nuclear exclusion of the transcription factor Nrf2. J Biol Chem. 2006;281(21):14841-51.

121. Yang WS, SriRamaratnam R, Welsch ME, Shimada K, Skouta R, Viswanathan VS, Cheah JH, Clemons PA, Shamji AF, Clish CB, Brown LM, Girotti AW, Cornish VW, Schreiber SL, Stockwell BR. Regulation of ferroptotic cancer cell death by GPX4. Cell. 2014;156(1-2):317-31.

122. Zenke-Kawasaki Y, Dohi Y, Katoh Y, Ikura T, Ikura M, Asahara T, Tokunaga F, Iwai K, Igarashi K. Heme induces ubiquitination and degradation of the transcription factor Bach1. Mol Cell Biol. 2007;27(19):6962-71.

123. Reichard JF, Motz GT, Puga A. Heme oxygenase-1 induction by NRF2 requires inactivation of the transcriptional repressor BACH1. Nucleic Acids Res. 2007;35(21):7074-86.

124. Singh A, Misra V, Thimmulappa RK, Lee H, Ames S, Hoque MO, Herman JG, Baylin SB, Sidransky D, Gabrielson E, Brock MV, Biswal S. Dysfunctional KEAP1-NRF2 interaction in non-small-cell lung cancer. PLoS Med. 2006;3(10):e420.

125. Shibata T, Ohta T, Tong KI, Kokubu A, Odogawa R, Tsuta K, Asamura H, Yamamoto M, Hirohashi S. Cancer related mutations in NRF2 impair its recognition by Keap1-Cul3 E3 ligase and promote malignancy. Proc Natl Acad Sci U S A. 2008;105(36):13568-73.

126. Wang R, An J, Ji F, Jiao H, Sun H, Zhou D. Hypermethylation of the Keap1 gene in human lung cancer cell lines and lung cancer tissues. Biochem Biophys Res Commun. 2008;373(1):151-4.

127. Kim YR, Oh JE, Kim MS, Kang MR, Park SW, Han JY, Eom HS, Yoo NJ, Lee SH. Oncogenic NRF2 mutations in squamous cell carcinomas of oesophagus and skin. J Pathol. 2010;220(4):446-51.

128. Solis LM, Behrens C, Dong W, Suraokar M, Ozburn NC, Moran CA, Corvalan AH, Biswal S, Swisher SG, Bekele BN, Minna JD, Stewart DJ, Wistuba, II. Nrf2 and Keap1 abnormalities in non-small cell lung carcinoma and association with clinicopathologic features. Clin Cancer Res. 2010;16(14):3743-53.

129. Zhang P, Singh A, Yegnasubramanian S, Esopi D, Kombairaju P, Bodas M, Wu H, Bova SG, Biswal S. Loss of Kelch-like ECH-associated protein 1 function in prostate cancer cells causes chemoresistance and radioresistance and promotes tumor growth. Mol Cancer Ther. 2010;9(2):336-46.

130. Berger AH, Brooks AN, Wu X, Shrestha Y, Chouinard C, Piccioni F, Bagul M, Kamburov A, Imielinski M, Hogstrom L, Zhu C, Yang X, Pantel S, Sakai R, Watson J, Kaplan N, Campbell JD, Singh S, Root DE, Narayan R, Natoli T, Lahr DL, Tirosh I, Tamayo P, Getz G, Wong B, Doench J, Subramanian A, Golub TR, Meyerson M, Boehm JS. High-throughput Phenotyping of Lung Cancer Somatic Mutations. Cancer Cell. 2016;30(2):214-28.

131. Goldstein Leonard D, Lee J, Gnad F, Klijn C, Schaub A, Reeder J, Daemen A, Bakalarski Corey E, Holcomb T, Shames David S, Hartmaier Ryan J, Chmielecki J, Seshagiri S, Gentleman R, Stokoe D. Recurrent Loss of NFE2L2 Exon 2 Is a Mechanism for Nrf2 Pathway Activation in Human Cancers. Cell Reports. 2016;16(10):2605-17.

132. Jeong Y, Hoang NT, Lovejoy A, Stehr H, Newman AM, Gentles AJ, Kong W, Truong D, Martin S, Chaudhuri A, Heiser D, Zhou L, Say C, Carter JN, Hiniker SM, Loo BW, West RB, Beachy P, Alizadeh AA, Diehn M. Role of KEAP1/NRF2 and TP53 mutations in lung squamous cell carcinoma development and radiation resistance. Cancer Discovery. 2017;7(1):86-101.

133. Best SA, De Souza DP, Kersbergen A, Policheni AN, Dayalan S, Tull D, Rathi V, Gray DH, Ritchie ME, McConville MJ, Sutherland KD. Synergy between the KEAP1/NRF2 and PI3K Pathways Drives Non-Small-Cell Lung Cancer with an Altered Immune Microenvironment. Cell Metabolism. 2018;27(4):935-43.e4.

134. Rogers ZN, McFarland CD, Winters IP, Seoane JA, Brady JJ, Yoon S, Curtis C, Petrov DA, Winslow MM. Mapping the in vivo fitness landscape of lung adenocarcinoma tumor suppression in mice. Nature Genetics. 2018.

135. Fu J, Xiong Z, Huang C, Li J, Yang W, Han Y, Paiboonrungruan C, Major MB, Chen KN, Kang X, Chen X. Hyperactivity of the transcription factor Nrf2 causes metabolic reprogramming in mouse esophagus. Journal of Biological Chemistry. 2019;294(1):327-40.

136. Romero R, Sánchez-Rivera FJ, Westcott PMK, Mercer KL, Bhutkar A, Muir A, González Robles TJ, Lamboy Rodríguez S, Liao LZ, Ng SR, Li L, Colón CI, Naranjo S, Beytagh MC, Lewis CA, Hsu PP, Bronson RT, Vander Heiden MG, Jacks T. Keap1 mutation renders lung adenocarcinomas dependent on Slc33a1. Nature Cancer. 2020;1(6):589-602.

137. Denicola GM, Karreth FA, Humpton TJ, Gopinathan A, Wei C, Frese K, Mangal D, Yu KH, Yeo CJ, Calhoun ES, Scrimieri F, Winter JM, Hruban RH, Iacobuzio-Donahue C, Kern SE, Blair IA, Tuveson DA. Oncogene-induced Nrf2 transcription promotes ROS detoxification and tumorigenesis. Nature. 2011;475(7354):106-10.

138. Sporn MB, Liby KT. NRF2 and cancer: the good, the bad and the importance of context. Nat Rev Cancer. 2012;12(8):564-71.

139. Hagiya Y, Adachi T, Ogura S, An R, Tamura A, Nakagawa H, Okura I, Mochizuki T, Ishikawa T. Nrf2-dependent induction of human ABC transporter ABCG2 and heme oxygenase-1 in HepG2 cells by photoactivation of porphyrins: biochemical implications for cancer cell response to photodynamic therapy. J Exp Ther Oncol. 2008;7(2):153-67.

140. Singh A, Wu H, Zhang P, Happel C, Ma J, Biswal S. Expression of ABCG2 (BCRP) is regulated by Nrf2 in cancer cells that confers side population and chemoresistance phenotype. Mol Cancer Ther. 2010;9(8):2365-76.

141. Sargazi Z, Yazdani Y, Tahavvori A, Youshanlouei HR, Alivirdiloo V, Beilankouhi EAV, Valilo M. NFR2/ABC transporter axis in drug resistance of breast cancer cells. Mol Biol Rep. 2023;50(6):5407-14.

142. Wang Q, Xu L, Wang G, Chen L, Li C, Jiang X, Gao H, Yang B, Tian W. Prognostic and clinicopathological significance of NRF2 expression in non-small cell lung cancer: A meta-analysis. PLoS One. 2020;15(11):e0241241.

143. Zhao J, Lin X, Meng D, Zeng L, Zhuang R, Huang S, Lv W, Hu J. Nrf2 Mediates Metabolic Reprogramming in Non-Small Cell Lung Cancer. Front Oncol. 2020;10:578315.

144. Hayashi M, Kuga A, Suzuki M, Panda H, Kitamura H, Motohashi H, Yamamoto M. Microenvironmental Activation of Nrf2 Restricts the Progression of Nrf2-Activated Malignant Tumors. Cancer Res. 2020;80(16):3331-44.

145. Singh A, Daemen A, Nickles D, Jeon S-M, Foreman O, Sudini K, Gnad F, Lajoie S, Gour N, Mitzner W, Chatterjee S, Choi E-J, Ravishankar B, Rappaport A, Patil N, McCleland M, Johnson L, Acquaah-Mensah G, Gabrielson E, Biswal S, Hatzivassiliou G. NRF2 Activation Promotes Aggressive Lung Cancer and Associates with Poor Clinical Outcomes. Clinical Cancer Research. 2021;27(3):877.

146. Foggetti G, Li C, Cai H, Hellyer JA, Lin W-Y, Ayeni D, Hastings K, Choi J, Wurtz A, Andrejka L, Maghini DG, Rashleigh N, Levy S, Homer R, Gettinger SN, Diehn M, Wakelee HA, Petrov DA, Winslow MM, Politi K. Genetic Determinants of EGFR-Driven Lung Cancer Growth and Therapeutic Response In Vivo. Cancer Discovery. 2021;11(7):1736-53.

147. Cai H, Chew SK, Li C, Tsai MK, Andrejka L, Murray CW, Hughes NW, Shuldiner EG, Ashkin EL, Tang R, Hung KL, Chen LC, Lee SYC, Yousefi M, Lin WY, Kunder CA, Cong L, McFarland CD, Petrov DA, Swanton C, Winslow MM. A Functional Taxonomy of Tumor Suppression in Oncogenic KRAS-Driven Lung Cancer. Cancer Discov. 2021;11(7):1754-73.

148. Rogers ZN, McFarland CD, Winters IP, Naranjo S, Chuang C-H, Petrov D, Winslow MM. A quantitative and multiplexed approach to uncover the fitness landscape of tumor suppression in vivo. Nature Methods. 2017;14(7):737-42.

149. Cheung EC, DeNicola GM, Nixon C, Blyth K, Labuschagne CF, Tuveson DA, Vousden KH. Dynamic ROS Control by TIGAR Regulates the Initiation and Progression of Pancreatic Cancer. Cancer Cell. 2020.

150. Khor TO, Huang MT, Prawan A, Liu Y, Hao X, Yu S, Cheung WK, Chan JY, Reddy BS, Yang CS, Kong AN. Increased susceptibility of Nrf2 knockout mice to colitis-associated colorectal cancer. Cancer Prev Res (Phila). 2008;1(3):187-91.

151. Xu C, Huang MT, Shen G, Yuan X, Lin W, Khor TO, Conney AH, Kong AN. Inhibition of 7,12-dimethylbenz(a)anthracene-induced skin tumorigenesis in C57BL/6 mice by sulforaphane is mediated by nuclear factor E2-related factor 2. Cancer Res. 2006;66(16):8293-6.

152. Elkashty OA, Tran SD. Sulforaphane as a Promising Natural Molecule for Cancer Prevention and Treatment. Current Medical Science. 2021;41(2):250-69.

153. Pouremamali F, Pouremamali A, Dadashpour M, Soozangar N, Jeddi F. An update of Nrf2 activators and inhibitors in cancer prevention/promotion. Cell Commun Signal. 2022;20(1):100.

154. DeBlasi JM, Falzone A, Caldwell S, Prieto-Farigua N, Prigge JR, Schmidt EE, Chio IIC, Karreth FA, DeNicola GM. Distinct Nrf2 Signaling Thresholds Mediate Lung Tumor Initiation and Progression. Cancer Res. 2023.

155. Wakabayashi N, Itoh K, Wakabayashi J, Motohashi H, Noda S, Takahashi S, Imakado S, Kotsuji T, Otsuka F, Roop DR, Harada T, Engel JD, Yamamoto M. Keap1-null mutation leads to postnatal lethality due to constitutive Nrf2 activation. Nature Genetics. 2003.

156. Hast BE, Cloer EW, Goldfarb D, Li H, Siesser PF, Yan F, Walter V, Zheng N, Hayes DN, Major MB. Cancer-derived mutations in KEAP1 impair NRF2 degradation but not ubiquitination. Cancer Research. 2014.

157. Tong KI, Padmanabhan B, Kobayashi A, Shang C, Hirotsu Y, Yokoyama S, Yamamoto M. Different Electrostatic Potentials Define ETGE and DLG Motifs as Hinge and Latch in Oxidative Stress Response. Molecular and Cellular Biology. 2007.

158. Taguchi K, Maher JM, Suzuki T, Kawatani Y, Motohashi H, Yamamoto M. Genetic Analysis of Cytoprotective Functions Supported by Graded Expression of Keap1. Molecular and Cellular Biology. 2010.

159. Huppke P, Weissbach S, Church JA, Schnur R, Krusen M, Dreha-Kulaczewski S, Kühn-Velten WN, Wolf A, Huppke B, Millan F, Begtrup A, Almusafri F, Thiele H, Altmüller J, Nürnberg P, Müller M, Gärtner J. Activating de novo mutations in NFE2L2 encoding NRF2 cause a multisystem disorder. Nature Communications. 2017;8(1):818.

160. Wohlhieter CA, Richards AL, Uddin F, Hulton CH, Quintanal-Villalonga À, Martin A, de Stanchina E, Bhanot U, Asher M, Shah NS, Hayatt O, Buonocore DJ, Rekhtman N, Shen R, Arbour KC, Donoghue M, Poirier JT, Sen T, Rudin CM. Concurrent Mutations in STK11 and KEAP1 Promote Ferroptosis Protection and SCD1 Dependence in Lung Cancer. Cell Rep. 2020;33(9):108444.

161. Dayalan Naidu S, Dinkova-Kostova AT. Omaveloxolone (Skyclarys(TM)) for patients with Friedreich's ataxia. Trends Pharmacol Sci. 2023;44(6):394-5.

162. Wang D, Mou H, Li S, Li Y, Hough S, Tran K, Li J, Yin H, Anderson DG, Sontheimer EJ, Weng Z, Gao G, Xue W. Adenovirus-Mediated Somatic Genome Editing of Pten by CRISPR/Cas9 in Mouse Liver in Spite of Cas9-Specific Immune Responses. Human Gene Therapy. 2015;26(7):432-42.

163. Jackson EL, Willis N, Mercer K, Bronson RT, Crowley D, Montoya R, Jacks T, Tuveson DA. Analysis of lung tumor initiation and progression using conditional expression of oncogenic K-ras. Genes and Development. 2001.

164. Hamad SH, Montgomery SA, Simon JM, Bowman BM, Spainhower KB, Murphy RM, Knudsen ES, Fenton SE, Randell SH, Holt JR, Hayes DN, Witkiewicz AK, Oliver TG, Major MB, Weissman BE. TP53, CDKN2A/P16, and NFE2L2/NRF2 regulate the incidence of pure- and combined-small cell lung cancer in mice. Oncogene. 2022;41(25):3423-32.

165. Taguchi K, Motohashi H, Yamamoto M. Molecular mechanisms of the Keap1–Nrf2 pathway in stress response and cancer evolution. Genes to Cells. 2011;16(2):123-40.

166. Jackson EL, Olive KP, Tuveson DA, Bronson R, Crowley D, Brown M, Jacks T. The differential effects of mutant p53 alleles on advanced murine lung cancer. Cancer Research. 2005;65(22):10280-8.

167. Nam LB, Keum Y-S. Binding partners of NRF2: Functions and regulatory mechanisms. Archives of Biochemistry and Biophysics. 2019;678:108184.

168. Pan X, Song X, Wang C, Cheng T, Luan D, Xu K, Tang B. H2Se induces reductive stress in HepG2 cells and activates cell autophagy by regulating the redox of HMGB1 protein under hypoxia. Theranostics. 2019.

169. Weiss-Sadan T, Ge M, Hayashi M, Gohar M, Yao C-H, de Groot A, Harry S, Carlin A, Fischer H, Shi L, Wei T-Y, Adelmann CH, Wolf K, Vornbäumen T, Dürr BR, Takahashi M, Richter M, Zhang J, Yang T-Y, Vijay V, Fisher DE, Hata AN, Haigis MC, Mostoslavsky R, Bardeesy N, Papagiannakopoulos T, Bar-Peled L. NRF2 activation induces NADH-reductive stress, providing a metabolic vulnerability in lung cancer. Cell Metabolism. 2023.

170. Hamada S, Shimosegawa T, Taguchi K, Nabeshima T, Yamamoto M, Masamune A. Simultaneous K-ras activation and Keap1 deletion cause atrophy of pancreatic parenchyma. American Journal of Physiology - Gastrointestinal and Liver Physiology. 2018.

171. Faraonio R, Vergara P, Di Marzo D, Pierantoni MG, Napolitano M, Russo T, Cimino F. p53 suppresses the Nrf2-dependent transcription of antioxidant response genes. Journal of Biological Chemistry. 2006.

172. Lengel HB, Mastrogiacomo B, Connolly JG, Tan KS, Liu Y, Fick CN, Dunne EG, He D, Lankadasari MB, Satravada BA, Sun Y, Kundra R, Fong C, Smith S, Riely GJ, Rudin CM, Gomez DR, Solit DB, Berger MF, Li BT, Mayo MW, Matei I, Lyden DC, Adusumilli PS, Schultz N, Sanchez-Vega F, Jones DR. Genomic mapping of metastatic organotropism in lung adenocarcinoma. Cancer Cell. 2023;41(5):970-85.e3.

173. Lo SC, Hannink M. PGAM5 tethers a ternary complex containing Keap1 and Nrf2 to mitochondria. Exp Cell Res. 2008;314(8):1789-803.

174. Ma J, Cai H, Wu T, Sobhian B, Huo Y, Alcivar A, Mehta M, Cheung KL, Ganesan S, Kong AN, Zhang DD, Xia B. PALB2 interacts with KEAP1 to promote NRF2 nuclear accumulation and function. Mol Cell Biol. 2012;32(8):1506-17.

175. Mulvaney KM, Matson JP, Siesser PF, Tamir TY, Goldfarb D, Jacobs TM, Cloer EW, Harrison JS, Vaziri C, Cook JG, Major MB. Identification and characterization of MCM3 as a kelch-like ECH-associated protein 1 (KEAP1) substrate. Journal of Biological Chemistry. 2016;291(45):23719-33.

176. Marzio A, Kurz E, Sahni JM, Di Feo G, Puccini J, Jiang S, Hirsch CA, Arbini AA, Wu WL, Pass HI, Bar-Sagi D, Papagiannakopoulos T, Pagano M. EMSY inhibits homologous recombination repair and the interferon response, promoting lung cancer immune evasion. Cell. 2022;185(1):169-83.e19.

177. Satoh H, Moriguchi T, Taguchi K, Takai J, Maher JM, Suzuki T, Winnard PT, Jr., Raman V, Ebina M, Nukiwa T, Yamamoto M. Nrf2-deficiency creates a responsive microenvironment for metastasis to the lung. Carcinogenesis. 2010;31(10):1833-43.

178. Satoh H, Moriguchi T, Saigusa D, Baird L, Yu L, Rokutan H, Igarashi K, Ebina M, Shibata T, Yamamoto M. NRF2 Intensifies Host Defense Systems to Prevent Lung Carcinogenesis, but After Tumor Initiation Accelerates Malignant Cell Growth. Cancer Res. 2016;76(10):3088-96.

179. Cerami E, Gao J, Dogrusoz U, Gross BE, Sumer SO, Aksoy BA, Jacobsen A, Byrne CJ, Heuer ML, Larsson E, Antipin Y, Reva B, Goldberg AP, Sander C, Schultz N. The cBio Cancer Genomics Portal: An open platform for exploring multidimensional cancer genomics data. Cancer Discovery. 2012.

180. Gao J, Aksoy BA, Dogrusoz U, Dresdner G, Gross B, Sumer SO, Sun Y, Jacobsen A, Sinha R, Larsson E, Cerami E, Sander C, Schultz N. Integrative analysis of complex cancer genomics and clinical profiles using the cBioPortal. Science Signaling. 2013.

181. Ji H, Ramsey MR, Hayes DN, Fan C, McNamara K, Kozlowski P, Torrice C, Wu MC, Shimamura T, Perera SA, Liang MC, Cai D, Naumov GN, Bao L, Contreras CM, Li D, Chen L, Krishnamurthy J, Koivunen J, Chirieac LR, Padera RF, Bronson RT, Lindeman NI, Christiani DC, Lin X, Shapiro GI, Jänne PA, Johnson BE, Meyerson M, Kwiatkowski DJ, Castrillon DH, Bardeesy N, Sharpless NE, Wong KK. LKB1 modulates lung cancer differentiation and metastasis. Nature. 2007.

182. Zhang H, Brainson CF, Koyama S, Redig AJ, Chen T, Li S, Gupta M, Garcia-De-Alba C, Paschini M, Herter-Sprie GS, Lu G, Zhang X, Marsh BP, Tuminello SJ, Xu C, Chen Z, Wang X, Akbay EA, Zheng M, Palakurthi S, Sholl LM, Rustgi AK, Kwiatkowski DJ, Diehl JA, Bass AJ, Sharpless NE, Dranoff G, Hammerman PS, Ji H, Bardeesy N, Saur D, Watanabe H, Kim CF, Wong KK. Lkb1 inactivation drives lung cancer lineage switching governed by Polycomb Repressive Complex 2. Nature Communications. 2017.

183. Lin C, Song H, Huang C, Yao E, Gacayan R, Xu SM, Chuang PT. Alveolar Type II Cells Possess the Capability of Initiating Lung Tumor Development. PLoS ONE. 2012.

184. Xu X, Rock JR, Lu Y, Futtner C, Schwab B, Guinney J, Hogan BL, Onaitis MW. Evidence for type II cells as cells of origin of K-Ras-induced distal lung adenocarcinoma. Proc Natl Acad Sci U S A. 2012;109(13):4910-5.

185. Mainardi S, Mijimolle N, Francoz S, Vicente-Dueñas C, Sánchez-García I, Barbacid M. Identification of cancer initiating cells in K-Ras driven lung adenocarcinoma. Proc Natl Acad Sci U S A. 2014;111(1):255-60.

186. Joo MS, Kim WD, Lee KY, Kim JH, Koo JH, Kim SG. AMPK Facilitates Nuclear Accumulation of Nrf2 by Phosphorylating at Serine 550. Mol Cell Biol. 2016;36(14):1931-42.

187. Kitamura H, Motohashi H. NRF2 addiction in cancer cells. Cancer Sci. 2018;109(4):900-11.

188. Institute B. DepMap Public 22Q2 2022.

189. Torrente L, Prieto-Farigua N, Falzone A, Elkins CM, Boothman DA, Haura EB, DeNicola GM. Inhibition of TXNRD or SOD1 overcomes NRF2-mediated resistance to β-lapachone. Redox Biology. 2020;30(January):101440-.

190. Feldser DM, Kostova KK, Winslow MM, Taylor SE, Cashman C, Whittaker CA, Sanchez-Rivera FJ, Resnick R, Bronson R, Hemann MT, Jacks T. Stage-specific sensitivity to p53 restoration during lung cancer progression. Nature. 2010;468(7323):572-5.

191. Dodson M, Castro-Portuguez R, Zhang DD. NRF2 plays a critical role in mitigating lipid peroxidation and ferroptosis. Redox Biol. 2019;23:101107.

192. Chen ZH, Saito Y, Yoshida Y, Sekine A, Noguchi N, Niki E. 4-Hydroxynonenal induces adaptive response and enhances PC12 cell tolerance primarily through induction of thioredoxin reductase 1 via activation of Nrf2. J Biol Chem. 2005;280(51):41921-7.

193. Dupage M, Dooley AL, Jacks T. Conditional mouse lung cancer models using adenoviral or lentiviral delivery of Cre recombinase. 2009;4(8):1064-73.

194. Tuveson DA, Shaw AT, Willis NA, Silver DP, Jackson EL, Chang S, Mercer KL, Grochow R, Hock H, Crowley D, Hingorani SR, Zaks T, King C, Jacobetz MA, Wang L, Bronson RT, Orkin SH, DePinho RA, Jacks T. Endogenous oncogenic K-ras(G12D) stimulates proliferation and widespread neoplastic and developmental defects. Cancer Cell. 2004;5(4):375-87.

195. Murphy DJ, Junttila MR, Pouyet L, Karnezis A, Shchors K, Bui DA, Brown-Swigart L, Johnson L, Evan GI. Distinct thresholds govern Myc's biological output in vivo. Cancer Cell. 2008;14(6):447-57.

196. Jamal-Hanjani M, Wilson GA, McGranahan N, Birkbak NJ, Watkins TBK, Veeriah S, Shafi S, Johnson DH, Mitter R, Rosenthal R, Salm M, Horswell S, Escudero M, Matthews N, Rowan A, Chambers T, Moore DA, Turajlic S, Xu H, Lee S-M, Forster MD, Ahmad T, Hiley CT, Abbosh C, Falzon M, Borg E, Marafioti T, Lawrence D, Hayward M, Kolvekar S, Panagiotopoulos N, Janes SM, Thakrar R, Ahmed A, Blackhall F, Summers Y, Shah R, Joseph L, Quinn AM, Crosbie PA, Naidu B, Middleton G, Langman G, Trotter S, Nicolson M, Remmen H, Kerr K, Chetty M, Gomersall L, Fennell DA, Nakas A, Rathinam S, Anand G, Khan S, Russell P, Ezhil V, Ismail B, Irvin-Sellers M, Prakash V, Lester JF, Kornaszewska M, Attanoos R, Adams H, Davies H, Dentro S, Taniere P, O'Sullivan B, Lowe HL, Hartley JA, Iles N, Bell H, Ngai Y, Shaw JA, Herrero J, Szallasi Z, Schwarz RF, Stewart A, Quezada SA, Le Quesne J, Van Loo P, Dive C, Hackshaw A, Swanton C. Tracking the Evolution of Non–Small-Cell Lung Cancer. New England Journal of Medicine. 2017;376(22):2109-21.

197. Ohta T, Iijima K, Miyamoto M, Nakahara I, Tanaka H, Ohtsuji M, Suzuki T, Kobayashi A, Yokota J, Sakiyama T, Shibata T, Yamamoto M, Hirohashi S. Loss of Keap1 function activates Nrf2 and provides advantages for lung cancer cell growth. Cancer Res. 2008;68(5):1303-9.

198. Clasquin MF, Melamud E, Rabinowitz JD. LC-MS data processing with MAVEN: a metabolomic analysis and visualization engine. Curr Protoc Bioinformatics. 2012;Chapter 14:Unit14.1.

199. McLoughlin MR, Orlicky DJ, Prigge JR, Krishna P, Talago EA, Cavigli IR, Eriksson S, Miller CG, Kundert JA, Sayin VI, Sabol RA, Heinemann J, Brandenberger LO, Iverson SV, Bothner B, Papagiannakopoulos T, Shearn CT, Arnér ESJ, Schmidt EE. TrxR1, Gsr, and oxidative stress determine hepatocellular carcinoma malignancy. Proc Natl Acad Sci U S A. 2019;116(23):11408-17.

200. Bankhead P, Loughrey MB, Fernandez JA, Dombrowski Y, McArt DG, Dunne PD, McQuaid S, Gray RT, Murray LJ, Coleman HG, James JA, Salto-Tellez M, Hamilton PW. QuPath: Open source software for digital pathology image analysis. Sci Rep. 2017;7(1):16878.

201. Jiang C, Ward NP, Prieto-Farigua N, Kang YP, Thalakola A, Teng M, DeNicola GM. A CRISPR screen identifies redox vulnerabilities for KEAP1/NRF2 mutant non-small cell lung cancer. Redox Biology. 2022;54:102358.

Appendix A: Keap1$^{R554Q/R5554Q}$ Metabolomics

	Fold Change	p-value	FDR
3-SULFINO-L-ALANINE_neg	**29.502**	**0.0022559**	**0.080067**
GLUTATHIONE_neg	**18.148**	**0.00020636**	**0.020171**
GLUTATHIONE_pos	**13.179**	**3.08E-05**	**0.010066**
HYPOTAURINE_neg	**6.6494**	**0.0028703**	**0.080409**
HYPOTAURINE_pos	**5.866**	**0.0023674**	**0.080067**
N-ACETYL-L-CYSTEINE_neg	**5.5681**	**0.0023646**	**0.080067**
N-ACETYL-L-CYSTEINE_pos	**5.3289**	**0.00031396**	**0.024551**
L-CYSTATHIONINE_neg	**5.1072**	**0.0013865**	**0.080067**
S-5'-ADENOSYL-L-HOMOCYSTEINE_neg	**4.4167**	**0.0021156**	**0.080067**
S-5'-ADENOSYL-L-HOMOCYSTEINE_pos	**4.0788**	**0.0024573**	**0.080067**
URIDINE 5'-DIPHOSPHO-N-ACETYLGLUCOSAMINE_neg	**3.6978**	**0.038236**	**0.30511**
PHENYLACETALDEHYDE_pos	**3.3232**	**0.0051765**	**0.13493**
L-CYSTEIC ACID_neg	**3.1211**	**0.00014838**	**0.019339**
L-CYSTATHIONINE_pos	**3.0515**	**0.041104**	**0.30907**
4-HYDROXY-L-PHENYLGLYCINE_pos	2.7458	0.10797	0.47576
MONO-METHYL GLUTARATE_pos	**2.7136**	**0.030428**	**0.29744**
XANTHOSINE_neg	**2.4639**	**0.0086153**	**0.1767**
GUANOSINE 5'-TRIPHOSPHATE_neg	2.2639	0.1841	0.56139
URIDINE-5-MONOPHOSPHATE_neg	2.244	0.077708	0.43406
3-METHOXY-4-HYDROXYMANDELATE_neg	2.2199	0.13156	0.49563
METHYL JASMONATE_neg	1.9189	0.19595	0.56752
GUANOSINE 5'-TRIPHOSPHATE_pos	1.8349	0.16971	0.53572
D-GLUCOSAMINE 6-PHOSPHATE_neg	**1.785**	**0.017219**	**0.21718**
2,6-DIHYDROXYPYRIDINE_pos	1.776	0.062761	0.39732
N-ACETYL-L-ASPARTIC ACID_neg	1.7219	0.085461	0.44827
D-GLUCONATE_neg	**1.6973**	**0.013536**	**0.19309**
RIBITOL_neg	1.6226	0.16016	0.52328

IS_L-HISTIDINE_pos	1.6217	0.062302	0.39732
HOMOCYSTEINE_pos	1.5946	0.23384	0.61363
N-ACETYL-DL-METHIONINE_pos	**1.5935**	**0.04487**	**0.32489**
O-ACETYL-L-CARNITINE_pos	**1.59**	**0.012122**	**0.18837**
CITRATE_neg	1.5741	0.084073	0.44827
3-METHYL-2-OXINDOLE_pos	1.5736	0.35769	0.73583
N-ACETYL-D-MANNOSAMINE_neg	**1.5623**	**0.014815**	**0.19309**
ALPHA-AMINOADIPATE_pos	**1.5461**	**0.035121**	**0.30511**
FORMYL-L-METHIONYL PEPTIDE_pos	1.5442	0.1606	0.52328
ALPHA-AMINOADIPATE_neg	**1.5213**	**0.025041**	**0.27197**
ADENOSINE 5'-TRIPHOSPHATE_pos	1.514	0.099695	0.47531
CREATININE_neg	1.5138	0.16231	0.52448
DEOXYCYTIDINE_neg	1.507	0.10151	0.47531
MESO-TARTARIC ACID_neg	1.5046	0.20591	0.5834
IS_L-ARGININE_neg	1.504	0.063413	0.39732
URATE_neg	1.4991	0.44435	0.75191
PYRIDOXAL 5'-PHOSPHATE_neg	1.4858	0.43215	0.75191
OMEGA-HYDROXYDODECANOIC ACID_neg	1.4857	0.13502	0.49563
IS_L-SERINE_pos	1.4855	0.090176	0.45791
IS_L-LYSINE_neg	**1.4832**	**0.03276**	**0.30511**
URIDINE 5'-DIPHOSPHOGLUCURONIC ACID_neg	**1.4783**	**0.03311**	**0.30511**
CYTIDINE 5'-TRIPHOSPHATE_pos	1.4691	0.32045	0.7086
CREATININE_pos	1.4677	0.15142	0.50604
2-OXOADIPIC ACID_neg	1.4644	0.22086	0.59971
URIDINE 5'-DIPHOSPHOGLUCOSE_neg	**1.4553**	**0.042238**	**0.3116**
PYRIDOXAMINE_pos	1.4489	0.30061	0.67744
SN-GLYCEROL 3-PHOSPHATE_neg	1.4473	0.053891	0.37627
CAFFEATE_neg	1.4397	0.52957	0.77182
TRANS-ACONITATE_neg	1.4256	0.13538	0.49563
N-ACETYL-L-ASPARTIC ACID_pos	**1.4252**	**0.014461**	**0.19309**
SHIKIMATE_neg	**1.4131**	**0.020877**	**0.24009**
O-PHOSPHORYLETHANOLAMINE_pos	1.4107	0.2258	0.60471
N-ACETYL-DL-GLUTAMIC ACID_neg	1.4089	0.34298	0.72882
D-GLUCURONOLACTONE_neg	1.3955	0.12428	0.49563
ALPHA-D-GLUCOSE 1-PHOSPHATE_neg	1.3892	0.071234	0.42201
TAURINE_pos	1.387	0.089804	0.45791
TRANS-CINNAMALDEHYDE_pos	1.3838	0.053626	0.37627
Beta-ALANINE_pos	1.3784	0.095146	0.47308
N-ACETYL-DL-METHIONINE_neg	1.3759	0.21863	0.59971

L-ALANINE_neg	1.3558	0.15115	0.50604
PROPIONATE_neg	1.3552	0.4733	0.75534
N-ACETYLSEROTONIN_pos	1.3469	0.35095	0.73026
D-GLUCOSE-6-PHOSPHATE_neg	1.3467	0.12775	0.49563
UROCANATE_pos	1.3351	0.64995	0.81805
GAMMA-LINOLENIC ACID_pos	1.3342	0.12712	0.49563
IS_GLYCINE_neg	1.3276	0.39224	0.74152
METHYL JASMONATE_pos	1.3252	0.21299	0.59914
S-HEXYL-GLUTATHIONE_pos	**1.3246**	**0.0062141**	**0.15186**
PHOSPHOCHOLINE_pos	1.3233	0.10868	0.47576
IS_LEUCINE_neg	**1.3088**	**0.028627**	**0.29744**
IS_L-VALINE_neg	**1.3048**	**0.0094197**	**0.1767**
IS_L-PROLINE_pos	**1.3035**	**0.012526**	**0.18837**
CREATINE_neg	1.3007	0.26171	0.65177
IS_L-PROLINE_neg	1.3003	0.070193	0.42201
4-AMINOBUTANOATE_pos	1.3002	0.14891	0.50604
IS_L-HISTIDINE_neg	1.296	0.13077	0.49563
TRIGONELLINE_pos	**1.2946**	**0.029835**	**0.29744**
CYTIDINE_pos	1.2931	0.29324	0.67744
GLUTARIC ACID_neg	**1.2913**	**0.006809**	**0.15661**
N-ACETYL-DL-SERINE_neg	1.2911	0.095585	0.47308
IS_L-THREONINE_pos	1.2891	0.085986	0.44827
IS_L-TYROSINE_pos	1.2856	0.1445	0.50604
IS_D-ASPARTATE_neg	**1.2818**	**0.010207**	**0.1767**
CARNOSINE_pos	1.2814	0.3032	0.67744
CREATINE_pos	1.2757	0.12737	0.49563
L-SERINE_pos	1.2751	0.28535	0.6762
3-UREIDOPROPIONATE_neg	1.2723	0.65348	0.81805
ADENOSINE 5'-MONOPHOSPHATE_neg	1.2711	0.42822	0.75191
2-DEOXY-D-GLUCOSE_neg	1.2689	0.41939	0.75191
TRANS-CYCLOHEXANE-1,2-DIOL_pos	1.2671	0.064887	0.39732
10-HYDROXYDECANOATE_neg	1.2671	0.32082	0.7086
IS_L-VALINE_pos	**1.2595**	**0.030172**	**0.29744**
URIDINE 5'-DIPHOSPHO-N-ACETYLGLUCOSAMINE_pos	1.2595	0.081843	0.44445
SN-GLYCEROL 3-PHOSPHATE_pos	**1.2531**	**0.014034**	**0.19309**
IS_L-ISOLEUCINE_neg	1.2527	0.10707	0.47576
IS_L-PHENYLALANINE_neg	**1.2493**	**0.041009**	**0.30907**
MALONATE_neg	1.2482	0.08008	0.44101
IS_L-TYROSINE_neg	1.2481	0.16491	0.52854

QUINATE_neg	**1.2382**	**0.037163**	**0.30511**
PHOSPHOCREATINE_pos	1.237	0.37757	0.74152
IS_D-ASPARTATE_pos	1.2353	0.17328	0.53771
IS_L-THREONINE_neg	1.2321	0.64461	0.81805
GLYCINE_pos	1.2203	0.14741	0.50604
D-GLUCOSAMINE 6-PHOSPHATE_pos	1.2161	0.44336	0.75191
IS_L-ALANINE_neg	1.2144	0.25871	0.65177
GLYCEROL 2-PHOSPHATE_pos	1.2133	0.13377	0.49563
D-GLUCOSE 6-PHOSPHATE_pos	1.2083	0.2964	0.67744
cis-5,8,11,14,17-Eicosapentaenoic acid_pos	1.2039	0.074276	0.42363
URIDINE-5-MONOPHOSPHATE_pos	1.203	0.46089	0.75191
GUANOSINE 5'-DIPHOSPHATE_neg	1.202	0.33981	0.72683
URIDINE 5'-DIPHOSPHATE_neg	1.2007	0.25595	0.64985
IS_L-ALANINE_pos	1.2003	0.45934	0.75191
FORMYL-L-METHIONYL PEPTIDE_neg	1.1981	0.074758	0.42363
O-SUCCINYL-L-HOMOSERINE_neg	1.197	0.43611	0.75191
ADENOSINE 5'-DIPHOSPHATE_neg	1.1911	0.32383	0.7086
IS_L-PHENYLALANINE_pos	**1.1893**	**0.037649**	**0.30511**
N-ACETYL-D-MANNOSAMINE_pos	**1.1831**	**0.036701**	**0.30511**
2'-DEOXYGUANOSINE 5'-MONOPHOSPHATE_pos	1.1814	0.46732	0.75191
IS_GLYCINE_pos	1.1781	0.11091	0.47576
GUANOSINE 5'-MONOPHOSPHATE_pos	1.177	0.49039	0.76574
BIS2-ETHYLHEXYLPHTHALATE_pos	1.1748	0.68507	0.82419
MYO-INOSITOL_neg	1.1745	0.3352	0.7241
HEPTANOIC ACID_pos	1.1737	0.13706	0.4962
NAD_pos	1.1714	0.51899	0.77157
TAURINE_neg	1.171	0.18522	0.56139
GUANOSINE 5'-MONOPHOSPHATE_neg	1.1644	0.55017	0.7851
IS_L-GLUTAMIC ACID_pos	1.1608	0.45869	0.75191
OXALIC ACID_neg	1.1597	0.35111	0.73026
IS_L-GLUTAMIC ACID_neg	**1.1593**	**0.0028791**	**0.080409**
PHOSPHONOACETATE_neg	1.1565	0.4867	0.76574
CHOLINE_pos	1.1544	0.77478	0.88502
CYTIDINE 5'-DIPHOSPHOCHOLINE_pos	1.1535	0.32586	0.7086
GLYCINE_neg	**1.1528**	**0.04059**	**0.30907**
L-PROLINE_pos	1.1527	0.22371	0.60324
2,3-DIHYDROXYBENZOATE_neg	1.1507	0.65017	0.81805
L-CARNITINE_pos	1.1419	0.18682	0.56183
3-METHYLGLUTARIC ACID_neg	1.1384	0.27245	0.66166

148

BUTANAL_pos	1.123	0.41632	0.75191
4-HYDROXY-2-QUINOLINECARBOXYLIC ACID_pos	1.1211	0.73595	0.85642
N6-DELTA2-ISOPENTENYL-ADENINE_pos	1.1188	0.61336	0.81805
L-PROLINE_neg	1.1141	0.36886	0.73583
CAPRYLIC ACID_neg	1.1137	0.1002	0.47531
OROTIC ACID_neg	1.1113	0.45714	0.75191
L-ARABITOL_pos	1.1033	0.69075	0.82594
ADENOSINE 5'-DIPHOSPHATE_pos	1.1027	0.53484	0.77182
CYTIDINE 5'-DIPHOSPHATE_neg	1.1016	0.59305	0.81362
DEOXYCYTIDINE_pos	1.0973	0.46816	0.75191
N-ACETYL-L-ALANINE_neg	1.0925	0.38035	0.74152
SORBATE_neg	1.0904	0.65596	0.81805
ACETYLCHOLINE_pos	1.0869	0.528	0.77182
DEOXYCARNITINE_pos	1.0869	0.528	0.77182
DIACETYL_pos	1.0858	0.52519	0.77182
PALMITOYL-DL-CARNITINE CHLORIDE_pos	**1.084**	**0.036223**	**0.30511**
GUANOSINE 5'-DIPHOSPHATE_pos	1.0834	0.44795	0.75191
URIDINE 5'-DIPHOSPHATE_pos	1.0815	0.36871	0.73583
5-AMINOPENTANOATE_neg	1.0791	0.62111	0.81805
D---ARABINOSE_neg	1.0749	0.8046	0.89629
CYTIDINE 5'-DIPHOSPHATE_pos	1.0747	0.59218	0.81362
GUANIDINOACETATE_pos	1.0675	0.56589	0.79306
S-DIHYDROOROTATE_neg	1.0591	0.86095	0.9325
ADENINE_pos	1.0578	0.6702	0.82147
CITRAMALATE_neg	1.0569	0.80747	0.89694
D-XYLOSE_neg	1.0558	0.84011	0.92531
ADENOSINE 5'-MONOPHOSPHATE_pos	1.0553	0.79084	0.88939
PYRIDINE-2,3-DICARBOXYLATE_neg	1.0505	0.85901	0.9325
5,6-DIHYDROURACIL_pos	1.0501	0.55695	0.78617
METHYL ACETOACETATE_pos	1.0438	0.8836	0.93992
3-NITRO-L-TYROSINE_neg	1.0424	0.30162	0.67744
1-AMINOCYCLOPROPANE-1-CARBOXYLATE_pos	1.041	0.79386	0.88939
THYMIDINE 5'-MONOPHOSPHATE_neg	1.041	0.92165	0.95766
NG-NG-DIMETHYLARGININE DIHYDROCHLORIDE_neg	1.0329	0.91175	0.95507
N-METHYL-D-ASPARTIC ACID_neg	1.0313	0.8873	0.9402
L-RHAMNOSE_neg	1.029	0.84635	0.92956
3-AMINOISOBUTANOATE_neg	1.0259	0.9217	0.95766
4-HYDROXY-L-PROLINE_neg	1.0254	0.91319	0.95507

S-MALATE_neg	1.0242	0.85939	0.9325
L-THREONINE_pos	1.0221	0.87874	0.93992
L-GLUTAMIC ACID_pos	1.0179	0.92854	0.96047
3-HYDROXY-3-METHYLGLUTARATE_neg	1.0143	0.9568	0.97934
BETAINE_pos	1.0078	0.94634	0.97118
ITACONATE_neg	1.0075	0.963	0.98131
L-ALANINE_pos	1.0074	0.96637	0.98143
S-HEXYL-GLUTATHIONE_neg	1.0033	0.97417	0.98373
5'-CMP_pos	1.0026	0.99208	0.99219
L-ASPARAGINE_pos	0.99768	0.98566	0.99072
PYRIDOXAL 5'-PHOSPHATE_pos	0.99673	0.99219	0.99219
TRANS-4-HYDROXYPROLINE_pos	0.99432	0.96374	0.98131
HIPPURATE_pos	0.99203	0.97618	0.98373
L-THREONINE_neg	0.98938	0.97609	0.98373
INOSINE_neg	0.98554	0.94462	0.97118
L-GLUTAMIC ACID_neg	0.98495	0.77627	0.88502
L-ASPARAGINE_neg	0.98363	0.94202	0.97118
DECANOATE_neg	0.97828	0.86444	0.9337
NICOTINAMIDE_pos	0.97745	0.89252	0.94318
IS_L-SERINE_neg	0.97691	0.92337	0.95766
N-METHYL-D-ASPARTIC ACID_pos	0.9754	0.85951	0.9325
3,4-DIHYDROXYPHENYL GLYCOL_neg	0.97515	0.88031	0.93992
D---3-PHOSPHOGLYCERIC ACID_neg	0.97506	0.78974	0.88939
GUANIDINOACETATE_neg	0.9747	0.88463	0.93992
SALICYLAMIDE_pos	0.97441	0.87755	0.93992
4-AMINOBUTANOATE_neg	0.97146	0.69006	0.82594
NEPSILON,NEPSILON,NEPSILON-TRIMETHYLLYSINE_pos	0.96789	0.8305	0.9173
O-PHOSPHORYLETHANOLAMINE_neg	0.96591	0.79745	0.89087
N-ACETYLNEURAMINATE_neg	0.96245	0.7203	0.85087
HYPOXANTHINE_neg	0.96024	0.87016	0.93728
N-ACETYL-DL-GLUTAMIC ACID_pos	0.95898	0.89724	0.94561
2-METHYLPROPANOATE_neg	0.95885	0.6811	0.82419
Beta-ALANINE_neg	0.95698	0.66876	0.82147
O-ACETYL-L-SERINE_pos	0.95695	0.66549	0.82147
N-ACETYL-L-LEUCINE_pos	0.95458	0.73014	0.85474
4-HYDROXY-3-METHOXYPHENYLGLYCOL_neg	0.94423	0.77637	0.88502
PHOSPHOCREATINE_neg	0.94347	0.4481	0.75191
5-OXO-L-PROLINE_pos	0.94253	0.65041	0.81805

NALPHA-ACETYL-L-LYSINE_pos	0.94182	0.75657	0.8752
L-LYSINE_neg	0.94113	0.77473	0.88502
ADENOSINE_pos	0.9402	0.63742	0.81805
DIACETYL_neg	0.93966	0.67807	0.82419
L-ORNITHINE_neg	0.9375	0.79208	0.88939
CYTOSINE_pos	0.93712	0.50669	0.76574
URIDINE_neg	0.92838	0.78253	0.88687
L-TYROSINE_pos	0.9278	0.48779	0.76574
SODIUM BENZOATE_neg	0.92779	0.68495	0.82419
RETINOATE_neg	0.92501	0.60865	0.81805
PYRIDOXINE_neg	0.92372	0.61732	0.81805
L-GLUTAMINE_pos	0.92369	0.23732	0.61659
LAURIC ACID_neg	0.92098	0.66867	0.82147
URACIL_neg	0.92045	0.66302	0.82147
HYPOXANTHINE_pos	0.917	0.7071	0.84035
L-ARGININE_neg	0.91696	0.69828	0.8324
2-QUINOLINECARBOXYLIC ACID_pos	0.91669	0.78165	0.88687
D-RIBOSE_neg	0.91382	0.60688	0.81805
cis-5,8,11,14,17-Eicosapentaenoic acid_neg	0.9137	0.60141	0.81649
ALLANTOIN_neg	0.91256	0.71096	0.84239
CYTIDINE_neg	0.91079	0.76256	0.87953
D-MANNOSAMINE_pos	0.91058	0.82157	0.91001
4-METHYLCATECHOL_neg	0.90967	0.7272	0.85386
ALLANTOIN_pos	0.90945	0.72308	0.85158
NG-NG-DIMETHYLARGININE DIHYDROCHLORIDE_pos	0.90895	0.68366	0.82419
NONANOATE_neg	0.90381	0.55248	0.78553
PHOSPHOCHOLINE_neg	0.90245	0.91354	0.95507
4-IMIDAZOLEACETIC ACID_pos	0.90186	0.2988	0.67744
FERULATE_neg	0.90186	0.85232	0.9325
PYRIDOXAL_neg	0.8998	0.49913	0.76574
D--GALACTOSAMINE_pos	0.89703	0.51778	0.77157
HEPTANOIC ACID_neg	0.89661	0.65695	0.81805
S-5'-ADENOSYL-L-METHIONINE_pos	0.89592	0.73356	0.85619
D--GLUCOSAMINE_pos	0.89589	0.51681	0.77157
2-DEOXY-D-GLUCOSE_pos	0.89506	0.63862	0.81805
DOCOSAHEXAENOIC ACID_neg	0.89486	0.63562	0.81805
N-ACETYL-L-ALANINE_pos	0.89396	0.20495	0.5834
D-GLYCERIC ACID_neg	0.89173	0.6399	0.81805
L-METHIONINE_neg	0.89044	0.48716	0.76574

N-ACETYL-L-PROLINE_pos	0.88913	0.54814	0.78507
N-ALPHA-ACETYL-L-ASPARAGINE_pos	0.88809	0.53243	0.77182
THYMINE_neg	0.88739	0.54666	0.78507
D-GLUCURONIC ACID_neg	0.88416	0.67853	0.82419
L-TRYPTOPHAN_neg	0.88398	0.59755	0.81408
FUMARATE_neg	0.8839	0.30231	0.67744
PALMITOLEIC ACID_neg	0.88148	0.59628	0.81408
L-TYROSINE_neg	0.87912	0.23034	0.61267
INOSINE_pos	0.87734	0.57044	0.79374
L-SERINE_neg	0.87691	0.22062	0.59971
L-ISOLEUCINE_neg	0.86862	0.51579	0.77157
D-SORBITOL_pos	0.8673	0.57886	0.79977
PIPECOLATE_pos	0.86514	0.27041	0.66082
ACETOACETATE_pos	0.86142	0.36407	0.73583
MONO-METHYL GLUTARATE_neg	0.85975	0.46922	0.75191
L-PHENYLALANINE_neg	0.85883	0.41987	0.75191
5-HYDROXYINDOLEACETATE_neg	0.85883	0.62492	0.81805
L-VALINE_pos	0.85797	0.56907	0.79374
D-SORBITOL_neg	0.85775	0.4987	0.76574
ETHYLMALONIC ACID_neg	0.85768	0.63327	0.81805
LEUCINE_neg	0.85694	0.50209	0.76574
L-HISTIDINE_neg	0.85639	0.32621	0.7086
DEOXYURIDINE_neg	0.85481	0.30036	0.67744
D-FRUCTOSE_neg	0.85377	0.64277	0.81805
MYRISTIC ACID_neg	0.85113	0.36565	0.73583
CARNOSINE_neg	0.84975	0.39458	0.74152
L-METHIONINE_pos	0.846	0.4967	0.76574
CITRULLINE_pos	0.84584	0.44704	0.75191
ADIPIC ACID_pos	0.84167	0.50058	0.76574
1-AMINOCYCLOPROPANE-1-CARBOXYLATE_neg	0.84093	0.74384	0.86303
INDOLE-3-ACETALDEHYDE_pos	0.83921	0.65516	0.81805
L-TRYPTOPHAN_pos	0.83771	0.57531	0.79769
XANTHINE_neg	0.83268	0.45241	0.75191
5-OXO-L-PROLINE_neg	0.83255	0.49058	0.76574
NICOTINATE_pos	0.83105	0.295	0.67744
O-SUCCINYL-L-HOMOSERINE_pos	0.82735	0.63782	0.81805
N-ACETYL-L-PHENYLALANINE_pos	0.82734	0.39605	0.74152
ACETOACETATE_neg	0.82541	0.35112	0.73026
L-ASPARTATE_neg	0.82365	0.15022	0.50604

DIETHYL 2-METHYL-3-OXOSUCCINATE_neg	0.82331	0.44718	0.75191
L-VALINE_neg	0.81968	0.46761	0.75191
5'-METHYLTHIOADENOSINE_neg	0.8196	0.065035	0.39732
2-QUINOLINECARBOXYLIC ACID_neg	0.81953	0.50662	0.76574
GLYCERALDEHYDE 3-PHOSPHATE DIETHYL ACETAL_neg	0.81817	0.39737	0.74152
L-ORNITHINE_pos	0.81796	0.53494	0.77182
FOLIC ACID_pos	0.81764	0.61828	0.81805
ADENINE_neg	**0.8154**	**0.010394**	**0.1767**
L-GLUTAMINE_neg	0.81414	0.12861	0.49563
L-ASPARTATE_pos	0.81216	0.11438	0.47576
4-PYRIDOXATE_pos	0.80866	0.56172	0.79005
N-FORMYLGLYCINE_pos	0.80494	0.64968	0.81805
4-COUMARATE_neg	0.80045	0.060974	0.39732
PHENYLPYRUVATE_neg	0.80045	0.060974	0.39732
N-ACETYL-L-PROLINE_neg	0.79327	0.11139	0.47576
2-HYDROXYPHENYLACETIC ACID_neg	0.79145	0.41644	0.75191
3-HYDROXYPHENYLACETATE_neg	0.79145	0.41644	0.75191
THYMINE_pos	0.78557	0.50723	0.76574
L-PHENYLALANINE_pos	0.78516	0.42684	0.75191
PYRROLE-2-CARBOXYLATE_neg	0.77929	0.38428	0.74152
QUINOLINE_pos	0.77913	0.23372	0.61363
THYMIDINE_neg	0.77773	0.25322	0.64713
4-HYDROXYBENZOATE_neg	0.77724	0.52418	0.77182
4-ACETAMIDOBUTANOATE_neg	0.77463	0.41264	0.75191
D---3-PHOSPHOGLYCERIC ACID_pos	0.77269	0.19025	0.56183
N,N-DIMETHYL-1,4-PHENYLENEDIAMINE_pos	0.76967	0.3869	0.74152
5'-METHYLTHIOADENOSINE_pos	**0.76926**	**0.020874**	**0.24009**
RS-MEVALONIC ACID LITHIUM SALT_neg	0.76388	0.46189	0.75191
GUANINE_pos	0.75887	0.12427	0.49563
GAMMA-LINOLENIC ACID_neg	0.75676	0.61989	0.81805
3-2-HYDROXYPHENYLPROPANOATE_neg	0.75334	0.34585	0.73026
DIMETHYLBENZIMIDAZOLE_pos	0.75254	0.45496	0.75191
N-ACETYLPUTRESCINE_pos	0.75074	0.34018	0.72683
URACIL_pos	0.75074	0.4414	0.75191
N-METHYL-L-GLUTAMATE_pos	0.74879	0.44378	0.75191
ERYTHRITOL_neg	0.74871	0.39787	0.74152
LINOLEATE_neg	0.74514	0.36732	0.73583
HISTAMINE_pos	0.74484	0.39826	0.74152

INDOLE-3-ACETAMIDE_pos	0.74187	0.55506	0.78617
ARACHIDIC ACID_neg	0.73868	0.65049	0.81805
ELAIDIC ACID_neg	0.73413	0.4194	0.75191
OLEATE_neg	0.73413	0.4194	0.75191
NICOTINATE_neg	0.73262	0.24875	0.63986
SODIUM GLYCOCHENODEOXYCHOLATE_neg	0.72892	0.37339	0.74109
N-FORMYLGLYCINE_neg	0.72632	0.63066	0.81805
PYRIDOXINE_pos	0.72	0.38382	0.74152
PENTANOATE_neg	0.70927	0.44807	0.75191
L-KYNURENINE_pos	0.70729	0.39001	0.74152
SUCCINIC ACID_neg	0.70495	0.28081	0.67323
D-PANTOTHENIC ACID_pos	0.69817	0.10211	0.47531
4-ACETAMIDOBUTANOATE_pos	0.69674	0.35932	0.73583
D-PANTOTHENIC ACID_neg	0.69616	0.14281	0.50604
N-ACETYLNEURAMINATE_pos	0.68571	0.26821	0.65957
NALPHA-ACETYL-L-LYSINE_neg	0.68521	0.1124	0.47576
HIPPURATE_neg	0.68287	0.42422	0.75191
PALMITATE_neg	0.67673	0.15647	0.51849
LAUROYLCARNITINE_pos	0.67161	0.26148	0.65177
4-PYRIDOXATE_neg	0.67126	0.44929	0.75191
L-LYSINE MONOHYDROCHLORIDE_pos	0.66755	0.49274	0.76574
IS_L-CYSTINE_neg	0.66297	0.19172	0.56183
N-ALPHA-ACETYL-L-ASPARAGINE_neg	0.65837	0.10923	0.47576
5-METHYLCYTOSINE HYDROCLORIDE_pos	0.63944	0.27814	0.6713
PYRIDOXAL_pos	0.63316	0.1699	0.53572
4-HYDROXY-2-QUINOLINECARBOXYLIC ACID_neg	0.62975	0.21851	0.59971
STEARATE_neg	0.6205	0.20358	0.5834
N-ACETYL-L-LEUCINE_neg	**0.61558**	**0.033756**	**0.30511**
DAMP_pos	0.61289	0.2174	0.59971
D-LACTOSE_pos	0.60994	0.23812	0.61659
HEPTADECANOATE_neg	0.60935	0.17882	0.55055
3-4-HYDROXYPHENYLLACTATE_neg	**0.60388**	**0.011767**	**0.18837**
2-HYDROXYBUTYRIC ACID_neg	0.60076	0.30097	0.67744
BETAINE_neg	0.59555	0.38968	0.74152
O-PHOSPHO-L-SERINE_pos	**0.56628**	**0.019883**	**0.24009**
O-ACETYL-L-CARNITINE_neg	0.55849	0.13563	0.49563
NICOTINAMIDE_neg	0.55796	0.26797	0.65957
CITRULLINE_neg	0.55482	0.17323	0.53771

O-PHOSPHO-L-SERINE_neg	**0.53678**	**0.024799**	**0.27197**
3-METHYL-2-OXOVALERIC ACID_neg	0.51788	0.11413	0.47576
N-ACETYL-D-TRYPTOPHAN_pos	0.50842	0.19254	0.56183
3-4-HYDROXYPHENYLPYRUVATE_neg	0.50645	0.14249	0.50604
RAC-GLYCEROL 1-MYRISTATE_neg	0.50189	0.073106	0.42363
D-RIBOSE 5-PHOSPHATE_neg	0.49613	0.099664	0.47531
L-KYNURENINE_neg	0.4952	0.10932	0.47576
4-GUANIDINOBUTANOATE_pos	**0.48556**	**0.0089583**	**0.1767**
2-HYDROXY-4-METHYLTHIOBUTYRIC ACID_neg	0.47779	0.062543	0.39732
OPHTHALMIC ACID_pos	**0.46432**	**0.0099405**	**0.1767**
OPHTHALMIC ACID_neg	0.42791	0.13287	0.49563
METHYL ACETOACETATE_neg	0.39206	0.14717	0.50604
ALPHA-KETOGLUTARIC ACID_neg	**0.35544**	**0.0018711**	**0.080067**
PYRUVATE_neg	0.21608	0.28238	0.67323
THIAMINE_pos	0.18406	0.36478	0.73583
THIAMINE MONOPHOSPHATE_pos	0.063524	0.19129	0.56183
IS_L-CYSTINE_pos	**0.011194**	**5.15E-05**	**0.010066**

Appendix A. Metabolites in Keap1$^{R554Q/R554Q}$ MEFs compared to Keap1$^{+/+}$ MEFs via LC-HRMS from our lab's previous study (43). N=3, representative of two individual MEF lines. Significantly altered metabolites with a p-value < 0.05 are **bold**.

Appendix B: Nrf2$^{D29H/D29H}$ Metabolomics

	Fold Change	p-value	FDR
GLUTATHIONE_neg	**9.7457**	**0.0004529**	**0.040811**
GLUTATHIONE_pos	**5.6944**	**0.00027915**	**0.036383**
3-SULFINO-L-ALANINE_neg	**4.3252**	**6.80E-05**	**0.013589**
N-ACETYL-L-CYSTEINE_pos	**3.715**	**0.0052455**	**0.083427**
N-ACETYL-L-CYSTEINE_neg	**2.576**	**6.95E-05**	**0.013589**
3-METHOXY-4-HYDROXYMANDELATE_neg	**2.5373**	**0.0032181**	**0.069903**
HYPOTAURINE_pos	**2.5249**	**0.00073063**	**0.040811**
3-UREIDOPROPIONATE_neg	2.3495	0.095864	0.25498
PYRIDOXAL 5'-PHOSPHATE_pos	2.215	0.11915	0.28234
HYPOTAURINE_neg	**2.1974**	**0.00056858**	**0.040811**
5-AMINOPENTANOATE_neg	**2.131**	**0.011989**	**0.097486**
L-CYSTATHIONINE_neg	**2.1221**	**0.036153**	**0.1415**
S-5'-ADENOSYL-L-METHIONINE_pos	2.0541	0.18387	0.38386
S-5'-ADENOSYL-L-HOMOCYSTEINE_pos	2.0346	0.11267	0.27881
S-5'-ADENOSYL-L-HOMOCYSTEINE_neg	1.9619	0.15749	0.34401
GAMMA-LINOLENIC ACID_neg	1.8054	0.16393	0.35217
HOMOCYSTEINE_pos	**1.6952**	**0.019998**	**0.10315**
PHENYLACETALDEHYDE_pos	**1.6616**	**0.010787**	**0.089742**
L-CYSTEIC ACID_neg	**1.615**	**0.0081453**	**0.083427**
ARACHIDIC ACID_neg	1.5959	0.19452	0.39832
OPHTHALMIC ACID_neg	**1.479**	**0.0025216**	**0.064642**
MONO-METHYL GLUTARATE_pos	**1.4508**	**0.026704**	**0.11474**
CREATININE_neg	1.4363	0.1065	0.27217
PYRIDOXAL 5'-PHOSPHATE_neg	1.4165	0.38193	0.58386
N-FORMYLGLYCINE_neg	1.4128	0.32882	0.55138
GUANIDINOACETATE_neg	1.4034	0.36536	0.56655
GUANOSINE 5'-TRIPHOSPHATE_neg	1.3999	0.19493	0.39832
L-CYSTATHIONINE_pos	1.3976	0.1093	0.27395
IS_L-CYSTINE_neg	1.3763	0.25075	0.47135
OPHTHALMIC ACID_pos	**1.3575**	**0.017711**	**0.10315**
ADENOSINE 5'-TRIPHOSPHATE_pos	1.3463	0.10084	0.26285
CREATININE_pos	1.322	0.0522	0.17151
D-GLUCURONOLACTONE_neg	1.3174	0.33934	0.55496
PHOSPHONOACETATE_neg	1.3113	0.10423	0.26812

IS_GLYCINE_neg	1.3041	0.11524	0.28125
URIDINE 5'-DIPHOSPHO-N-ACETYLGLUCOSAMINE_pos	1.3009	0.10018	0.26285
N,N-DIMETHYL-1,4-PHENYLENEDIAMINE_pos	**1.2924**	**0.019237**	**0.10315**
OXALIC ACID_neg	1.2861	0.48156	0.67677
N-ACETYL-DL-METHIONINE_neg	1.28	0.11862	0.28234
URACIL_pos	1.2779	0.34064	0.55496
LAUROYLCARNITINE_pos	1.2728	0.43924	0.63782
IS_L-SERINE_neg	1.2685	0.17406	0.3696
SN-GLYCEROL 3-PHOSPHATE_pos	**1.249**	**0.046638**	**0.15857**
D-GLUCONATE_neg	**1.2471**	**0.0062113**	**0.083427**
CYTIDINE 5'-TRIPHOSPHATE_pos	1.2391	0.3328	0.55138
N-ACETYL-DL-METHIONINE_pos	1.2335	0.24657	0.46575
IS_L-THREONINE_neg	1.2142	0.33144	0.55138
MALONATE_neg	1.2128	0.51588	0.70389
IS_L-TYROSINE_pos	1.2114	0.10842	0.27351
N-ACETYLPUTRESCINE_pos	1.2089	0.36499	0.56655
N-ACETYL-D-MANNOSAMINE_neg	1.2026	0.25768	0.4775
IS_L-GLUTAMIC ACID_pos	1.2025	0.097796	0.25837
THIAMINE MONOPHOSPHATE_pos	1.2014	0.30624	0.52518
IS_L-HISTIDINE_neg	**1.1993**	**0.01029**	**0.087466**
4-COUMARATE_neg	1.1966	0.56264	0.71995
PHENYLPYRUVATE_neg	1.1966	0.56264	0.71995
D-GLUCOSE 6-PHOSPHATE_pos	1.1935	0.33561	0.55368
MYO-INOSITOL_neg	1.184	0.1956	0.39832
IS_L-LYSINE_neg	1.1833	0.058419	0.18273
4-HYDROXYBENZOATE_neg	1.175	0.26215	0.48349
FERULATE_neg	1.1744	0.56568	0.71995
N6-DELTA2-ISOPENTENYL-ADENINE_pos	1.1728	0.38507	0.58386
FORMYL-L-METHIONYL PEPTIDE_pos	1.1722	0.36405	0.56655
4-AMINOBUTANOATE_pos	**1.1601**	**0.0026452**	**0.064642**
PALMITOLEIC ACID_neg	1.153	0.30461	0.52518
D-GLUCOSE-6-PHOSPHATE_neg	1.148	0.076573	0.22682
QUINATE_neg	1.1448	0.35199	0.56405
HEPTANOIC ACID_pos	1.1439	0.36344	0.56655
S-HEXYL-GLUTATHIONE_pos	1.1436	0.63715	0.77129
CREATINE_pos	1.1428	0.081607	0.23462
D-RIBOSE 5-PHOSPHATE_neg	1.142	0.51371	0.70389
DIETHYL 2-METHYL-3-OXOSUCCINATE_neg	1.1348	0.12582	0.29284
MESO-TARTARIC ACID_neg	1.1316	0.69917	0.80825
S-MALATE_neg	1.1301	0.28762	0.50429
BIS2-ETHYLHEXYLPHTHALATE_pos	1.1296	0.5495	0.71995
TRANS-CYCLOHEXANE-1,2-DIOL_pos	1.1284	0.61669	0.76015

IS_L-ARGININE_neg	1.1282	0.055874	0.17907
NAD_pos	1.1278	0.69362	0.80711
IS_L-ISOLEUCINE_neg	1.1267	0.060928	0.18758
L-GLUTAMINE_neg	1.1259	0.40736	0.60912
SALICYLAMIDE_pos	1.1258	0.41976	0.61934
L-SERINE_neg	1.1251	0.37314	0.5744
2-DEOXY-D-GLUCOSE_neg	1.12	0.72232	0.82823
GLYCEROL 2-PHOSPHATE_pos	1.1188	0.18035	0.37913
L-ASPARAGINE_neg	1.1183	0.32908	0.55138
2'-DEOXYGUANOSINE 5'-MONOPHOSPHATE_pos	1.1131	0.34532	0.55856
LAURIC ACID_neg	1.1122	0.44456	0.63782
L-ARABITOL_pos	1.1117	0.80454	0.88874
IS_LEUCINE_neg	1.1105	0.086324	0.24057
OROTIC ACID_neg	1.1093	0.33903	0.55496
Beta-ALANINE_pos	**1.1067**	**0.044107**	**0.15537**
N-ACETYL-L-ALANINE_neg	1.1065	0.12271	0.28904
N-ACETYL-DL-SERINE_neg	1.1063	0.10761	0.27321
METHYL JASMONATE_pos	1.1062	0.4	0.60387
HEPTADECANOATE_neg	1.0997	0.43409	0.63569
O-ACETYL-L-CARNITINE_pos	1.0944	0.13892	0.3104
ELAIDIC ACID_neg	1.0941	0.4597	0.65361
OLEATE_neg	1.0941	0.4597	0.65361
IS_L-TYROSINE_neg	1.0888	0.31462	0.53491
CITRATE_neg	1.088	0.080893	0.23429
N-ACETYLSEROTONIN_pos	1.0851	0.54461	0.71995
MYRISTIC ACID_neg	1.0836	0.50729	0.70088
TAURINE_neg	1.0825	0.15952	0.34467
4-HYDROXY-L-PHENYLGLYCINE_pos	1.0821	0.65717	0.7882
N-ACETYL-L-ASPARTIC ACID_pos	**1.081**	**0.0042965**	**0.08076**
DOCOSAHEXAENOIC ACID_neg	1.0783	0.44145	0.63782
IS_L-VALINE_pos	1.0773	0.22986	0.45012
PALMITATE_neg	1.0764	0.67121	0.79528
ALPHA-D-GLUCOSE 1-PHOSPHATE_neg	1.0739	0.58488	0.73533
S-HEXYL-GLUTATHIONE_neg	1.0715	0.15955	0.34467
10-HYDROXYDECANOATE_neg	1.0699	0.75905	0.84832
IS_L-PHENYLALANINE_neg	1.0696	0.3457	0.55856
STEARATE_neg	1.0695	0.61831	0.76015
PALMITOYL-DL-CARNITINE CHLORIDE_pos	1.0624	0.23024	0.45012
ADENOSINE 5'-DIPHOSPHATE_neg	1.0606	0.59871	0.74791
PYRROLE-2-CARBOXYLATE_neg	1.0591	0.4103	0.61
IS_L-PROLINE_neg	1.0575	0.52924	0.71546
ALPHA-AMINOADIPATE_neg	1.0572	0.64003	0.77238

4-HYDROXY-3-METHOXYPHENYLGLYCOL_neg	1.0554	0.62456	0.76313
DECANOATE_neg	1.0539	0.56712	0.71995
FUMARATE_neg	1.0472	0.71869	0.8265
PYRIDOXAMINE_pos	1.0459	0.85442	0.91779
IS_L-PROLINE_pos	1.0451	0.53318	0.71641
N-METHYL-D-ASPARTIC ACID_pos	1.0447	0.55473	0.71995
O-SUCCINYL-L-HOMOSERINE_neg	1.0408	0.69263	0.80711
IS_L-VALINE_neg	1.0333	0.40793	0.60912
IS_L-HISTIDINE_pos	1.0311	0.60348	0.75146
O-PHOSPHORYLETHANOLAMINE_neg	1.0302	0.66549	0.79331
URIDINE 5'-DIPHOSPHOGLUCURONIC ACID_neg	1.0286	0.7399	0.83855
MONO-METHYL GLUTARATE_neg	1.0273	0.72496	0.82883
CYTIDINE_pos	1.0271	0.82158	0.89731
GLYCINE_pos	1.0251	0.55925	0.71995
TAURINE_pos	1.0251	0.7872	0.87691
XANTHOSINE_neg	1.0244	0.91902	0.95744
GLYCINE_neg	1.0242	0.74755	0.83992
ADENOSINE 5'-DIPHOSPHATE_pos	1.0228	0.44533	0.63782
2-OXOADIPIC ACID_neg	1.0192	0.86389	0.92543
TRANS-4-HYDROXYPROLINE_pos	1.0188	0.81962	0.89731
URIDINE 5'-DIPHOSPHATE_pos	1.017	0.80691	0.88874
ADENOSINE 5'-MONOPHOSPHATE_pos	1.0133	0.86947	0.92561
METHYL JASMONATE_neg	1.0123	0.97067	0.99113
SN-GLYCEROL 3-PHOSPHATE_neg	1.0111	0.84021	0.90752
IS_D-ASPARTATE_pos	1.0102	0.92173	0.95744
TRANS-ACONITATE_neg	1.0086	0.89359	0.93923
RAC-GLYCEROL 1-MYRISTATE_neg	1.0067	0.97155	0.99113
QUINOLINE_pos	1.0063	0.98541	0.99113
cis-5,8,11,14,17-Eicosapentaenoic acid_pos	1.0055	0.98311	0.99113
Beta-ALANINE_neg	1.0052	0.89125	0.93923
N-ALPHA-ACETYL-L-ASPARAGINE_pos	1.0052	0.95065	0.97845
URIDINE 5'-DIPHOSPHATE_neg	1.004	0.96509	0.99042
L-THREONINE_neg	1.0034	0.98392	0.99113
PHOSPHOCHOLINE_neg	1.0027	0.98853	0.99113
IS_L-SERINE_pos	1.0015	0.98004	0.99113
5,6-DIHYDROURACIL_pos	0.99862	0.99497	0.99497
3-METHYLGLUTARIC ACID_neg	0.9974	0.98859	0.99113
4-HYDROXY-2-QUINOLINECARBOXYLIC ACID_pos	0.99735	0.98356	0.99113
IS_L-ALANINE_pos	0.9924	0.92408	0.95744
IS_L-GLUTAMIC ACID_neg	0.98934	0.87353	0.92561
CYTIDINE 5'-DIPHOSPHOCHOLINE_pos	0.98783	0.91542	0.95744
NONANOATE_neg	0.9874	0.95092	0.97845

PHOSPHOCHOLINE_pos	0.98704	0.79619	0.8844
N-ACETYL-D-MANNOSAMINE_pos	0.98702	0.83167	0.90329
N-METHYL-D-ASPARTIC ACID_neg	0.98581	0.86952	0.92561
URATE_neg	0.98349	0.92561	0.95744
IS_D-ASPARTATE_neg	0.98285	0.2926	0.51074
CYTIDINE_neg	0.98214	0.87289	0.92561
GUANOSINE 5'-DIPHOSPHATE_neg	0.98039	0.8064	0.88874
IS_L-ALANINE_neg	0.9798	0.53941	0.71983
2,6-DIHYDROXYPYRIDINE_pos	0.97959	0.8833	0.93343
3-AMINOISOBUTANOATE_neg	0.97945	0.84501	0.91019
N-ACETYL-L-ALANINE_pos	0.97848	0.5787	0.72991
4-METHYLCATECHOL_neg	0.97613	0.92162	0.95744
FORMYL-L-METHIONYL PEPTIDE_neg	0.97343	0.74755	0.83992
IS_L-PHENYLALANINE_pos	0.97259	0.36119	0.56655
4-IMIDAZOLEACETIC ACID_pos	0.97085	0.62017	0.76015
N-ACETYLNEURAMINATE_neg	0.97019	0.73558	0.83852
N-ACETYL-L-ASPARTIC ACID_neg	0.9676	0.608	0.75455
CITRAMALATE_neg	0.96611	0.60982	0.75455
N-METHYL-L-GLUTAMATE_pos	0.96606	0.67815	0.79972
CAPRYLIC ACID_neg	0.96433	0.53569	0.71731
L-SERINE_pos	0.9621	0.5467	0.71995
3,4-DIHYDROXYPHENYL GLYCOL_neg	0.96196	0.36391	0.56655
L-CARNITINE_pos	0.96126	0.59002	0.73942
DIMETHYLBENZIMIDAZOLE_pos	0.96058	0.68485	0.80276
SORBATE_neg	0.95933	0.74735	0.83992
RIBITOL_neg	0.95761	0.67904	0.79972
CYTIDINE 5'-DIPHOSPHATE_neg	0.95012	0.63151	0.76922
ADENOSINE 5'-MONOPHOSPHATE_neg	0.94978	0.83518	0.90459
IS_GLYCINE_pos	0.94872	0.38526	0.58386
SODIUM BENZOATE_neg	0.94823	0.53065	0.71546
D---3-PHOSPHOGLYCERIC ACID_neg	0.94598	0.55359	0.71995
INOSINE_neg	0.93889	0.48286	0.67677
ADENINE_pos	0.93657	0.2682	0.48997
L-KYNURENINE_neg	0.93552	0.73873	0.83855
4-HYDROXY-L-PROLINE_neg	0.93312	0.75937	0.84832
GUANIDINOACETATE_pos	0.93244	0.15723	0.34401
DEOXYCYTIDINE_pos	0.93187	0.095735	0.25498
L-ALANINE_pos	0.93085	0.18555	0.38386
N-ALPHA-ACETYL-L-ASPARAGINE_neg	0.93005	0.55281	0.71995
O-PHOSPHORYLETHANOLAMINE_pos	0.92984	0.34743	0.55903
2-METHYLPROPANOATE_neg	0.92893	0.38447	0.58386
ACETYLCHOLINE_pos	0.92777	0.11653	0.28125
DEOXYCARNITINE_pos	0.92777	0.11653	0.28125
LINOLEATE_neg	0.92598	0.82012	0.89731
DIACETYL_neg	0.92535	0.25391	0.47501

TRIGONELLINE_pos	**0.92372**	**0.001282**	**0.055695**
1-AMINOCYCLOPROPANE-1-CARBOXYLATE_pos	0.91846	0.13558	0.30824
3-HYDROXY-3-METHYLGLUTARATE_neg	0.91684	0.13809	0.3104
TRANS-CINNAMALDEHYDE_pos	0.91289	0.6701	0.79528
5'-CMP_pos	0.90994	0.66018	0.78939
BUTANAL_pos	0.90759	0.51667	0.70389
2,3-DIHYDROXYBENZOATE_neg	0.90709	0.70076	0.80825
L-GLUTAMIC ACID_pos	**0.90619**	**0.020073**	**0.10315**
5'-METHYLTHIOADENOSINE_pos	0.90328	0.28173	0.4962
DEOXYURIDINE_neg	0.90294	0.48291	0.67677
L-TYROSINE_pos	0.90188	0.21855	0.43602
N-ACETYL-DL-GLUTAMIC ACID_neg	0.9011	0.11356	0.27926
D-RIBOSE_neg	**0.89982**	**0.015457**	**0.10315**
L-GLUTAMINE_pos	0.89642	0.084324	0.23892
ALPHA-AMINOADIPATE_pos	0.89568	0.32673	0.55138
ACETOACETATE_pos	0.89524	0.68573	0.80276
3-NITRO-L-TYROSINE_neg	0.89336	0.28044	0.4962
GUANOSINE 5'-DIPHOSPHATE_pos	0.89264	0.41232	0.61067
ACETOACETATE_neg	0.89114	0.12761	0.29523
S-DIHYDROOROTATE_neg	0.88997	0.27037	0.48997
GAMMA-LINOLENIC ACID_pos	0.88845	0.57092	0.72243
THYMIDINE_neg	0.88755	0.18486	0.38386
SHIKIMATE_neg	0.88031	0.30614	0.52518
N-ACETYL-L-PROLINE_pos	**0.88016**	**0.0080898**	**0.083427**
D-LACTOSE_pos	0.87619	0.49608	0.69027
L-ASPARTATE_pos	0.87603	0.077549	0.22798
GUANOSINE 5'-TRIPHOSPHATE_pos	0.87531	0.69564	0.80711
3-METHYL-2-OXINDOLE_pos	0.87433	0.48762	0.68092
ITACONATE_neg	**0.87312**	**0.022439**	**0.10959**
N-ACETYL-L-PROLINE_neg	0.8706	0.36659	0.56655
L-METHIONINE_neg	**0.86784**	**0.015658**	**0.10315**
PIPECOLATE_pos	**0.86473**	**0.024584**	**0.11076**
URACIL_neg	0.86468	0.1356	0.30824
GUANOSINE 5'-MONOPHOSPHATE_pos	0.86104	0.52878	0.71546
L-HISTIDINE_neg	**0.85971**	**0.018669**	**0.10315**
L-PROLINE_neg	**0.85941**	**0.018018**	**0.10315**
THYMINE_pos	0.85932	0.65191	0.7843
D---3-PHOSPHOGLYCERIC ACID_pos	0.85906	0.48186	0.67677
NICOTINATE_pos	0.85821	0.27893	0.4962
L-ASPARTATE_neg	**0.85748**	**0.024929**	**0.11076**
RETINOATE_neg	0.85677	0.82699	0.9007
L-GLUTAMIC ACID_neg	**0.85634**	**0.020368**	**0.10315**
L-TYROSINE_neg	**0.85614**	**0.017427**	**0.10315**
GUANOSINE 5'-MONOPHOSPHATE_neg	0.85588	0.54557	0.71995

5'-METHYLTHIOADENOSINE_neg	0.85377	0.31465	0.53491
L-PROLINE_pos	**0.85184**	**0.0052661**	**0.083427**
4-AMINOBUTANOATE_neg	**0.85004**	**0.0054431**	**0.083427**
OMEGA-HYDROXYDODECANOIC ACID_neg	0.84905	0.40816	0.60912
CYTIDINE 5'-DIPHOSPHATE_pos	0.84794	0.25554	0.4758
NALPHA-ACETYL-L-LYSINE_pos	0.84518	0.1253	0.29284
L-ISOLEUCINE_neg	**0.84074**	**0.024043**	**0.11076**
PROPIONATE_neg	0.83996	0.17488	0.3696
LEUCINE_neg	**0.83773**	**0.0078476**	**0.083427**
PENTANOATE_neg	0.83101	0.050244	0.16649
ADIPIC ACID_pos	0.83086	0.056478	0.17954
5-OXO-L-PROLINE_pos	0.82624	0.16859	0.3602
PYRIDINE-2,3-DICARBOXYLATE_neg	0.8262	0.053594	0.17463
ADENINE_neg	0.82543	0.054993	0.17771
PYRIDOXINE_neg	**0.8229**	**0.03105**	**0.12779**
BETAINE_pos	**0.8217**	**0.0020985**	**0.064642**
1-AMINOCYCLOPROPANE-1-CARBOXYLATE_neg	0.82087	0.29899	0.51957
2-DEOXY-D-GLUCOSE_pos	0.81892	0.057901	0.18257
URIDINE 5'-DIPHOSPHOGLUCOSE_neg	0.81584	0.36338	0.56655
D-GLUCOSAMINE 6-PHOSPHATE_pos	0.8155	0.28052	0.4962
CARNOSINE_neg	0.81472	0.21857	0.43602
L-VALINE_neg	**0.8127**	**0.015207**	**0.10315**
D-SORBITOL_pos	0.81242	0.063626	0.19137
SODIUM GLYCOCHENODEOXYCHOLATE_neg	0.81226	0.15053	0.33315
HIPPURATE_pos	0.81111	0.49943	0.69247
D-GLYCERIC ACID_neg	0.81104	0.15081	0.33315
CYTOSINE_pos	**0.81004**	**0.0043375**	**0.08076**
THYMINE_neg	0.80967	0.062671	0.19137
cis-5,8,11,14,17-Eicosapentaenoic acid_neg	0.80834	0.56511	0.71995
GLYCERALDEHYDE 3-PHOSPHATE DIETHYL ACETAL_neg	**0.80719**	**0.032574**	**0.1313**
N-ACETYL-L-LEUCINE_pos	**0.80549**	**0.036855**	**0.1415**
2-HYDROXYPHENYLACETIC ACID_neg	0.80525	0.24294	0.46111
PYRIDOXAL_neg	0.80346	0.35638	0.56655
D---ARABINOSE_neg	0.80198	0.12985	0.29865
3-HYDROXYPHENYLACETATE_neg	0.80141	0.23488	0.45241
NICOTINATE_neg	0.80024	0.44407	0.63782
L-PHENYLALANINE_neg	**0.79953**	**0.0040483**	**0.08076**
THYMIDINE 5'-MONOPHOSPHATE_neg	0.79931	0.23437	0.45241
O-ACETYL-L-CARNITINE_neg	**0.79912**	**0.041453**	**0.15007**
URIDINE 5'-DIPHOSPHO-N-ACETYLGLUCOSAMINE_neg	0.79786	0.63535	0.77129

D-XYLOSE_neg	0.79702	0.11055	0.27533
N-ACETYL-L-LEUCINE_neg	0.79667	0.094133	0.25383
IS_L-THREONINE_pos	0.79624	0.23855	0.45722
L-RHAMNOSE_neg	0.79534	0.27548	0.4962
NEPSILON,NEPSILON,NEPSILON-TRIMETHYLLYSINE_pos	**0.79254**	**0.038186**	**0.14253**
L-VALINE_pos	**0.79186**	**0.035647**	**0.1415**
L-ASPARAGINE_pos	**0.7906**	**0.019886**	**0.10315**
D-PANTOTHENIC ACID_pos	**0.79045**	**0.039823**	**0.14552**
N-ACETYL-L-PHENYLALANINE_pos	**0.78881**	**0.024918**	**0.11076**
4-HYDROXY-2-QUINOLINECARBOXYLIC ACID_neg	0.78865	0.20955	0.42233
O-PHOSPHO-L-SERINE_neg	**0.78506**	**0.038276**	**0.14253**
ALLANTOIN_pos	**0.78304**	**0.037275**	**0.1415**
L-TRYPTOPHAN_neg	**0.78232**	**0.0024641**	**0.064642**
CHOLINE_pos	**0.78117**	**0.020266**	**0.10315**
URIDINE-5-MONOPHOSPHATE_pos	0.78098	0.093255	0.25321
N-ACETYLNEURAMINATE_pos	**0.77962**	**0.019507**	**0.10315**
5-HYDROXYINDOLEACETATE_neg	0.77684	0.22248	0.43934
O-ACETYL-L-SERINE_pos	0.77134	0.19808	0.40129
D-SORBITOL_neg	**0.77093**	**0.024637**	**0.11076**
L-THREONINE_pos	0.76844	0.085023	0.23917
GLUTARIC ACID_neg	0.76741	0.08344	0.23814
NICOTINAMIDE_pos	**0.76659**	**0.012977**	**0.097684**
NALPHA-ACETYL-L-LYSINE_neg	0.76382	0.078277	0.22841
L-ARGININE_neg	**0.7631**	**0.037102**	**0.1415**
L-METHIONINE_pos	**0.76246**	**0.0086969**	**0.083427**
L-TRYPTOPHAN_pos	**0.76169**	**0.0022501**	**0.064642**
ERYTHRITOL_neg	**0.76144**	**0.012991**	**0.097684**
D-PANTOTHENIC ACID_neg	**0.76136**	**0.0063876**	**0.083427**
NG-NG-DIMETHYLARGININE DIHYDROCHLORIDE_pos	**0.76113**	**0.014836**	**0.10315**
L-ALANINE_neg	0.75974	0.56355	0.71995
O-PHOSPHO-L-SERINE_pos	**0.7554**	**0.012738**	**0.097684**
L-LYSINE_neg	**0.75485**	**0.0075808**	**0.083427**
2-QUINOLINECARBOXYLIC ACID_neg	0.75145	0.074636	0.22277
3-2-HYDROXYPHENYLPROPANOATE_neg	0.74977	0.11876	0.28234
3-4-HYDROXYPHENYLLACTATE_neg	**0.74864**	**0.0088547**	**0.083427**
5-OXO-L-PROLINE_neg	**0.73188**	**0.012217**	**0.097486**
ALPHA-KETOGLUTARIC ACID_neg	**0.7297**	**0.018865**	**0.10315**
UROCANATE_pos	0.72783	0.43704	0.63762
PYRIDOXINE_pos	**0.7221**	**0.026603**	**0.11474**
FOLIC ACID_pos	0.72121	0.22162	0.43934
4-GUANIDINOBUTANOATE_pos	**0.72036**	**0.00069806**	**0.040811**
CAFFEATE_neg	0.71906	0.55709	0.71995

ADENOSINE_pos	0.71662	0.089267	0.24408
L-KYNURENINE_pos	**0.7151**	**0.005298**	**0.083427**
CREATINE_neg	0.71423	0.51295	0.70389
CITRULLINE_neg	0.71265	0.13877	0.3104
SUCCINIC ACID_neg	**0.71153**	**0.04225**	**0.15018**
L-PHENYLALANINE_pos	**0.709**	**0.0017179**	**0.064642**
ALLANTOIN_neg	**0.70799**	**0.0011254**	**0.055004**
L-ORNITHINE_neg	**0.70784**	**0.013682**	**0.10094**
XANTHINE_neg	**0.70701**	**0.0065134**	**0.083427**
NICOTINAMIDE_neg	**0.70305**	**0.018285**	**0.10315**
HYPOXANTHINE_pos	**0.69954**	**0.0066692**	**0.083427**
METHYL ACETOACETATE_pos	0.69901	0.24221	0.46111
2-QUINOLINECARBOXYLIC ACID_pos	**0.69608**	**0.021598**	**0.1069**
RS-MEVALONIC ACID LITHIUM SALT_neg	**0.69495**	**0.0084792**	**0.083427**
HISTAMINE_pos	**0.69377**	**0.026997**	**0.11474**
DEOXYCYTIDINE_neg	0.68887	0.27014	0.48997
L-ORNITHINE_pos	**0.68305**	**0.0088211**	**0.083427**
D--GALACTOSAMINE_pos	**0.67881**	**0.020268**	**0.10315**
D--GLUCOSAMINE_pos	**0.67881**	**0.020268**	**0.10315**
CITRULLINE_pos	**0.67836**	**0.042016**	**0.15018**
DIACETYL_pos	0.67031	0.27068	0.48997
HYPOXANTHINE_neg	**0.66774**	**0.017645**	**0.10315**
4-ACETAMIDOBUTANOATE_neg	**0.6647**	**0.020578**	**0.10315**
URIDINE_neg	**0.66263**	**0.036519**	**0.1415**
N-ACETYL-DL-GLUTAMIC ACID_pos	0.66099	0.42956	0.63142
HEPTANOIC ACID_neg	0.65916	0.27923	0.4962
CARNOSINE_pos	0.65914	0.10351	0.26802
GUANINE_pos	**0.65852**	**0.010048**	**0.087306**
5-METHYLCYTOSINE HYDROCLORIDE_pos	0.65791	0.059148	0.18355
2-HYDROXYBUTYRIC ACID_neg	**0.65036**	**0.047508**	**0.16013**
INOSINE_pos	**0.64809**	**0.02306**	**0.10996**
PHOSPHOCREATINE_neg	**0.64702**	**0.039283**	**0.1449**
N-FORMYLGLYCINE_pos	**0.64314**	**0.048741**	**0.16289**
D-FRUCTOSE_neg	**0.64299**	**0.017994**	**0.10315**
3-4-HYDROXYPHENYLPYRUVATE_neg	**0.639**	**0.0029627**	**0.068141**
4-PYRIDOXATE_pos	0.63402	0.06325	0.19137
HIPPURATE_neg	**0.63178**	**0.032574**	**0.1313**
2-HYDROXY-4-METHYLTHIOBUTYRIC ACID_neg	**0.63**	**0.045629**	**0.1565**
4-ACETAMIDOBUTANOATE_pos	**0.62601**	**0.028353**	**0.11921**
THIAMINE_pos	**0.61056**	**0.019006**	**0.10315**
BETAINE_neg	**0.60556**	**0.044796**	**0.15565**
URIDINE-5-MONOPHOSPHATE_neg	0.6021	0.33237	0.55138
O-SUCCINYL-L-HOMOSERINE_pos	**0.59994**	**0.0072478**	**0.083427**

164

DAMP_pos	0.59627	0.087149	0.24057
PYRIDOXAL_pos	**0.59594**	**0.0091261**	**0.083427**
ETHYLMALONIC ACID_neg	**0.59158**	**0.025868**	**0.11365**
PHOSPHOCREATINE_pos	0.5862	0.087367	0.24057
L-LYSINE MONOHYDROCHLORIDE_pos	**0.58473**	**0.0293**	**0.12187**
INDOLE-3-ACETALDEHYDE_pos	**0.58309**	**0.0093936**	**0.083475**
D-GLUCOSAMINE 6-PHOSPHATE_neg	0.56353	0.23326	0.45241
INDOLE-3-ACETAMIDE_pos	**0.54456**	**0.020499**	**0.10315**
3-METHYL-2-OXOVALERIC ACID_neg	**0.53609**	**0.016897**	**0.10315**
NG-NG-DIMETHYLARGININE DIHYDROCHLORIDE_neg	**0.52195**	**0.0089341**	**0.083427**
4-PYRIDOXATE_neg	**0.50189**	**0.008741**	**0.083427**
METHYL ACETOACETATE_neg	**0.49196**	**0.0068957**	**0.083427**
D-GLUCURONIC ACID_neg	**0.46323**	**0.0091749**	**0.083427**
N-ACETYL-D-TRYPTOPHAN_pos	**0.43048**	**0.024359**	**0.11076**
D-MANNOSAMINE_pos	**0.32083**	**0.0018402**	**0.064642**
PYRUVATE_neg	**0.22695**	**0.044983**	**0.15565**
IS_L-CYSTINE_pos	**0.13481**	**0.022703**	**0.10959**

Appendix B. Metabolites in Nrf2$^{D29H/D29H}$ MEFs compared to Nrf2$^{LSL/LSL}$ MEFs via LC-HRMS. N=3, representative of two individual MEF lines. Significantly altered metabolites with a p-value < 0.05 are **bold**.

Appendix C: Copyright Permissions

Cancers Journal (Review) https://creativecommons.org/licenses/by/4.0/

Dear Janine,

Thanks for your email. Cancers is an open access journal and copyright is retained by the authors. The papers published in Cancers can be accessed for free.

More information is available at: https://www.mdpi.com/authors/rights

By the way, may I know if you or your team have/has any proposal in preparation? If so, would you consider Cancers as one of your possible options? Please feel free to contact us if you have any other questions.

Have a nice day.

Best regards,
Editorial Office
cancers@mdpi.com

Journal Editor
Ms. Fiona Huang
fiona.huang@mdpi.com

Cancers received an updated Journal Impact Factor of 5.2 (2022, 72/241 (Q2)), 5-Year Impact Factor: 5.6: https://www.mdpi.com/journal/cancers Welcome to follow us at https://twitter.com/Cancers_MDPI, https://linkedin.com/company/cancers-mdpi and https://facebook.com/CancersMDPI

On 9/13/2023 5:34 PM, Deblasi, Janine M wrote:
> CAUTION - EXTERNAL: This email originated from outside of MDPI
> organisation. BE CAUTIOUS especially to click links or open
> attachments.
>
> Hello,
>

1

> We published a review article in your Cancers journal in 2020, and I
> would like to use some of the figures and text in my PhD
> dissertation. As long as properly cited, is it allowed to adapt
> figures and text? It looks like this should be ok based on
> https://creativecommons.org/licenses/by/4.0/

167

Cancer Research (Article): https://creativecommons.org/licenses/by-nc-nd/4.0/

This page is available in the following languages:

Creative Commons License Deed

Attribution-NonCommercial-NoDerivatives 4.0 International (CC BY-NC-ND 4.0)

This is a human-readable summary of (and not a substitute for) the license.

You are free to:

Share — copy and redistribute the material in any medium or format

The licensor cannot revoke these freedoms as long as you follow the license terms.

Under the following terms:

Attribution — You must give appropriate credit, provide a link to the license, and indicate if changes were made. You may do so in any reasonable manner, but not in any way that suggests the licensor endorses you or your use.

NonCommercial — You may not use the material for commercial purposes.

NoDerivatives — If you remix, transform, or build upon the material, you may not distribute the modified material.

No additional restrictions — You may not apply legal terms or technological measures that legally restrict others from doing anything the license permits.

Notices:

You do not have to comply with the license for elements of the material in the public domain or where your use is permitted by an applicable exception or limitation.

No warranties are given. The license may not give you all of the permissions necessary for your intended use. For example, other rights such as publicity, privacy, or moral rights may limit how you use the material.

Deblasi, Janine M

From:	Beeler, Sierra <sierra.beeler@aacr.org> on behalf of Cancer Research <Cancerres@aacr.org>
Sent:	Wednesday, May 24, 2023 9:55 AM
To:	Deblasi, Janine M
Cc:	DeNicola, Gina M
Subject:	EXT:Re: Copyright Inquiry

Hi Dr. Deblasi,

Thank you for your email. Please note that per AACR policy authors are allowed to "Submit a copy of the article to a doctoral candidate's university in support of a doctoral thesis or dissertation" without requesting permission. Additional information is available at: https://aacrjournals.org/pages/copyright.

Additionally, as this manuscript was published under a CC-BY-NC-ND license: "The CC-BY-NC-ND License permits use, distribution, and reproduction of the published article in any medium, provided that the article is properly cited, the use is non-commercial, and no modifications or adaptations are made."

In sum, it is acceptable for you to include the manuscript in your thesis along with proper citation, but any manuscript figures should not be modified. I hope this clarifies. Please let me know if you have any further questions.

Best,
Sierra Beeler
Staff
Cancer Research

From: Deblasi, Janine M <Janine.Deblasi@moffitt.org>
Sent: Tuesday, May 23, 2023 5:17 PM
To: Cancer Research <Cancerres@aacr.org>
Cc: DeNicola, Gina M <Gina.DeNicola@moffitt.org>
Subject: Copyright Inquiry

Hello,

We recently published an article in your journal, and I would like to use some of the figures and text in my PhD thesis. As long as properly cited, is it allowed to modify figures and/ or reuse text?

https://aacrjournals.org/cancerres/article/doi/10.1158/0008-5472.CAN-22-3848/725886/Distinct-Nrf2-Signaling-Thresholds-Mediate-Lung

Appendix D: Institutional Animal Care and Use Committee Approval

UNIVERSITY OF SOUTH FLORIDA

RESEARCH INTEGRITY AND COMPLIANCE
INSTITUTIONAL ANIMAL CARE & USE COMMITTEE

MEMORANDUM

TO: Gina DeNicola,

FROM:

Farah Moulvi, MSPH, IACUC Coordinator
Institutional Animal Care & Use Committee
Research Integrity & Compliance

DATE: 7/11/2017

PROJECT TITLE: Therapeutic Targeting of NRF2-Regulated Metabolism in Lung Cancer.

FUNDING SOURCE: H Lee Moffitt Cancer Center

IACUC PROTOCOL #: R IS00003893

PROTOCOL STATUS: **APPROVED**

The Institutional Animal Care and Use Committee (IACUC) reviewed your application requesting the use of animals in research for the above-entitled study. The IACUC **APPROVED** your request to use the following animals in your **protocol for a one-year period beginning 7/11/2017:**

Mouse: LSL-K-RasG12D x LSL-Nfe2l2D29H ((4–8wks/15–20gms/M-F))	195
Mouse: nu/nu or NOD/scid ((4–8wks/15–20gms/M-F))	650
Mouse: p53FL/FL x LSL-Nfe2l2D29H ((4–8wks/15–20gms/M-F))	195
Mouse: LSL-K-RasG12D x p53FL/FL ((4–8w,s/15–20gms/M-F))	195
Mouse: LSL-K-RasG12D x Keap1R554Q ((4–8wks/15–20gms/M-F))	195
Mouse: LSL-K-RasG12D x Keap1R470C ((4–8wks/15–20gms/M-F))	195
Mouse: C57BL/6 ((4–8wks/15–20gms/M-F))	450
Mouse: LSL-Nfe2l2E79Q ((4–8wks/15–20gms/M-F))	195
Mouse: LSL-Nfe2l2D29H ((4–8wks/15–20gms/M-F))	195
Mouse: p53FL/FL x Keap1R554Q ((4–8wks/15–20gms/M-F))	195
Mouse: LSL-K-RasG12D x LSL-Nfe2l2E79Q ((4–8wks/15–20gms/M-F))	195
	195

Mouse: p53FL/FL x LSL-Nfe2I2E79Q ((4–8wks/15–20gms/M-F))	
Mouse: p53FL/FL ((4–8wks/15–20gms/M-F))	310
Mouse: p53FL/FL x Keap1R470C ((4–8wks/15–20gms/M-F))	195
Mouse: Keap1R554Q ((4–8wks/15–20gms/M-F))	195
Mouse: LSL-K–RasG12D p53Fl/Fl x Keap1R470C ((4–8wks/15–20gms/M-F))	195
Mouse: LSL-K–RasG12D p53Fl/Fl x Keap1R554Q ((4–8wks/15–20gms/M-F))	195
Mouse: LSL-K–RasG12D p53Fl/Fl x LSL-Nfe2I2E79Q ((4–8wks/15–20gms/M-F))	195
Mouse: LSL-K–RasG12D ((4–8wks/15–20gms/M-F))	310
Mouse: LSL-K–RasG12D p53Fl/Fl x LSL-Nfe2I2D29H ((4–8wks/15–20gms/M-F))	195
Mouse: Keap1R470C ((4–8wks/15–20gms/M-F))	195
Mouse: Nrf2 flox ((4–8wks/15–20gms/M-F))	195

Please take note of the following:

• **IACUC approval is granted for a one-year period at the end of which, an annual renewal form must be submitted for years two (2) and three (3) of the protocol through the eIACUC system.** After three years all continuing studies must be completely re-described in a new electronic application and submitted to IACUC for review.

• **All modifications to the IACUC-Approved Protocol must be approved by the IACUC prior to initiating the modification.** Modifications can be submitted to the IACUC for review and approval as an Amendment or Procedural Change through the eIACUC system. These changes must be within the scope of the original research hypothesis, involve the original species and justified in writing. Any change in the IACUC-approved protocol that does not meet the latter definition is considered a major protocol change and requires the submission of a new application.

• **All costs invoiced to a grant account must be allocable to the purpose of the grant.** Costs allocable to one protocol may not be shifted to another in order to meet deficiencies caused by overruns, or for other reasons convenience. Rotation of charges among protocols by month without establishing that the rotation schedule credibly reflects the relative benefit to each protocol is unacceptable.

171

MEMORANDUM

TO: Gina DeNicola,

FROM:

Farah Moulvi, MSPH, IACUC Coordinator
Institutional Animal Care & Use Committee
Research Integrity & Compliance

DATE: 6/3/2020

PROJECT TITLE: Investigation of NRF2-dependent Metabolic Liabilities
                             Therapeutic Targeting of NRF2-Regulated Metabolism in Lung and Pancreatic Cancer

FUNDING SOURCE: Federal government or major agency that awards grants based on peer-reviewed
                             proposals (NIH, NSF, DOD, AHA, ACS, etc.)
                             Non-Profit (Private Foundations, H. Lee Moffitt Cancer Center, etc.), For Profit (Industry
                             Sponsored) or Other
                             National Institute of Health; H Lee Moffitt Cancer Center

IACUC PROTOCOL #:   R IS00007922

PROTOCOL STATUS: **APPROVED**

The Institutional Animal Care and Use Committee (IACUC) reviewed your application requesting the use of animals in
research for the above-entitled study, The IACUC **APPROVED** your request to use the following animals in your
protocol for a one-year period beginning 6/3/2020:

Mouse: C57BL/6 ((4-8wks/15-20gms/M-F))	120
Mouse: p53FL/FL x LSL-Nfe2l2D29H ((4-8wks/15-20gms/M-F))	85
Mouse: LSL-Nfe2l2D29H ((4-8wks/15-20gms/M-F))	85
Mouse: LSL-K-RasG12D x p53FL/FL ((4-8w,s/15-20gms/M-F))	85
Mouse: Nrf2 flox ((4-8wks/15-20gms/M-F))	85
Mouse: p53FL/FL x Keap1R554Q ((4-8wks/15-20gms/M-F))	85
Mouse: LSL-K-RasG12D x LSL-Nfe2l2D29H ((4-8wks/15-20gms/M-F))	85
Mouse: LSL-K-RasG12D p53Fl/Fl x Keap1R554Q ((4-8wks/15-20gms/M-F))	85
Mouse: p53FL/FL ((4-8wks/15-20gms/M-F))	85
Mouse: LSL-K-RasG12D x Keap1R554Q ((4-8wks/15-20gms/M-F))	85

Mouse: LSL-K-RasG12D p53Fl/Fl x LSL-Nfe2l2D29H ((4-8wks/15-20gms/M-F))	85
Mouse: Keap1R554Q ((4-8wks/15-20gms/M-F))	85
Mouse: LSL-K-RasG12D ((4-8wks/15-20gms/M-F))	85
Mouse: NSG SCID (6-40 weeks/15-30g/male and female)	600
Mouse: Stk11 Flox/flox (4-8wks/15-20gms/M-F)	85
Mouse: Stk11 Flox/Flox x LSL-Nfe2l2D29H (4-8wks/15-20gms/M-F)	85
Mouse: Stk11 Flox/Flox x Keap1R554Q (4-8wks/15-20gms/M-F)	85
Mouse: LSL-K-RasG12D x Stk11 Flox/Flox (4-8wks/15-20gms/M-F)	85
Mouse: LSL-K-RasG12D x Stk11 Flox/Flox x LSL-Nfe2l2D29H (4-8wks/15-20gms/M-F)	85
Mouse: LSL-K-RasG12D x Stk11 Flox/Flox x Keap1R554Q (4-8wks/15-20gms/M-F)	85
Mouse: LSL-K-RasG12D x p53Fl/Fl x H11LSL-Cas9 x Keap1R554Q ((4-8wks/15-20gms/M-F))	100
Mouse: LSL-K-RasG12D x p53Fl/Fl x H11LSL-Cas9 ((4-8wks/15-20gms/M-F))	100
Mouse: LSL-K-RasG12D x p53Fl/Fl x H11LSL-Cas9 x LSL-Nfe2l2D29H ((4-8wks/15-20gms/M-F))	100

Please take note of the following:

• IACUC approval is granted for a one-year period at the end of which, an annual renewal form must be submitted for years two (2) and three (3) of the protocol through the eIACUC system. After three years all continuing studies must be completely re-described in a new electronic application and submitted to IACUC for review.

• All modifications to the IACUC-Approved Protocol must be approved by the IACUC prior to initiating the modification. Modifications can be submitted to the IACUC for review and approval as an Amendment or Procedural Change through the eIACUC system. These changes must be within the scope of the original research hypothesis, involve the original species and justified in writing. Any change in the IACUC-approved protocol that does not meet the latter definition is considered a major protocol change and requires the submission of a new application.

• All costs invoiced to a grant account must be allocable to the purpose of the grant. Costs allocable to one protocol may not be shifted to another in order to meet deficiencies caused by overruns, or for other reasons convenience. Rotation of charges among protocols by month without establishing that the rotation schedule credibly reflects the relative benefit to each protocol is unacceptable.